ELECTROCHEMICAL CHARACTERIZATION OF NONAQUEOUS SYSTEMS FOR SECONDARY BATTERY APPLICATION

by Manny Shaw, O. A. Paez, and Frank A. Ludwig

Prepared by
WHITTAKER CORPORATION
San Diego, Calif.
for Lewis Research Center

NATIONAL AERONAUTICS AND SPACE ADMINISTRATION • WASHINGTON, D. C. • SEPTEMBER 1969

ABSTRACT

Approximately one thousand electrode - organic electrolyte combinations have been characterized relative to their use as rechargeable battery systems, using the method of cyclic voltammetry. Electrode systems consisted of silver, copper, nickel, cobalt, zinc, cadmium, indium, iron, molybdenum, chromium, manganese, vanadium, lithium, calcium, and magnesium. In general, the most promising positive metals were silver, copper, zinc, cadmium, and indium. A large majority of the nickel, cobalt, and iron systems exhibited no discharge peaks at all, and in most cases negligible discharge current. Twenty-four recommended systems comprising silver, copper, zinc, and cadmium, were further characterized by constant-current charge and discharge of sintered electrodes.

FOREWORD

The research described in this report was conducted by the Whittaker Corporation under NASA contract NAS 3-8509 with Mr. Robert B. King, of the Lewis Research Center, as NASA Project Manager. The report was originally issued as Whittaker report WRD-392.

TABLE OF CONTENTS

		Page
I.	INTRODUCTION	1
II.	DISCUSSION OF RESULTS	14
	A. Introduction	14
	B. Parameters Derived from Cyclic Voltammograms	15
	C. Reporting Procedure for Present Report	19
	D. Roster of Systems Screened	19
	E. Systems Causing Amplifier Overload	19
	F. Cyclic Voltammetry of Positive Electrode - Electrolyte Systems	40
	1. Cyclic Voltammetry of Silver Systems	43
	2. Cyclic Voltammetry of Copper Systems	51
	3. Cyclic Voltammetry of Nickel Systems	59
	4. Cyclic Voltammetry of Cobalt Systems	60
	5. Cyclic Voltammetry of Zinc Systems	61
	6. Cyclic Voltammetry of Cadmium Systems	64
	7. Cyclic Voltammetry of Indium Systems	66
	8. Cyclic Voltammetry of Mo, Fe, Cr, Mn and V	67
	G. The Effect of Water on Cyclic Voltammograms	70
	1. Silver Systems	70
	2. Copper Systems	71
	3. Other Systems	71
	H. The Effect of Solute Concentration on Cyclic Voltammograms	72
	I. Cyclic Voltammetry of Negative-Electrolyte Systems	80
	1. Lithium Systems	80
	2. Magnesium Systems	83
	3. Calcium Systems	83

TABLE OF CONTENTS (Cont'd)

		Page
II.	DISCUSSION OF RESULTS (Cont'd)	
	J. Recommended Positive - Electrolyte Systems	89
	K. Galvanostatic Charge-Discharge Measurements	114
	L. Chronopotentiometry of Some Recommended Systems	164
III.	EXPERIMENTAL	174
	A. Material Purification and Characterization	174
	1. Solvent Purification and Characterization	175
	2. Solute Purification and Characterization	179
	3. Solution Preparation	186
	4. Electrode Preparation and Characterization	192
	B. Cyclic Voltammetric Measurements	200
	1. Instrumentation	200
	2. Measurement Procedure	202
	3. Instrument Overloading	203
	4. Electrochemical Cell	204
	5. Effect of ir Drop on Cyclic Voltammograms	206
	C. Galvanostatic Charge-Discharge Measurements	208
	D. Chronopotentiometric Measurements	212
IV.	REFERENCES	214

LIST OF FIGURES

Figure		Page
1.	Cyclic voltammogram for silver in KOH.	11
2.	Cyclic voltammogram for mercury in KOH.	12
3.	Useful parameters of cyclic voltammogram.	16
4.	Percent distribution of cyclic voltammetric parameters for total systems screened.	42
5.	Effect of cycling on cyclic voltammogram for Ag/PC-KPF_6.	50
6.	Typical cyclic voltammogram showing non-reducible secondary anodic product.	56
7.	Cyclic voltammogram for zinc in dimethylformamide - KPF_6, 1.75 m, containing 1000 ppm water.	73
8.	Cyclic voltammogram for zinc in dimethylformamide - KPF_6, 0.75 m.	74
9.	Cyclic voltammogram for zinc in dimethylformamide - KPF_6, 1.0 m.	75
10.	Cyclic voltammogram for zinc in dimethylformamide - KPF_6, 2.0 m.	76
11.	Cyclic voltammogram for zinc in dimethylformamide - KPF_6, 3.0 m.	77
12.	Cyclic voltammogram for nickel in KOH.	79
	CYCLIC VOLTAMMOGRAMS OF RECOMMENDED SYSTEMS	
13.	Ag in Butyrolactone - $AlCl_3$ + LiCl	90
14.	AgF_2 in Propylene carbonate - $LiBF_4$	91
15.	Cu in Acetonitrile - KPF_6 + $LiPF_6$	92
16.	Cu in Dimethylformamide - $LiPF_6$	93
17.	$CuCl_2$ in Acetonitrile - $LiPF_6$	94
18.	$CuCl_2$ in Butyrolactone - $AlCl_3$	95
19.	$CuCl_2$ in Dimethylformamide - LiCl + $LiClO_4$	96
20.	$CuCl_2$ in Dimethylformamide - $LiPF_6$	97
21.	$CuCl_2$ in Propylene carbonate - $LiClO_4$	98

LIST OF FIGURES (Cont'd)

Figure		Page
22.	CuF_2 in Dimethylformamide - $LiPF_6$	99
23.	CuF_2 in Propylene carbonate - $LiPF_6$	100
24.	CuF_2 in Propylene carbonate - $LiClO_4$	101
25.	Zn in Acetonitrile - $LiClO_4$	102
26.	Zn in Butyrolactone - KPF_6	103
27.	Zn in Dimethylformamide - KPF_6	104
28.	Zn in Dimethylformamide - $LiPF_6$	105
29.	Zn in Dimethylformamide - $LiClO_4$	106
30.	Zn in Propylene carbonate - KPF_6	107
31.	ZnF_2 in Dimethylformamide - KPF_6	108
32.	ZnF_2 in Dimethylformamide - $LiClO_4$	109
33.	Cd in Butyrolactone - KPF_6	110
34.	Cd in Dimethylformamide - KPF_6	111
35.	Cd in Dimethylformamide - $LiBF_4$	112
36.	Cd in Dimethylformamide - $LiClO_4$	113
	DISCHARGE CAPACITY VERSUS CHARGE CAPACITY	
37.	AgO in Butyrolactone - $AlCl_3$ + LiCl (1 ma/cm^2)	118
38.	AgO in Butyrolactone - $AlCl_3$ + LiCl (5 ma/cm^2)	119
39.	Cu in Dimethylformamide - $LiPF_6$	121
40.	CuF_2 in Dimethylformamide - $LiPF_6$	123
42.	CuF_2 in Propylene carbonate - $LiPF_6$ (1 ma/cm^2)	125
43.	CuF_2 in Propylene carbonate - $LiPF_6$ (5 ma/cm^2)	126
44.	$CuCl_2$ in Dimethylformamide - $LiPF_6$	128
45.	$CuCl_2$ in Propylene carbonate - $LiClO_4$	130
46.	Zn in Acetonitrile - $LiClO_4$	132
47.	Zn in Dimethylformamide - $LiClO_4$	133
48.	Zn in Dimethylformamide - $LiPF_6$	134

Figure		Page
	DISCHARGE CAPACITY VERSUS CHARGE CAPACITY	
50.	Zn in Dimethylformamide - KPF_6 (0.75 m)	137
51.	Zn in Dimethylformamide - KPF_6 (2.0 m)	138
53.	Zn in Butyrolactone - KPF_6	140
54.	Zn in Propylene carbonate - KPF_6	141
55.	Cd in Dimethylformamide - KPF_6	143
56.	Cd in Dimethylformamide - $LiBF_4$	145
57.	Cd in Dimethylformamide - $LiClO_4$	146
59.	Cd in Butyrolactone - KPF_6	149
60.	AgF_2 in Propylene carbonate - $LiBF_4$	151
61.	$CuCl_2$ in Butyrolactone - $AlCl_3$	153
62.	$CuCl_2$ in Dimethylformamide - LiCl + $LiClO_4$	154
63.	CuF_2 in Propylene carbonate - $LiClO_4$ (1 ma/cm^2)	155
64.	CuF_2 in Propylene carbonate - $LiClO_4$ (5 ma/cm^2)	156
65.	ZnF_2 in Dimethylformamide - $LiClO_4$	158
66.	ZnF_2 in Dimethylformamide - KPF_6	159
41.	Discharge curve for CuF_2/DMF-$LiPF_6$.	124
49.	Charge and discharge curves for Zn/DMF-KPF_6.	135
52.	Discharge curve for Zn/BL-KPF_6.	139
58.	Discharge curve for Cd/BL-KPF_6.	147
67.	Representative charge and discharge curve.	162
68.	Chronopotentiometric curve.	168
69.	Schematic of apparatus for preparing complex fluoride salts in-situ.	189
70.	Block diagram of instrumentation.	201
71.	Measuring cell for cyclic voltammetry.	205

LIST OF FIGURES (Cont'd)

Figure		Page
72.	Effect of solution ir-drop on cyclic voltammogram.	207
73.	Experimental cell.	209
74.	Block diagram for CPM experimental circuit.	213

LIST OF TABLES

Table		Page
1.	Chart of Systems Screened - Acetonitrile	20
2.	Chart of Systems Screened - Butyrolactone	22
3.	Chart of Systems Screened - Dimethylformamide	24
4.	Chart of Systems Screened - Propylene Carbonate	27
5.	Electrolyte Conductivity	30
6.	Voltage Overload Systems	35
7.	Current Overload Systems	39
8.	Percent Distribution of Cyclic Voltammetric Parameters for Total Systems Screened	41
9.	Percent Distribution of Systems Having Peak Separations Less than 0.5 Volt	44
10.	Percent Distribution of Cyclic Voltammetric Parameters for Silver Systems	45
11.	Peak Current Densities and Peak Separation, Silver Systems	46
12.	Specific Discharge Capacity and Coulombic Ratio of Some Silver Systems	48
13.	Percent Distribution of Cyclic Voltammetric Parameters for Copper Systems	51
14.	Peak Current Densities and Peak Separation, Copper Systems	53
15.	Specific Discharge Capacity and Coulombic Ratio of Some Copper Systems	57
16.	Percent Distribution of Cyclic Voltammetric Parameters for Nickel Systems	60

LIST OF TABLES (Cont'd)

Table		Page
17.	Percent Distribution of Cyclic Voltammetric Parameters for Cobalt Systems	61
18.	Percent Distribution of Cyclic Voltammetric Parameters for Zinc Systems	62
19.	Specific Discharge Capacity and Coulombic Ratio of Some Zinc Systems	62
20.	Peak Current Densities and Peak Separation, Zinc Systems	63
21.	Percent Distribution of Cyclic Voltammetric Parameters for Cadmium Systems	64
22.	Peak Current Densities and Peak Separation, Cadmium Systems	65
23.	Specific Discharge Capacity and Coulombic Ratio of Some Cadmium Systems	66
24.	Percent Distribution of Cyclic Voltammetric Parameters for Indium Systems	67
25.	Peak Current Densities and Peak Separation, Indium Systems	68
26.	Peak Current Densities and Peak Separation, Other Systems	69
27.	Specific Capacity of Zn/DMF-KPF_6 as a Function of Solute Concentration	78
28.	Lithium Systems	81
29.	Magnesium Systems	84
30.	Calcium Systems	86
31.	Charge-Discharge Data for Sintered Electrodes	161
32.	Chronopotentiometric Data for Zn/BL-KPF_6 (0.80 M)	169
33.	Chronopotentiometric Data for Zn/BL-KPF_6 (0.40 M)	169
34.	Chronopotentiometric Data for Zn/BL-KPF_6 (0.20 M)	171
35.	Chronopotentiometric Data for Zn/BL-KPF_6 (0.80 M)	171
36.	Chronopotentiometric Data for Cd/BL-KPF_6 (0.80 M)	172
37.	Chronopotentiometric Data for Cu/PC-LiCl + $AlCl_3$ (0.80 M)	172

LIST OF TABLES (Cont'd)

Table		Page
38.	Vapor Phase Chromatography Conditions	176
39.	Spectrographic Analysis of Metal Salts	180
40.	Spectrographic Analysis of Wire Electrodes	193
41.	Fluorination Conditions	196
42.	Chlorination Conditions	197
43.	Oxidation Conditions	197
44.	Fluorination and Chlorination of Sintered Metal Electrodes	199

SUMMARY

Cyclic voltammetric measurements have been applied to the screening of 940 individual electrochemical systems in organic electrolytes. Using this technique for the electrochemical characterization of so many systems at the molecular level of the electrode reaction, it was therefore possible to eliminate hundreds of electrode-electrolyte combinations from further consideration as potential systems for high energy density batteries. Furthermore, the program resulted in the selection of a limited number of systems that have been recommended for further characterization and cell development into practical high energy density rechargeable battery systems.

Despite the large number of systems screened, it should be noted that obviously not all possibilities have been covered. In terms of the electrolyte, the program was limited to four solvents of known desirability as organic electrolyte media, and twenty-three solutes, a number of which have already been demonstrated as being advantageous. The thirty-one electrode materials, however, represent a rather complete survey of electrode choice.

Throughout the program particular emphasis was made on the chemical characterization of all materials prior to the electrochemical characterization of the systems. It was considered that within the limits of practicability this was an important factor, considering the molecular complexity of organic-inorganic solutions. As a result, confidence in the significance of the data was established, and the reproducibility of the cyclic voltammograms was satisfactory except in the few cases representing very unstable systems. The effect of water on the voltammograms was determined by the deliberate addition of known amounts to nonaqueous solutions. For some systems the effect was pronounced, while for others, amounts up to 3000 ppm had no apparent effect on the sweep curve characteristics.

Although measurements were made at 200, 80, and 40 mv/sec, the systems were evaluated relative to each other at the lowest sweep rate. According to theory and confirmed experimentally, peaks are better defined in terms of being more narrow and less displaced from each other (i.e. anodic to cathodic), making evaluation by comparison of the systems more concise. For meaningful comparison of the very large number of cyclic voltammograms, use was made of certain parameters defining the primary characteristics of the curves. Peak height, separation, and enclosed area were chosen as being indicative, in a relative manner, of electrode activity, charge-discharge voltage separation, specific capacity, and charge-discharge efficiency. The slope of the ascending portion of the peak is a measure of the extent of activation polarization, while the descending branch reflects the rate of depletion of the available anions. There was no need to measure these however, since the overall effect is shown by the height, separation, and area of the peaks.

876 positive electrode-electrolyte systems were screened. These consisted of the oxides, chlorides, and fluorides of silver, copper, nickel, and cobalt, the chlorides and fluorides of zinc, cadmium, indium, and iron, and molybdenum, chromium, manganese, and vanadium metals. Of this number, 217 systems caused amplifier voltage overload as a result of a combination of high solution resistivities and appreciable current densities, or by high current densities alone. The former usually occurred in solutions of BF_3, PF_5, and the magnesium or calcium salts of the complex fluorides. In general, silver, copper, zinc, cadmium, and indium systems, showed a greater proportion of high or appreciable currents. An overwhelming majority of the nickel, cobalt, and iron systems exhibited no discharge peaks at all, and in most cases negligible discharge current. On the other hand, only a small percent of the copper, silver, zinc, and cadmium systems failed to show a discharge peak. The fact that only a limited number

of nickel, cobalt, and iron systems caused instrument overload is due to the very low or negligible currents for these systems.

The magnitude of the specific charge capacity was interpreted as an indication of the formation of a more dense (compact) or less dense anodic product. Support for this belief came from cyclic voltammetry of a given system having varying solute concentrations. It was suspected that a less dense, spongy anodic product was associated with a higher rate of solubility.

A total of 64 systems involving lithium, calcium, and magnesium electrodes, was screened by cyclic voltammetry. Only five of the 17 lithium systems exhibited both charge and discharge peaks, but with large peak separations. In nearly all cases, neither magnesium nor calcium exhibited charge peaks, and the charge currents were negligible or non-existent.

Twenty-four systems were chosen for further characterization by means other than voltage sweep. Constant current charge and discharge measurements were made on sintered-type electrodes. The purpose of this effort was to measure the discharge capacity as a function of charge input, and to provide information on utilization efficiency and system reversibility as indicated by the voltage separation between charge and discharge plateaus. As a result of this further characterization, seven systems were recommended for cell development. These were silver oxide in butyrolactone - $LiCl + AlCl_3$, copper fluoride in either dimethylformamide or propylene carbonate - $LiPF_6$, copper chloride in propylene carbonate - $LiClO_4$, zinc in dimethylformamide - KPF_6, cadmium in dimethylformamide - $LiClO_4$, and silver difluoride in

propylene carbonate - $LiBF_4$.

An emphatic point to be made is that the original recommended 24 systems were chosen by setting an arbitrary standard of high discharge current densities and low peak-to-peak separations. It is likely that of the other systems measured, a number having lower discharge current peaks or slightly larger peak separations would also be suitable candidates for further characterization. This is a reasonable expectation based on the very large number of systems screened.

It was not the intent of the program to obtain any mechanistic information regarding the electrode-electrolyte systems. The purpose, as stated, was to conduct a rapid yet systematic screening of many systems. This was accomplished with the above results. Certain points stand out in clarity. There is much hope for a number of silver and copper systems. There is little hope for nickel and cobalt systems. New candidates such as zinc, cadmium, and indium have made their appearance.

Another fact made evident is the great utilitarian aspect of the method of cyclic voltammetry for electrochemical characterization of potential battery candidates. It has become apparent that when applied to a limited number of systems, the voltage sweep technique is capable of more fully describing a system in terms of its macroscopic properties.

I. INTRODUCTION

The large number of electrochemical systems that can be considered for possible application in nonaqueous high energy density batteries, together with the variability of plate fabrication and its consequent effect on cell performance, involves the screening of thousands of combinations. Previous work (Ref. 1) has indicated that 30 solvent-solute systems exist having sufficient conductance to be considered as electrolytes for high energy density batteries. Using these electrolytes, the screening of 10 cathode materials comprising plates fabricated according to four types of binders, five variations of mix ratio, three sintering temperatures, three sintering times, and three values of plate compression, involves the testing of 162,000 combinations. This does not consider other determining factors of plate fabrication. It is apparent that a logical and systematic screening procedure is required to choose from the many electrode-electrolyte combinations those having the most promise for development into practical high energy density batteries.

The screening problem can be resolved by considering that even though the performance of any battery depends on a multitude of factors, they can all be grouped into the following:

Molecular Level Factors

These are the kinetic and mass transfer factors related to the electrode processes that determine the initial availability of energy.

Plate Level Factors

These are the structural factors necessary to the practical operation of the battery.

In essence, the initial release of energy is at the molecular level of the charge-transfer reaction and transport of reactive species. If the electrons cannot be removed from the anode at a useable rate, and at the same time be taken up at the cathode at a useable rate, the system warrants no further consideration. The magnitude of the reaction rate constant, number of electrons involved in the charge transfer reaction, mass transfer effects, and magnitude of energy loss, are those factors at the molecular level which initially determine the availability of energy. Molecular level screening chooses those systems having the most desirable electrochemical properties. Whether these systems will have any promise in an actual battery can only be determined by a cell development program at the plate level.

The various techniques of plate fabrication methods, such as pasting, molding, sintering, electro- and chemoformation, will determine the actual cell performance. Plate porosity and surface availability are dependent on the specific methods used for plate fabrication, and are tied in with the type of binder and vehicle employed. The proper choice of the mix ratio, involving these with the active material and the conductive diluent, is essential to optimum cell performance.

In order to properly screen an electrode-electrolyte combination it is necessary to do so in the absence of such considerations as method of plate preparation, additives, separators, etc. In other words, the screening must be done under conditions distinguishing those factors that determine the efficiency at the molecular level of the reaction from those imposed upon it by the requirements of plate composition. If this is not done, or if the screening is performed solely at the plate level, then an attempt to determine optimum plate conditions for those couples that do not posses the basic electrochemical requirements represents a wasted and futile effort. In addition the elimination of desirable electrochemical couples is made possible because of the unfortunate choice of mix ratio, particle size, binder, or other variations. Pre-

liminary screening at the molecular level permits the systematic and rapid elimination of the electrochemically-undesirable systems, so that a more thorough investigation of the promising systems can be made at the plate level.

Choice of a Molecular Level Screening Technique

The voltage sweep technique (also variously known as sweep voltammetry, triangular voltage sweep, linear potential scan voltammetry) is particularly suited to the electrochemical characterization of electrode-electrolyte systems in a molecular level screening program. Inherent in this single technique is the ability to obtain information as to the extent of electrode polarization, reaction potential, charge-discharge efficiency, reaction complexity, solvent decomposition, surface passivation, and separation of individual discharge steps with their relative efficiency. Although the instrumentation is complex, the technique is simple and rapid - necessary requirements for a screening technique.

The measuring technique used in these studies will be referred to as Cyclic Voltammetry, inasmuch as it involves the characterization of systems for secondary battery application, so that a single voltammogram will exhibit both the charge and discharge reactions.

Simply described, cyclic voltammetry is a procedure by which the voltage is varied continuously in a linear manner in an unstirred solution using a stationary microelectrode. Basically, a linearly varying voltage is applied between the working and reference electrodes over a given range. This voltage is a triangular function of time and is supplied by a function generator. Since the voltage applied to the cell varies linearly with time, the X-axis corresponds to either voltage or time units. Variations of the current flowing between the working and counterelectrodes are followed by

means of a suitable recorder. The current-voltage (current-time) curve is characterized by peaks resulting from the opposing effects of increasing rate of electron transfer and depletion of the electroactive species. With appropriate instrumentation the sweep rate (rate at which the applied voltage changes) can be varied over any desired range. This allows interpretation of the curves in terms of both reaction and diffusion rates at various applied voltages and scan rates. The processes can be separated as to type by comparison of the area under the current-time plots as a function of sweep rate. Information regarding the mechanism of the various processes can be derived from the slope of the current rise. Integration of the areas enclosed by the peaks gives a measure of depth of material conversion, while comparison of the anodic and cathodic peak areas gives the charge-discharge efficiency. Decomposition of the solvent is made evident by the appearance of peaks due to solvent oxidation or reduction.

Interpretation of Cyclic Voltammograms

Cyclic voltammetry has been extensively used in electroanalysis and the determination of reaction mechanisms for the oxidation and reduction of soluble species both organic and inorganic. Mathematical relationships have been derived relating the electrode kinetic parameters of such systems. Nicholson and Shain (Ref. 2) review developments in this area and have extended the theory to include additional kinetic cases (Refs. 2-5). Cyclic voltammetric data have been qualitatively analyzed for platinum electrodes in the case of the electro-oxidation of organic compounds (Refs. 6-14). Within the broad application of cyclic voltammetry such parameters as peak current, peak potential, and sweep rate, have been related to concentration of the reactive species for single scan (Ref. 15) and multicycle sweeps (Ref. 2). Equations have been obtained for linear, cylindric, and spherical diffusion in sweep voltammetry (Refs. 2, 15). Analysis is usually simpler for linear diffusion. However if the quantity $\left(\frac{1}{r_o}\right)\left(\frac{D}{n\nu}\right)^{1/2} < 0.2$

then the treatment of linear diffusion is applicable to cylindric diffusion. The quantity r_o is the radius of the wire electrode in cm., D is the diffusion coefficient in $cm^2/sec.$, ν is the sweep rate in volts/sec., and n is the number of Faradays. For the sweep rates used in this work, the assumption of linear diffusion is usually applicable.*

When insoluble films form at the electrode surface, the ohmic drop through the film (the thickness of which theoretically varies as the inverse square root of the sweep rate) will have a marked effect on the peak current. A drop of 0.100 volts through a film of constant thickness will decrease the peak current to 71% of its theoretical value (Ref. 15). Under actual conditions of changing film thickness and a non-linear variation of resistance with film growth, the deviation is probably greater than for the example given.

The theoretical derivation of kinetic relationships in the case of consummable electrodes, or electrodes forming insoluble oxidation products, as for those systems of interest to battery application, is an almost impossible task. The changing nature of the electrode surface and the formation of semiconducting layers makes even a qualitative analysis more difficult than for the soluble species - inert electrode systems. Nevertheless, the cyclic voltammetric method serves as a valuable tool for the rapid screening of electrochemical systems in evaluating their possible use in nonaqueous battery systems.

In the case of an electrochemically reversible dissolved species reacting at an inert electrode, and where the electrode reaction is limited only by mass transfer of ions, the cyclic voltammogram would be typified by the following:

* e.g. for $r_o = 0.064$ cm, n is 2, ν is 0.04 v/sec, and D is 2×10^{-6} cm^2/sec (propylene carbonate), the quantity is 0.08. Less viscous solvents give a value of 0.2 - 0.3.

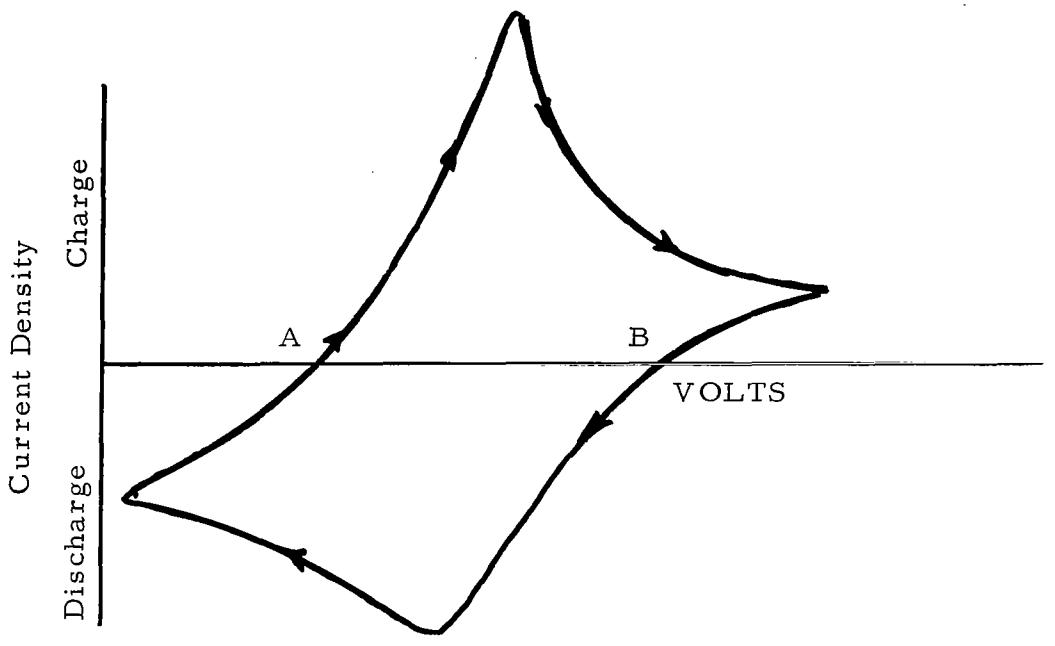

Dissolved species, reversible (mass transfer limited)

The scan is in a clockwise direction with the potential becoming more positive towards the right. For a homogeneous reversible reaction, the peak potential (the potential at the peak current) depends only on the polarographic half-wave potential. Where a solid product is involved however, the peak potential is a function of concentration. For both the reversible homogeneous reaction and reversible solid product cases, the sweep curve indication of concentration polarization is characterized by having the peak currents at close to the same potential, and proportional to the bulk concentration as well as to the square root of the sweep rate. The simple relationships of peak potential, peak current, concentration, and sweep rate need modification when considering multi-cycle sweeps.

In addition, stirring greatly increases the current. Increasing the sweep rate has the effect of increasing the distance between points A and B at which the forward and return portions of the curve cross the zero-current axis. Finally, currents related to adsorption capacities are negligible in comparison to the diffusion currents.

An irreversible process would exhibit the following type of curve,

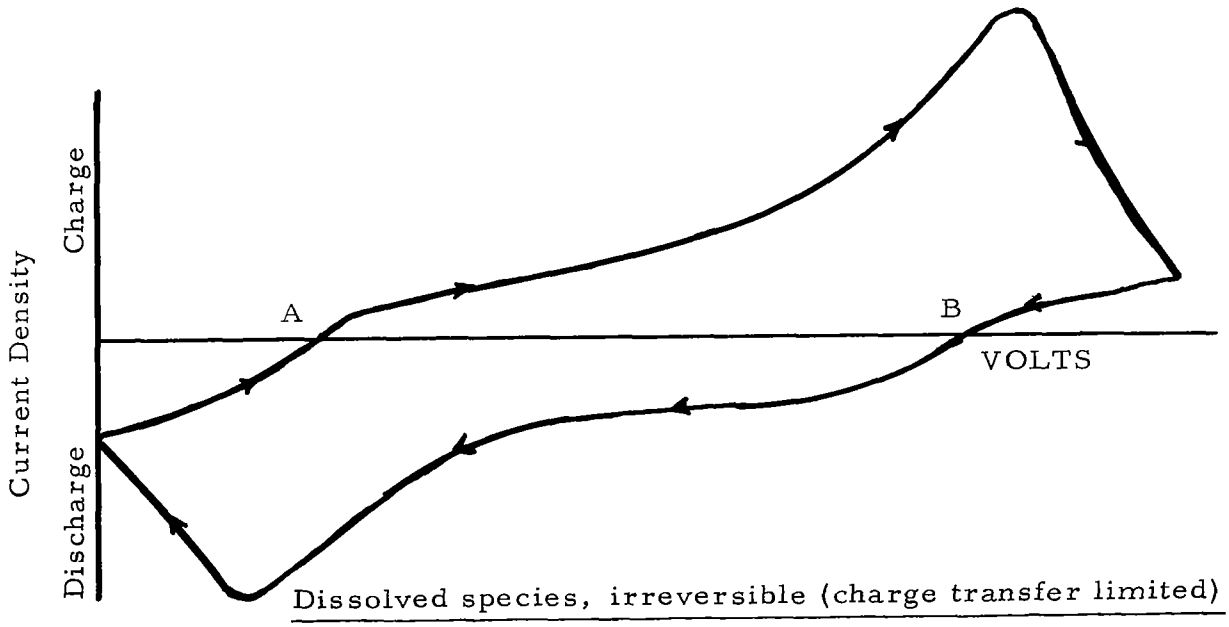

in which the peaks are considerably displaced from the ocv (E_o) value and from each other. In general, the distance between the two points (A and B), where the curve intersects the zero-current axis, is a relative measure of the concentration polarization.

We consider the following reaction,

$$M + A^- \longrightarrow MA + e^-$$

where M is a solid metal electrode, A^- is a soluble anion, and MA is a relatively insoluble solid product. This situation is therefore schematically represented as,

M	MA	A^-
Metal	Insoluble Compound	Solution

The layer MA is represented as having some finite depth since prior work at Whittaker has demonstrated a thickness of at least 5 monolayers existing at solid electrodes. This representation requires that the MA layer also contains some M species. Charge transfer may therefore be possible either at the M-MA or at the MA-solution interfaces. Determination of which occurs involves consideration of the characteristics of the MA layer. Current must be accompanied by transport through the MA phase of M, M^+, or A^-. It is generally accepted (though not proven) that only M and M^+ are transportable. In metal-excess types, the metal atoms are assumed to migrate interstitially with electron transfer occurring at the MA-solution interface. The electrons must then also cross the MA phase, constituting a semiconductor process. In metal-defect materials, it is assumed that the M^+ ion is the migrating species (via defect lattice sites), and that electron transfer occurs at the M-MA interface. This does not require the electron to be carried across

the MA layer. The activational energy losses associated with electron transfer, electron migration across the MA layer, and migration of M, M^+, or A^- across the MA layer, must be considered together as one since they cannot be individually measured.

Because charged particles must be transported across the MA layer, the latter acts similar to a resistance in series with the chemical reaction. A voltage loss will occur across this film, and will be proportional to the current density, the film thickness, and the film resistivity. The effective resistance of the layer, termed transfer resistance, is a more complex parameter than solution resistance since it is a function of the number of charge carriers. These have an uncertain nature because different phases of the same material may have differing semiconductor properties, so that the number of charge carriers may also be a function of the current density and time (total charge). The film thickness is also a function of time and current density. For a solid state type of reaction therefore, the total non-linear polarization must include the polarization due to film transfer resistance in addition to that due to normal mass and charge transfer at the solid-electrolyte interface. In such a case, for a relatively reversible system, the following sweep curve would be obtained:

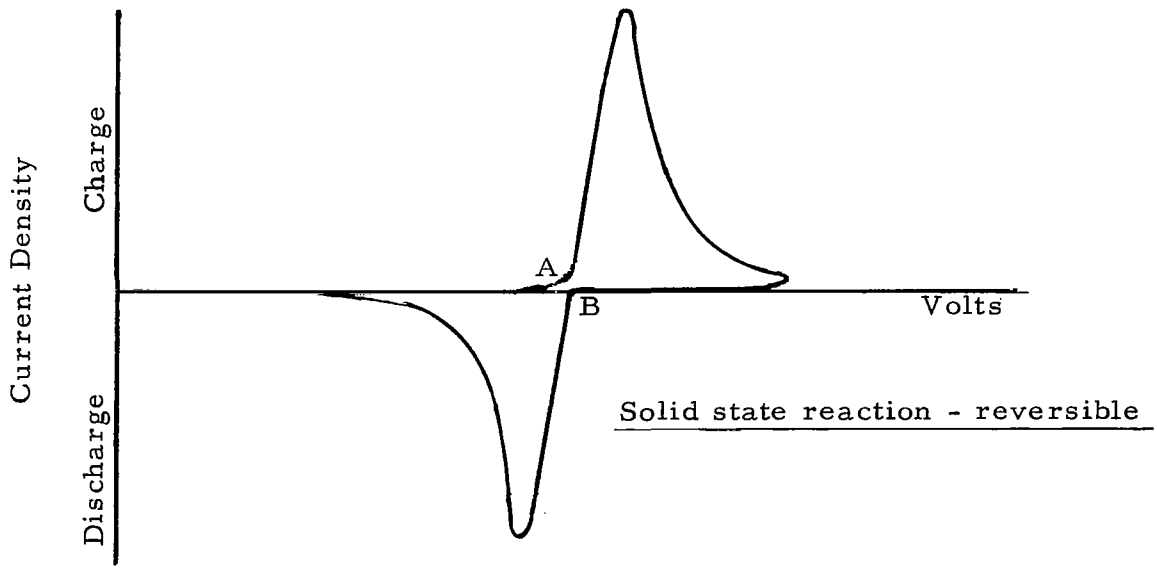

Solid state reaction - reversible

For irreversible systems where the charge transfer process is limiting, the following type of curve will result:

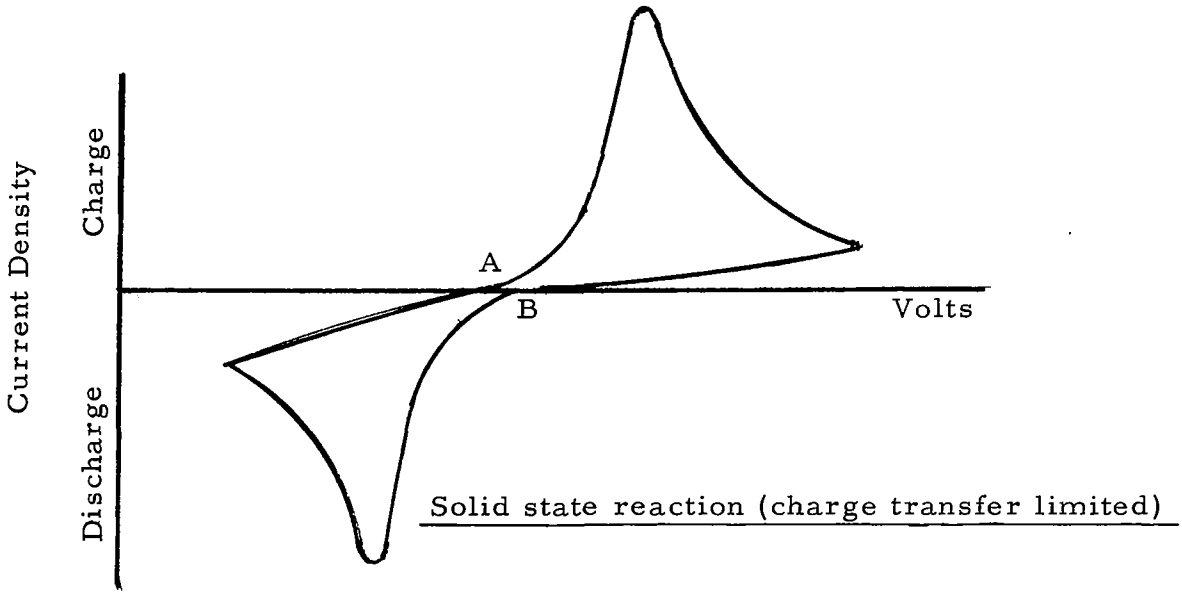

The relatively small displacement between points A and B indicates the minor contribution of concentration polarization relative to the transfer film type of polarization. This displacement will become larger with increasing concentration polarization.

Almost all of the sweep curves obtained during this program, and having both anodic and cathodic peaks, exhibited this type of pattern with varying displacement of points A and B. The fact that aqueous systems also display the solid state type of cyclic voltammogram is shown in Figures 1 and 2 for silver oxide and mercuric oxide in potassium hydroxide, these two representing typical battery positives.

Figure 1. Cyclic voltammogram for silver in KOH*

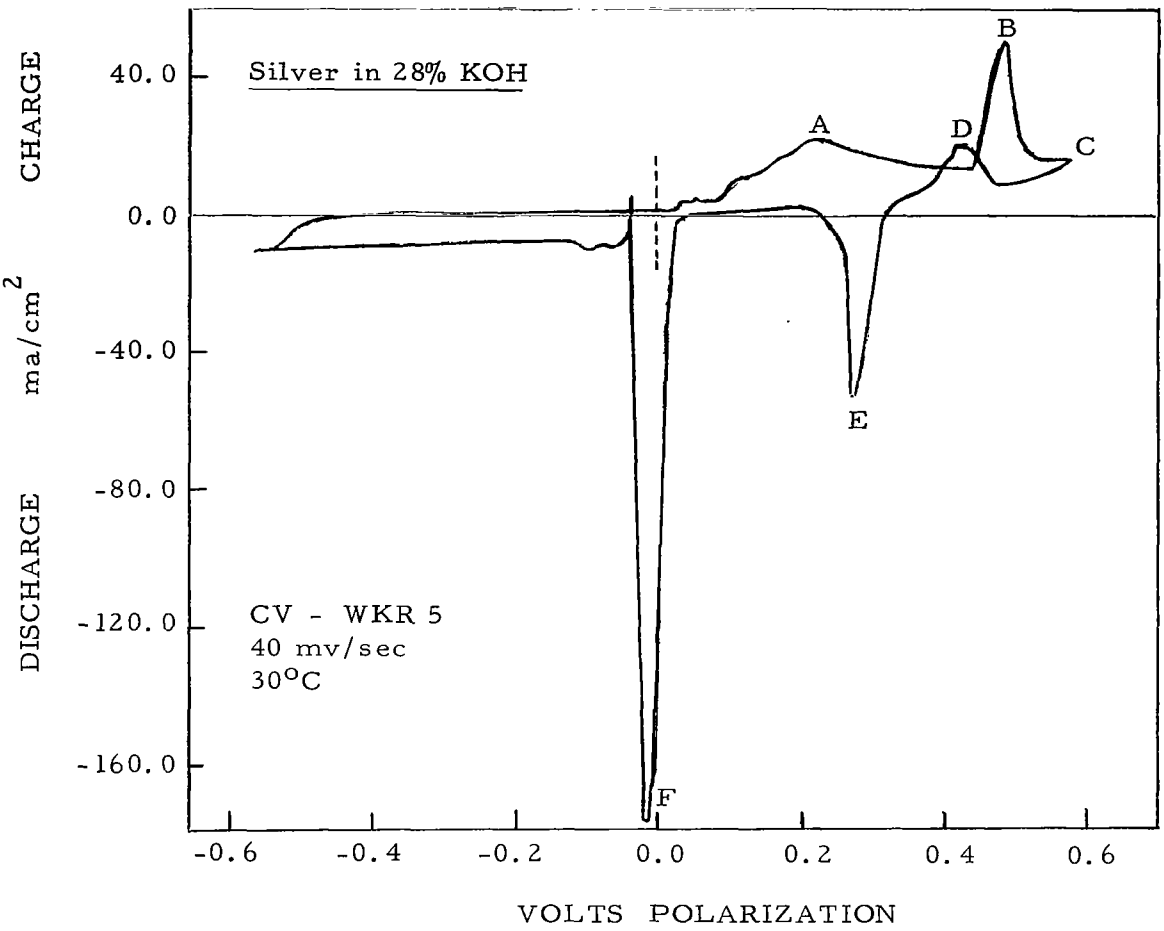

*Previous work at Whittaker has tentatively explained the peaks as follows:

Peak	Reaction	Peak	Reaction
A	$Ag \longrightarrow Ag_2O$	D	$Ag_2O \longrightarrow AgO$
B	$Ag_2O \longrightarrow Ag_2O_3$	E	$AgO \longrightarrow Ag_2O$
C	$H_2O \longrightarrow O_2$	F	$Ag_2O \longrightarrow Ag$

Direct formation of divalent Ag from monovalent is not observed during the charge sweep, but rather the formation of trivalent (Ag_2O_3) shown by peak B. This disproportionates rapidly with silver to form divalent (AgO), which nucleates the oxidation of monovalent to further AgO (peak D). The higher voltage for peak B causes the typical spike found at full charge of the monovalent Ag. Formation of divalent Ag during conventional charging corresponds to peak D, but since Ag_2O_3 formed at B is essentially converted to AgO, the area of B gives the formation capacity of the divalent form.

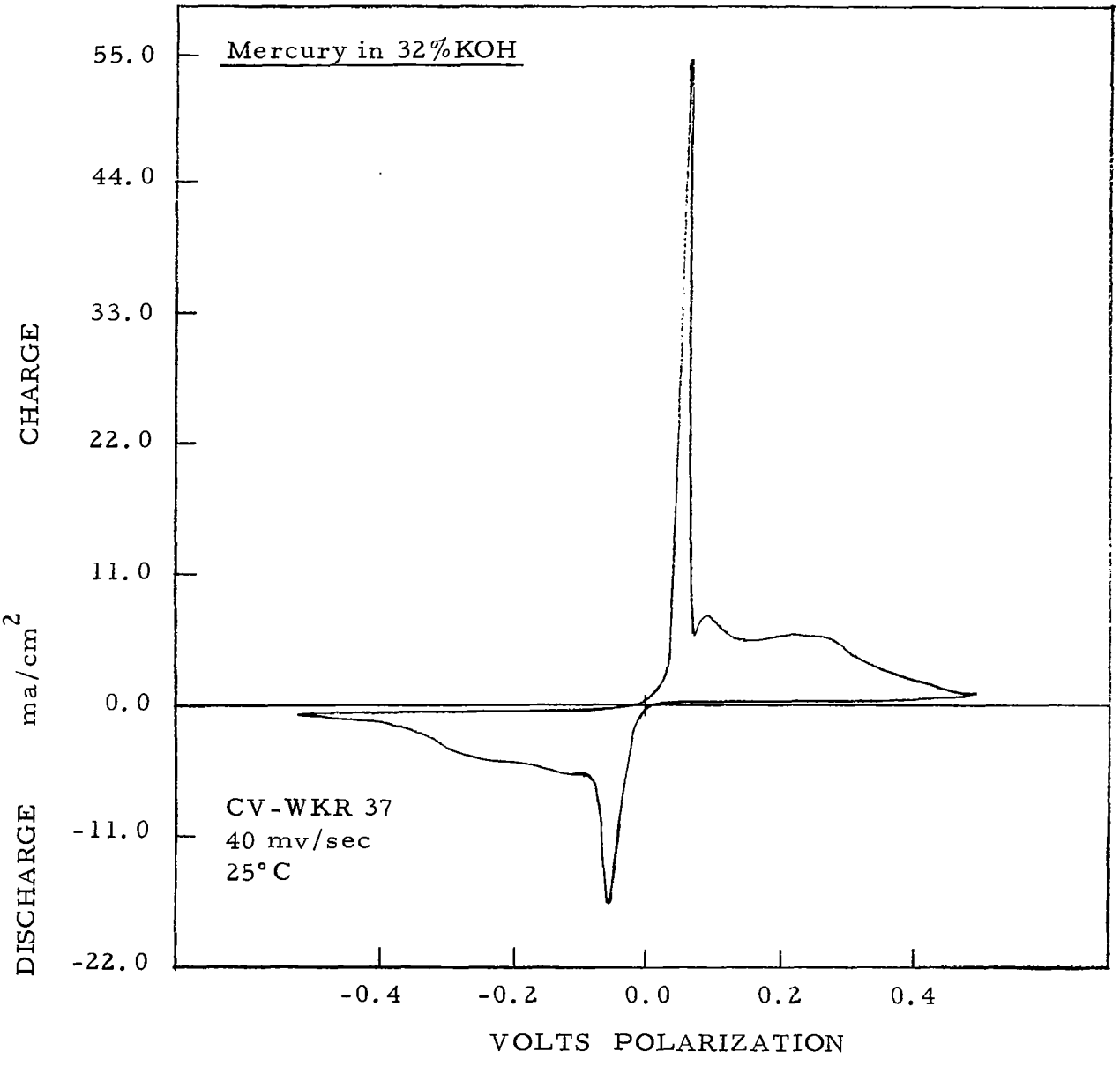

Figure 2. Cyclic voltammogram for mercury in KOH

With only one or two exceptions all systems screened indicated the solid state type of cyclic voltammogram. A large number of systems exhibited however, a decrease in the discharge peak area (with respect to the charge peak area) with decreasing sweep rate. At sufficiently low sweep rates, many systems failed to show any cathodic current. Apparently the product formed during the anodic portion of the sweep was less available, or no longer existed at the lower sweep rates for subsequent reduction. This would be explained by dissolution of the anodic product in the electrolyte, and due to convection was dissipated throughout the bulk solution, so was not available for reduction at the working electrode. At lower sweep rates, a longer time would have elapsed before the reduction potential would have been reached, thereby explaining the decrease in discharge capacity with decreasing sweep rate. The reduction current, due to the small amount of dissolved material remaining at the reaction interface, would not be registered since the sensitivity of the X-Y recorder was adjusted to accommodate the excessively large currents resulting from the anodic reaction.

In confirmation of this, measurements were made in a few cases using a pyrolytic graphite electrode in used solutions, where cyclic voltammetry had been performed on systems showing the effect of a vanishing discharge peak with decreasing sweep rate. Discharge currents were obtained but of two or three orders of magnitude lower than when the system electrode was run. In these cases, also, the discharge coulombs decreased with cycling, and no anodic current was evident.

II. DISCUSSION OF RESULTS

A. Introduction

Cyclic voltammograms were obtained for 940 separate electrochemical systems comprising four solvents, twenty-three solutes, and thirty-one electrode materials. The exceedingly large number of systems screened made it mandatory that a systematic and routine procedure be adopted for analysis and reporting of the results. Analysis of the data as reported during the program was accomplished by dividing all systems into those involving chloride and perchlorate electrolytes, and those involving fluoride electrolytes. Each main group was then subdivided according to the identity of the working electrode. Each of these subgroups was further broken down according to the identity of the solvent portion of the solution. The cyclic voltammograms were then discussed in terms of the total solution. Since a few thousand cyclic voltammograms were obtained, it was impossible, nor was it necessary, to reproduce all curves. As it was, 280 cyclic voltammograms were reproduced in the quarterly reports.

Electrochemical characterization of 940 separate systems required a system in which parametric data derived from the cyclic voltammograms could be recorded and then retrieved. Such data detailed information regarding the existence or absence of charge or discharge peaks, their height, area, and separation.

In addition to the derived data were the number of separate characteristics merely defining the systems, such as electrode material, solvent, solute, solute concentration, and conductance. Ideal for the purposes of information storage and retrieval was the use of manually punched cards which could be sorted, also manually, by needle selection. The use of punch cards greatly facilitated data analysis and system comparison. It also simplified the pre-

paration of tabular data for report presentation.

Prior to presentation and discussion of the results, it is first necessary to describe in more detail the data derived from the cyclic voltammograms. The use of these cyclic voltammetric parameters permits the evaluation and direct comparison of the electrochemical systems. It also allows the reporting of many more systems within reasonable limits of a report size.

B. Parameters Derived from Cyclic Voltammograms

Figure 3 shows a typical cyclic voltammogram. The sweep is in a clockwise direction, the potential becoming more positive to the right. Positive currents represent anodic reactions, and negative currents represent cathodic reactions. In the case of positive plate materials, this orientation corresponds to the charge reaction above, and the discharge reaction below, the voltage axis (X-axis). In the case of negative plate materials, this corresponds to the discharge and charge reactions respectively. The current axis is in units of ma/cm^2, each unit being of variable scale depending on the X-Y recorder sensitivity setting. The voltage axis units are relative to the ocv, E_o, so that voltage units are in terms of electrode polarization.

Except in those cases where the metal is converted to a cathodic material prior to assembly in the measuring cell, the working electrode is the base metal itself. During the voltage sweep the metal is oxidized to some species, this anodic product then serving as the cathode which is subsequently reduced during the cathodic portion of the sweep. Each sweep cycle thus corresponds to a charge-discharge cycle.

Analysis is based on the cyclic voltammograms obtained at the lowest sweep rate, 40 mv/sec, except where additional information is required from the higher sweep rate curves to aid in the analysis.

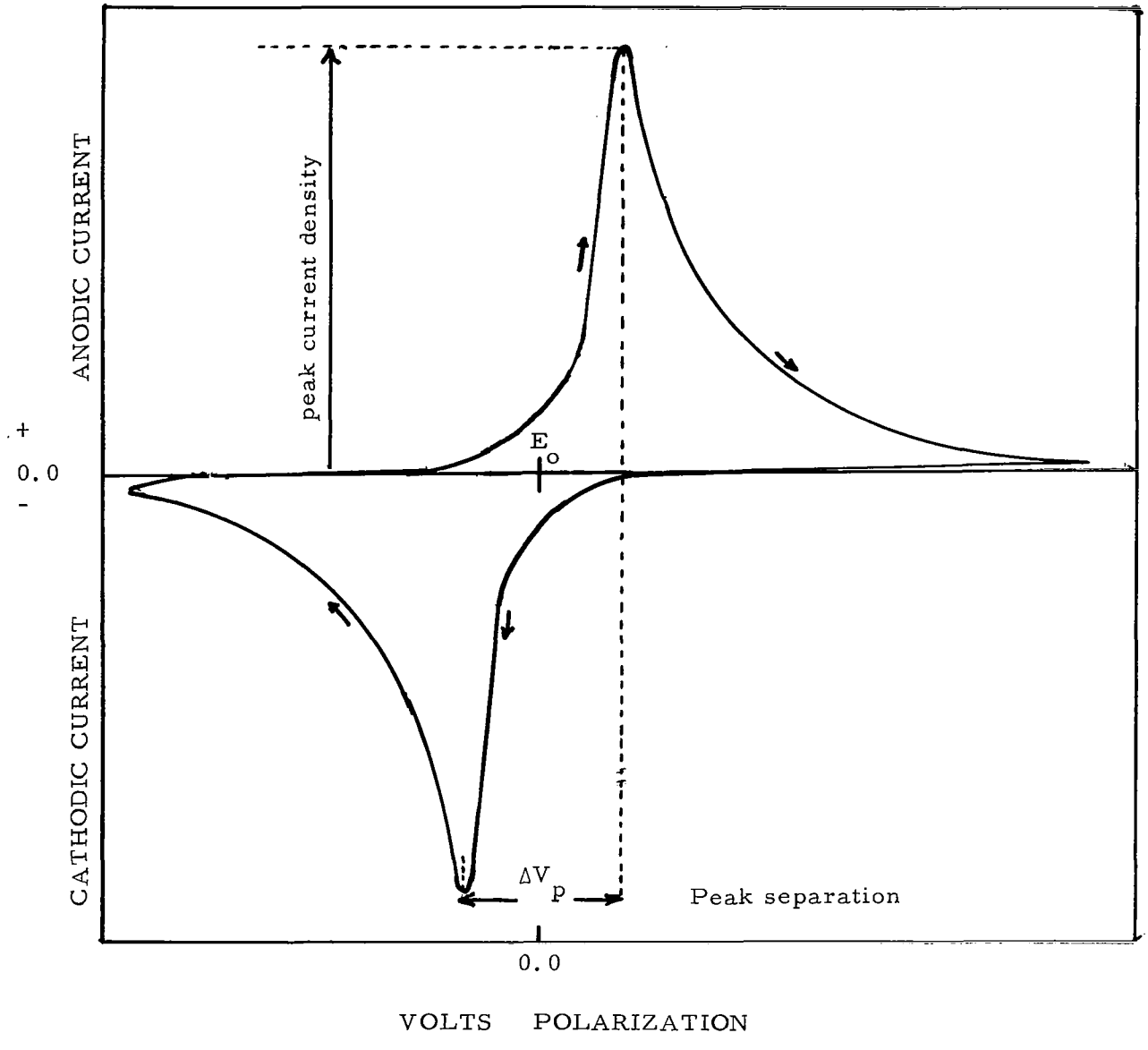

Figure 3. Useful parameters of cyclic voltammogram

The following parameters are of significance:

1. Peak Current Density

During the screening program the peak current densities (both anodic and cathodic) of all systems were reported relative to one another according to a peak current density range. For comparative purposes the current density magnitude was classified according to very high (more than 300 ma/cm^2), high (100-300 ma/cm^2), medium high (50-100 ma/cm^2), medium low (10-50 ma/cm^2), low (1-10 ma/cm^2), and very low (less than 1 ma/cm^2). For the purpose of this report only those systems will be tabulated whose discharge current densities are in the medium-high or greater range, i.e. those having discharge current densities (at 40 mv/sec) greater than 50 ma/cm^2.

2. Peak-to-Peak Separation

This value, ΔV_p, measured in millivolts, represents the distance between the peak voltages of the charge and discharge reactions, giving a qualitative measure of overall electrode reversibility. In more practical terms, it gives a measure of suitability of the electrochemical system for secondary battery application. The greater the separation of the peaks, the less suitable is the system, either because of the greater polarization of the charge or the discharge reaction or both. Since it was not practical in a screening program of this nature to use electrochemically reversible reference electrodes, it was not always possible to determine whether the charge or discharge reaction was the more polarized. In any case however, a system would have no interest as a rechargeable battery if ΔV_p were significantly large.

3. Specific Capacity

Integration of the area under the peak gives the specific capacity in cou-

lombs/cm^2. This is obtained by the following calculation,

$$\text{coul/cm}^2 = \frac{A\, I_p\, \Delta X}{\nu\, h}$$

where A is the peak area in cm^2, I_p is the peak current density in amps/cm^2, ΔX is the XY recorder range setting for the voltage axis in volts/cm, h is the peak height in cms, and ν is the sweep rate in volts/second.

The specific charge capacity represents the amount of material converted to the oxidized state per unit area of electrode. Similarly, the specific discharge capacity is the amount of material discharged per unit area of electrode. Calculations of specific capacity are possible only for simple well-defined peaks. In many cases, a peak may be well-formed with a sharp ascending portion, and a sharp descending portion until a current density value of 20-30% of the peak value is reached, after which the current flattens out and remains at this value until the maximum scan is reached and retraced. In such cases, a choice should be made as to the maximum area to be integrated, being confined chiefly to the sharp peak region. In the case of a charge peak, this is equivalent to limiting the charge voltage, which is a standard procedure. If the maximum coulombic input chosen represents most of the total charge coulombs, this procedure is particularly justified.

4. Coulombic Ratio

This is the ratio of the specific discharge capacity to the specific charge capacity, thus representing a charge-discharge efficiency, or percent utilization of the charged material.

C. Reporting Procedure for Present Report

The procedure described above for reporting the results during the program is not appropriate for a final report having the purpose of reporting on and summarizing the total program. Results and discussion for this report will therefore be categorized according to the metal systems comprising the electrodes, e.g. copper systems including copper metal, copper oxide, copper chloride, and copper fluoride.

Inclusion of all the tabular data for 940 systems, as reported in the quarterlies, would result in an excessively bulky report having no particular advantage. Therefore, as stated earlier, tabular data relative to the cyclic voltammetric characteristics will be reported only for those systems exhibiting a discharge current density greater than 50 ma/cm^2 at a sweep rate of 40 mv/sec. This comprises 117 of the total 940 systems. Only the peak current densities and the peak separation will be reported for all 117 systems. Coulombic ratios will only be reported for those systems where meaningful peak area measurements can be made, and where the values serve a purpose.

D. Roster of Systems Screened

The 940 electrochemical systems screened comprised four solvents, twenty-three solutes, and thirty-one electrode materials. Tables 1, 2, 3, and 4 list 160 acetonitrile, 148 butyrolactone, 341 dimethylformamide, and 295 propylene carbonate systems respectively. Solution conductivities are tabulated in Table 5.

E. Systems Causing Amplifier Overload

Cyclic voltammograms could not be obtained for 217 positive electrolyte systems due to amplifier overload caused by a combination of low conductivity

TABLE 1

CHART OF SYSTEMS SCREENED

ACETONITRILE

Solutes \ Electrodes	Cu	CuO	$CuCl_2$	CuF_2	Ag	AgO	AgCl	AgF_2	Ni	NiO	$NiCl_2$	NiF_2
LiCl	x				x				x			
$AlCl_3$	x		x		x		x		x		x	
$LiCl + AlCl_3$	x	x	x	x	x	x	x	x	x	x	x	x
$MgCl_2$	x		x		x		x		x		x	
$LiClO_4$	x	x	x	x	x	x	x	x	x	x	x	x
PF_5	x			x	x			x	x			x
KPF_6	x	x		x	x	x		x	x	x		x
$LiPF_6$	x	x	x	x	x	x	x	x	x	x	x	x
$LiPF_6 + KPF_6$	x				x							
BF_3	x			x	x			x	x			x
$LiBF_4$	x			x	x			x	x			
$Mg(BF_4)_2$	x			x	x			x	x			x
$LiF + MgF_2$	x											
$LiF + KPF_6$	x	x		x	x	x		x	x	x		x

TABLE 1 (Cont'd)

CHART OF SYSTEMS SCREENED

ACETONITRILE (Cont'd)

Solutes \ Electrodes	Co	CoO	$CoCl_2$	CoF_3	Zn	Cd	Mo	Mg	Ca
$AlCl_3$	x	x	x					x	x
$LiCl + AlCl_3$	x	x	x	x	x			x	x
$MgCl_2$	x	x	x	x					
$LiClO_4$	x	x	x	x	x	x	x	x	x
$Mg(ClO_4)_2$								x	
PF_5	x			x					
KPF_6	x	x		x	x	x	x	x	
$LiPF_6$	x	x	x	x				x	x
$LiPF_6 + KPF_6$					x	x		x	x
BF_3	x			x					
$LiBF_4$	x			x	x	x		x	x
$Mg(BF_4)_2$	x			x					
$LiF + KPF_6$	x			x	x	x	x		

TABLE 2

CHART OF SYSTEMS SCREENED

BUTYROLACTONE

Solutes \ Electrodes	Cu	CuO	$CuCl_2$	CuF_2	Ag	AgO	AgCl	AgF_2	Ni	NiO	$NiCl_2$	NiF_2
LiCl	x	x	x		x	x	x		x	x	x	
$AlCl_3$	x		x		x		x		x		x	
$LiCl + AlCl_3$	x	x	x	x	x	x	x	x	x	x	x	x
$MgCl_2$	x		x		x		x		x		x	
$LiCl + MgCl_2$	x		x		x		x		x		x	
$LiClO_4$	x	x	x	x	x	x	x	x	x	x	x	x
$LiCl + LiClO_4$	x		x		x		x		x		x	
$AlCl_3 + LiClO_4$	x				x				x			
PF_5	x				x				x			x
KPF_6	x	x		x	x	x		x	x	x		x
BF_3	x			x	x			x	x			x
MgF_2	x				x				x			
$LiF + KPF_6$	x	x		x	x	x		x	x	x		x
$LiF + MgF_2$	x				x				x			

TABLE 2 (Cont'd)

CHART OF SYSTEMS SCREENED

BUTYROLACTONE (Cont'd)

Solutes \ Electrodes	Co	CoO	$CoCl_2$	CoF_3	Zn	Cd	Mo	Li	Mg	Ca
LiCl	x	x	x							
$AlCl_3$	x		x					x	x	x
LiCl + $AlCl_3$	x	x	x	x				x	x	x
$MgCl_2$	x	x	x							
LiCl + $MgCl_2$	x	x	x							
$LiClO_4$	x	x	x	x	x	x	x	x	x	x
LiCl + $LiClO_4$	x	x	x							
KPF_6	x	x		x	x	x	x	x	x	x
BF_3	x			x						
MgF_2					x	x	x			
LiF + KPF_6	x	x		x	x	x	x			

TABLE 3

CHART OF SYSTEMS SCREENED

DIMETHYLFORMAMIDE

Solutes \ Electrodes	Cu	CuO	$CuCl_2$	CuF_2	Ag	AgO	AgCl	AgF_2	Ni	NiO
LiCl	x	x	x		x	x	x		x	x
$AlCl_3$	x		x		x		x		x	x
$LiCl + AlCl_3$	x	x	x	x	x	x	x	x	x	x
$MgCl_2$	x		x		x		x		x	
$LiCl + MgCl_2$	x		x		x		x		x	
$LiClO_4$	x	x	x	x	x	x	x	x	x	x
$LiCl + LiClO_4$	x		x		x		x		x	
$AlCl_3 + LiClO_4$	x					x			x	
PF_5	x			x	x			x	x	
KPF_6	x	x		x	x	x		x	x	x
$LiPF_6$	x	x	x	x	x	x	x	x	x	x
BF_3	x			x	x			x	x	
$LiBF_4$	x			x	x			x	x	
$Mg(BF_4)_2$	x			x	x			x	x	
MgF_2	x				x				x	
$LiF + KPF_6$	x	x		x	x	x		x	x	x

TABLE 3 (Cont'd)

CHART OF SYSTEMS SCREENED

DIMETHYLFORMAMIDE (Cont'd)

Solutes \ Electrodes	$NiCl_2$	NiF_2	Co	CoO	$CoCl_2$	CoF_2	Zn	ZnF_2	Cd	CdF_2
LiCl	x		x	x	x		x		x	
$AlCl_3$			x	x	x					
$LiCl + AlCl_3$	x	x	x	x	x	x	x	x	x	x
$MgCl_2$	x		x	x	x	x	x	x	x	x
$LiCl + MgCl_2$	x		x		x					
$CaCl_2$							x	x	x	x
$LiClO_4$	x	x	x	x	x	x				
$LiCl + LiClO_4$	x		x	x	x		x		x	
$Mg(ClO_4)_2$						x		x	x	x
PF_5		x	x			x	x	x	x	x
KPF_6		x	x	x		x	x	x	x	x
$LiPF_6$	x	x	x	x	x	x	x	x	x	x
$Ca(PF_6)_2$							x	x	x	x
$Mg(PF_6)_2$							x	x	x	x
BF_3		x	x			x	x	x	x	x
$LiBF_4$	x		x			x	x	x	x	x
$Ca(BF_4)_2$							x	x	x	x
$Mg(BF_4)_2$		x	x			x	x	x	x	x
$LiF + KPF_6$		x	x	x		x				

TABLE 3 (Cont'd)

CHART OF SYSTEMS SCREENED

DIMETHYLFORMAMIDE (Cont'd)

Solutes \ Electrodes	Mo	In	InF_3	Fe	FeF_3	Cr	Mn	V	Li	Mg	Ca
LiCl	x	x	x	x	x	x	x	x	x	x	x
$LiCl + AlCl_3$	x	x	x	x	x	x	x	x			
$MgCl_2$	x	x	x	x						x	
$CaCl_2$	x	x	x	x	x			x			
$LiClO_4$	x	x		x	x	x	x	x	x	x	x
$LiCl + LiClO_4$									x	x	x
$Mg(ClO_4)_2$	x	x	x	x	x	x	x	x		x	
PF_5	x	x		x	x	x	x	x			
KPF_6	x	x	x	x	x	x	x	x	x	x	x
$LiPF_6$	x	x	x	x	x	x	x	x	x	x	x
$Ca(PF_6)_2$	x	x	x	x	x	x	x	x			
$Mg(PF_6)_2$	x	x	x	x				x			
BF_3	x	x	x	x	x	x	x	x			
$LiBF_4$	x	x	x	x	x	x	x	x	x	x	x
$Ca(BF_4)_2$	x	x	x	x	x	x	x	x			
$Mg(BF_4)_2$	x	x		x		x	x	x			

TABLE 4

CHART OF SYSTEMS SCREENED

PROPYLENE CARBONATE

Solutes \ Electrodes	Cu	CuO	$CuCl_2$	CuF_3	Ag	AgO	AgCl	AgF_2	Ni	NiO
$AlCl_3$	x		x		x		x		x	x
$LiCl + AlCl_3$	x	x	x	x	x	x	x	x	x	x
$MgCl_2$	x		x		x		x		x	x
$LiCl + MgCl_2$	x		x		x		x		x	
$LiClO_4$	x	x	x	x	x	x	x	x	x	x
PF_5	x			x	x			x	x	
KPF_6	x	x		x	x	x		x	x	x
$LiPF_6$	x	x	x	x	x	x	x	x	x	x
BF_3	x			x	x			x	x	
$LiBF_4$	x			x	x			x	x	
$Mg(BF_4)_2$	x			x	x			x	x	
$LiF + KPF_6$	x	x		x	x	x		x	x	x

TABLE 4 (Cont'd)

CHART OF SYSTEMS SCREENED

PROPYLENE CARBONATE (Cont'd)

Solutes \ Electrodes	$NiCl_2$	NiF_2	Co	CoO	$CoCl_2$	CoF_3	Zn	ZnF_2	Cd	CdF_2
$AlCl_3$	x		x	x	x					
$LiCl + AlCl_3$	x	x	x	x	x	x	x		x	
$MgCl_2$	x		x	x	x	x	x		x	
$LiCl + MgCl_2$	x		x		x					
$CaCl_2$							x	x	x	x
$LiClO_4$	x	x	x	x	x	x	x	x	x	x
$LiCl + LiClO_4$							x	x	x	x
$AlCl_3 + LiClO_4$							x	x	x	x
$Mg(ClO_4)_2$							x		x	
PF_5		x	x			x	x	x	x	x
KPF_6		x	x	x		x	x	x	x	x
$LiPF_6$	x	x	x	x	x	x	x	x	x	x
$Ca(PF_6)_2$							x	x	x	x
$Mg(PF_6)_2$							x	x	x	
BF_3		x	x			x				
$LiBF_4$		x	x			x	x	x	x	x
$Ca(BF_4)_2$							x	x	x	x
$Mg(BF_4)_2$		x	x			x	x	x	x	x
$LiF + KPF_6$		x	x	x		x				

TABLE 4 (Cont'd)

CHART OF SYSTEMS SCREENED

PROPYLENE CARBONATE (Cont'd)

Solutes \ Electrodes	Mo	In	InF_3	Fe	FeF_3	Cr	Mn	V	Li	Mg	Ca
$LiCl + AlCl_3$	x	x		x		x	x	x	x	x	x
$MgCl_2$	x	x		x					x	x	
$CaCl_2$	x	x	x	x	x			x			
$LiClO_4$	x	x	x	x	x	x	x	x	x	x	x
$LiCl + LiClO_4$	x	x	x	x	x			x			
$AlCl_3 + LiClO_4$	x	x	x	x	x			x			
$Mg(ClO_4)_2$	x	x		x					x		
PF_5	x	x	x	x	x	x	x	x			
KPF_6	x	x	x	x		x	x	x	x	x	x
$LiPF_6$	x	x		x	x			x	x	x	x
$Ca(PF_6)_2$	x	x	x	x	x	x	x	x			
$Mg(PF_6)_2$	x	x	x	x	x			x			
$LiBF_4$	x	x	x	x	x			x	x	x	x
$Ca(BF_4)_2$	x	x	x	x	x	x	x	x			
$Mg(BF_4)_2$	x	x		x		x	x	x			

TABLE 5. ELECTROLYTE CONDUCTIVITY

Solute		AN	BL	DMF	PC
LiCl	(0.5 m)	5.1×10^{-4}	7.6×10^{-4}	7.7×10^{-3}	-
LiCl	(0.75 m)	-	1.3×10^{-3}	8.7×10^{-3}	-
LiCl	(1.0 m)	-	-	9.7×10^{-3}	-
LiCl	(1.5 m)	-	-	9.4×10^{-3}	-
LiCl	(2.5 m)	-	-	6.6×10^{-3}	-
$AlCl_3$	(0.5 m)	-	1.1×10^{-2}	3.4×10^{-3}	8.0×10^{-3}
$AlCl_3$	(1.0 m)	4.2×10^{-2}	-	-	-
$LiCl + AlCl_3$	(0.25 m)	1.5×10^{-2}	-	-	-
$LiCl + AlCl_3$	(0.5 m)	-	1.1×10^{-2}	1.0×10^{-2}	7.1×10^{-3}
$MgCl_2$	(0.5 m)	6.3×10^{-4}	1.3×10^{-3}	7.7×10^{-3}	3.6×10^{-3}
$LiCl + MgCl_2$	(0.5 m)	-	-	1.0×10^{-2}	5.8×10^{-3}
$LiCl + MgCl_2$	(0.75 m)	-	6.3×10^{-3}	-	-
$CaCl_2$	(0.25 m)	-	-	5.3×10^{-3}	6.9×10^{-4}
$LiClO_4$	(0.5 m)	-	-	2.0×10^{-2}	-

TABLE 5. ELECTROLYTE CONDUCTIVITY (Cont'd)

Solute		AN	BL	DMF	PC
$LiClO_4$	(0.75 m)	3.0×10^{-2}	1.3×10^{-2}	3.4×10^{-2}	-
$LiClO_4$	(1.0 m)	-	-	2.6×10^{-2}	6.1×10^{-3}
$LiClO_4$	(1.5 m)	-	-	2.6×10^{-2}	-
$LiClO_4$	(2.5 m)	-	-	1.4×10^{-2}	-
$LiCl + LiClO_4$	(sat/0.5 m)	-	-	-	1.3×10^{-3}
$LiCl + LiClO_4$	(sat/0.75 m)	-	8.3×10^{-3}	1.8×10^{-2}	-
$AlCl_3 + LiClO_4$	(0.5 m)	-	1.7×10^{-2}	1.8×10^{-2}	5.6×10^{-3}
$Mg(ClO_4)_2$	(0.5 m)	-	-	-	5.5×10^{-3}
$Mg(ClO_4)_2$	(0.75 m)	-	-	2.0×10^{-2}	-
$Mg(ClO_4)_2$	(1.0 m)	3.3×10^{-2}	-	-	-
PF_5	(0.06 m)	-	8.1×10^{-4}	-	7.9×10^{-4}
PF_5	(0.5 m)	2.2×10^{-3}	-	2.2×10^{-3}	1.3×10^{-3}
KPF_6	(0.5 m)	1.5×10^{-2}	1.2×10^{-2}	-	-
KPF_6	(0.75 m)	3.3×10^{-2}	7.1×10^{-3}	2.1×10^{-2}	4.5×10^{-3}

TABLE 5. ELECTROLYTE CONDUCTIVITY (Cont'd)

Solute		AN	BL	DMF	PC
KPF_6	(1.0 m)	-	-	2.4×10^{-2}	5.3×10^{-3}
KPF_6	(1.5 m)	-	-	2.4×10^{-2}	-
KPF_6	(1.75 m)	-	-	1.3×10^{-2}	-
KPF_6	(2.0 m)	-	-	2.5×10^{-2}	-
KPF_6	(3.0 m)	-	-	5.8×10^{-3}	-
$LiPF_6$	(0.5 m)	1.7×10^{-2}	-	9.0×10^{-3}	5.8×10^{-3}
$LiPF_6 + KPF_6$	(0.5 m)	4.3×10^{-2}	-	-	-
$Ca(PF_6)_2$	(0.25 m)	-	-	5.8×10^{-3}	2.8×10^{-3}
$Mg(PF_6)_2$	(0.25 m)	-	-	2.8×10^{-3}	2.4×10^{-3}
BF_3	(0.5 m)	1.9×10^{-4}	5.6×10^{-4}	1.6×10^{-3}	1.3×10^{-4}
$LiBF_4$	(0.5 m)	1.6×10^{-2}	-	6.6×10^{-3}	3.4×10^{-3}
$Ca(BF_4)_2$	(0.5 m)	-	-	1.9×10^{-3}	8.2×10^{-4}
$Mg(BF_4)_2$	(0.25 m)	9.2×10^{-4}	-	2.6×10^{-3}	4.8×10^{-4}
MgF_2	(0.5 m)	-	2.0×10^{-6}	2.2×10^{-6}	-

TABLE 5. ELECTROLYTE CONDUCTIVITY (Cont'd)

Solute	AN	BL	DMF	PC
$LiF + MgF_2$ (0.5 m)	1.0×10^{-4}	4.6×10^{-5}	-	-
$LiF + KPF_6$ (0.5 m)	-	7.1×10^{-3}	-	-
$LiF + KPF_6$ (0.75 m)	3.6×10^{-2}	1.6×10^{-2}	1.7×10^{-2}	7.1×10^{-3}

and relatively high currents, or by exceedingly high currents alone. With few exceptions, overload due to combined low conductivity and high current occurred with BF_3 and PF_5 solutions and the magnesium and calcium complex fluorides. Where the current densities were within the capability of the amplifier (less than 4.8 ma/cm^2), current readings were indicated on the meter. Table 6 lists those systems causing instrument overload, and is restricted to systems in which the maximum discharge current was greater than 50 ma/cm^2. This represents about 50% of the systems registering overload. The remaining systems generally gave negligible discharge currents, the overload condition being due to the anodic (charge) current. Those indicating negligible discharge currents were predominantly nickel and cobalt systems, and a limited number of vanadium, chromium, and molybdenum metal electrodes. A number of systems screened did not register overload, even though they contained BF_3, PF_5, and the magnesium and calcium salts of the complex fluorides. In all such cases, both the anodic and cathodic currents were very low. Again, these consisted of nickel, cobalt, iron, vanadium, molybdenum, chromium, as well as indium.

Twenty-three systems registered excessively high charge and discharge current densities beyond the range of the amplifier meter (>4.8 amps/cm^2). Only five of these had low conductivities. To distinguish these from those systems whose currents were recordable, these are referred to as giving "current overload". Such systems are listed in Table 7. In some cases, obvious dissolution of the electrodes occurred accompanied by gassing, as for the silver or AgCl systems in $LiClO_4$. In other cases, however, a black reaction product formed at the working electrode, and appeared visibly insoluble. This occurred for the zinc and cadmium systems. $CuCl_2$ in propylene carbonate - LiCl + $AlCl_3$ formed a black reaction product which passed into suspension in the solution.

TABLE 6

VOLTAGE OVERLOAD SYSTEMS[#]

3200 ma/cm^2

AgF_2/DMF-$Mg(BF_4)_2$ *
InF_3/DMF-BF_3 *

2400 ma/cm^2

AgF_2/DMF-PF_5 *
Cu/PC-LiCl + $AlCl_3$
Cu/PC-$LiBF_4$

2000 ma/cm^2

AgCl/DMF-$AlCl_3$
AgF_2/DMF-$AlCl_3$
CdF_2/PC-$LiPF_6$ *

1600 ma/cm^2

AgF_2/DMF-BF_3 *
CuF_2/DMF-PF_5 *
Zn/DMF-$Ca(BF_4)_2$ *
Cd/DMF-$Ca(BF_4)_2$ *
CdF_2/DMF-PF_5 *
In/DMF-$Ca(BF_4)_2$ *
Mn/DMF-$Mg(BF_4)_2$ *

1400 ma/cm^2

InF_3/DMF-$Mg(PF_6)_2$ *

\# Listing only those systems having discharge current densities greater than 50 ma/cm^2.

* Electrolyte conductivity less than 5.0×10^{-3} ohm^{-1}cm^{-1}

NOTE: The following abbreviations for the solvents will be used throughout this report:

AN - Acetonitrile
BL - γ-Butyrolactone
DMF - Dimethylformamide
PC - Propylene carbonate

TABLE 6 (Cont'd)

VOLTAGE OVERLOAD SYSTEMS#

1200 ma/cm^2

CuF_2/AN-PF_5 *
Cd/DMF-$Mg(BF_4)_2$ *
Cd/DMF-$Mg(PF_6)_2$ *
Cd/PC-$LiBF_4$
Cd/PC-$Mg(BF_4)_2$ *
In/DMF-$Mg(BF_4)_2$ *
InF_3/PC-$Mg(BF_4)_2$ *
Mn/DMF-$Ca(BF_4)_2$ *
Mn/PC-$Ca(BF_4)_2$ *

920 ma/cm^2

AgO/PC-$LiPF_6$

800 ma/cm^2

Ag/DMF-$Mg(BF_4)_2$ *
AgO/DMF-$LiPF_6$
Zn/DMF-$Mg(BF_4)_2$ *
Zn/PC-$Mg(BF_4)_2$ *
Cd/DMF-$Ca(PF_6)_2$
Cd/PC-$Mg(BF_4)_2$ *
In/DMF-BF_3 *
In/DMF-$Ca(PF_6)_2$
In/PC-KPF_6
In/PC-$Ca(PF_6)_2$ *
Mn/DMF-PF_5 *
Mn/PC-PF_5 *
Li/PC-$LiPF_6$

700 ma/cm^2

AgO/DMF-$LiClO_4$

640 ma/cm^2

Cu/DMF-BF_3 *

Listing only those systems having discharge current densities greater than 50 ma/cm^2.

* Electrolyte conductivity less than 5.0×10^{-3} ohm^{-1}cm^{-1}

TABLE 6 (Cont'd)

VOLTAGE OVERLOAD SYSTEMS[#]

600 ma/cm^2

CuF_2/AN-$Mg(BF_4)_2$ *
Zn/DMF-PF_5 *
Zn/DMF-$Mg(PF_6)_2$ *

500 ma/cm^2

ZnF_2/DMF-PF_5 *
In/PC-$Mg(PF_6)_2$ *
InF_3/PC-KPF_6

450 ma/cm^2

Zn/DMF-BF_3 *
Cd/DMF-BF_3 *

400 ma/cm^2

Ag/AN-$Mg(BF_4)_2$ *
Ag/PC-$LiBF_4$ *
AgF_2/BL-BF_3 *
AgF_2/PC-PF_5 *
AgF_2/DMF-$LiBF_4$
CuF_2/PC-PF_5 *
In/DMF-$Mg(PF_6)_2$ *
In/PC-$Ca(BF_4)_2$ *
Mn/DMF-BF_3 *
Mn/DMF-$Ca(PF_6)_2$

300 ma/cm^2

Cd/PC-$Ca(PF_6)_2$ *
InF_3/DMF-$LiBF_4$
InF_3/PC-LiCl + $LiClO_4$

Listing only those systems having discharge current densities greater than 50 ma/cm^2.

* Electrolyte conductivity less than 5.0×10^{-3} $ohm^{-1} cm^{-1}$

TABLE 6 (Cont'd)

VOLTAGE OVERLOAD SYSTEMS#

200 ma/cm^2	150 ma/cm^2
$Ag/BL\text{-}BF_3$ *	$InF_3/DMF\text{-}LiPF_6$
$Ag/DMF\text{-}BF_3$ *	$CdF_2/PC\text{-}Mg(BF_4)_2$ *
$Ag/PC\text{-}Mg(BF_4)_2$ *	
$AgCl/BL\text{-}MgCl_2$ *	100 ma/cm^2
$AgF_2/AN\text{-}BF_3$ *	$Cu/PC\text{-}Mg(BF_4)_2$ *
$AgF_2/PC\text{-}BF_3$ *	$Co/AN\text{-}BF_3$ *
$AgF_2/PC\text{-}Mg(BF_4)_2$ *	$Zn/DMF\text{-}CaCl_2$
$CuF_2/AN\text{-}BF_3$ *	$Mo/DMF\text{-}Ca(PF_6)_2$
$Co/DMF\text{-}Mg(BF_4)_2$ *	
$Cd/PC\text{-}Ca(BF_4)_2$ *	
$Fe/DMF\text{-}BF_3$ *	
$V/PC\text{-}PF_5$ *	

Listing only those systems having discharge current densities greater than 50 ma/cm^2.

* Electrolyte conductivity less than 5.0×10^{-3} ohm^{-1}cm^{-1}

TABLE 7

CURRENT OVERLOAD SYSTEMS[#]

$Ag/DMF\text{-}LiCl + LiClO_4$	$AgCl/PC\text{-}LiClO_4$ *
$AgO/BL\text{-}KPF_6$	$CuCl_2/AN\text{-}LiCl$ *
$AgO/BL\text{-}LiF + KPF_6$	$CuCl_2/PC\text{-}LiCl + AlCl_3$
$AgO/PC\text{-}LiCl + AlCl_3$	$Zn/AN\text{-}LiCl + AlCl_3$
$AgO/PC\text{-}LiClO_4$ *	$Zn/AN\text{-}LiF + KPF_6$
$AgCl/AN\text{-}LiClO_4$	$Zn/DMF\text{-}LiCl$
$AgCl/BL\text{-}LiCl$ *	$Zn/DMF\text{-}LiCl + AlCl_3$
$AgCl/BL\text{-}LiClO_4$	$Cd/AN\text{-}LiClO_4$
$AgCl/BL\text{-}LiCl + LiClO_4$	$Cd/BL\text{-}LiClO_4$
$AgCl/DMF\text{-}LiClO_4$	$Cd/DMF\text{-}LiPF_6$
$AgCl/DMF\text{-}LiPF_6$	$Cd/PC\text{-}LiClO_4$ *

Having discharge current densities in excess of 4.8 amps/cm^2.

* Electrolyte conductivity less than 5×10^{-3} $ohm^{-1}\text{-}cm^{-1}$.

These observations indicate that even though cyclic voltammograms were not obtainable, these systems should be investigated further because of the high currents they can support. Their interest may well lie in the reserve type battery if it is suspected that such high currents would be accompanied by high chemical activity.

F. Cyclic Voltammetry of Positive Electrode - Electrolyte Systems

Table 8 shows the breakdown of the total number of positive - electrolyte systems screened according to the metal species contained within the electrode, whether it be the base metal, oxide, or halide. Listed also are the percent distributions of the following cyclic voltammetric parameters:

Percent of systems having discharge peak current densities greater than 50 ma/cm^2.

Percent of systems having discharge peak current densities less than 50 ma/cm^2.

Percent of systems exhibiting no discharge peaks.

Percent of systems causing istrument overload.

Figure 4 displays the same data in bar graph form to permit immediate visual comparison of the systems relative to these parameters. In no case was there a majority of systems in any group species having discharge peak current densities in excess of 50 ma/cm^2. Systems having the greater number of discharge peaks in excess of this value were copper, silver, zinc, and indium, with manganese and cadmium having a lower number of systems. Again, copper, silver, zinc, indium, and cadmium systems gave the highest percentage of discharge peaks less than 50 ma/cm^2, with the zinc and cadmium groups being the more predominant.

TABLE 8

PERCENT DISTRIBUTION OF CYCLIC VOLTAMMETRIC PARAMETERS FOR TOTAL SYSTEMS SCREENED

Electrode	Qty.	Discharge Peak >50 ma/cm^2 %	Discharge Peak <50 ma/cm^2 %	None %	Overload %
Ag	134	22	39	5	34
Cu	135	30	40	9	21
Ni	135	0	10	79	11
Co	139	1	14	68	17
Zn	64	28	35	9	28
Cd	63	11	40	14	35
Mo	37	0	14	51	35
In	52	22	29	9	40
Fe	52	6	14	73	7
Cr	19	0	0	42	58
Mn	19	16	16	26	42
V	27	0	11	67	22

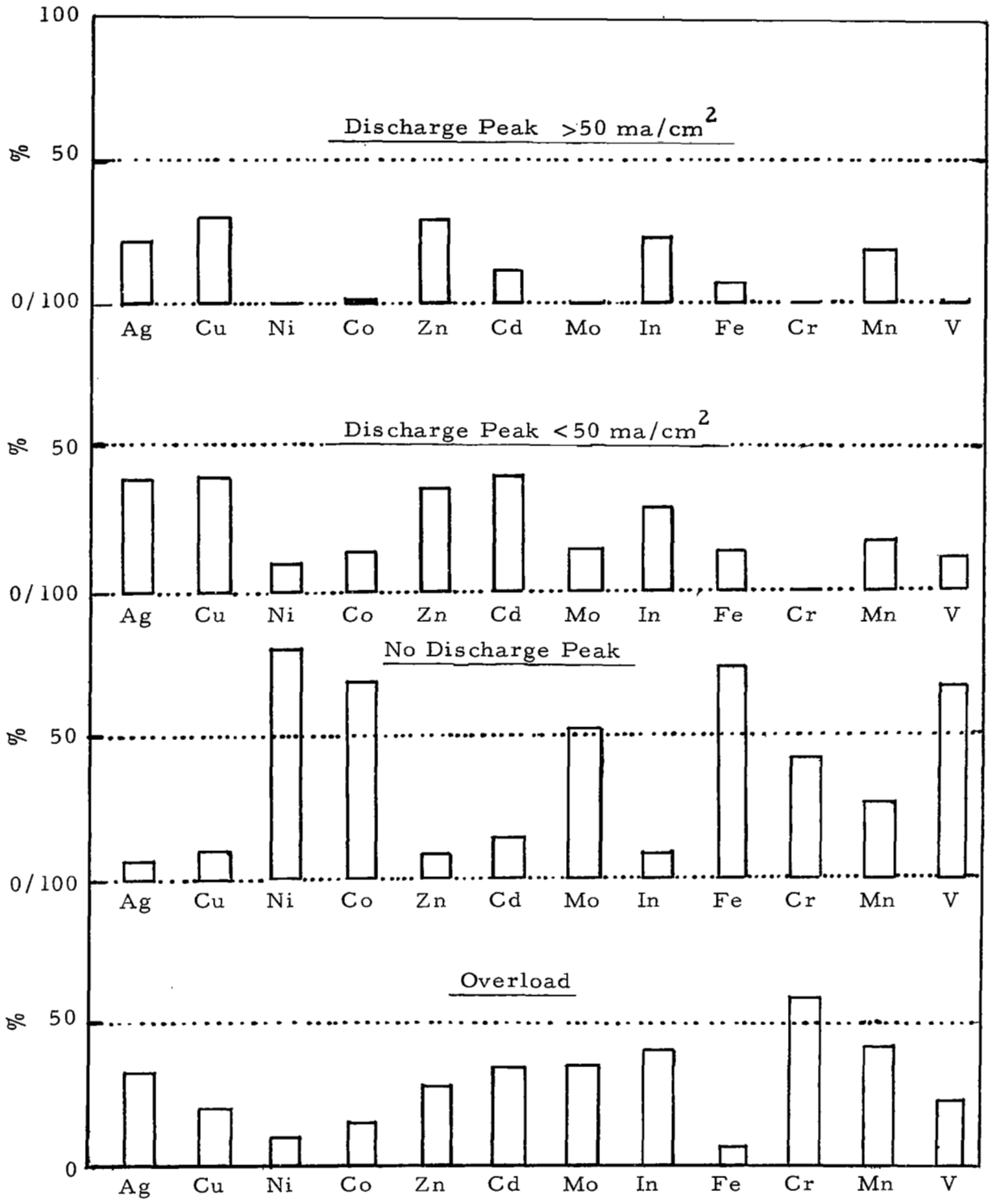

Figure 4. Percent distribution of cyclic voltammetric parameters for total systems screened.

None of the nickel, molybdenum, nor chromium systems gave discharge peak current densities greater than 50 ma/cm^2, whereas only 1 and 5% of the cobalt and iron systems registered peak current densities in this range. A large majority of the nickel, cobalt, and iron systems exhibited no discharge peaks at all, and in most cases negligible reduction current. On the other hand, only a small percent of the copper, silver, zinc, and cadmium systems failed to show a discharge peak. The fact that only a limited number of nickel, cobalt, and iron systems caused instrument overload is due to the very low or negligible currents for these systems.

Table 9 lists those systems having discharge peak current densities in excess of 50 ma/cm^2, and peak separations less than 0.5 v. All seven cadmium systems meeting this minimum current density have peak separations less than 0.5 v. 89% of the zinc systems and 78% of the copper systems, having a discharge peak in excess of 50 ma/cm^2, have peak separations less than 0.5 v. Included in the group also are indium (54%), silver (43%) and iron (33%).

1. Cyclic Voltammetry of Silver Systems

A total of 134 silver systems were screened, including silver metal, silver oxide, silver chloride, and silver fluoride. Of these, 60% had both charge and discharge peaks, while 35% overloaded the instrumentation preventing voltammetric recording. The percent distribution of the voltammetric data for the separate groups of silver species systems is shown in Table 10.

The peak current densities and peak separation, as well as visual observations of changes in electrode or electrolyte appearance, are shown in Table 11. Only those systems having discharge peaks in excess of 50 ma/cm^2 are listed.

TABLE 9

PERCENT DISTRIBUTION OF SYSTEMS
HAVING PEAK SEPARATIONS LESS THAN 0.5 VOLT *

Electrode	Qty.	ΔV less than 0.5 v %
Ag	30	43
Cu	41	78
Ni	nil	0
Co	1	0
Zn	18	89
Cd	7	100
Mo	nil	0
In	6	54
Fe	3	33
Cr	nil	0
Mn	3	0
V	nil	0

* Having discharge peaks greater than 50 ma/cm^2.

TABLE 10

PERCENT DISTRIBUTION OF CYCLIC VOLTAMMETRIC PARAMETERS FOR SILVER SYSTEMS

134 Systems

Electrode	Qty.	Discharge Peak >50 ma/cm^2 %	Discharge Peak <50 ma/cm^2 %	None %	Overload %
Ag	54	21	46	0	33
AgO	22	27	32	5	36
AgCl	26	46	12	4	38
AgF_2	32	3	53	10	34

a. Silver metal

Of the 54 silver metal electrodes screened, 67% exhibited both charge and discharge peaks, the remainder being overload systems. Eleven silver systems (21%) had discharge peaks in excess of 50 ma/cm^2. Of this group, five (or 45%) had peak separations less than 0.5 volt. One system (Ag/PC-$LiPF_6$) showed a decreasing coulombic ratio with decreasing sweep rate. A number of the systems were observed to form reaction products at the electrode, with suspended material in the electrolyte. Table 12 lists specific discharge capacities and coulombic ratios for some silver electrode systems.

Although not a listed system (those having discharge peaks less than 50 ma/cm^2), of particular interest is the system Ag/PC-KPF_6, in which the cyclic voltammogram is a marked function of cycling as shown in Figure 5.

TABLE 11

PEAK CURRENT DENSITIES AND PEAK SEPARATION

SILVER SYSTEMS

Systems	Peak c.d. Disch.	Peak c.d. Chge.	ΔV	Visual
	ma/cm^2		mv	
Ag metal				
Ag/DMF-LiCl	1120	960	300	SY
Ag/DMF-$MgCl_2$	560	145	160	S
Ag/AN-LiCl + $AlCl_3$	400	1300	520	FB
Ag/BL-$AlCl_3$	270	210	870	N
Ag/DMF-LiCl + $MgCl_2$	220	170	250	N
Ag/BL-$AlCl_3$ + $LiClO_4$	220	240	850	N
Ag/AN-KPF_6	150	490	490	S
Ag/BL-LiCl + $LiClO_4$	150	160	550	N
Ag/PC-$LiPF_6$	140	600	70	C
Ag/AN-LiF + KPF_6	100	65	700	S
Ag/BL-$MgCl_2$	70	65	700	N
AgO				
AgO/BL-LiCl + $AlCl_3$	1024	576	230	N
AgO/DMF-LiCl	360	200	440	N
AgO/PC-KPF_6	170	170	980	N
AgO/BL-$LiClO_4$	150	490	980	N
AgO/AN-KPF_6	130	320	1000	S
AgO/DMF-LiCl + $AlCl_3$	110	40	20	N
AgO/BL-LiCl	90	60	1100	N

B solution turns blue
C coulombic ratio decreases with decreasing sweep rate
F dark reaction product forms at working electrode and drops off
N no noticeable change
S reaction product from working electrode forms suspension
Y solution turns yellow

TABLE 11 (Cont'd)

PEAK CURRENT DENSITIES AND PEAK SEPARATION

SILVER SYSTEMS

Systems	Peak c.d. Disch.	Peak c.d. Chge.	ΔV	Visual
	ma/cm^2		mv	
AgCl				
AgCl/DMF-LiCl	1500	1500	90	K
AgCl/BL-$AlCl_3$	960	480	550	N
AgCl/AN-LiCl + $AlCl_3$	800	700	490	S
AgCl/PC-$AlCl_3$	800	600	850	N
AgCl/AN-$LiPF_6$	210	1120	630	SE
AgCl/DMF-LiCl + $AlCl_3$	190	330	150	N
AgCl/DMF-$MgCl_2$	170	290	710	W
AgCl/BL-LiCl + $AlCl_3$	170	100	870	B
AgCl/DMF-LiCl + $MgCl_2$	160	40	300	W
AgCl/DMF-LiCl + $LiClO_4$	110	60	300	W
AgCl/PC-$LiPF_6$	90	100	620	N
AgCl/BL-LiCl + $MgCl_2$	60	40	700	W
AgF_2				
AgF_2/PC-$LiBF_4$*	160	190	200	W

* Charge and discharge peaks grow with continued cycling.

B solution turns blue
E erratic peak reproducibility
K solution turns dark color
N no noticeable change
S reaction product from working electrode forms suspension
W dark reaction product remains at working electrode

TABLE 12

SPECIFIC DISCHARGE CAPACITY AND COULOMBIC RATIO OF SOME SILVER SYSTEMS *

System	Specific Discharge Capacity coul/cm^2	Coulombic Ratio
Ag		
Ag/BL-$MgCl_2$	0.7	1.0
Ag/BL-$AlCl_3$	2.2	1.0
Ag/BL-$AlCl_3$ + $LiClO_4$	1.5	0.8
Ag/DMF-LiCl	3.7	0.5
AgCl		
AgCl/BL-$AlCl_3$	3.9	3.5
AgCl/AN-LiCl + $AlCl_3$	3.1	1.2
AgCl/BL-LiCl + $AlCl_3$	2.6	1.0
AgCl/BL-LiCl + $MgCl_2$	0.7	1.0
AgCl/PC-$LiPF_6$	1.1	1.0
AgCl/DMF-LiCl + $MgCl_2$	0.6	0.8
AgCl/DMF-LiCl + $AlCl_3$	1.2	0.6

* In order of decreasing coulombic ratio.

This set of curves was obtained by raising the X-Y recorder pen for a few minutes each time, but allowing the system to cycle continuously at 200 mv/sec. Successive curves were recorded over a 30-minute period proceeding in the order 1-6 as labelled. Of interest is the absence of a lower oxidation peak and corresponding reduction peak during the early cycles, but with continued cycling, these peaks begin to occur and gain in magnitude, indicating the formation of a double oxidation species of silver. In confirmation, shown as an inset in Figure 5 is a reproduction of a cyclic voltammogram recorded at 800 mv/sec, nineteen months previously during an independent investigation by Whittaker Corporation.

b. Silver oxide

Of the 22 silver oxide systems, 59% had both charge and discharge peaks. 27% of the systems had discharge peaks in excess of 50 ma/cm^2, and only three had peak separations less than 0.5 v. Only in the case of AgO/AN-KPF_6 was there any noticeable change, with the formation of a dark reaction product at the electrode, and the presence of suspended material in the solution. The coulombic ratio and specific discharge capacity for the one system calculated, AgO/BL-LiCl, was 0.8 and 0.7 $coul/cm^2$ respectively.

c. Silver chloride

58% of the 26 AgCl systems exhibited both anodic and cathodic peaks, with 46% having discharge current densities greater than 50 ma/cm^2. This is compared with 21% and 27% for Ag and AgO respectively. Specific discharge capacities and coulombic ratios are listed in Table 12. Of particular interest is the high coulombic ratio of AgCl/BL-$AlCl_3$. Since coulombic ratio is a measure of charge-discharge efficiency, the maximum value should be unity. A value of 3.5, as in this case, must be due to discharge of the preformed AgCl in addition to any material formed during the sweep charge.

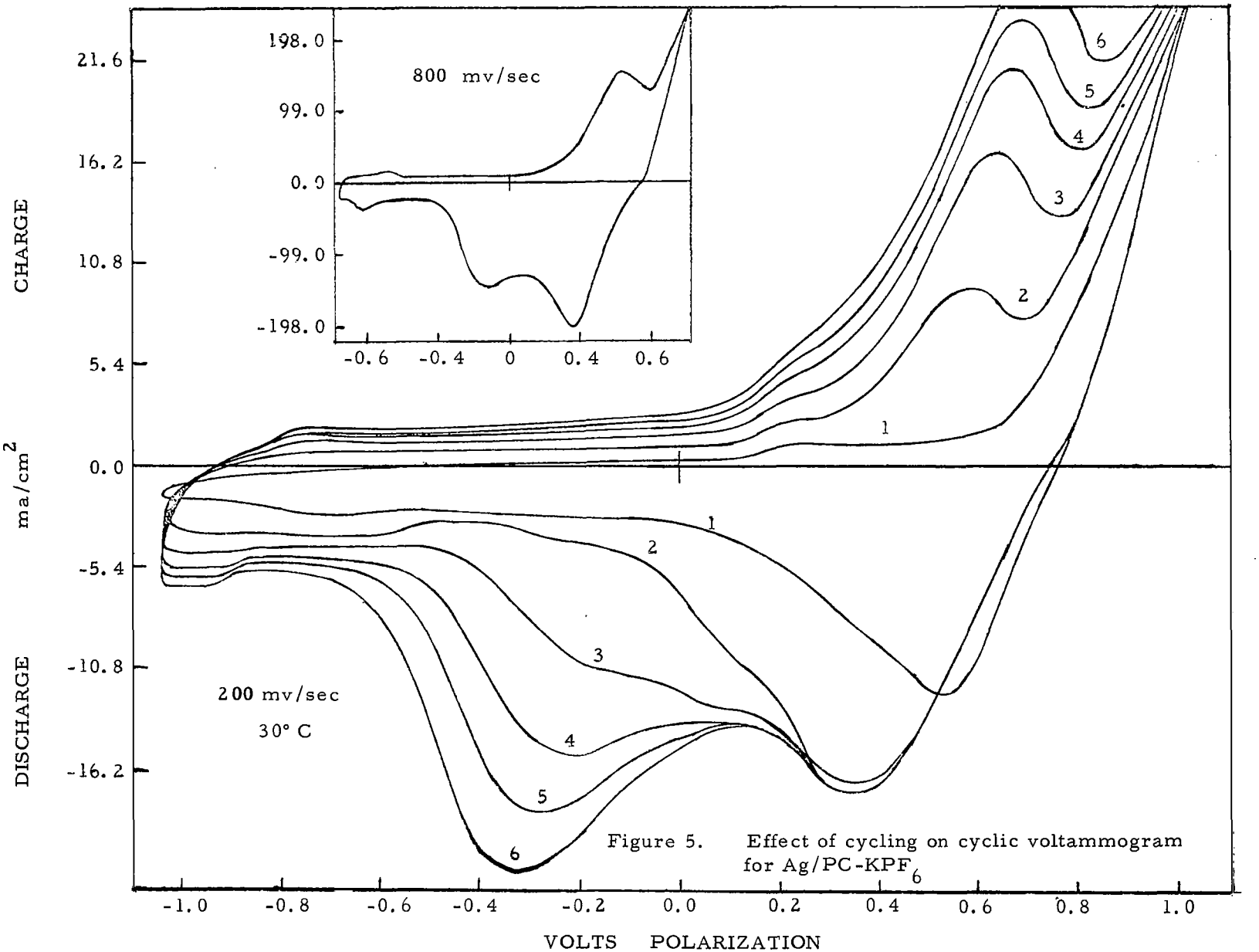

Figure 5. Effect of cycling on cyclic voltammogram for Ag/PC-KPF_6

d. Silver difluoride

Thirty-two AgF_2 systems were screened, and only one, AgF_2/PC-$LiBF_4$, had a discharge peak greater than 50 ma/cm^2. 53% of the systems had discharge current densities in the medium low and low ranges, and 34% overloaded the amplifier.

2. Cyclic Voltammetry of Copper Systems

A total of 135 copper systems were screened. Of these, 70% had both charge and discharge peaks, and 21% resulted in instrument overload. The percent distribution of the voltammetric data of the separate copper species is shown in Table 13.

TABLE 13

PERCENT DISTRIBUTION OF CYCLIC VOLTAMMETRIC PARAMETERS FOR COPPER SYSTEMS

135 Systems

		Discharge Peak			
Electrode	Qty.	>50 ma/cm^2 %	<50 ma/cm^2 %	None %	Overload %
Cu	56	16	50	9	25
CuO	21	34	52	14	0
$CuCl_2$	26	54	23	8	15
CuF_2	32	35	28	6	31

Table 14 lists the peak current densities, peak separations, and visual observations, for those systems having discharge peaks in excess of 50 ma/cm^2.

a. Copper metal

Fifty-six copper electrode systems were screened, of which 66% showed both charge and discharge peaks. Only nine systems (16%) had discharge peaks greater than 50 ma/cm^2. Of these, eight (89%) had peak separations less than 0.5 v, compared with only 45% for the silver electrode. Unlike the silver systems, copper systems showed a yellow discoloration of many of the cell solutions. Typical for a number of the copper systems is the cyclic voltammogram shown in Figure 6. Integration of the entire anodic region for this type of curve would give too low a coulombic ratio for the main reaction, e.g. 0.3. Confining the integration to the main reaction results in a value of 1.0.

In a program of this nature, where nearly a thousand systems are screened at three different sweep rates for each system, one is very hesitant to make any interpretation such as above, since there is simply insufficient data to support any hypothesis. For this reason, it may not be proper to exclude the portion of the anodic sweep positive to +0.2 v. Possible the lower value for the coulombic ratio (0.3) may be more significant, in that it may indicate dissolution of anodic material. Coulombic ratios of some copper systems are listed in Table 15. In most cases, the entire anodic portion of the curve was included in the area measurement.

TABLE 14

PEAK CURRENT DENSITIES AND PEAK SEPARATION

COPPER SYSTEMS

Systems	Peak c.d. Disch.	Chge.	ΔV	Visual
	ma/cm^2		mv	
Cu metal				
Cu/DMF-$LiPF_6$	1600	780	140	FYP
Cu/DMF-$AlCl_3$ + $LiClO_4$	940	300	130	SY
Cu/AN-$LiPF_6$ + KPF_6	420	350	60	W
Cu/AN-$LiPF_6$	270	350	90	W
Cu/AN-$LiBF_4$	160	710	100	F
Cu/DMF-LiCl + $LiClO_4$	140	230	250	WY
Cu/DMF-LiCl	140	170	340	WY
Cu/DMF-$LiClO_4$	100	290	460	SY
Cu/PC-$LiClO_4$	80	7(	1300	N
CuO				
CuO/DMF-LiCl + $AlCl_3$	530	170	170	WY
CuO/PC-$LiClO_4$	220	50	390	N
CuO/BL-$LiClO_4$	130	250	1270	W
CuO/AN-KPF_6	120	300	540	Y
CuO/BL-KPF_6	90	200	1280	N
CuO/DMF-LiCl	80	230	300	C
CuO/AN-LiF + KPF_6	80	230	700	Y

C coulombic ratio decreases with decreasing sweep rate
F dark reaction product forms at working electrode and drops off
N no noticeable change
P plating at counterelectrode
S reaction product from working electrode forms suspension
W dark reaction product remains at working electrode
Y solution turns yellow

TABLE 14 (Cont'd)

PEAK CURRENT DENSITIES AND PEAK SEPARATION

COPPER SYSTEMS

Systems	Peak c.d. Disch.	Chge.	ΔV	Visual
	ma/cm^2		mv	
$CuCl_2$				
$CuCl_2$/BL-$AlCl_3$	1600	910	300	N
$CuCl_2$/PC-$AlCl_3$	1120	290	550	W
$CuCl_2$/BL-$LiClO_4$	1020	860	190	WG
$CuCl_2$/PC-$LiClO_4$	1010	420	170	W
$CuCl_2$/DMF-$AlCl_3$	910	400	110	FY
$CuCl_2$/DMF-LiCl + $MgCl_2$	900	190	100	WY
$CuCl_2$/DMF-$LiPF_6$	700	570	40	W
$CuCl_2$/AN-LiCl + $AlCl_3$	400	600	60	WDB
$CuCl_2$/BL-LiCl + $LiClO_4$	350	210	1150	WY
$CuCl_2$/DMF-LiCl + $AlCl_3$	290	490	80	FE
$CuCl_2$/AN-$LiPF_6$	160	350	110	D
$CuCl_2$/DMF-LiCl + $LiClO_4$	140	130	230	SY
$CuCl_2$/BL-LiCl + $AlCl_3$	90	490	130	F
$CuCl_2$/BL-$MgCl_2$	80	80	10	W

B solution turns blue
D electrode dissolution
E erratic peak reproducibility
F dark reaction product forms at working electrode and drops off
G solution turns green
N no noticeable change
S reaction product from working electrode forms suspension
W dark reaction product remains at working electrode
Y solution turns yellow

TABLE 14 (Cont'd)

PEAK CURRENT DENSITIES AND PEAK SEPARATION

COPPER SYSTEMS

Systems	Peak c.d. Disch.	Peak c.d. Chge.	ΔV	Visual
	ma/cm^2		mv	
CuF_2				
CuF_2/DMF-$LiPF_6$	1800	1080	10	W
CuF_2/PC-LiCl + $AlCl_3$	1600	120	160	W
CuF_2/BL-$LiClO_4$	880	250	250	WY
CuF_2/DMF-LiCl + $AlCl_3$	300	410	100	YCE
CuF_2/PC-$LiPF_6$	180	100	170	W
CuF_2/BL-LiCl + $AlCl_3$	150	700	880	C
CuF_2/AN-$LiBF_4$	110	390	170	W
CuF_2/PC-$LiClO_4$	110	80	330	W
CuF_2/AN-KPF_6	80	340	40	WY
CuF_2/AN-$LiClO_4$	70	90	1100	W
CuF_2/AN-LiF + KPF_6	60	240	230	WY

C coulombic ratio decreases with decreasing sweep rate
E erratic peak reproducibility
W dark reaction product remains at working electrode
Y solution turns yellow

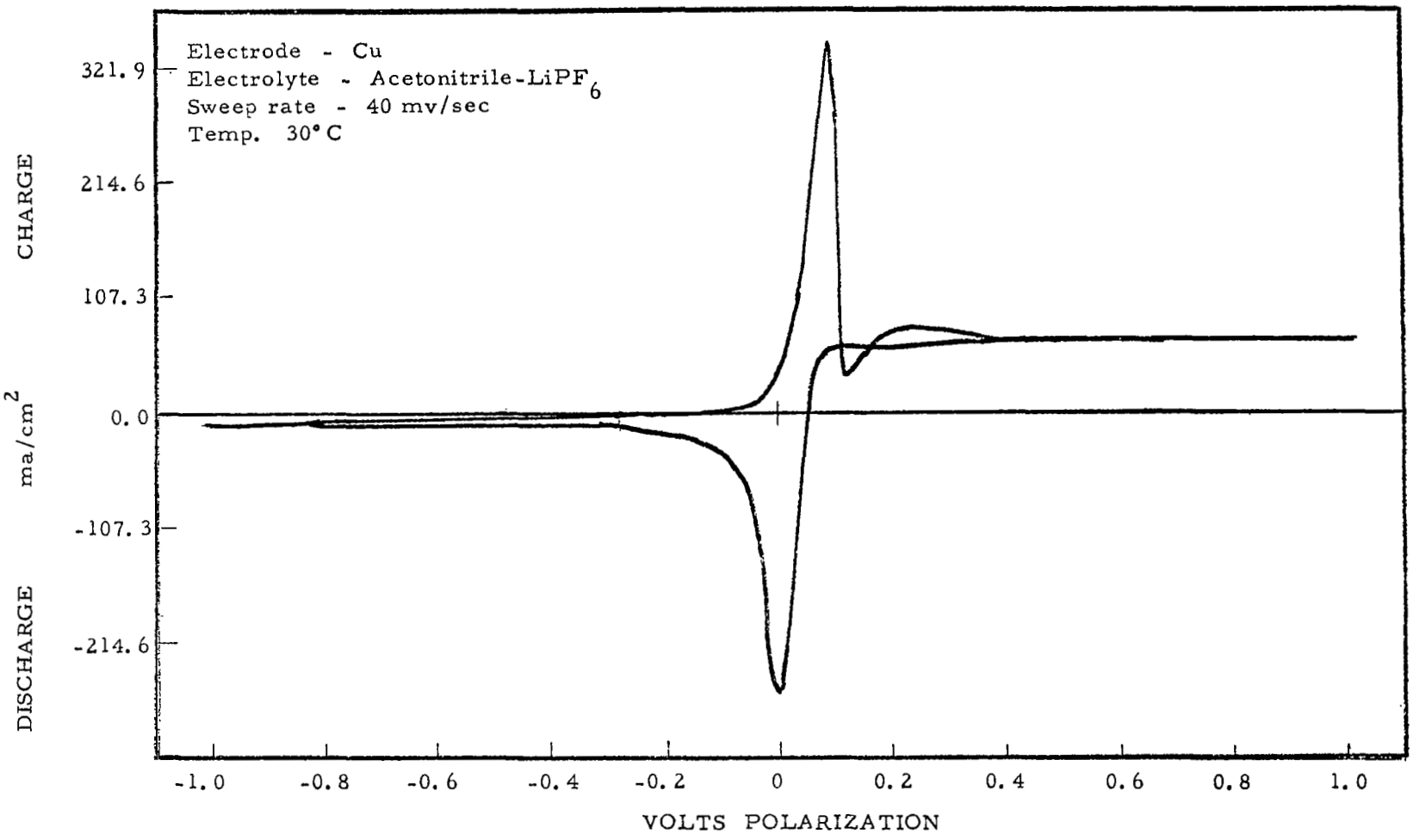

Figure 6. Typical cyclic voltammogram showing non-reducible secondary anodic product.

TABLE 15

SPECIFIC DISCHARGE CAPACITY AND COULOMBIC RATIO OF SOME COPPER SYSTEMS*

System	Specific Discharge Capacity coul/cm^2	Coulombic Ratio
Cu		
Cu/AN-KPF_6 + $LiPF_6$	6.0	1.0
Cu/DMF-$AlCl_3$ + $LiClO_4$	4.2	0.8
Cu/AN-$LiBF_4$	0.2	0.2
CuO		
CuO/BL-$LiClO_4$	1.9	0.5
CuO/AN-LiF + KPF_6	1.1	0.5
CuO/BL-KPF_6	1.2	0.3
CuO/AN-KPF_6	1.0	0.2
$CuCl_2$		
$CuCl_2$/PC-$AlCl_3$	4.3	1.6
$CuCl_2$/BL-$AlCl_3$	4.8	1.0
$CuCl_2$/PC-$LiClO_4$	2.9	1.0
$CuCl_2$/BL-$MgCl_2$	0.2	1.0
$CuCl_2$/BL-$LiClO_4$	0.2	0.7
$CuCl_2$/AN-$LiPF_6$	0.4	0.5
$CuCl_2$/DMF-LiCl + $LiClO_4$	0.7	0.2
$CuCl_2$/DMF-$LiPF_6$	0.1	0.1

* In order of decreasing coulombic ratio.

TABLE 15 (Cont'd)

SPECIFIC DISCHARGE CAPACITY AND COULOMBIC RATIO OF SOME COPPER SYSTEMS *

System	Specific Discharge Capacity coul/cm^2	Coulombic Ratio
CuF_2		
CuF_2/BL-$LiClO_4$	2.3	0.7
CuF_2/PC-$LiClO_4$	0.5	0.6
CuF_2/PC-$LiPF_6$	1.0	0.5
CuF_2/AN-KPF_6	0.2	0.5
CuF_2/DMF-$LiPF_6$	3.3	0.4
CuF_2/AN-$LiBF_4$	0.3	0.1

* In order of decreasing coulombic ratio.

b. Copper oxide

Twenty-one copper oxide systems were screened, of which 86% showed both charge and discharge peaks. No "overload" systems were obtained. Seven of the systems (34%) had discharge peaks greater than 50 ma/cm^2. Of these, three (43%) had peak separations less than 0.5 v. A number of the CuO systems, similar to copper metal, showed a secondary low charge peak. Coulombic ratios of some CuO systems are listed in Table 15.

c. Copper chloride

Twenty-six copper chloride systems were screened, of which 77% showed both charge and discharge peaks. Fourteen systems had discharge peaks in excess of 50 ma/cm^2 (54%). Of these, twelve (86%) had peak separations less than 0.5 v., matching that of copper metal and copper oxide. In general, the $CuCl_2$ systems exhibited considerably higher discharge peaks than the Cu and CuO systems. Coulombic ratios of some $CuCl_2$ systems are listed in Table 15.

d. Copper fluoride

Thirty-two copper fluoride systems were screened, of which 63% exhibited both charge and discharge peaks. Eleven systems (54%) had discharge peaks in excess of 50 ma/cm^2, and of these, nine (82%) had peak separations less than 0.5 v. Coulombic ratios of some CuF_2 systems are listed in Table 15.

3. Cyclic Voltammetry of Nickel Systems

A total of 135 nickel systems were screened. Most of these either showed negligible charge current, or a gradually increasing current (as the voltage was scanned towards +1.0 v.) without reaching a peak. This latter behavior is typical of continuous anodic dissolution of electrode material. In either case, no discharge current was evident, so that 79% of these failed

to show a discharge peak. Table 16 presents the percent distribution of the voltammetric data of the separate nickel systems.

TABLE 16

PERCENT DISTRIBUTION OF CYCLIC VOLTAMMETRIC PARAMETERS FOR NICKEL SYSTEMS

135 Systems

Electrode	Qty.	Discharge Peak >50 ma/cm^2 %	Discharge Peak <50 ma/cm^2 %	None %	Overload %
Ni	54	0	7	82	11
NiO	24	0	17	79	4
$NiCl_2$	26	0	8	73	19
NiF_2	31	0	9	81	10

4. Cyclic Voltammetry of Cobalt Systems

A total of 139 cobalt systems were screened, of which 68% exhibited no discharge peaks. In general, cobalt systems behaved similarly to nickel systems. Table 17 shows the percent distribution of the voltammetric parameters.

TABLE 17

PERCENT DISTRIBUTION OF CYCLIC VOLTAMMETRIC PARAMETERS FOR COBALT SYSTEMS

139 Systems

Electrode	Qty.	Discharge Peak >50 ma/cm^2 %	Discharge Peak <50 ma/cm^2 %	None %	Overload %
Co	47	0	15	53	32
CoO	30	0	20	67	13
$CoCl_2$	26	4	27	50	19
CoF_3	36	0	0	100	0

5. Cyclic Voltammetry of Zinc Systems

A total of 64 zinc systems were screened, comprising zinc metal and zinc fluoride electrodes. 63% indicated both charge and discharge peaks, with 28% of the systems having discharge peaks in excess of 50 ma/cm^2. Nearly 90% of the latter systems had peak separation less than 0.5 v. The percent distribution of voltammetric data for the separate zinc groups is shown in Table 18

Coulombic ratios of some zinc systems are listed in Table 19. Table 20 lists the peak current densities, peak separations, and visual observations for those systems having discharge peaks in excess of 50 ma/cm^2.

a. Zinc metal

Of the 39 zinc metal systems screened, 51% showed both charge and discharge peaks, 41% overloaded the amplifier, and 8% had no discharge peaks.

TABLE 18

PERCENT DISTRIBUTION OF CYCLIC VOLTAMMETRIC PARAMETERS FOR ZINC SYSTEMS

64 Systems

Electrode	Qty.	Discharge Peak >50 ma/cm^2 %	Discharge Peak <50 ma/cm^2 %	None %	Overload %
Zn	39	39	12	8	41
ZnF_2	25	12	72	8	8

TABLE 19

SPECIFIC DISCHARGE CAPACITY AND COULOMBIC RATIO OF SOME ZINC SYSTEMS *

System	Specific Discharge Capacity coul/cm^2	Coulumbic Ratio
Zn		
$Zn/AN\text{-}LiClO_4$	5.6	1.1
$Zn/BL\text{-}KPF_6$	0.5	1.0
$Zn/PC\text{-}KPF_6$	0.4	0.7
$Zn/DMF\text{-}LiPF_6$	2.4	0.5
$Zn/DMF\text{-}LiClO_4$	1.0	0.4
$Zn/DMF\text{-}Mg(ClO_4)_2$	1.0	0.4
$Zn/DMF\text{-}KPF_6$	1.7	0.3
ZnF_2		
$ZnF_2/DMF\text{-}KPF_6$	1.1	0.3
$ZnF_2/DMF\text{-}LiClO_4$	0.8	0.2

* In order of decreasing coulombic ratio.

TABLE 20

PEAK CURRENT DENSITIES AND PEAK SEPARATION

ZINC SYSTEMS

Systems	Peak c.d. Disch. (ma/cm^2)	Peak c.d. Chge. (ma/cm^2)	ΔV (mv)	Visual
Zn metal				
$Zn/DMF-LiClO_4$	470	470	80	F
$Zn/DMF-KPF_6$	400	610	80	F
$Zn/DMF-Mg(ClO_4)_2$	400	30	210	F
$Zn/AN-LiClO_4$	390	580	160	S
$Zn/DMF-LiPF_6$	370	370	50	WY
$Zn/AN-LiCl + AlCl_3$	270	1100	120	FC
$Zn/DMF-Ca(PF_6)_2$	220	240	300	FY
$Zn/DMF-LiCl + LiClO_4$	130	130	100	W
$Zn/DMF-LiBF_4$	100	220	410	WY
$Zn/PC-Ca(PF_6)_2$	100	16	380	N
$Zn/BL-KPF_6$	90	96	110	N
$Zn/PC-KPF_6$	60	55	340	N
$Zn/PC-Mg(PF_6)_2$	60	100	1100	N
$Zn/PC-LiClO_4$	60	110	1470	W
$Zn/BL-LiF + KPF_6$	50	40	240	N
ZnF_2				
$ZnF_2/DMF-KPF_6$	500	400	10	N
$ZnF_2/DMF-LiClO_4$	160	270	160	N
$ZnF_2/DMF-BF_3$	80	240	340	N

C coulombic ratio decreases with decreasing sweep rate
F dark reaction product forms at working electrode and drops off
N no noticeable change
S reaction product forms suspension
W dark reaction product remains at working electrode
Y solution turns yellow

Fifteen zinc systems (39%) had discharge peaks in excess of 50 ma/cm^2. Of this group thirteen (or 87%) had peak separations less than 0.5 v. A number of the metal zinc systems displayed the limited diffusion current region during the anodic sweep, similar to the copper systems.

b. Zinc fluoride

Only three of the 25 ZnF_2 systems exhibited discharge peaks in excess of 50 ma/cm^2. All three had peak separations less than 0.5 v., and one (ZnF_2/DMF-KPF_6) an extreme low of 10 mv.

6. Cyclic Voltammetry of Cadmium Systems

A total of 63 cadmium systems were screened, comprising cadmium metal and cadmium fluoride electrodes. Of these 51% had both charge and discharge peaks, with 11% of the systems having discharge peaks in excess of 50 ma/cm^2. Table 21 lists the distribution of the separate cadmium group.

TABLE 21

PERCENT DISTRIBUTION OF CYCLIC VOLTAMMETRIC PARAMETERS FOR CADMIUM SYSTEMS

63 Systems

		Discharge Peak			
Electrode	Qty.	>50 ma/cm^2 %	<50 ma/cm^2 %	None %	Overload %
Cd	39	18	28	10	46
CdF_2	24	0	59	24	17

TABLE 22

PEAK CURRENT DENSITIES AND PEAK SEPARATION

CADMIUM SYSTEMS

Systems	Peak c.d. Disch.	Chge.	ΔV	Visual
	ma/cm^2		mv	
Cd metal				
$Cd/DMF-LiClO_4$	1300	480	10	S
$Cd/DMF-LiBF_4$	1200	1280	60	WY
$Cd/DMF-Mg(ClO_4)_2$	880	220	130	W
$Cd/DMF-KPF_6$	400	320	400	N
$Cd/BL-KPF_6$	370	250	340	N
$Cd/DMF-CaCl_2$	100	210	60	F
$Cd/BL-LiF + KPF_6$	80	80	400	N

F dark reaction product forms at working electrode and drops off
N no noticeable change
S reaction product from working electrode forms suspension
W dark reaction product remains at working electrode
Y solution turns yellow

None of the CdF_2 systems exhibited discharge peaks in excess of 50 ma/cm^2, while only seven (18%) of the Cd metal systems were in this group. All of the seven had peak separations less than 0.5 v. Table 22 lists the voltammetric data for all systems having discharge peaks in excess of 50 ma/cm^2. Coulombic ratios of some cadmium systems are listed in Table 23.

TABLE 23

SPECIFIC DISCHARGE CAPACITY AND COULOMBIC RATIO OF SOME CADMIUM SYSTEMS*

System	Specific Discharge Capacity coul/cm^2	Coulombic Ratio
Cd		
Cd/BL-KPF_6	1.7	1.0
Cd/DMF-KPF_6	2.8	0.5
Cd/DMF-$LiBF_4$	4.8	0.4
Cd/DMF-$LiClO_4$	2.0	0.3

* In order of decreasing coulombic ratio.

7. Cyclic Voltammetry of Indium Systems

A total of 52 indium systems were screened, comprising indium metal and the fluoride. Of these 51% exhibited both charge and discharge peaks, with 22% having discharge peaks in excess of 50 ma/cm^2. Table 24 shows the percent distribution of voltammetric parameters for indium and indium fluoride systems.

TABLE 24

PERCENT DISTRIBUTION OF CYCLIC VOLTAMMETRIC PARAMETERS FOR INDIUM SYSTEMS

52 Systems

Electrode	Qty.	Discharge Peak >50 ma/cm^2 %	Discharge Peak <50 ma/cm^2 %	None %	Overload %
In	30	17	27	16	40
InF_3	22	27	32	0	41

Table 25 lists the peak current densities, peak separations, and visual observations for the indium systems.

8. Cyclic Voltammetry of Mo, Fe, Cr, Mn, and V

Molybdenum, chromium, and vanadium, behaved similar to nickel and cobalt, in showing very little electrochemical activity, as shown in Table 8. The three or four Fe and Mn systems showing a discharge peak in excess of 50 ma/cm^2 are shown in Table 26.

TABLE 25

PEAK CURRENT DENSITIES AND PEAK SEPARATION

INDIUM SYSTEMS

Systems	Peak c.d. Disch.	Peak c.d. Chge.	ΔV	Visual
	ma/cm^2		mv	
In metal				
In/PC-$Mg(ClO_4)_2$	560	220	200	W
In/PC-$MgCl_2$	130	130	450	N
In/PC-$LiPF_6$	65	290	700	DP
In/DMF-$Mg(ClO_4)_2$	60	280	350	SY
In/PC-$LiBF_4$	60	270	900	N
InF_3				
InF_3/PC-KPF_6	400	440	400	D
InF_3/PC-PF_5	220	120	550	D
InF_3/PC-$Mg(PF_6)_2$	200	150	950	N
InF_3/DMF-$CaCl_2$	165	270	250	N
InF_3/PC-$Ca(PF_6)_2$	140	90	650	N
InF_3/DMF-KPF_6	70	660	190	Y

D electrode dissolution
N no noticeable change
P plating at counterelectrode
S reaction product from working electrode forms suspension
W dark reaction product remains at working electrode
Y solution turns yellow

TABLE 26

PEAK CURRENT DENSITIES AND PEAK SEPARATION

OTHER SYSTEMS

Systems	Peak c.d. Disch	Chge.	ΔV	Visual
	ma/cm^2		mv	
Cobalt metal				
$CoCl_2$/AN-$LiPF_6$	90	90	1270	FB
Iron metal				
Fe/PC-$Mg(BF_4)_2$	130	280	1500	N
Fe/DMF-$Ca(PF_6)_2$	120	290	490	N
Fe/DMF-$LiPF_6$	120	320	1000	WYP
Manganese metal				
Mn/DMF-$LiPF_6$	190	310	910	WYP
Mn/DMF-$LiBF_4$	120	620	720	YC
Mn/DMF-KPF_6	130	190	700	WY

B solution turns blue
C coulombic ratio decreases with decreasing sweep rate
F dark reaction product forms at working electrode and drops off
N no noticeable change
P plating at counterelectrode
W dark reaction product remains at working electrode
Y solution turns yellow

G. The Effect of Water on Cyclic Voltammograms

Known amounts of water were added to a few systems to determine the effect on the cyclic voltammograms. In some cases the effect was sufficiently marked to entirely change the character of the voltammogram, whereas in other cases, additions of water to 3000 ppm had no apparent effect on the curve.

1. Silver Systems

The addition of 500 ppm water to butyrolactone-$MgCl_2$ caused voltage overload for the silver electrode, possibly resulting from high peak currents and low conductance of the electrolyte. Since the discharge and charge current densities for the anhydrous systems were only 70 and 65 ma/cm^2 respectively, the presence of water has a major influence on this system. On the other hand, the only major effect that 2000 ppm of water had on the cyclogram for silver in dimethylformamide - $MgCl_2$ was to increase the peak separation by about 200 mv. The addition of 1000 ppm water to dimethylformamide - $MgCl_2$ caused a 25% increase in current densities for both the cathodic and anodic peaks for AgCl. Addition of 2000 ppm water resulted in voltage overload. In the case of AgCl/DMF-LiCl, the addition of 2000 ppm water gave a much higher discharge peak, as well as a very large decrease in ΔV_p from 400 to 160 mv. This is unusual in that water resulted in a voltammogram indicating a better system, in terms of discharge current density and rechargeability, than the dry solution.

Addition of 500 and 1000 ppm water to systems of silver electrodes in propylene carbonate-$MgCl_2$ showed only minor effects. Small increases in peak current densities, and a decrease in ΔV_p were observed on addition of 1000 ppm water. The addition of 1000 ppm water to propylene carbonate - $MgCl_2$ causes a significant increase in current densities for both anodic and cathodic peaks in the case of the AgCl electrode. Voltage overload occurs at 2000 ppm water.

In addition the peaks are much sharper than those obtained in solutions without water additive.

2. Copper Systems

The addition of either 1000 or 2000 ppm to dimethylformamide - LiCl had no effect on the cyclic voltammograms of copper metal in this solution. For lithium perchlorate solutions in dimethylformamide, 1000 ppm of water had a devastating effect on the sweep curve by entirely eliminating the high, sharp charge and discharge peaks, leaving only low peak-less currents within the ± 1.0 volt scan range. The addition of 1000 ppm water to acetonitrile - KPF_6 had no significant effect on the anodic reaction of CuO but the specific discharge capacity was considerably reduced. This was not due to anodic product dissolution since the coulombic ratio remains invariant with sweep rate. The effect of adding 2000 ppm water caused a pronounced decrease in anodic peak current density and a large increase in peak separation. The specific discharge capacity remained relatively unchanged from the 1000 ppm value.

The cyclic voltammogram for copper oxide showed a secondary charge about 400 mv positive to the charge peak associated with the discharge peak. The addition of 500 and 1000 ppm water caused the disappearance of one of the anodic peaks and increased the current density of the remaining anodic peaks as well as the cathodic peak. Copper chloride electrodes which exhibited very high anodic and cathodic currents in dry propylene carbonate - $LiClO_4$, resulted in voltage overload in solutions containing 500 and 1000 ppm water.

3. Other Systems

Nickel, which exhibited zero charge and discharge currents in butyrolactone - $MgCl_2$, gave voltage overload on the addition of 1000 ppm water. This was all due to the charge reaction, the discharge current remaining zero.

Cobalt in acetonitrile solution of KPF_6 showed anodic but no cathodic activity. Addition of 500 ppm and 1000 ppm water to this system increased the anodic activity but failed to show any improvement in cathodic behavior.

In the case of zinc metal the addition of 1000 ppm water to dimethylformamide-KPF_6 solution results in the very peculiar cyclic voltammogram shown in Figure 7. Peaks A and B are the original peaks (in the absence of water), as shown in Figure 7, with a separate charge-discharge reaction occurring 0.70 volt negative to this. Addition of 2000 ppm water results in poorly reproducible curves, but are consistent in exhibiting two pronounced cathodic peaks of very high current density at about 0.0 and -0.9 volts. Only low spurious anodic peaks are obtained. Obviously the presence of water impurity is detrimental to this system. The charge-discharge reaction (D, E) at -0.7 v may involve formation and subsequent discharge of zinc oxide. Discharge peak C maintains its potential at -0.1 v for the 40 and 80 mv/sec sweep rates, but at 200 mv/sec the peak potential is non-reproducible, but remaining in the range of -0.1 to -0.4 v.

H. The Effect of Solute Concentration on Cyclic Voltammograms

The effect on the cyclic voltammograms by varying the solute concentration was determined for four systems: Ag/DMF-LiCl, Zn/DMF-$LiClO_4$, Zn/DMF-KPF_6, and Cd/DMF-$LiClO_4$. Sweep curves were obtained for solutions of varying molality from 0.5 to 3.0 m. If the data has been correctly interpreted, then analysis of the cyclic voltammograms resulted in significant information related to the degree of solubility of the anodic product formed during the anodic sweep.

Reference is made to the cyclic voltammograms for the zinc electrode in varying concentrations of dimethylformamide - KPF_6 shown in Figures 8-11. The descending branch of the charge peak is more gradual at the lower con-

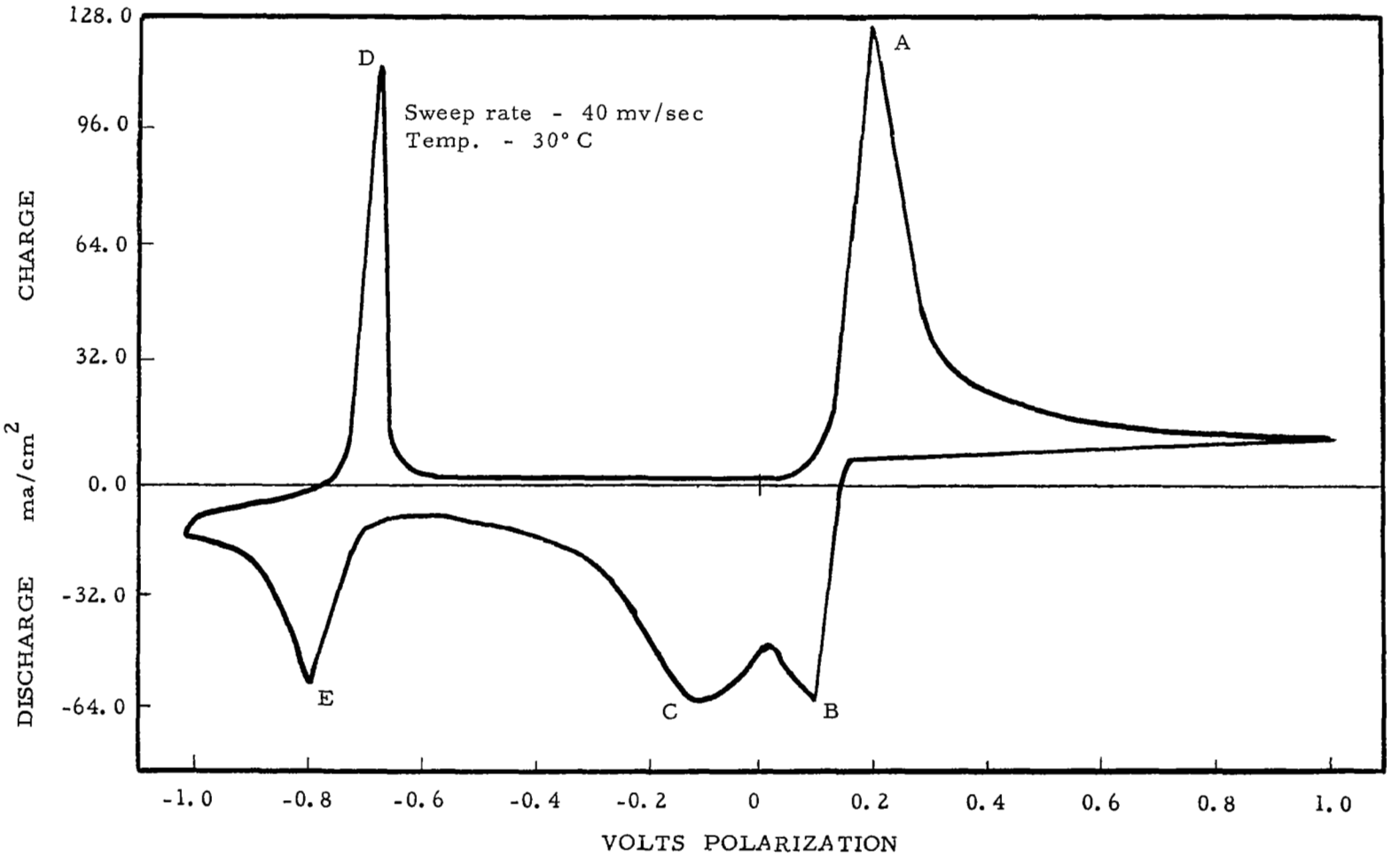

Figure 7. Cyclic voltammogram for zinc in dimethylformamide - KPF_6, 1.75 m, containing 1000 ppm water.

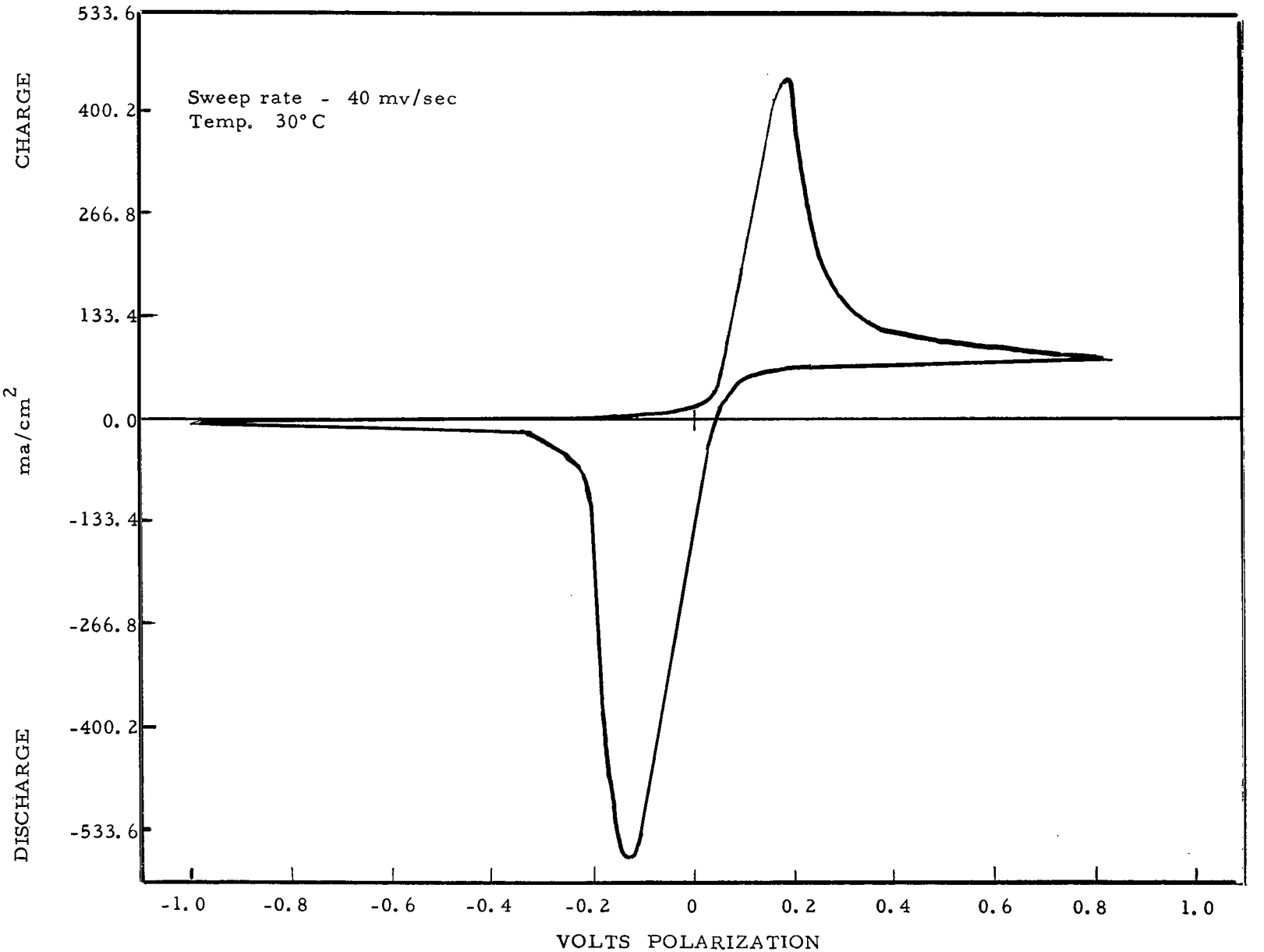

Figure 8. Cyclic voltammogram for zinc in dimethylformamide - KPF_6, 0.75 m.

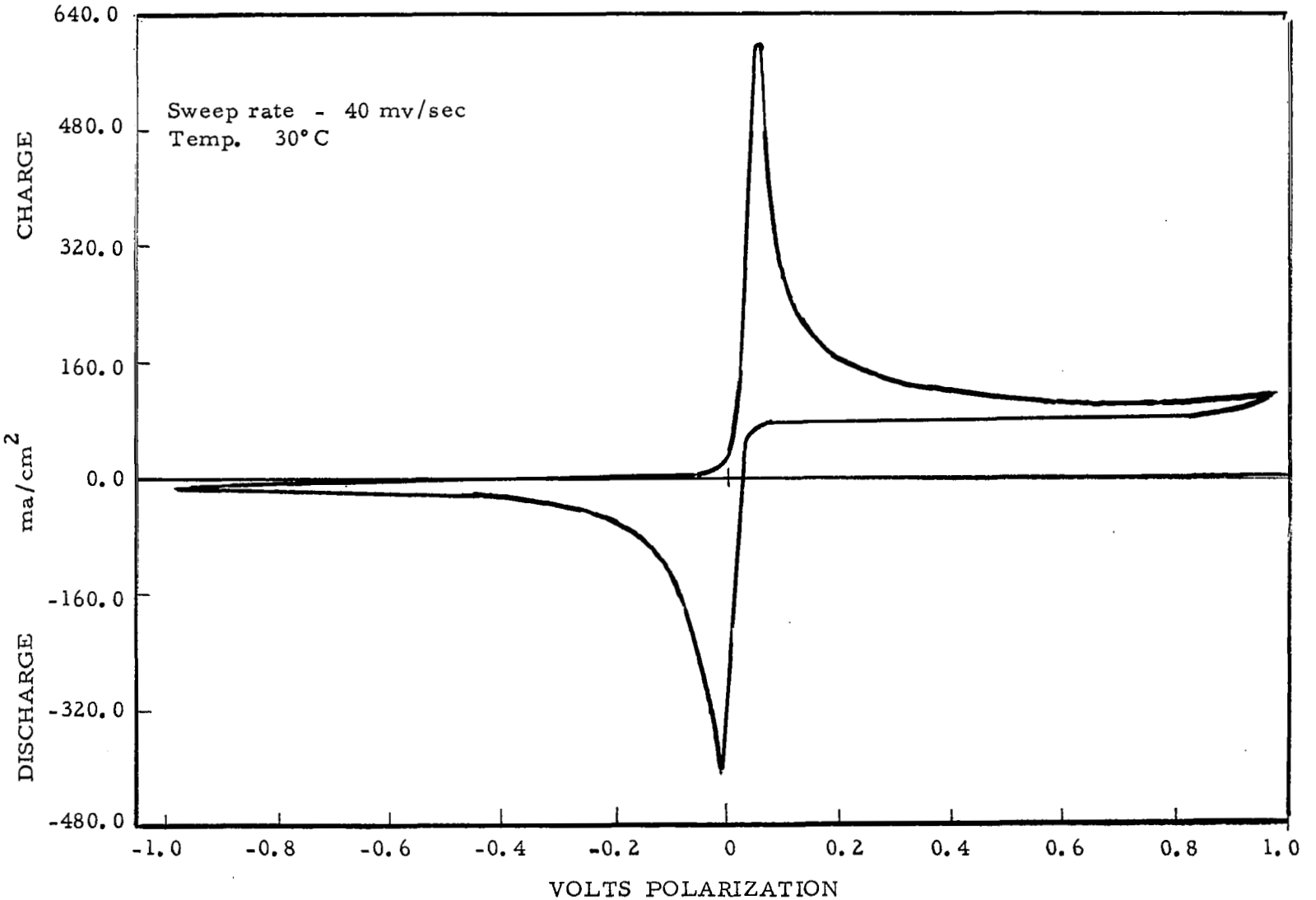

Figure 9. Cyclic voltammogram for zinc in dimethylformamide - KPF_6, 1.0 m.

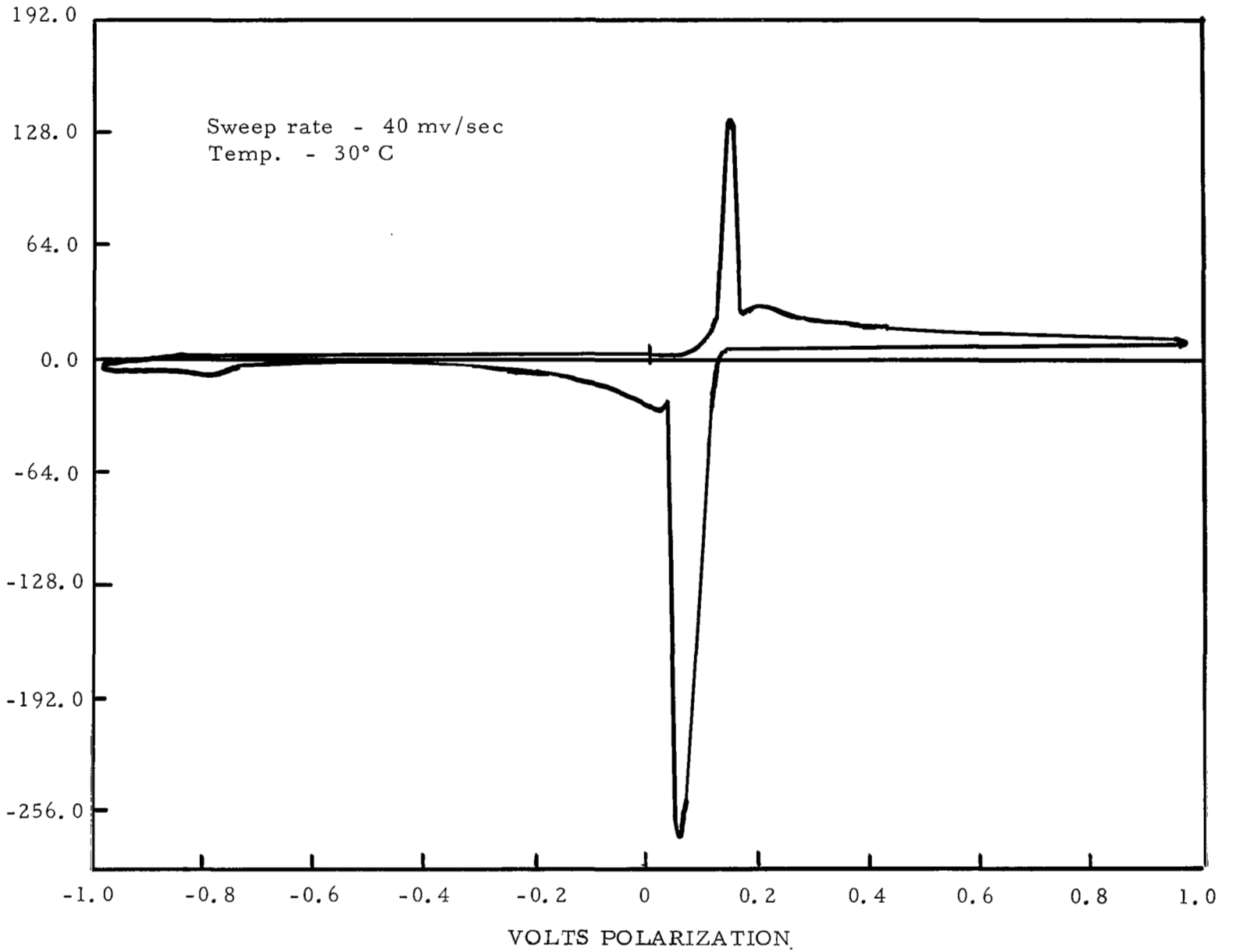

Figure 10. Cyclic voltammogram for zinc in dimethylformamide - KPF_6, 2.0 m.

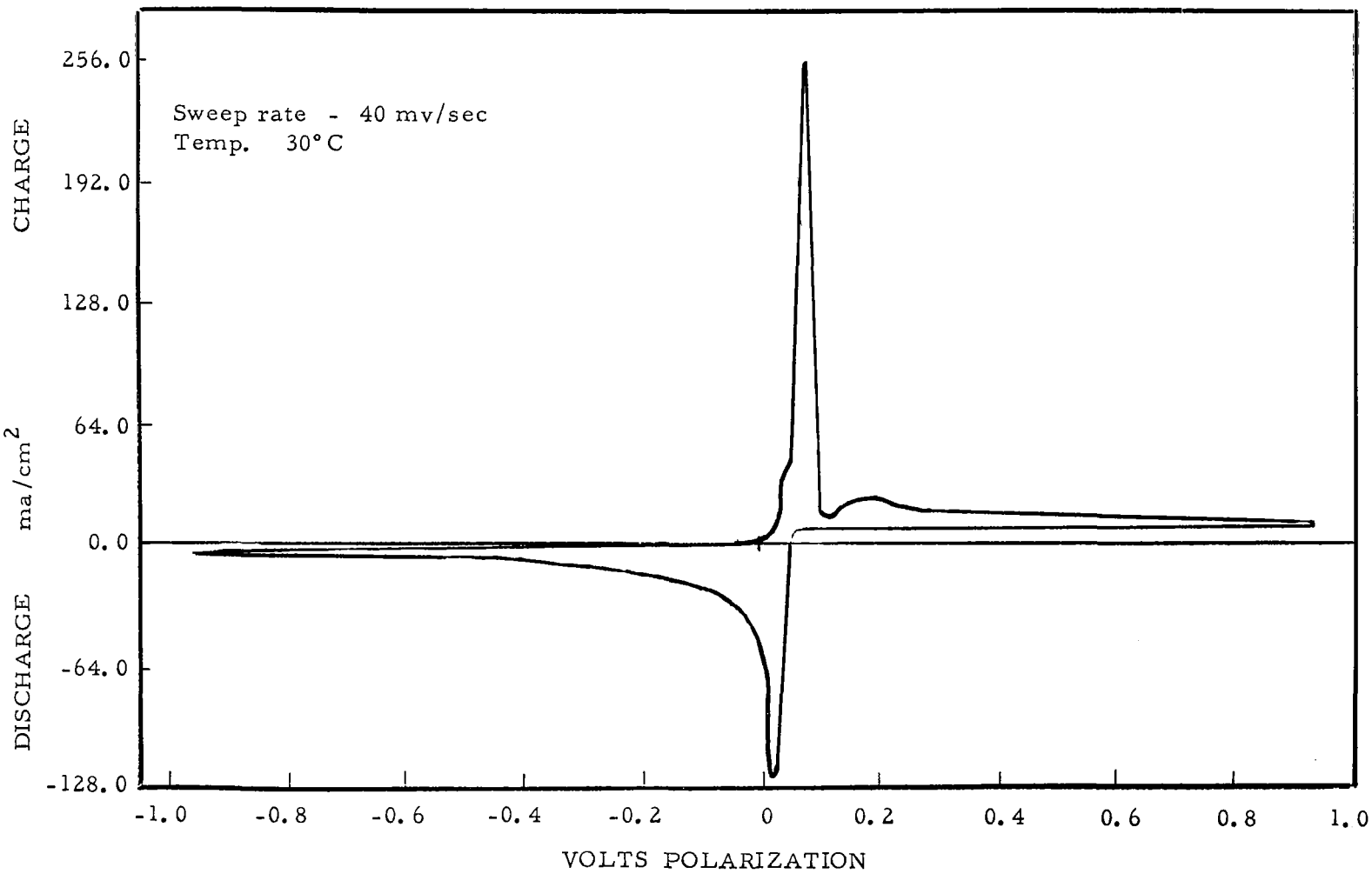

Figure 11. Cyclic voltammogram for zinc in dimethylformamide - KPF_6, 3.0 m.

A possible explanation is that since the anion concentration within the dense layer is depleted, further increase of voltage will cause metal ions within this layer to migrate to the layer-solution interface where they can react with available anions forming a second broader peak. This latter peak may be associated with the formation of a more porous, looser deposit.

The tendency to produce a thicker, secondary layer, which may be relatively soluble, suggests that a penalty is paid in terms of coulombic ratio by sweeping to anodic voltages well beyond the main peak. Convection, as well as pure diffusion, could distribute the dissolved material throughout the cell, making it only partially available for reduction within reasonable confines of a reduction peak. If the voltage sweep was limited from -0.4 volt to +0.4 volt for the higher concentrations, the coulombic ratios would be close to unity. The more limited sweep would also be more realistic in terms of actual battery performance. Thus the scan need vary only over the range of the primary charge and discharge plateaus (or peaks, in sweep terminology).

I. Cyclic Voltammetry of Negative-Electrolyte Systems

A total of 64 systems involving lithium, calcium, and magnesium electrodes, were screened by cyclic voltammetry. Only nine of the 17 lithium systems exhibited both charge and discharge peaks, but with large peak separations. In nearly all cases, neither magnesium nor calcium exhibited charge peaks, and the charge currents were negligible or non-existent.

1. Lithium Systems

Table 28 summarizes the lithium data. Lithium was not screened in acetonitrile because of known lack of compatibility in this solvent. There was visual evidence of lithium decomposition in dimethylformamide on both

TABLE 28

LITHIUM SYSTEMS

System		Max. Charge Current Density ma/cm^2
Disch. c.d. >300 ma/cm^2 (vh)		
Li/PC-$LiPF_6$	vo	very high
Li/DMF-$LiBF_4$	a	med low
Li/DMF-$LiClO_4$	np	med low
Disch. c.d. 100-300 ma/cm^2 (h)		
Li/BL-KPF_6	a	very low
Li/BL-$LiClO_4$		high
Li/BL-$AlCl_3$		high
Li/DMF-$LiPF_6$		high
Li/PC-$LiBF_4$		high
Disch. c.d. 50-100 ma/cm^2 (mh)		
Li/DMF-KPF_6	a	very low
Disch. c.d. 10-50 ma/cm^2 (ml)		
Li/PC-$Mg(ClO_4)_2$		low
Li/PC-$LiClO_4$	a	med low
Li/PC-$AlCl_3$ + LiCl		med low
Li/PC-$MgCl_2$		med low

vh	very high	vo	voltage overload
h	high	a	discharge (anodic) peak only
mh	med high	np	no peaks
ml	med low		

TABLE 28 (Cont'd)

LITHIUM SYSTEMS

System		Max. Charge Current Density ma/cm^2
Disch. c.d. 1-10 ma/cm^2 (l)		
Li/PC-KPF_6		low
Li/BL-$AlCl_3$ + LiCl		med high
Li/DMF-LiCl + $LiClO_4$	np	very low
Disch. c.d. < 1 ma/cm^2 (vl)		
Li/DMF-LiCl	np	very low

l low

vl very low

np no peaks

the working and reference electrodes. In general, lithium exhibited higher current densities than either magnesium or calcium electrodes.

2. Magnesium Systems

Table 29 lists the magnesium systems screened. These showed generally high anodic activity (discharge), but very little or no cathodic activity. The anodic activity was generally higher in acetonitrile and dimethylformamide solutions than in butyrolactone and propylene carbonate solutions. Electrolytes containing potassium, lithium, aluminum, and magnesium, all behaved similarly in this respect. Only three systems, DMF-$LiPF_6$, DMF-$LiBF_4$, and AN-$LiBF_4$, gave maximum cathodic current densities greater than 10 ma/cm^2, and this activity occurred only at about 1 volt negative to the open circuit voltage at potentials near the lithium ion reduction, which suggests that even these current densities may be due to lithium reduction.

3. Calcium Systems

Table 30 lists the calcium systems screened. Results were similar to those obtained with magnesium in that relatively little cathodic acitivity was obtained. Generally, greater anodic activity was observed in acetonitrile and dimethylformamide solutions, and less in butyrolactone and propylene carbonate solutions. An exception was Ca/PC-$LiBF_4$, but it is uncertain that the cathodic reaction is due to calcium or lithium ions from the electrolyte, because of the close proximity of the electrode potentials for both metals. The cathodic peak current density (285 ma/cm^2) was about twice what would be expected for lithium ions for the 0.5 m $LiBF_4$ electrolyte. However the curve was recorded after ten sweep cycles, and by this time changes in concentration at the electrode surface as well as the presence of convection currents could account for the large cathodic current.

TABLE 29

MAGNESIUM SYSTEMS

System		Max. Charge Current Density ma/cm^2
Disch. c.d. >300 ma/cm^2 (vh)		
Mg/AN-$LiPF_6$	a	very low
Mg/AN-$LiClO_4$	a	very low
Disch. c.d. 100-300 ma/cm^2 (h)		
Mg/AN-KPF_6 + $LiPF_6$	a	very low
Mg/DMF-$LiBF_4$	a	med low
Mg/AN-$Mg(ClO_4)_2$	a	very low
Mg/AN-$AlCl_3$	a	very low
Mg/AN-$AlCl_3$ + LiCl	a	low
Mg/BL-$AlCl_3$	a	very low
Mg/BL-$AlCl_3$ + LiCl	a	very low
Mg/DMF-$LiClO_4$	ad	very low
Mg/DMF-LiCl	a	very low
Mg/DMF-$MgCl_2$	a	very low
Mg/PC-$AlCl_3$ + LiCl	a	very low
Disch. c.d. 50-100 ma/cm^2 (mh)		
Mg/DMF-$LiPF_6$		med low
Mg/DMF-LiCl + $LiClO_4$	a	very low

vh very high
h high
mh med high

a discharge (anodic) peak only.
d electrode volume reduced more than 50% by dissolution.

TABLE 29 (Cont'd)

MAGNESIUM SYSTEMS

System		Max. Charge Current Density ma/cm^2
Disch. c.d. 10-50 ma/cm^2 (ml)		
$Mg/DMF-KPF_6$	a	very low
$Mg/BL-LiClO_4$	a	very low
$Mg/DMF-Mg(ClO_4)_2$	ad	very low
$Mg/AN-KPF_6$	np	very low
Disch. c.d. 1-10 ma/cm^2 (l)		
$Mg/PC-LiPF_6$	a	very low
$Mg/PC-LiBF_4$	a	very low
$Mg/AN-LiBF_4$	np	med low
Disch. c.d. <1 ma/cm^2 (vl)		
$Mg/BL-KPF_6$	np	very low
$Mg/PC-LiClO_4$	np	very low
$Mg/PC-KPF_6$	np	very low
$Mg/PC-MgCl_2$	a	very low

ml	med low	a	discharge (anodic) peak only.
l	low	np	no peaks
vl	very low	d	electrode volume reduced more than 50% by dissolution.

TABLE 30

CALCIUM SYSTEMS

Systems		Max. Charge Current Density ma/cm^2
Disch. c.d. >300 ma/cm^2		
Ca/AN-$AlCl_3$ + LiCl		med low
Disch. c.d. 100-300 ma/cm^2		
Ca/AN-$AlCl_3$		low
Ca/AN-$LiPF_6$ + KPF_6	a	low
Disch. c.d. 50-100 ma/cm^2		
Ca/AN-$LiPF_6$	np	med low
Ca/DMF-KPF_6	a	low
Ca/DMF-LiCl	a	low
Disch. c.d. 10-50 ma/cm^2		
Ca/PC-$LiBF_4$	np	high
Ca/DMF-LiCl + $LiClO_4$		very low
Ca/BL-$AlCl_3$	a	very low
Ca/BL-$AlCl_3$ + LiCl	a	very low

a discharge (anodic peak only

np no peaks

TABLE 30 (Cont'd)

CALCIUM SYSTEMS

Systems		Max. Charge Current Density ma/cm^2
Disch. c.d. 1-10 ma/cm^2		
Ca/DMF-$LiPF_6$	a	very low
Ca/PC-$LiPF_6$	a	low
Ca/PC-KPF_6	a	very low
Ca/AN-$LiClO_4$	a	very low
Disch. c.d. <1 ma/cm^2		
Ca/AN-$LiBF_4$	np	very low
Ca/BL-$LiClO_4$	np	very low
Ca/DMF-$LiClO_4$	np	very low
Ca/DMF-$LiBF_4$	np	low
Ca/PC-$AlCl_3$ + LiCl	np	very low
Ca/BL-KPF_6	a	very low
Ca/PC-$LiClO_4$	a	very low

a discharge (anodic) peak only

np no peaks

In addition the specific charge capacity was several times that for the anodic peak, again suggesting the reduction of species from solution.

These results indicate that at least according to the cyclic voltammetry data none of the calcium or magnesium systems, and few of the lithium systems, would be suitable for secondary battery application. The soft electrode made it difficult to accurately reproduce the electrode position at the luggin capillary, thereby introducing appreciable ohmic effect on the voltammograms. This would have affected only the lithium data since calcium or magnesium showed no charge current at all even though well-defined discharge peaks were obtained. There is a strong question whether these results can be considered valid in terms of system performance, since experience on the positive systems has shown the absence of a reduction peak when the anodic product undergoes immediate dissolution as it is formed.

J. Recommended Positive - Electrolyte Systems

The following systems were recommended on the basis of high discharge peaks and low peak separation:

$AgO/BL\text{-}LiCl + AlCl_3$
$AgF_2/PC\text{-}LiBF_4$
$Cu/AN\text{-}LiPF_6 + KPF_6$
$Cu/DMF\text{-}LiPF_6$
$CuCl_2/AN\text{-}LiPF_6$
$CuCl_2/BL\text{-}AlCl_3$
$CuCl_2/DMF\text{-}LiCl + LiClO_4$
$CuCl_2/DMF\text{-}LiPF_6$
$CuCl_2/PC\text{-}LiClO_4$
$CuF_2/DMF\text{-}LiPF_6$
$CuF_2/PC\text{-}LiPF_6$
$CuF_2/PC\text{-}LiClO_4$
$Zn/AN\text{-}LiClO_4$
$Zn/BL\text{-}KPF_6$
$Zn/DMF\text{-}KPF_6$
$Zn/DMF\text{-}LiPF_6$
$Zn/DMF\text{-}LiClO_4$
$Zn/PC\text{-}KPF_6$
$ZnF_2/DMF\text{-}KPF_6$
$ZnF_2/DMF\text{-}LiClO_4$
$Cd/BL\text{-}KPF_6$
$Cd/DMF\text{-}KPF_6$
$Cd/DMF\text{-}LiBF_4$
$Cd/DMF\text{-}LiClO_4$

The cyclic voltammograms for these systems are shown in the following pages.

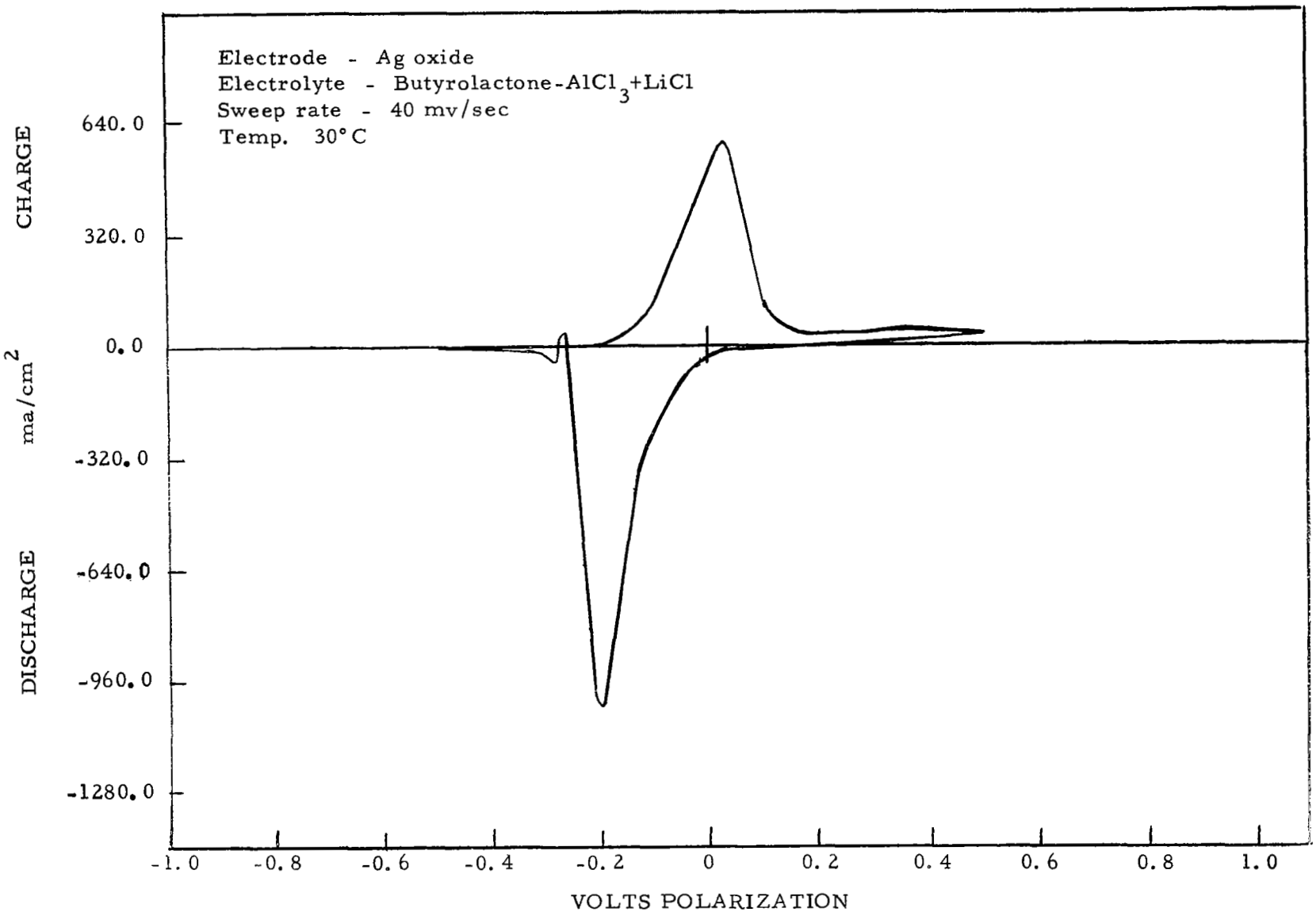
Electrode - Ag oxide
Electrolyte - Butyrolactone-AlCl3+LiCl
Sweep rate - 40 mv/sec
Temp. 30°C
CHARGE
DISCHARGE
ma/cm2
640.0
320.0
0.0
-320.0
-640.0
-960.0
-1280.0
-1.0
-0.8
-0.6
-0.4
-0.2
0
0.2
0.4
0.6
0.8
1.0
VOLTS POLARIZATION

Figure 13

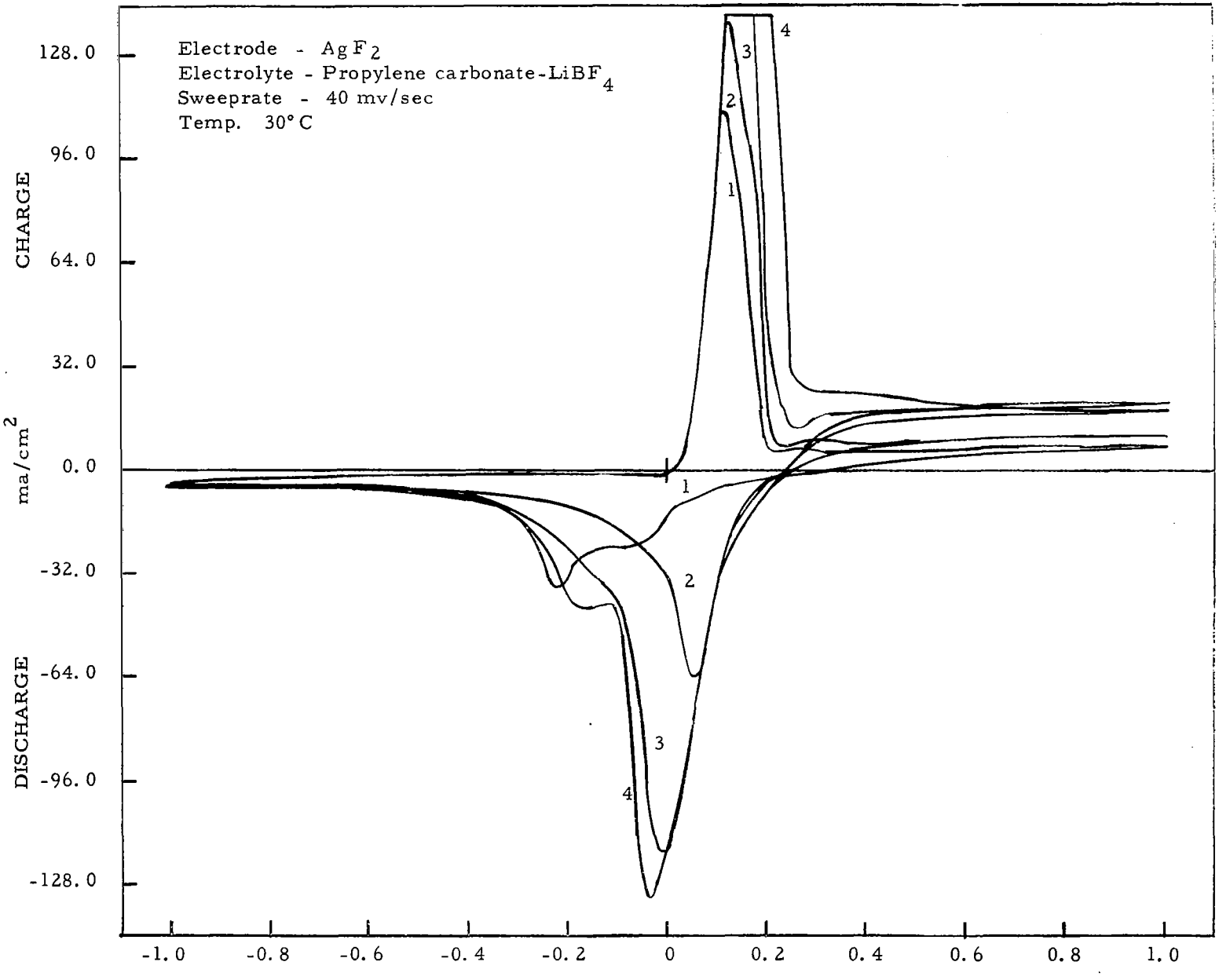

VOLTS POLARIZATION

Figure 14

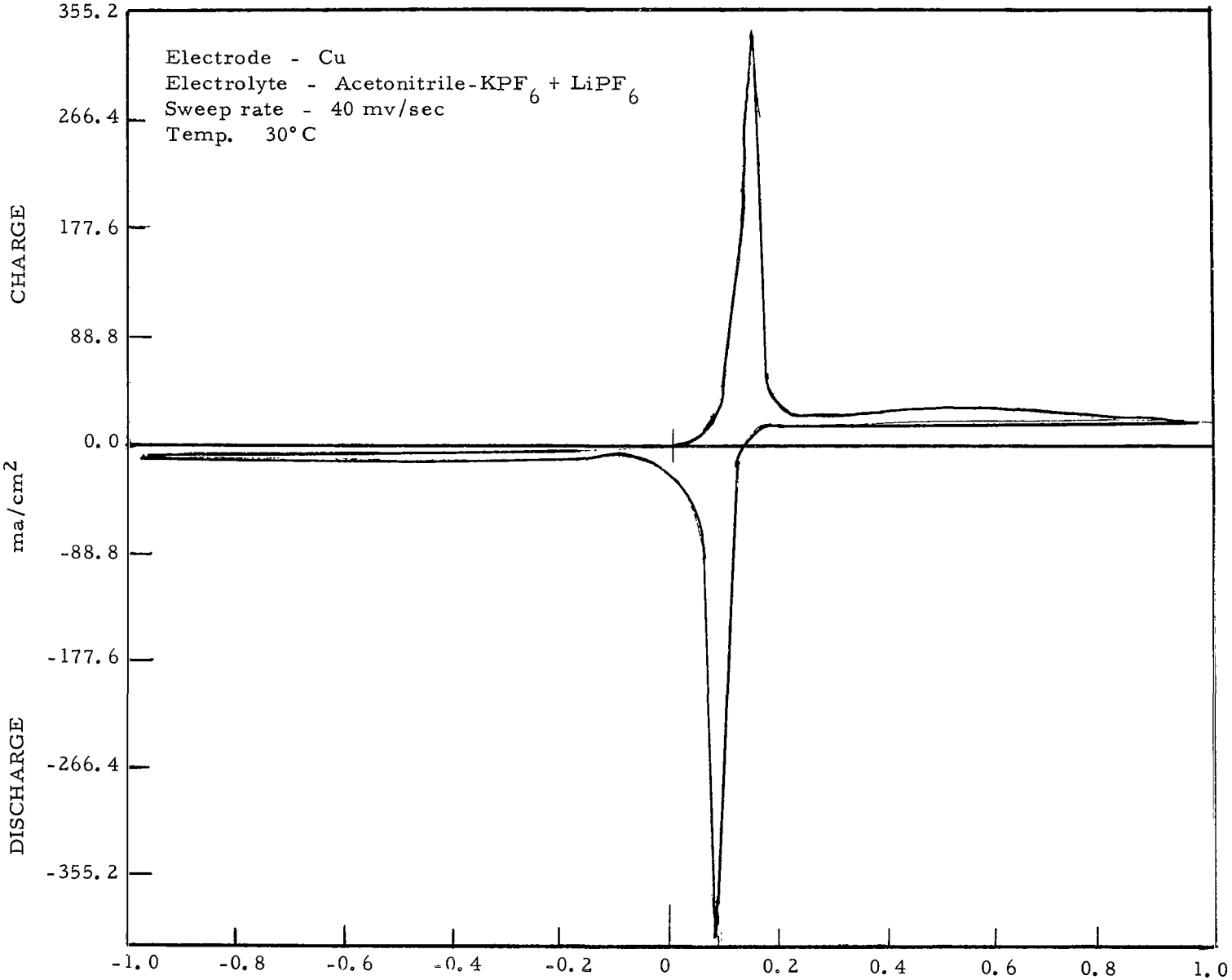
Electrode - Cu
Electrolyte - Acetonitrile-KPF_6 + $LiPF_6$
Sweep rate - 40 mv/sec
Temp. 30° C
355.2
266.4
177.6
88.8
0.0
-88.8
-177.6
-266.4
-355.2
CHARGE
DISCHARGE
ma/cm²
-1.0
-0.8
-0.6
-0.4
-0.2
0
0.2
0.4
0.6
0.8
1.0
VOLTS POLARIZATION

Figure 15

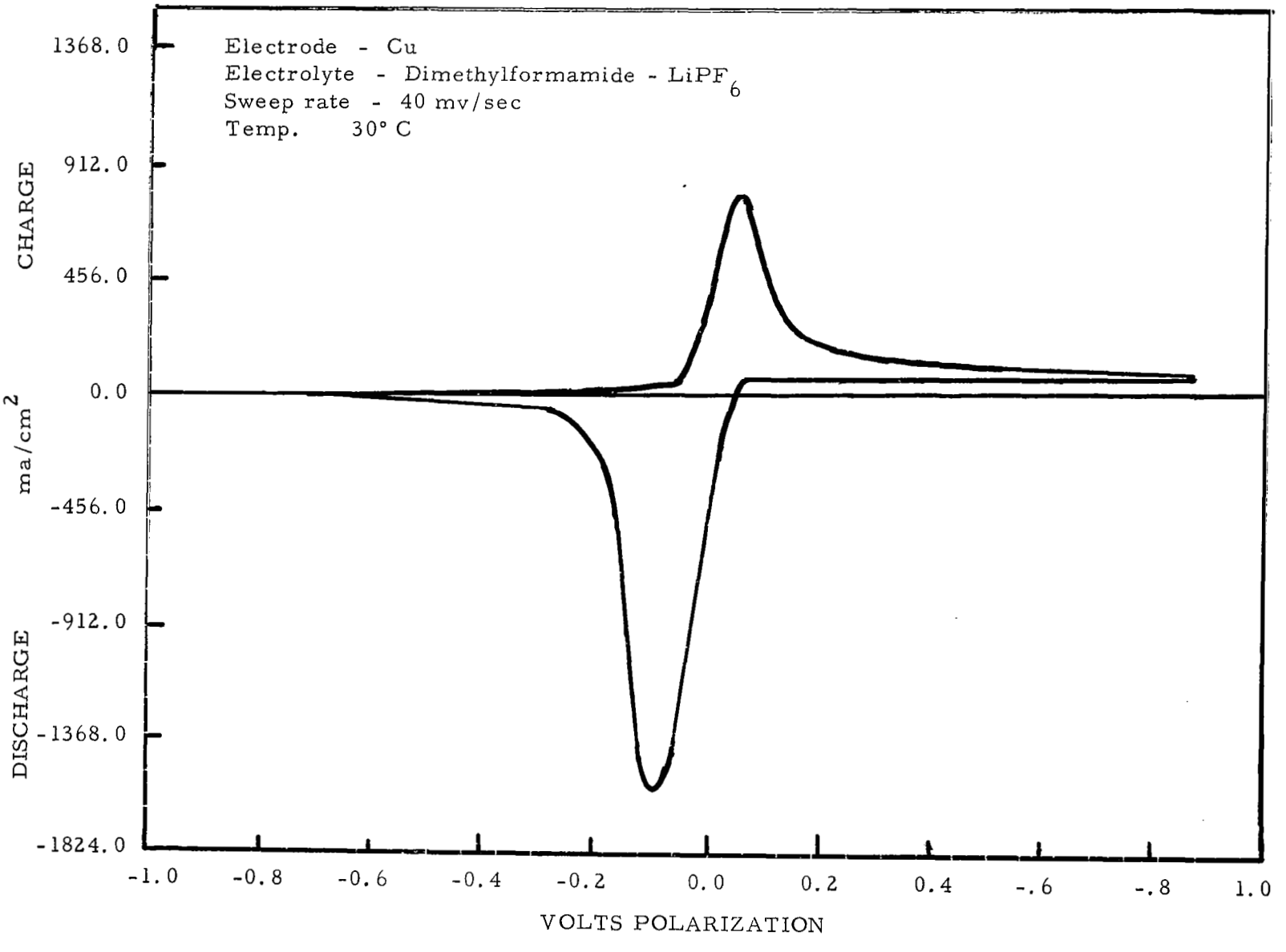
Electrode - Cu
Electrolyte - Dimethylformamide - $LiPF_6$
Sweep rate - 40 mv/sec
Temp. 30° C
1368.0
912.0
456.0
0.0
-456.0
-912.0
-1368.0
-1824.0
CHARGE
DISCHARGE
ma/cm^2
-1.0
-0.8
-0.6
-0.4
-0.2
0.0
0.2
0.4
-.6
-.8
1.0
VOLTS POLARIZATION

Figure 16

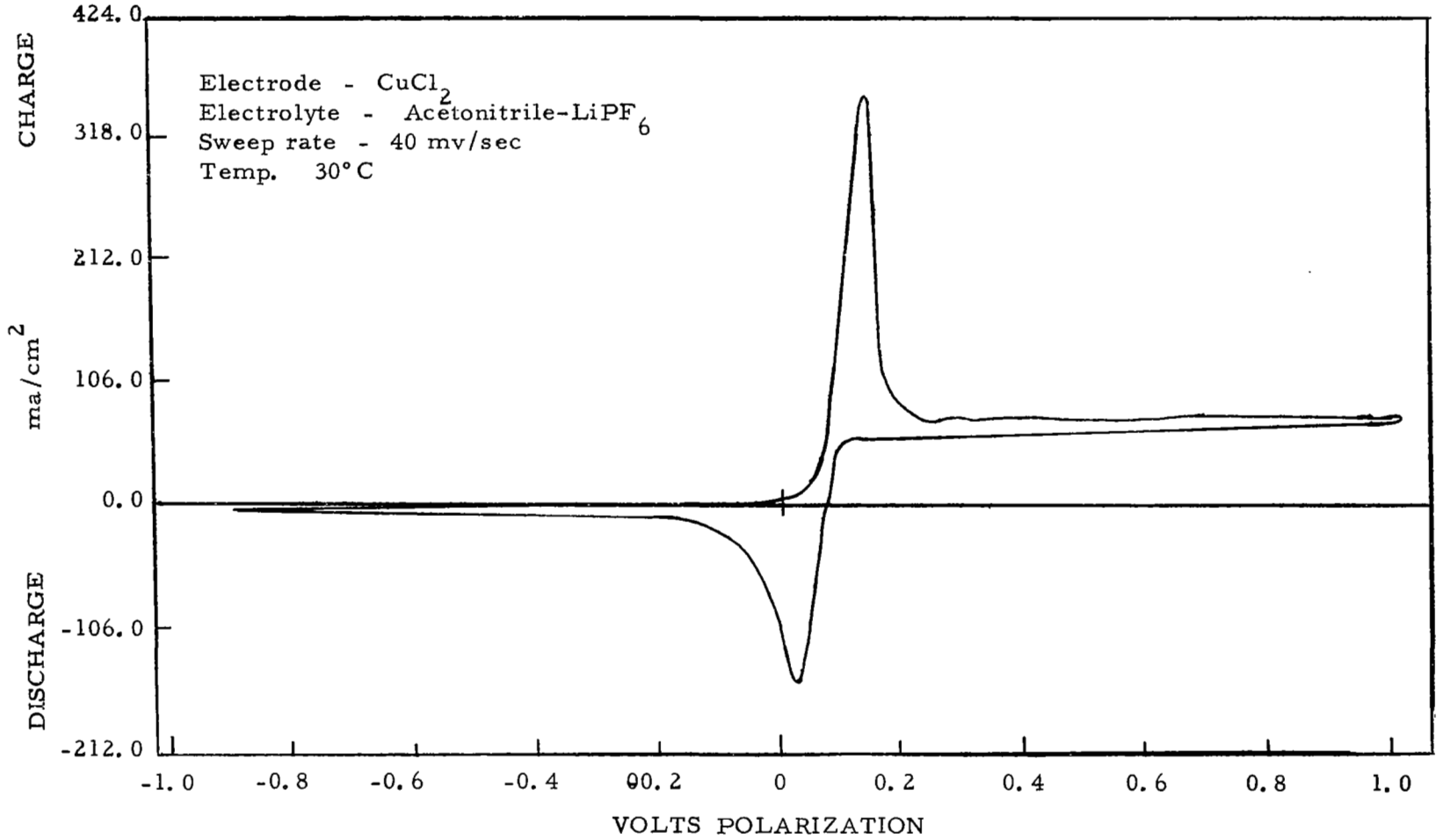
Electrode - $CuCl_2$
Electrolyte - Acetonitrile-$LiPF_6$
Sweep rate - 40 mv/sec
Temp. 30°C
CHARGE
DISCHARGE
ma/cm^2
424.0
318.0
212.0
106.0
0.0
-106.0
-212.0
-1.0
-0.8
-0.6
-0.4
-0.2
0
0.2
0.4
0.6
0.8
1.0
VOLTS POLARIZATION

Figure 17

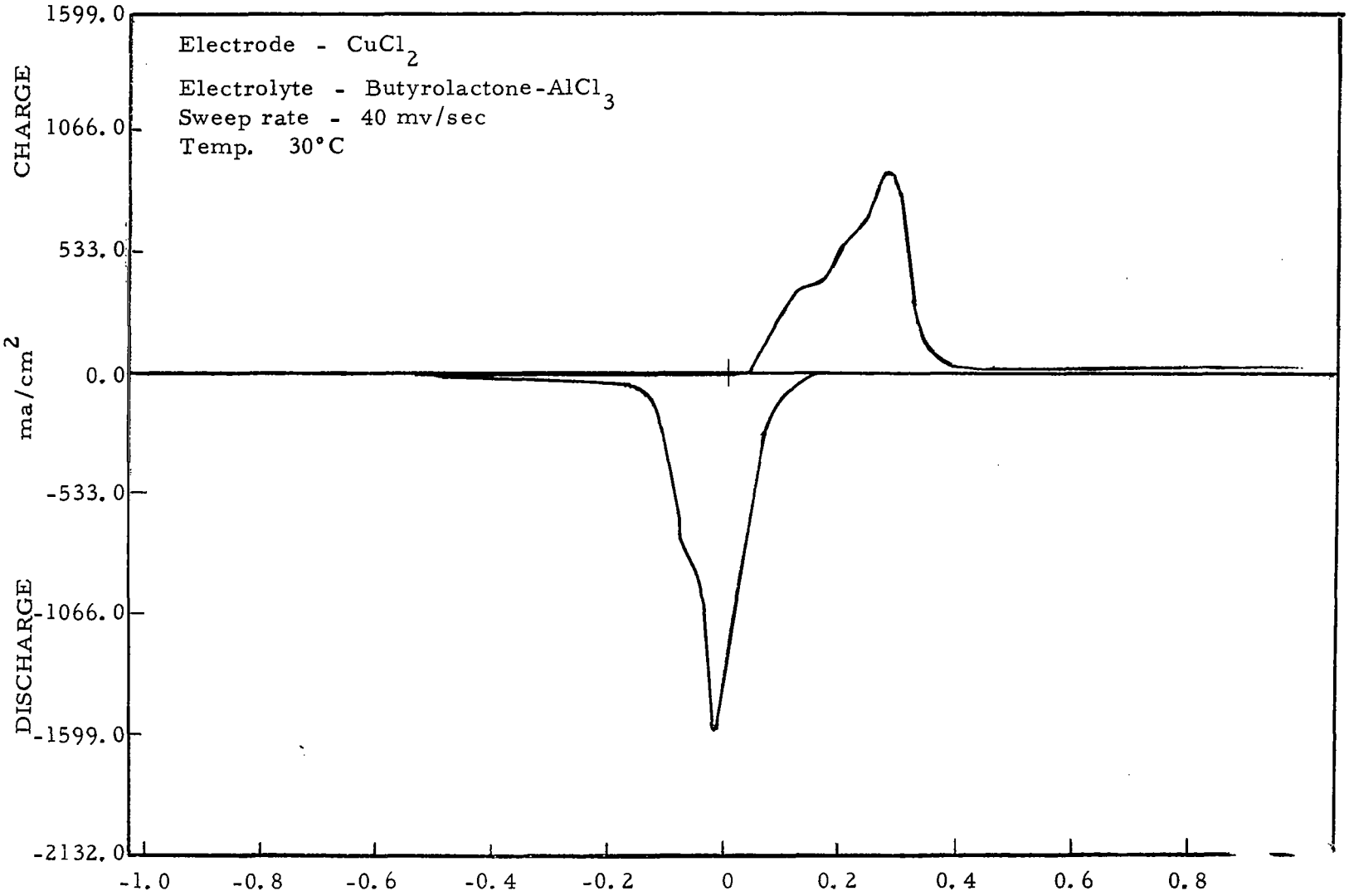
Electrode - $CuCl_2$
Electrolyte - Butyrolactone-$AlCl_3$
Sweep rate - 40 mv/sec
Temp. 30°C
CHARGE
DISCHARGE
ma/cm^2
1599.0
1066.0
533.0
0.0
-533.0
-1066.0
-1599.0
-2132.0
-1.0
-0.8
-0.6
-0.4
-0.2
0
0.2
0.4
0.6
0.8

Figure 18

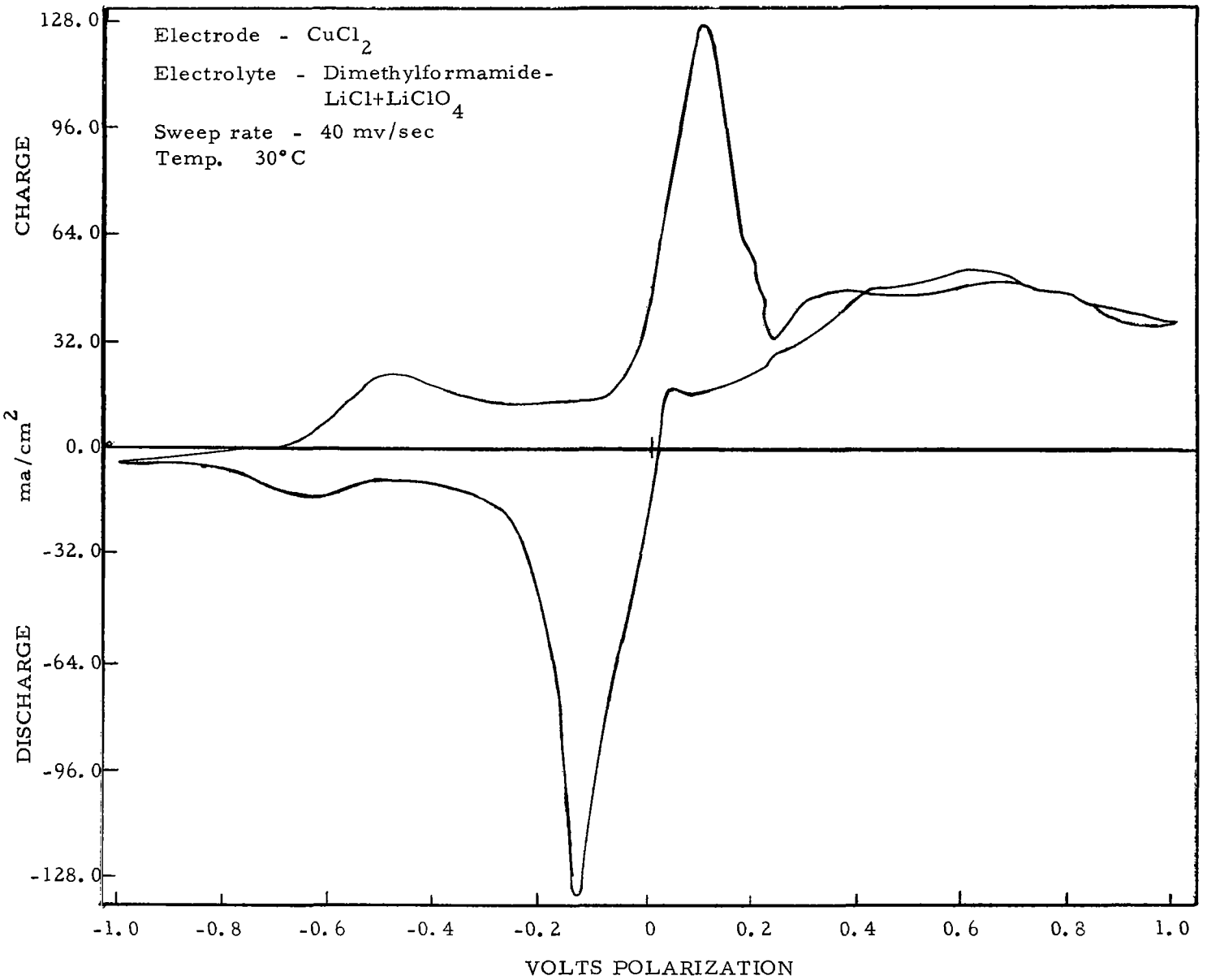
Electrode - $CuCl_2$
Electrolyte - Dimethylformamide-
$LiCl+LiClO_4$
Sweep rate - 40 mv/sec
Temp. 30°C
CHARGE
DISCHARGE
ma/cm^2
128.0
96.0
64.0
32.0
0.0
-32.0
-64.0
-96.0
-128.0
-1.0
-0.8
-0.6
-0.4
-0.2
0
0.2
0.4
0.6
0.8
1.0
VOLTS POLARIZATION

Figure 19

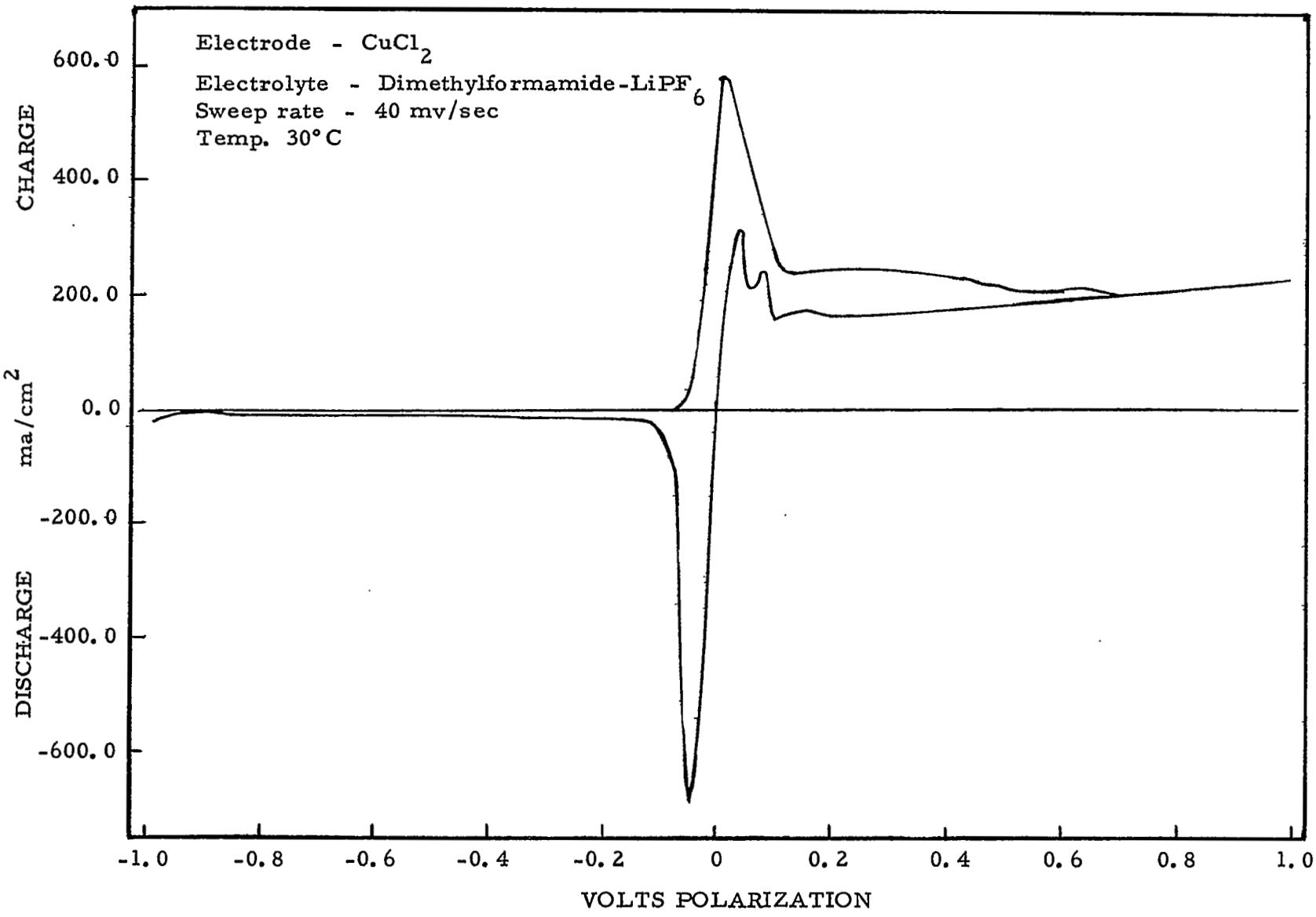
Electrode - $CuCl_2$
Electrolyte - Dimethylformamide-$LiPF_6$
Sweep rate - 40 mv/sec
Temp. 30°C
CHARGE
DISCHARGE
ma/cm^2
600.0
400.0
200.0
0.0
-200.0
-400.0
-600.0
-1.0
-0.8
-0.6
-0.4
-0.2
0
0.2
0.4
0.6
0.8
1.0
VOLTS POLARIZATION

Figure 20

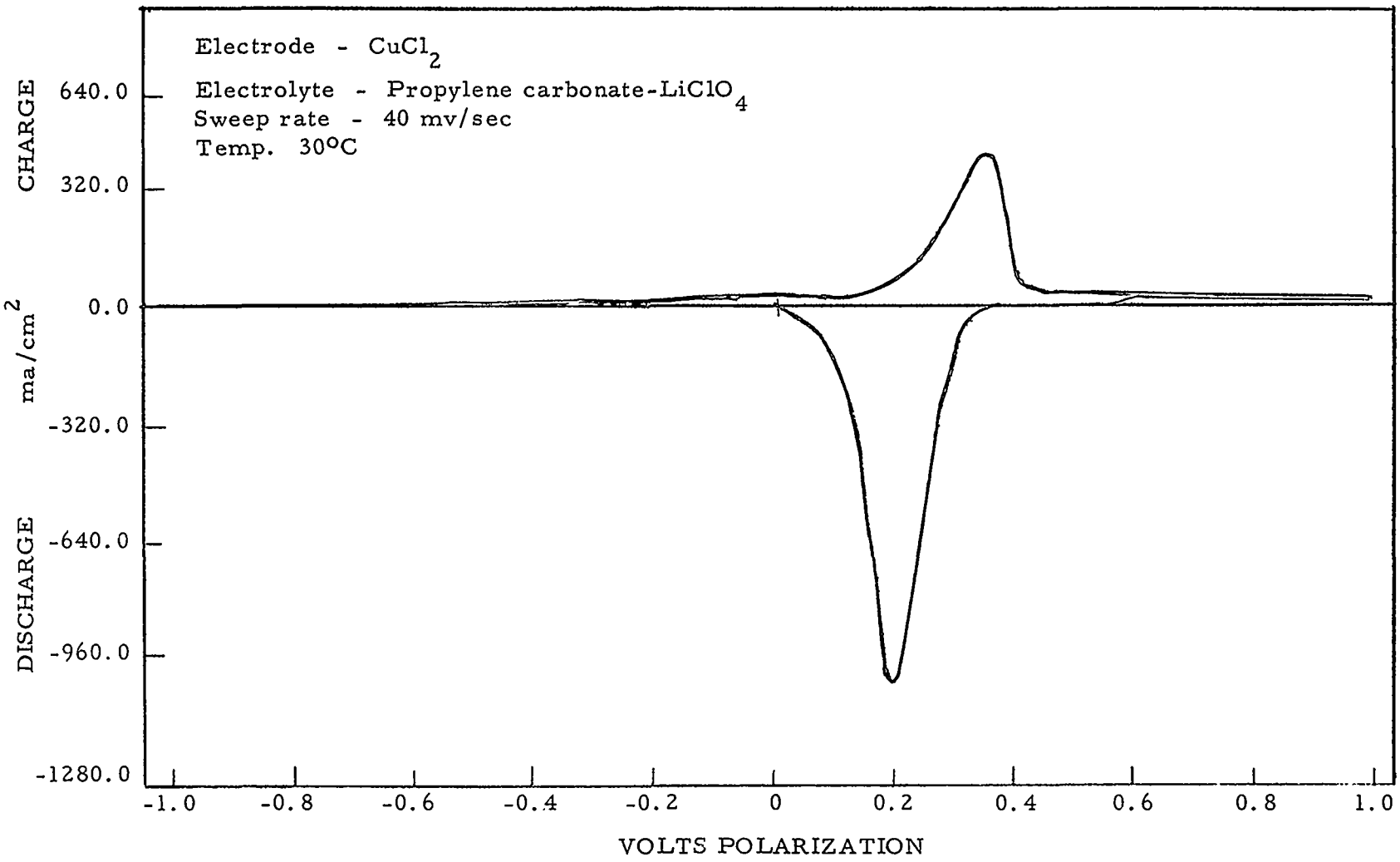
Electrode - $CuCl_2$
Electrolyte - Propylene carbonate-$LiClO_4$
Sweep rate - 40 mv/sec
Temp. 30°C
CHARGE
DISCHARGE
ma/cm^2
640.0
320.0
0.0
-320.0
-640.0
-960.0
-1280.0
-1.0
-0.8
-0.6
-0.4
-0.2
0
0.2
0.4
0.6
0.8
1.0
VOLTS POLARIZATION

Figure 21

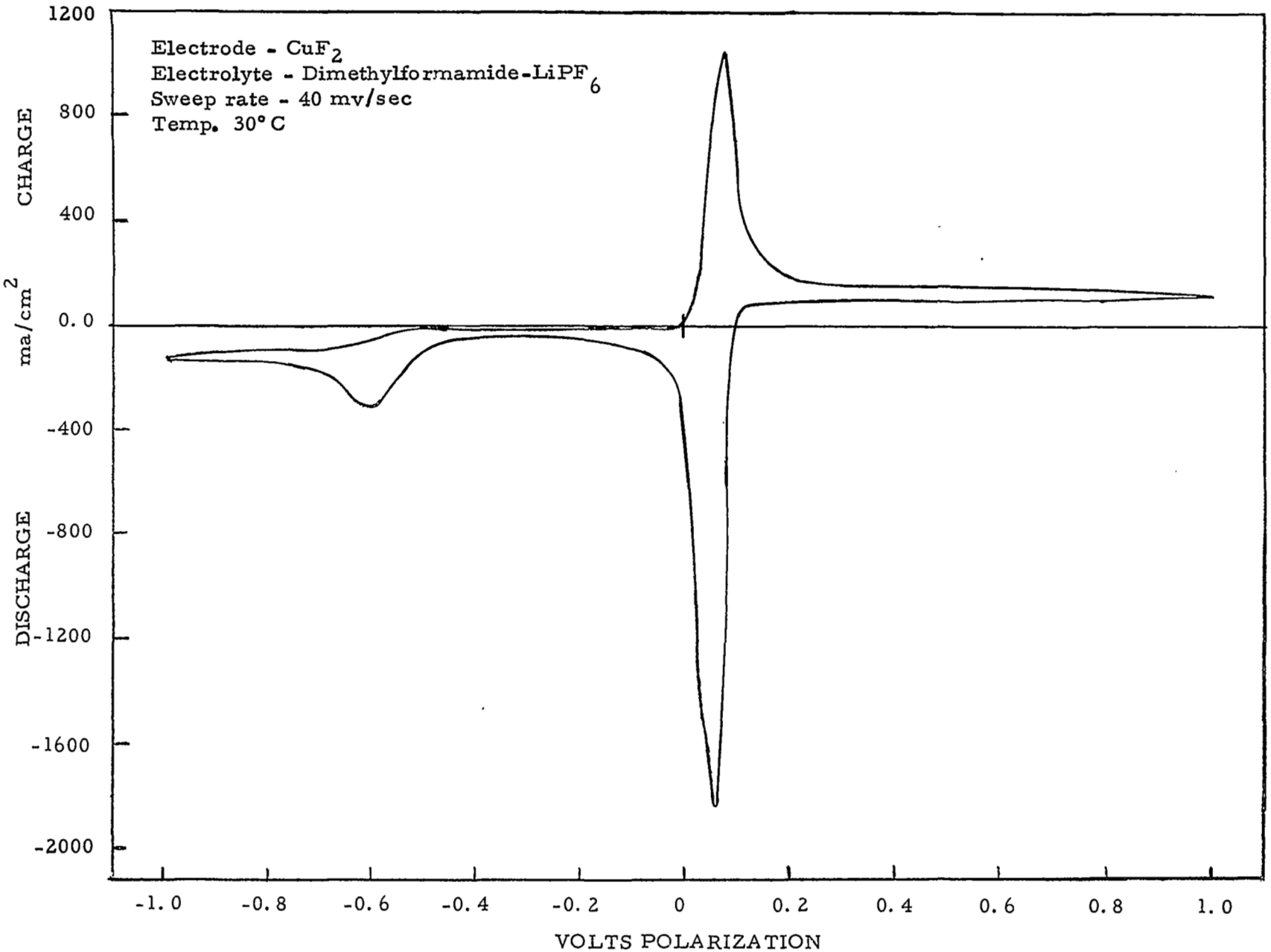
Electrode - CuF_2
Electrolyte - Dimethylformamide-$LiPF_6$
Sweep rate - 40 mv/sec
Temp. 30° C
CHARGE
DISCHARGE
ma/cm^2
1200
800
400
0.0
-400
-800
-1200
-1600
-2000
-1.0
-0.8
-0.6
-0.4
-0.2
0
0.2
0.4
0.6
0.8
1.0
VOLTS POLARIZATION

Figure 22

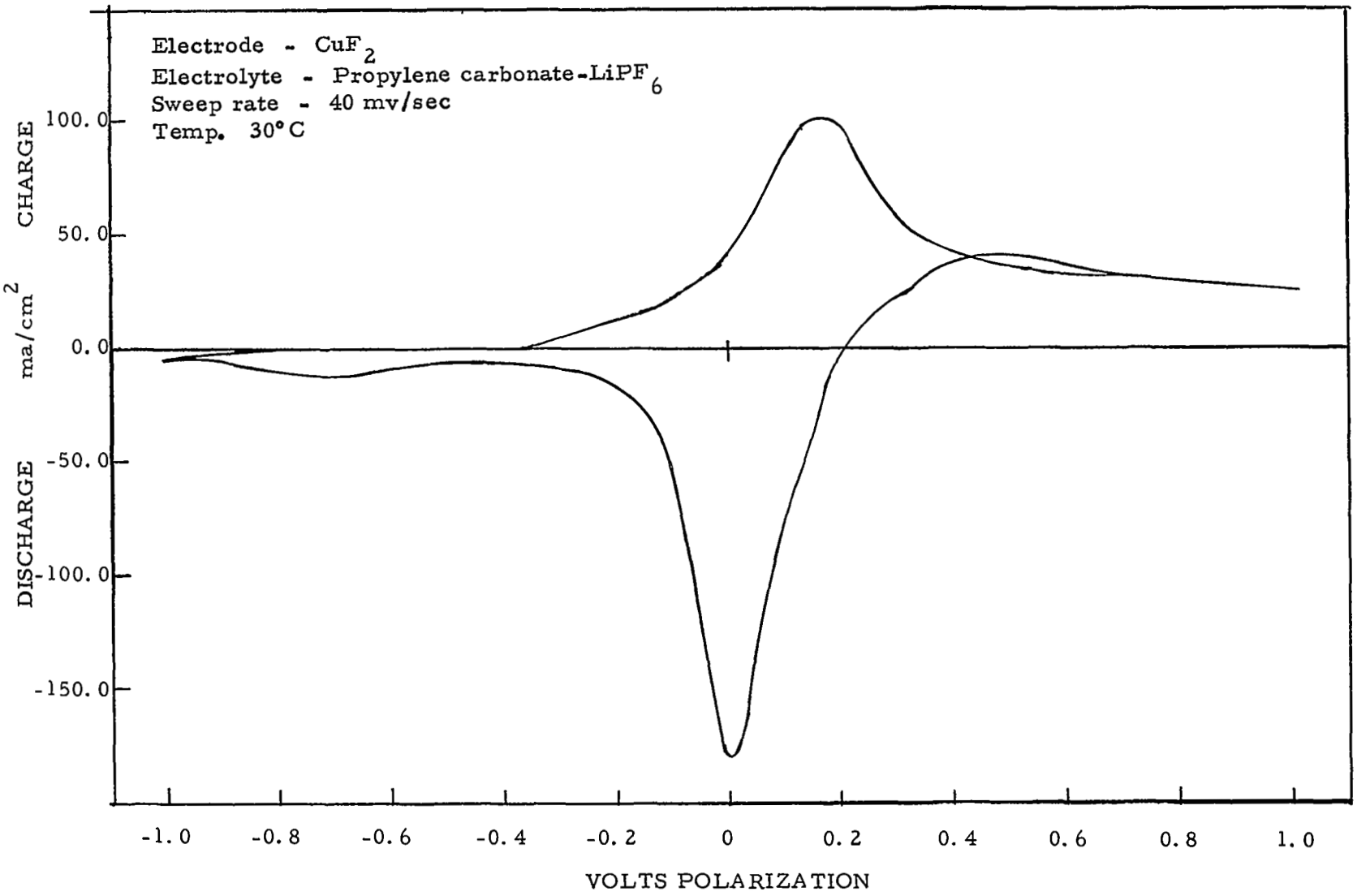
Electrode - CuF_2
Electrolyte - Propylene carbonate-$LiPF_6$
Sweep rate - 40 mv/sec
Temp. 30°C
CHARGE
DISCHARGE
ma/cm^2
100.0
50.0
0.0
-50.0
-100.0
-150.0
-1.0
-0.8
-0.6
-0.4
-0.2
0
0.2
0.4
0.6
0.8
1.0
VOLTS POLARIZATION

Figure 23

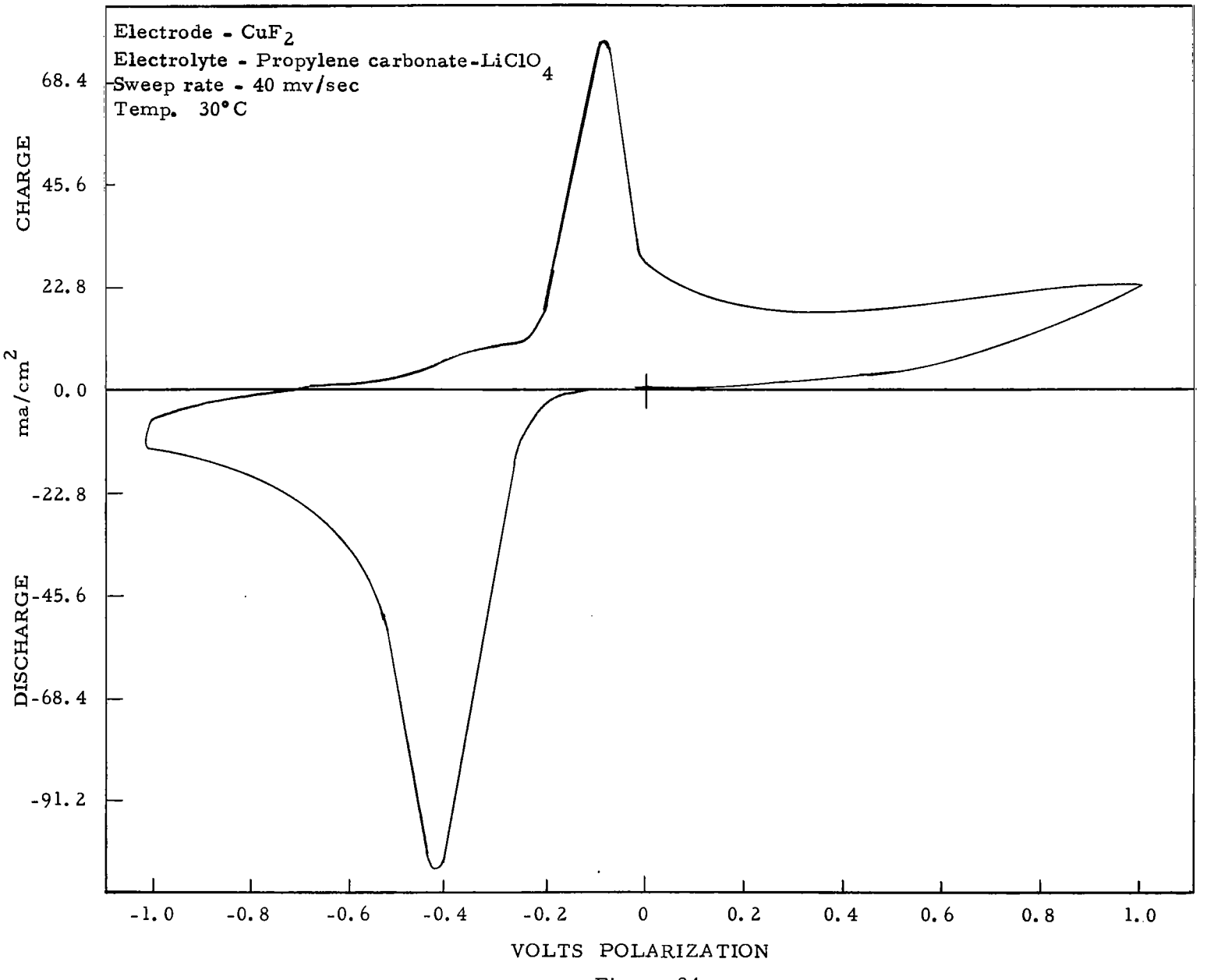
Electrode - CuF_2
Electrolyte - Propylene carbonate-$LiClO_4$
Sweep rate - 40 mv/sec
Temp. 30°C
CHARGE
DISCHARGE
ma/cm^2
68.4
45.6
22.8
0.0
-22.8
-45.6
-68.4
-91.2
-1.0
-0.8
-0.6
-0.4
-0.2
0
0.2
0.4
0.6
0.8
1.0
VOLTS POLARIZATION

Figure 24

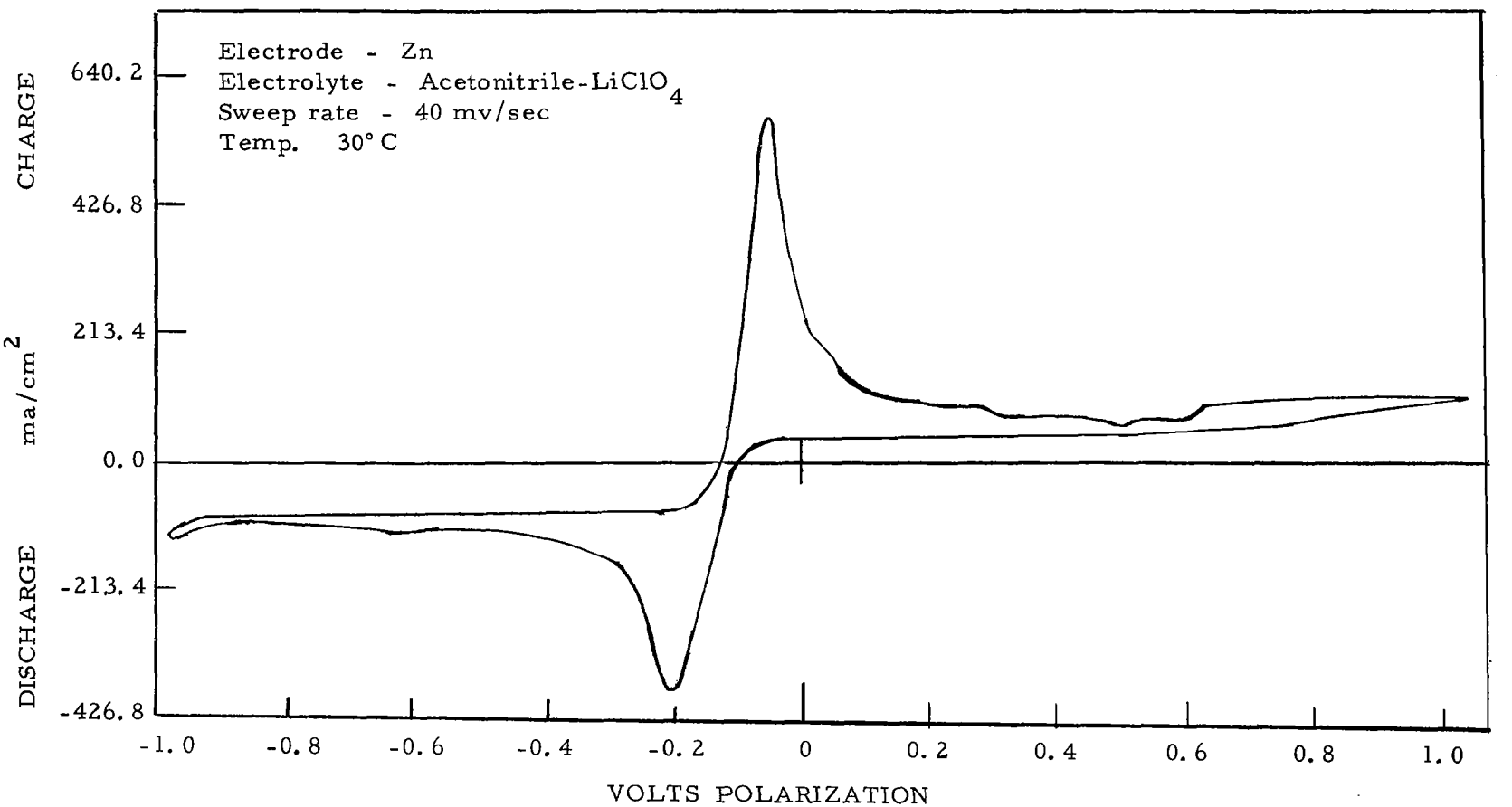
Electrode - Zn
Electrolyte - Acetonitrile-LiClO4
Sweep rate - 40 mv/sec
Temp. 30° C
CHARGE
DISCHARGE
ma/cm2
640.2
426.8
213.4
0.0
-213.4
-426.8
-1.0
-0.8
-0.6
-0.4
-0.2
0
0.2
0.4
0.6
0.8
1.0
VOLTS POLARIZATION

Figure 25

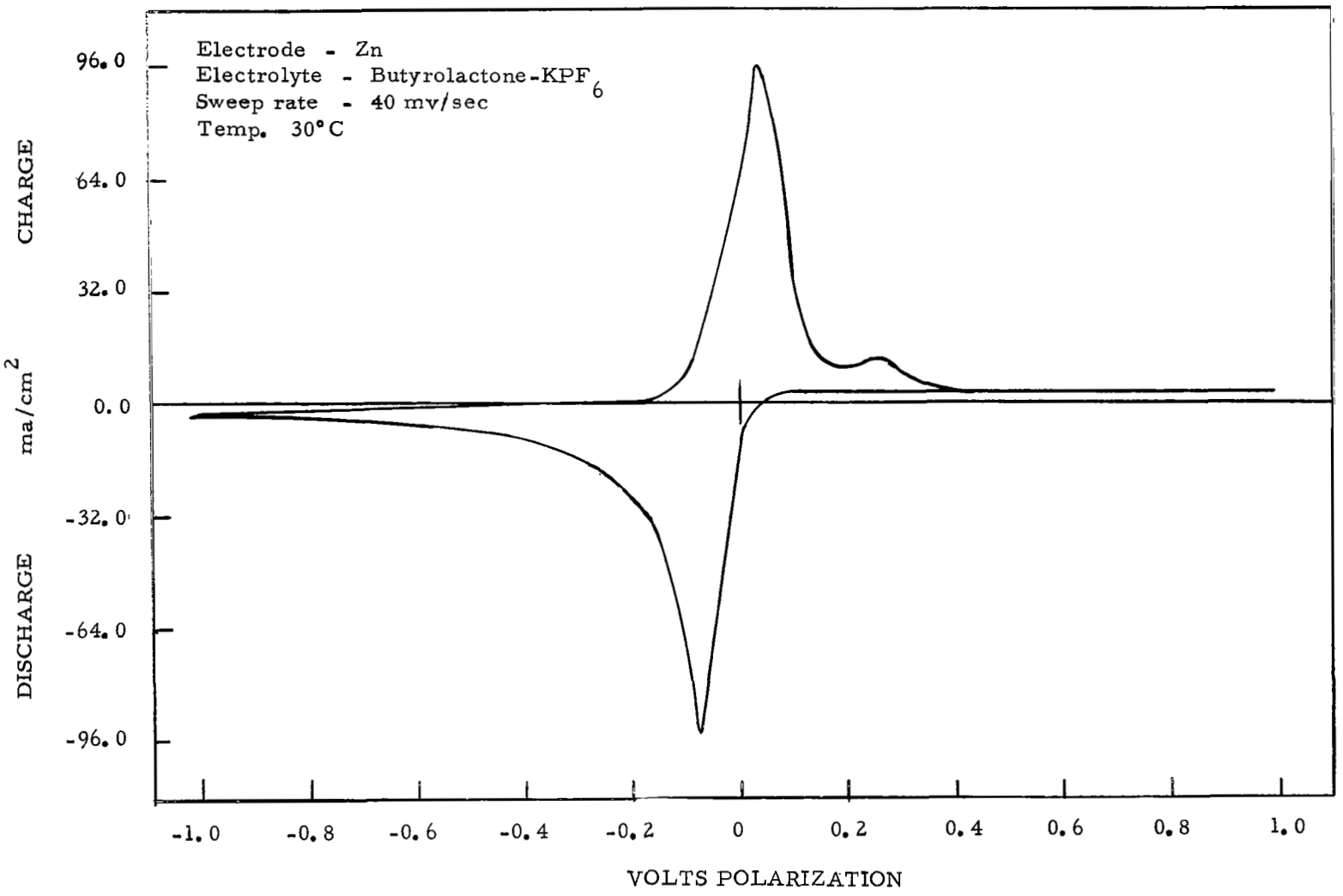
Electrode - Zn
Electrolyte - Butyrolactone-KPF6
Sweep rate - 40 mv/sec
Temp. 30°C
CHARGE
DISCHARGE
ma/cm2
96.0
64.0
32.0
0.0
-32.0
-64.0
-96.0
-1.0
-0.8
-0.6
-0.4
-0.2
0
0.2
0.4
0.6
0.8
1.0
VOLTS POLARIZATION

Figure 26

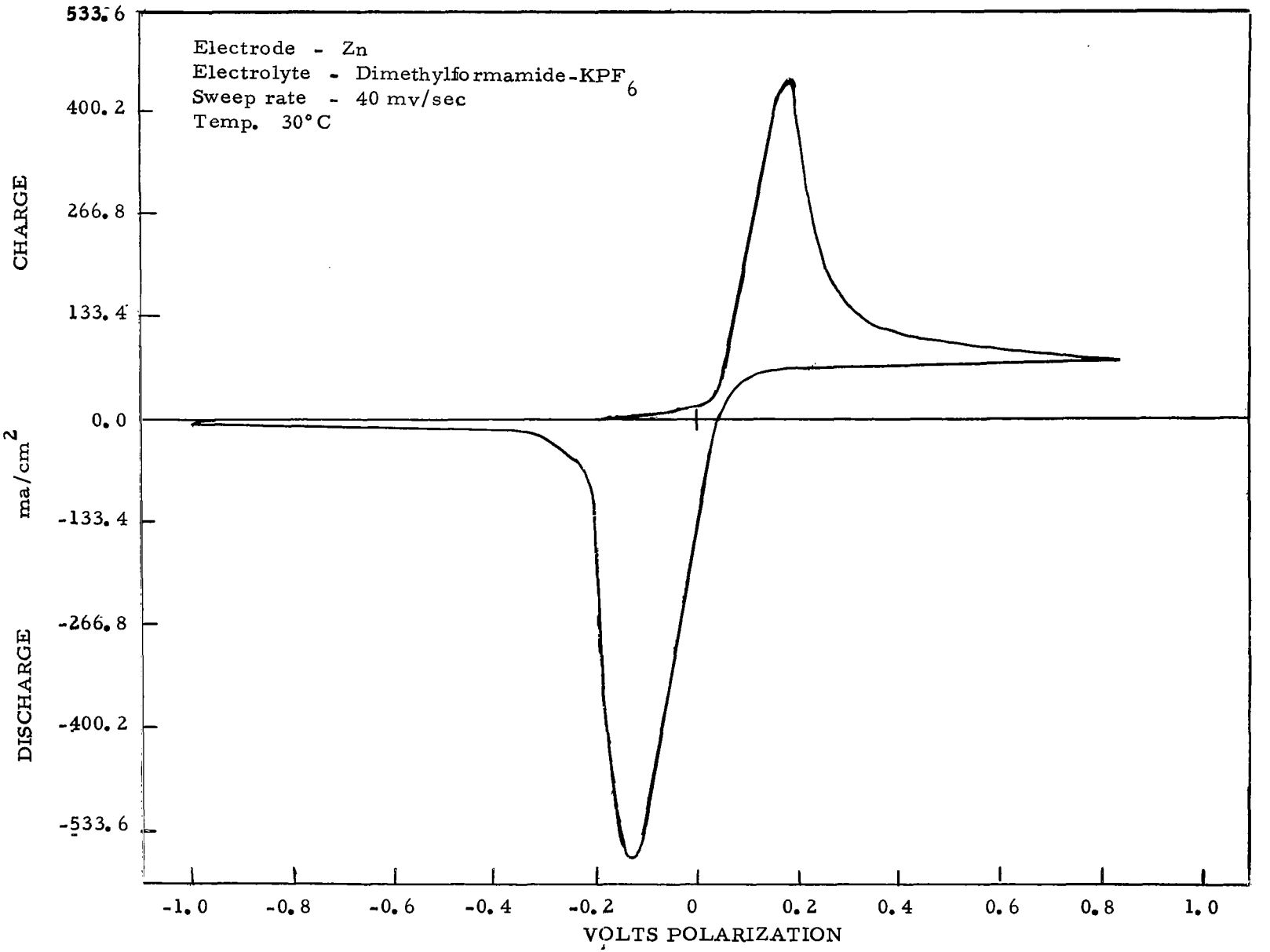
Electrode - Zn
Electrolyte - Dimethylformamide-KPF_6
Sweep rate - 40 mv/sec
Temp. 30°C
CHARGE
DISCHARGE
ma/cm^2
533.6
400.2
266.8
133.4
0.0
-133.4
-266.8
-400.2
-533.6
-1.0
-0.8
-0.6
-0.4
-0.2
0
0.2
0.4
0.6
0.8
1.0
VOLTS POLARIZATION

Figure 27

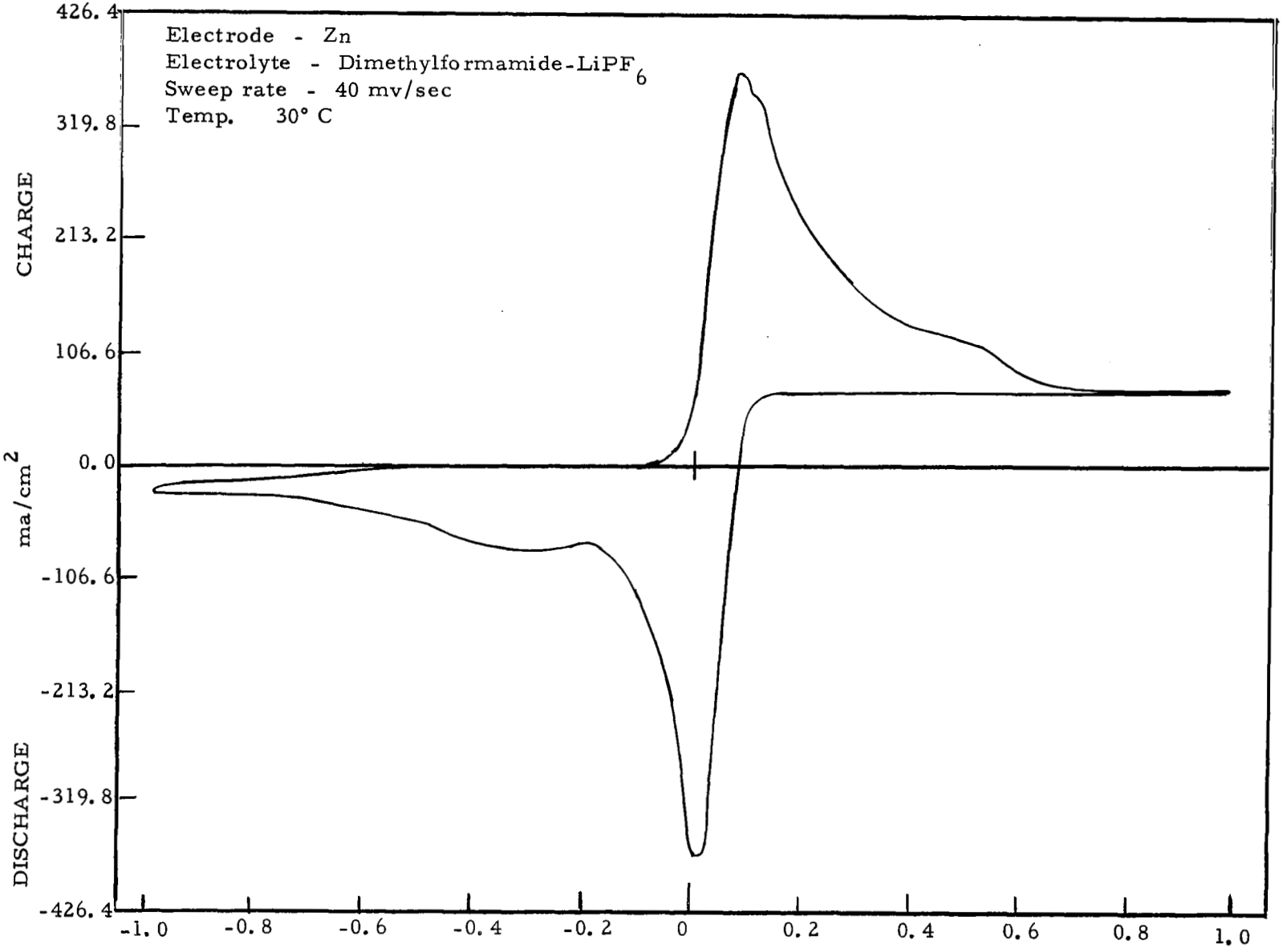
Electrode - Zn
Electrolyte - Dimethylformamide-LiPF6
Sweep rate - 40 mv/sec
Temp. 30° C
426.4
319.8
213.2
106.6
0.0
-106.6
-213.2
-319.8
-426.4
CHARGE
DISCHARGE
ma/cm2
-1.0
-0.8
-0.6
-0.4
-0.2
0
0.2
0.4
0.6
0.8
1.0
VOLTS POLARIZATION

Figure 28

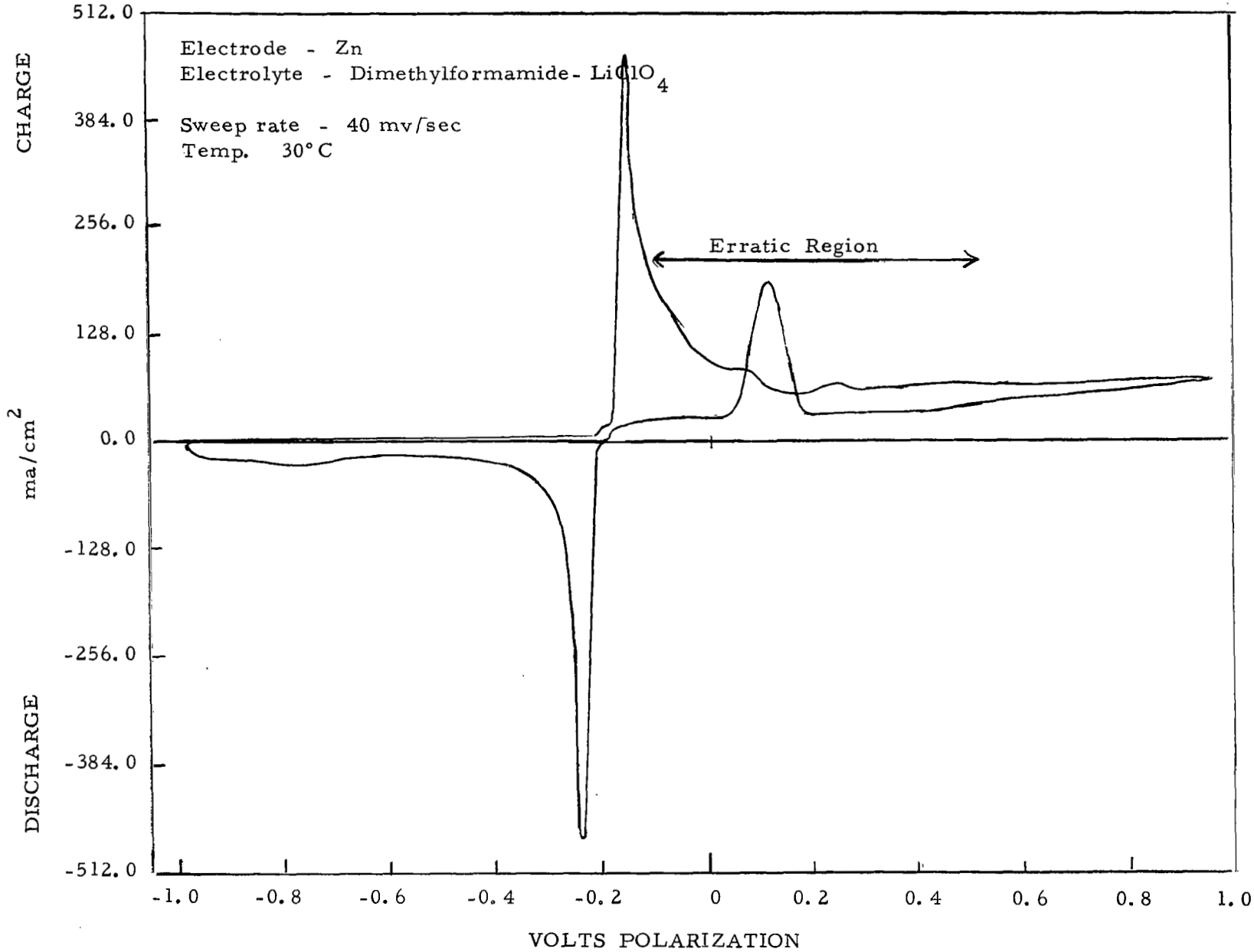
Electrode - Zn
Electrolyte - Dimethylformamide- $LiClO_4$
Sweep rate - 40 mv/sec
Temp. 30°C
Erratic Region
CHARGE
DISCHARGE
ma/cm^2
512.0
384.0
256.0
128.0
0.0
-128.0
-256.0
-384.0
-512.0
-1.0
-0.8
-0.6
-0.4
-0.2
0
0.2
0.4
0.6
0.8
1.0
VOLTS POLARIZATION

Figure 29

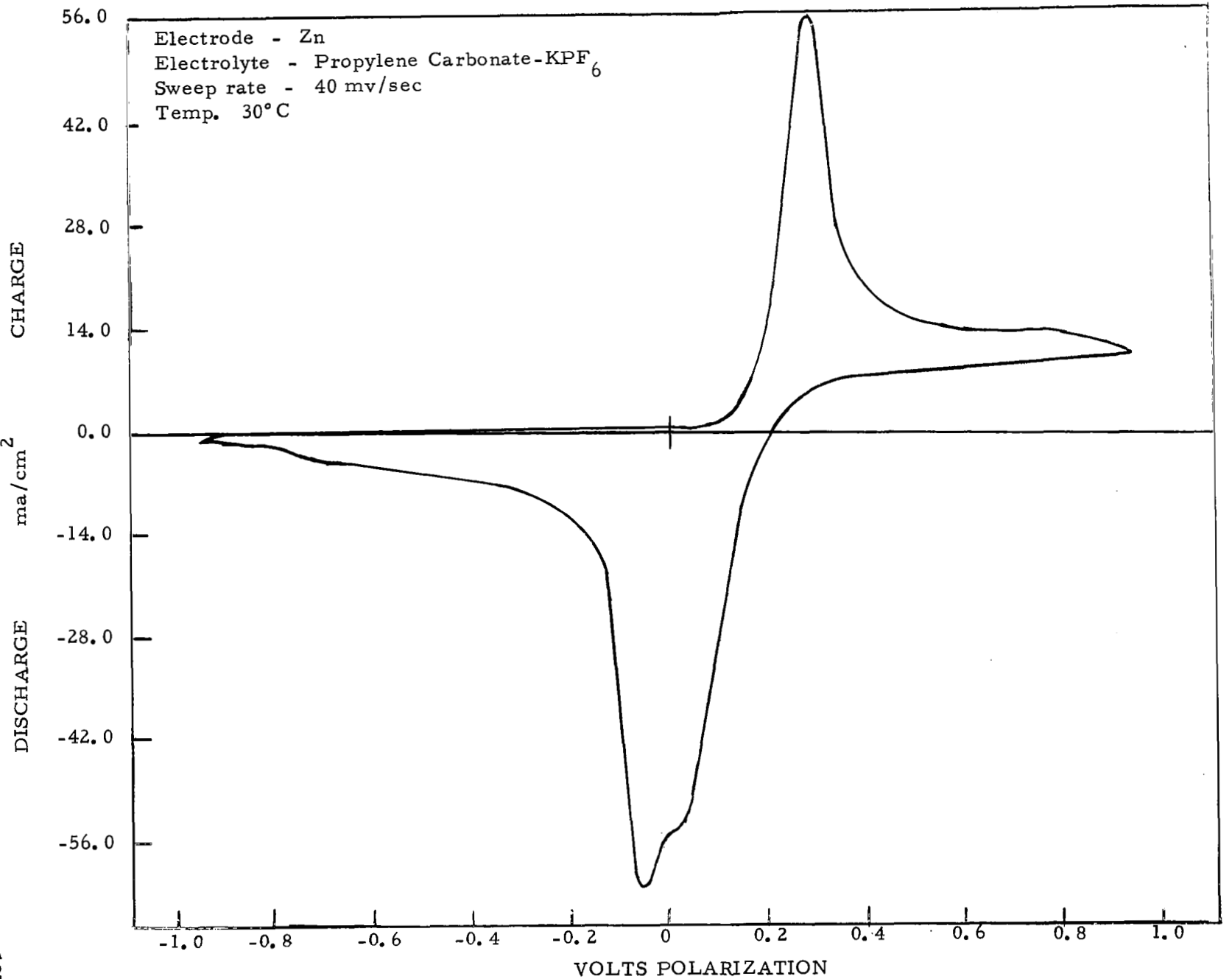
Electrode - Zn
Electrolyte - Propylene Carbonate-KPF_6
Sweep rate - 40 mv/sec
Temp. 30°C
56.0
42.0
28.0
14.0
0.0
-14.0
-28.0
-42.0
-56.0
CHARGE
DISCHARGE
ma/cm^2
-1.0
-0.8
-0.6
-0.4
-0.2
0
0.2
0.4
0.6
0.8
1.0
VOLTS POLARIZATION

Figure 30

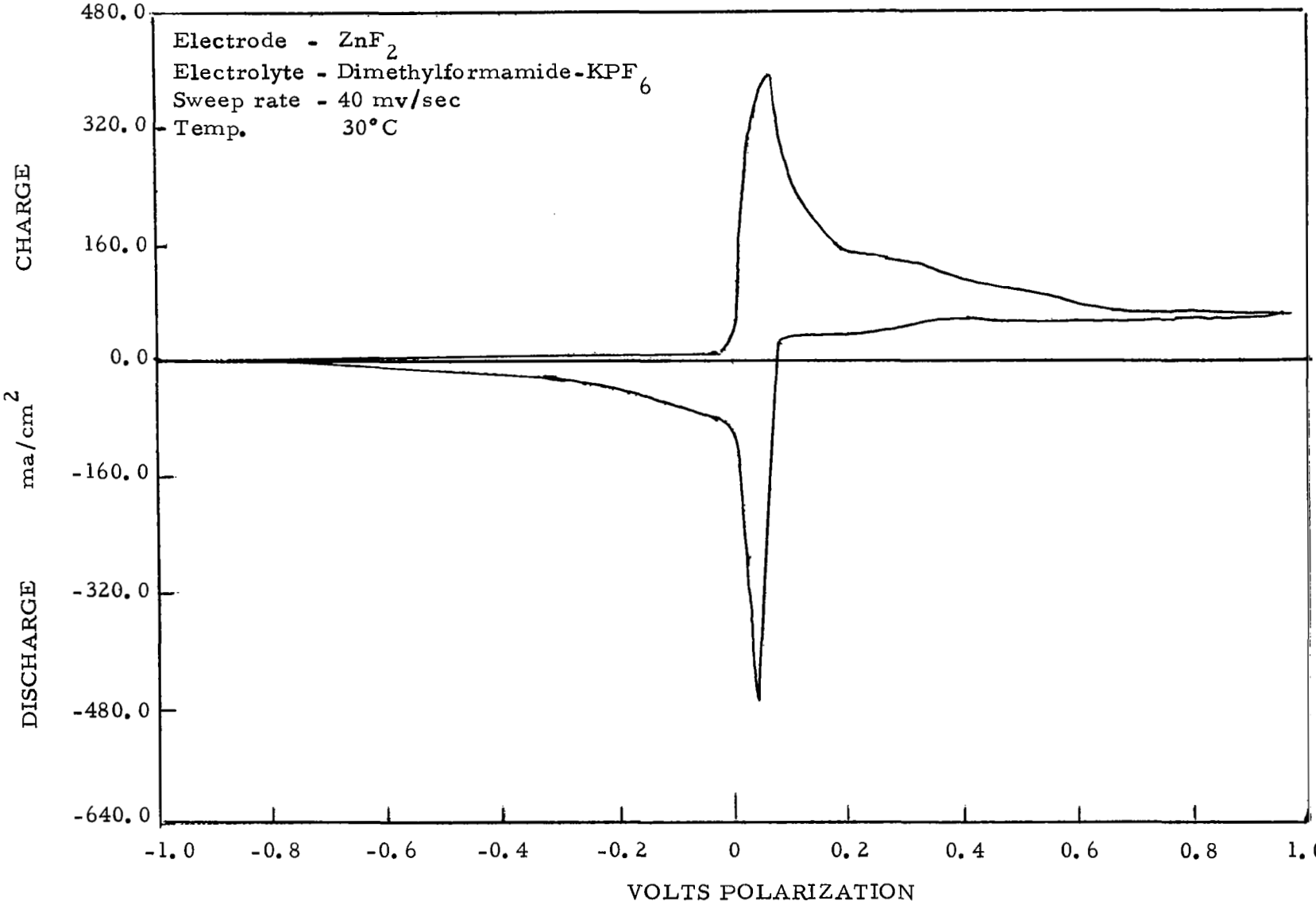
Electrode - ZnF_2
Electrolyte - Dimethylformamide-KPF_6
Sweep rate - 40 mv/sec
Temp. 30°C
480.0
320.0
160.0
0.0
-160.0
-320.0
-480.0
-640.0
CHARGE
DISCHARGE
ma/cm^2
-1.0
-0.8
-0.6
-0.4
-0.2
0
0.2
0.4
0.6
0.8
1.0
VOLTS POLARIZATION

Figure 31

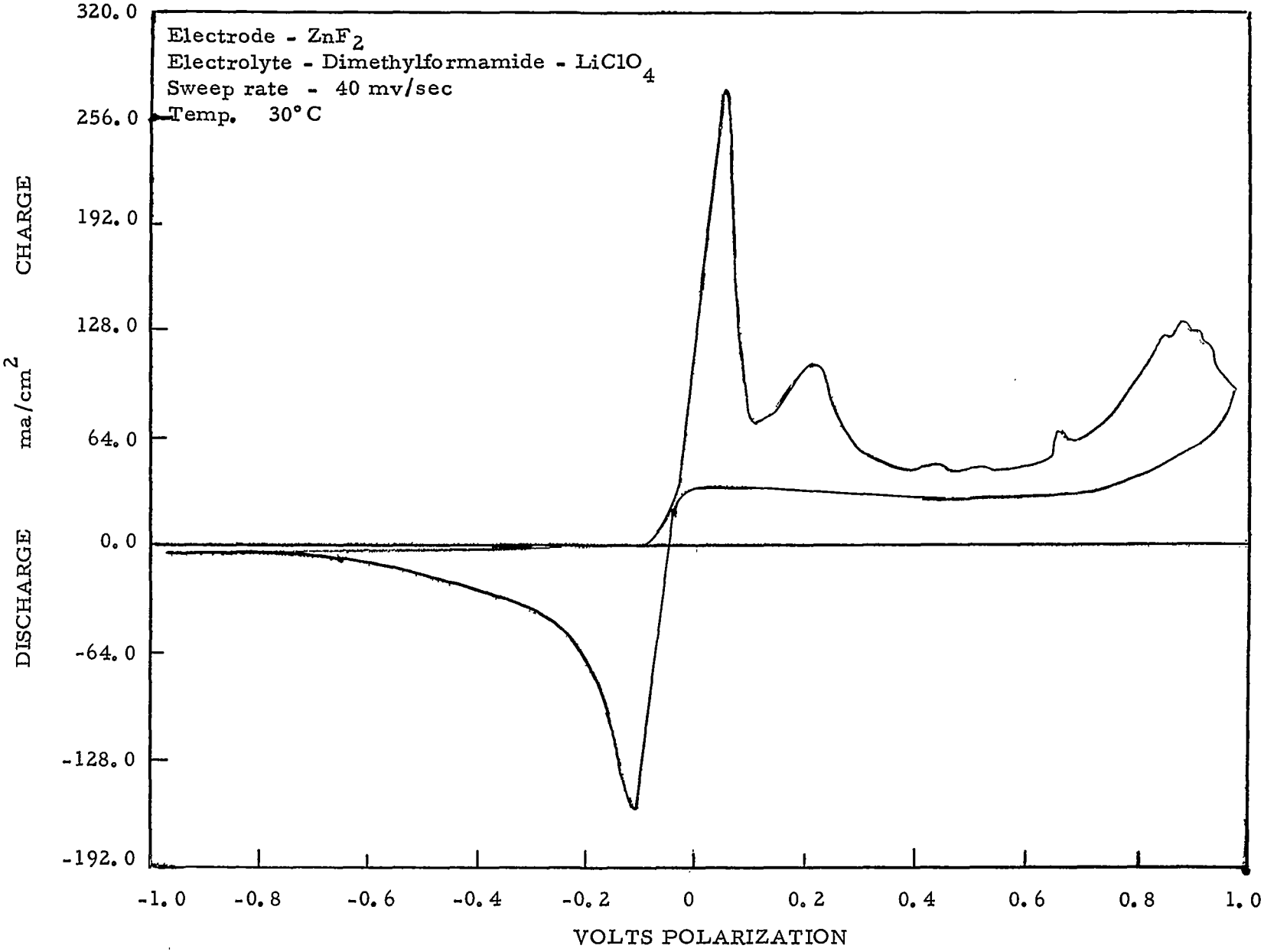
Electrode - ZnF_2
Electrolyte - Dimethylformamide - $LiClO_4$
Sweep rate - 40 mv/sec
Temp. 30° C
320.0
256.0
192.0
128.0
64.0
0.0
-64.0
-128.0
-192.0
CHARGE
DISCHARGE
ma/cm^2
-1.0
-0.8
-0.6
-0.4
-0.2
0
0.2
0.4
0.6
0.8
1.0
VOLTS POLARIZATION

Figure 32

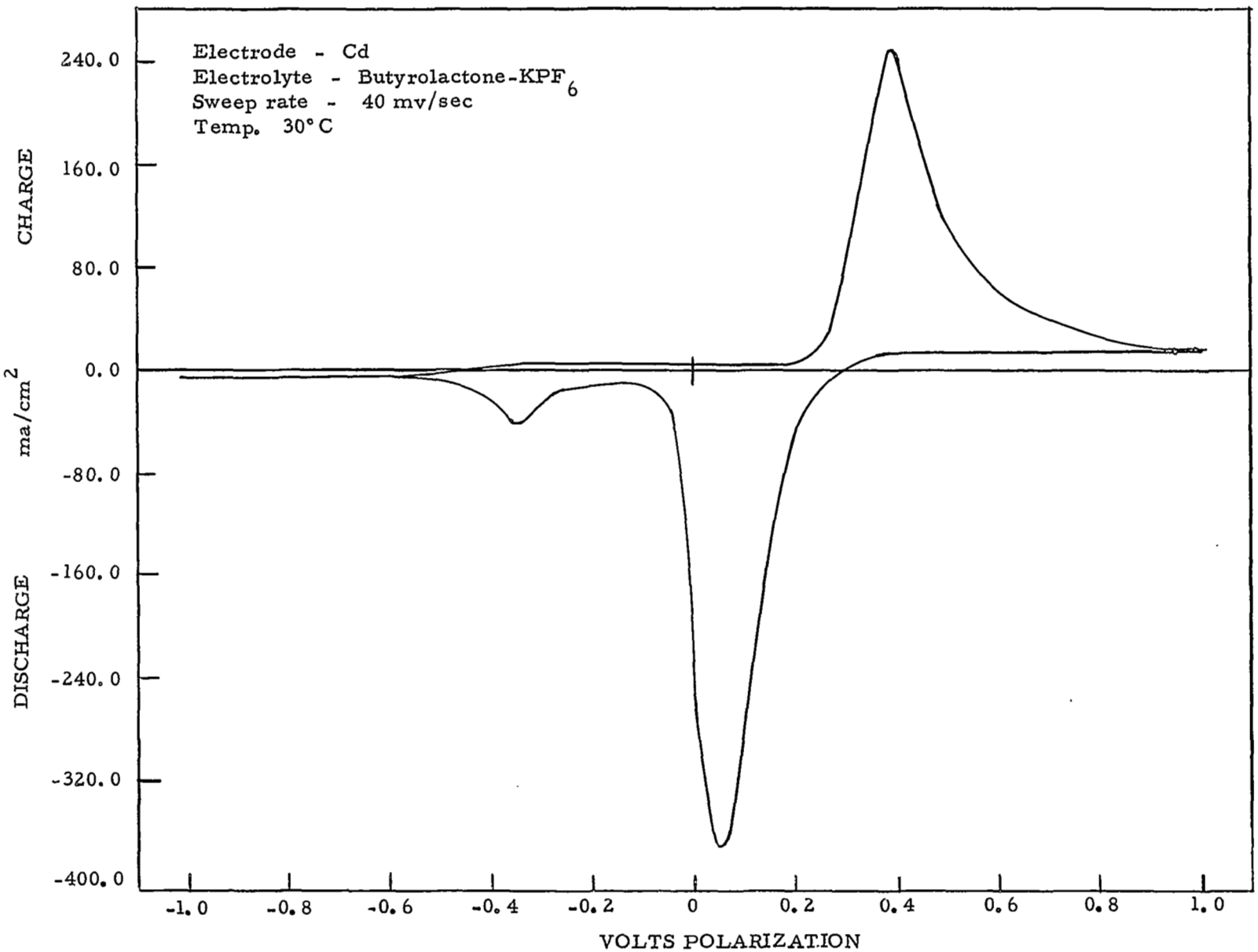
Electrode - Cd
Electrolyte - Butyrolactone-KPF6
Sweep rate - 40 mv/sec
Temp. 30° C
CHARGE
DISCHARGE
ma/cm2
240.0
160.0
80.0
0.0
-80.0
-160.0
-240.0
-320.0
-400.0
-1.0
-0.8
-0.6
-0.4
-0.2
0
0.2
0.4
0.6
0.8
1.0
VOLTS POLARIZATION

Figure 33

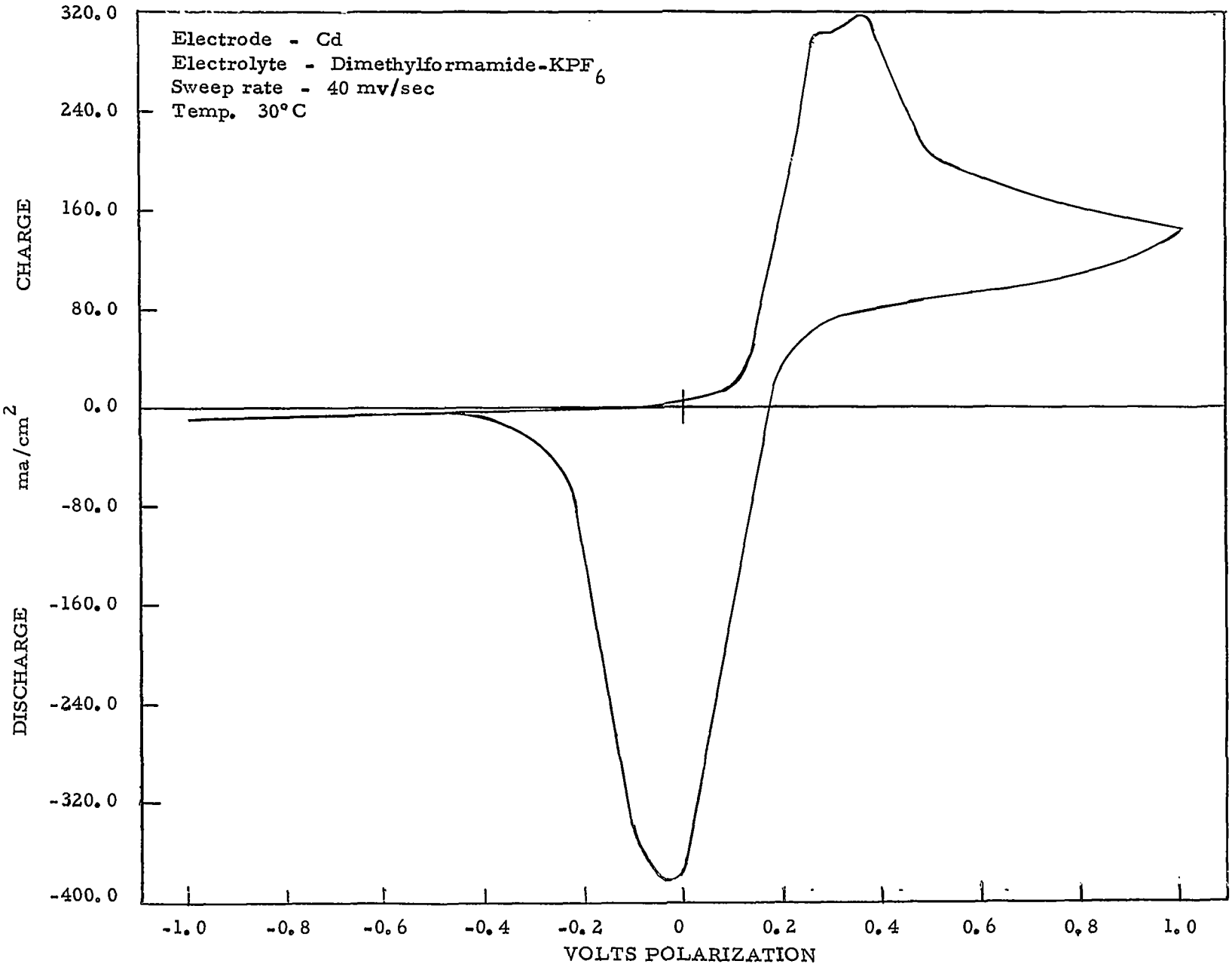
Electrode - Cd
Electrolyte - Dimethylformamide-KPF_6
Sweep rate - 40 mv/sec
Temp. 30°C
320.0
240.0
160.0
80.0
0.0
-80.0
-160.0
-240.0
-320.0
-400.0
CHARGE
DISCHARGE
ma/cm^2
-1.0
-0.8
-0.6
-0.4
-0.2
0
0.2
0.4
0.6
0.8
1.0
VOLTS POLARIZATION

Figure 34

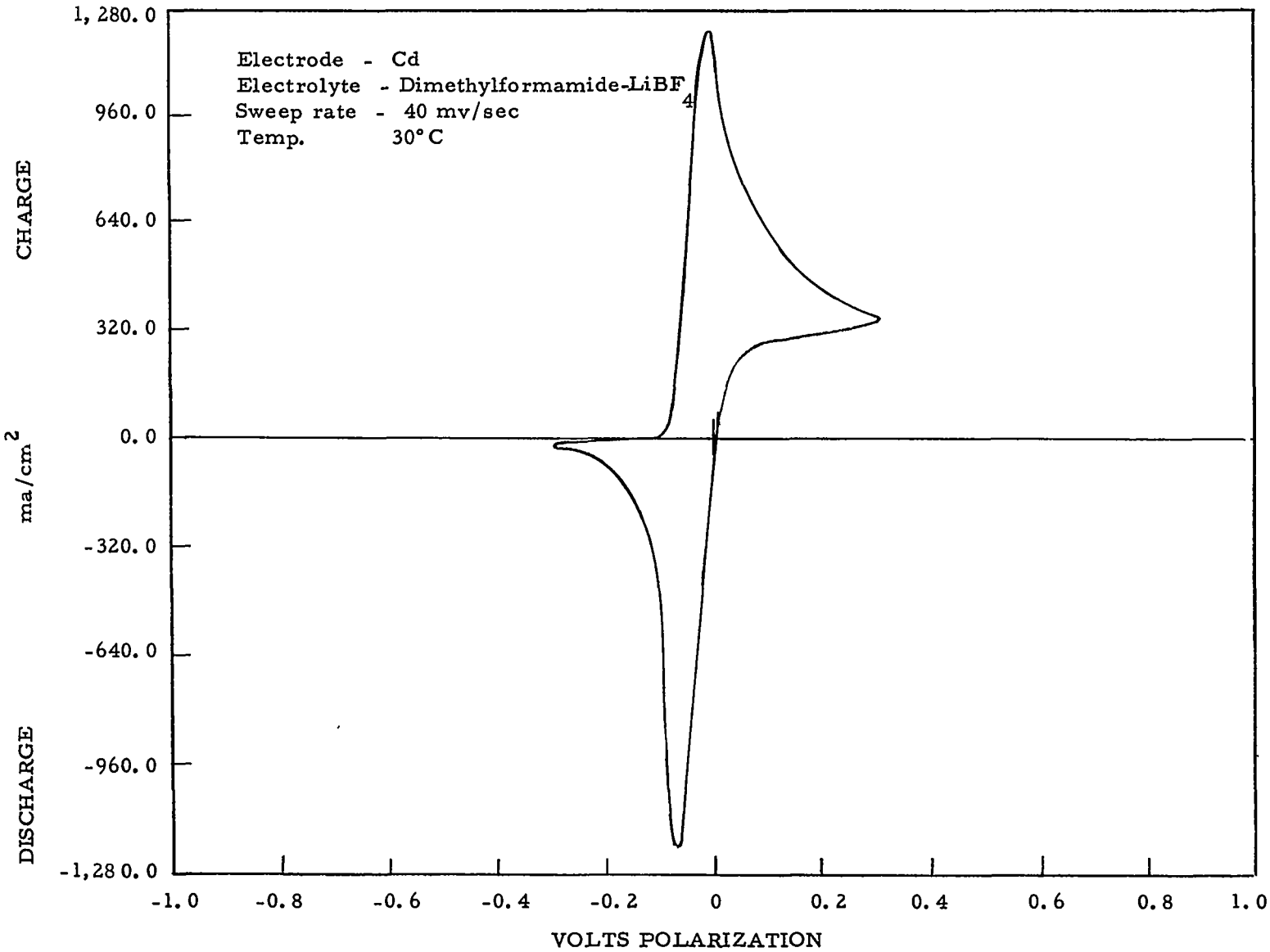
Electrode - Cd
Electrolyte - Dimethylformamide-LiBF4
Sweep rate - 40 mv/sec
Temp. 30° C
1,280.0
960.0
640.0
320.0
0.0
-320.0
-640.0
-960.0
-1,280.0
CHARGE
DISCHARGE
ma/cm2
-1.0
-0.8
-0.6
-0.4
-0.2
0
0.2
0.4
0.6
0.8
1.0
VOLTS POLARIZATION

Figure 35

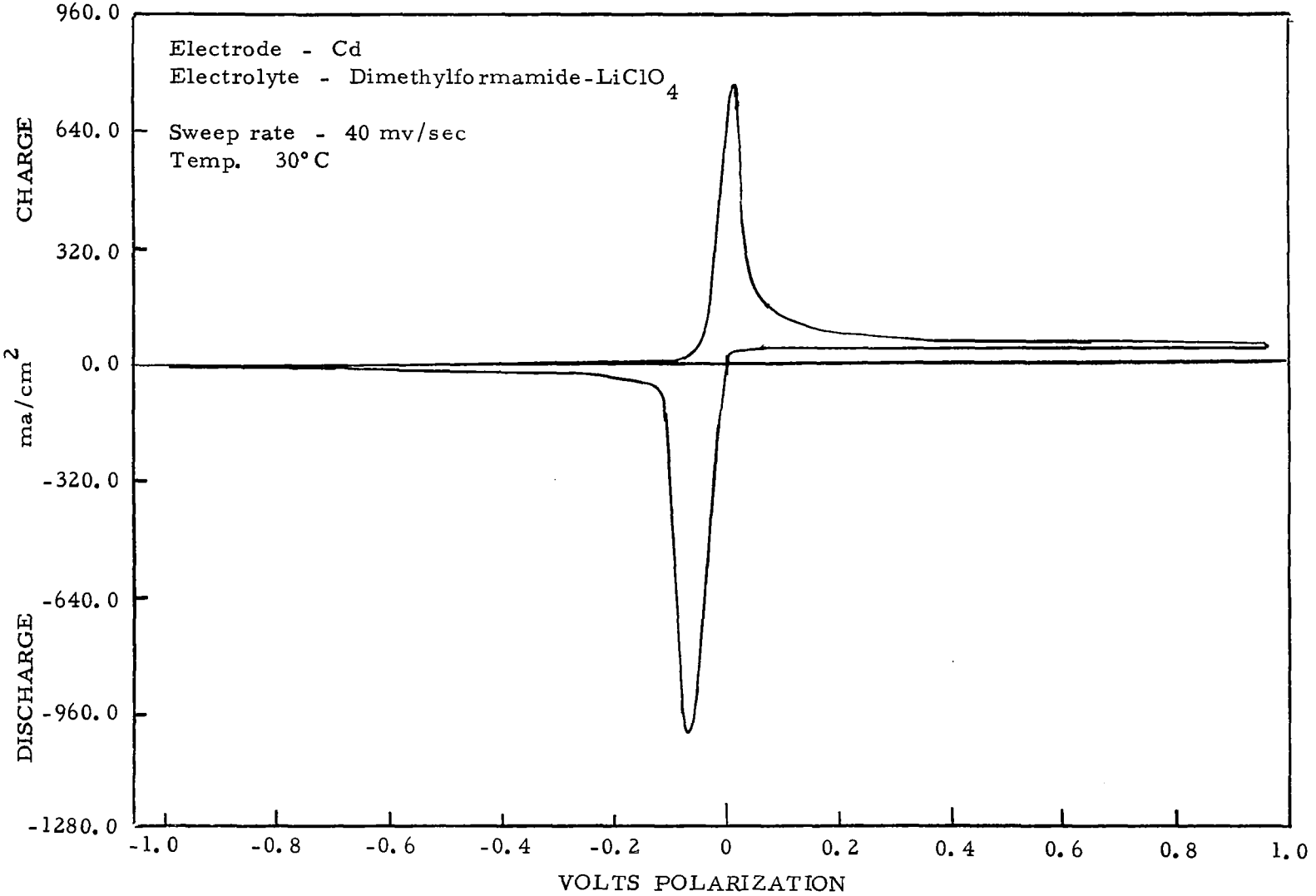
Electrode - Cd
Electrolyte - Dimethylformamide-$LiClO_4$
Sweep rate - 40 mv/sec
Temp. 30° C
960.0
640.0
320.0
0.0
-320.0
-640.0
-960.0
-1280.0
CHARGE
DISCHARGE
ma/cm^2
-1.0
-0.8
-0.6
-0.4
-0.2
0
0.2
0.4
0.6
0.8
1.0
VOLTS POLARIZATION

Figure 36

K. Galvanostatic Charge-Discharge Measurements

The major portion of the program was to screen by cyclic voltammetry a very large number of systems in order to choose those having sufficient interest for further analysis. In order to properly further evaluate the 24 recommended systems, constant current charge and discharge measurements were made on sintered-type electrodes. The purpose of this effort was to measure the discharge capacity as a function of charge input, to provide information on utilization efficiency and system reversibility as indicated by the voltage separation between charge and discharge plateaus.

Percent utilization, as used here, is defined as the ratio of the specific discharge capacity to the specific charge capacity, both expressed in coulombs per square centimeter. A plot of the discharge capacity (coulombs delivered) versus the charge capacity (coulombs passed) for different charge inputs should give a straight line whose slope represents the percent utilization. If the coulombic input exceeds that required for the desired charge reaction, so that the incremental coulombs are utilized for some other anodic reaction the product of which is not dischargeable, then the plot will depart from linearity and ultimately reach a slope of zero. This tendency towards a decreasing slope, or towards an asymptotic value, will also be indicated if the charged material becomes unavailable for discharge, either due to dissolution, material detachment, or deactivation of any kind. Also, the charge process may be more efficient than the discharge process, so that a lesser amount of charged material is discharged, this becoming more pronounced at the greater depths of conversion (higher charge capacity values).

Charge - discharge plots showing the coulombs delivered as a function of the charge input, and representative voltage-time curves are included in the figures. Discharge capacities were measured at a break in the discharge plateau at an appropriate cutoff voltage within 0.5 volt negative to the rest potential. In some instances the knee of the discharge plateau became less well-defined as the tests progressed, possibly due to increasing effective electrode area on cycling. In such cases the cutoff voltages were taken at potentials consistent within a given triplication of measurements.

Where the reduction of dissolved electroactive material was sufficient to cause a prolonged discharge, the cutoff was set at 120% of charge. Prolonged discharge occurs when the discharge current density is less than the limiting diffusion current for a given concentration of dissolved electroactive material. In this case a drop-off in the discharge plateau occurs gradually as a function of the concentration of electroactive material in the bulk solution. In most of the systems the concentration of electroactive material in the saturated electrolyte is sufficient to maintain diffusion currents of 1 ma/cm^2. If the reduction of dissolved material takes place at potentials coinciding with the discharge of solid material, the discharge may be masked or incomplete, and accordingly build up on the electrode as cycling is continued. It is likely in this case that higher limiting current values can result, depending on the dissolution rate of solid material on the electrode surface.

The highest metal ion concentration measured in previous work was 4×10^{-2} M. The limiting current for this concentration for a two-electron change at a planar electrode is less than 4 ma/cm^2 based on known results in aqeuous solution. Likewise, the contribution of dissolved material to

the transition time for a current density of 5 ma/cm^2 is of the order of 50 seconds, or less than 3% of the largest charge input (10 coul/cm^2) in these tests. Consequently a linear relationship between the coulombs passed during charge and discharge tests must represent a measure of the utilization efficiency for discharge of solid product formed during the charge reaction.

Almost all systems show a prolonged discharge at the low current density (1 ma/cm^2) giving utilization efficiencies greater than 120%. In these instances, triplicate measurements were taken only for the smallest charge input (0.10 coul/cm^2), where discharge was allowed to continue until 0.20 coul/cm^2 was passed. Single tests on all succeeding measurements at 1 ma/cm^2 were made allowing the discharge to proceed to 120% of the charge input. A minimum of three tests was made at all charge inputs where a drop-off in the voltage of the discharge plateau was evident prior to the 120% stopping point, except in those instances mentioned in the text.

In the charge-discharge plots, the circles represent the average of a minimum of three discharge tests unless otherwise indicated. The variation within each set of tests is shown by the vertical lines, the cross bars indicating individual test results. The sequence of a given test result within a set of measurements is indicated by the number next to each bar. In some cases the reproducibility of three tests lies within the range of the circle.

1. Silver Oxide Electrode in Butyrolactone-$LiCl + AlCl_3$

Initial discharge for this system was nil. Immediate polarization on discharge was greater than 0.8 volts. Less than 15% utilization of the 10 coul/cm^2 electroformed silver oxide was recovered at a current density of 3 ma/cm^2. The regular testing procedure was followed after these initial discharge tests. Charge-discharge plots for this system are linear with a slope indicating a utilization efficiency better than 80% for both the 1 and 5 ma/cm^2 tests. These are shown as Figures 37 and 38. The voltage separating charge and discharge plateaus at 1 and 5 ma/cm^2 are 0.3 and 0.5 volts respectively. Results indicate the discharge of solid state material formed during the charge cycle at all capacities. This system is recommended for further study.

2. Copper Electrode in Acetonitrile-$LiPF_6$ + KPF_6

This system exhibited prolonged discharge at all charge input values for both 1 and 5 ma/cm^2. The voltage separating the charge and discharge plateaus at 5 ma/cm^2 was 0.12 v, indicating high electrochemical activity for dissolved material. Examination of the electrode showed that extensive disintegration had taken place, with only a small portion remaining attached to the lead wire contact. Results indicate a high contribution to the discharge due to dissolved electroactive copper material, and loss of electrode integrity on charge. This system should be eliminated from further study.

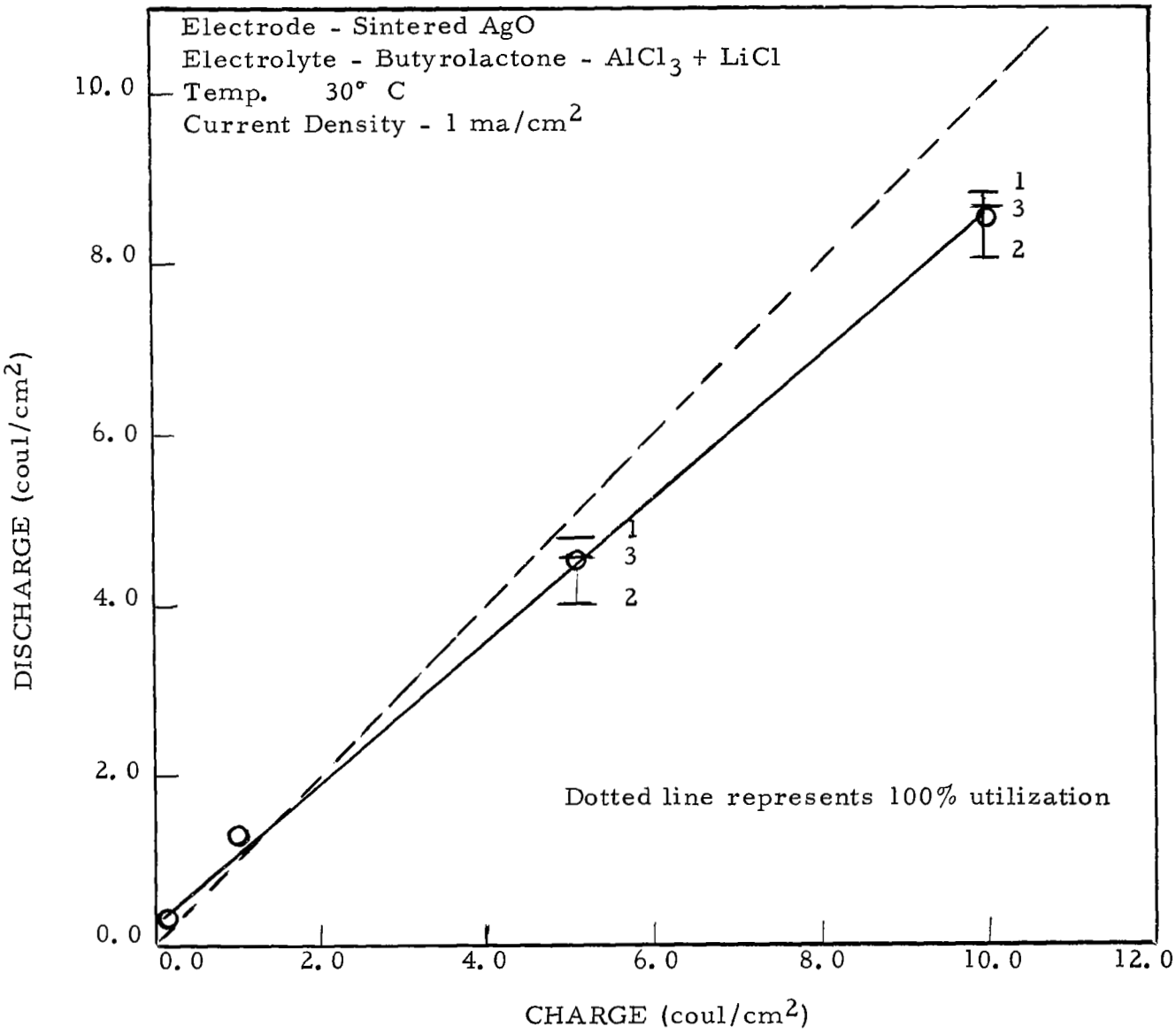

Figure 37. Coulombs delivered as a function of coulombs passed

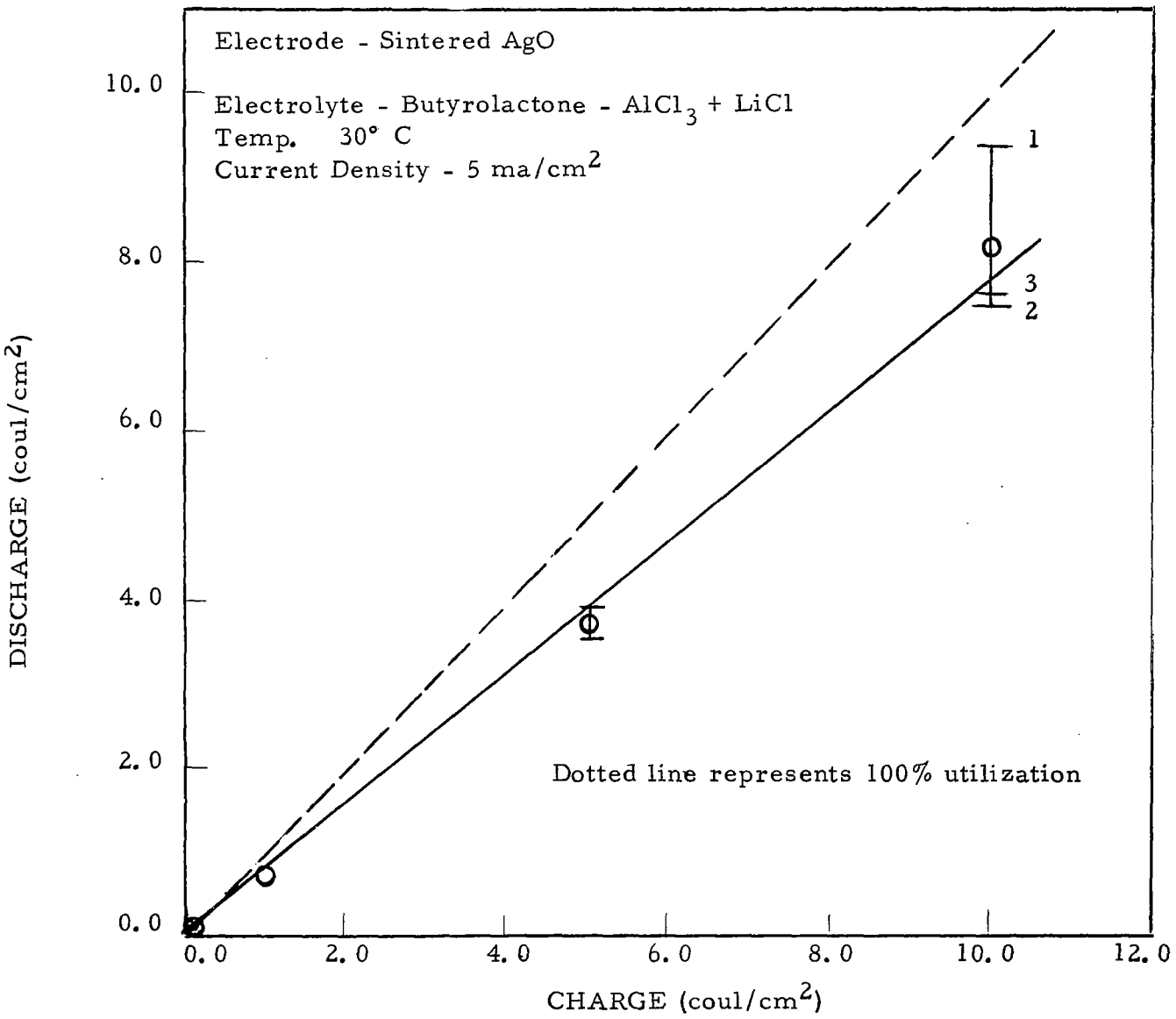

Figure 38. Coulombs delivered as a function of coulombs passed

3. Copper Electrode in Dimethylformamide-$LiPF_6$

This system showed prolonged discharge (utilization efficiency greater than 120%) for the 1 ma/cm^2 tests. The voltage separating the charge and discharge plateau was only 0.03 volts at 1 ma/cm^2 indicating high electrochemical activity for dissolved material. A drop-off in the discharge plateau occurred only for the 5 ma/cm^2 tests where the voltage separation was 0.1 volts. The charge-discharge plot is shown in Figure 39.

The average utilization efficiency for all charge inputs at 5 ma/cm^2 is 42%. Reproducibility is good for the two lowest charge input values, however a spread from 1.3 to 4.8 coul/cm^2 results at the 5 coul/cm^2 charge input, with values increasing with cycling. A similar effect is noted at the 10 coul/cm^2 charge input. Only two tests were made at this point since loss of contact caused by electrode disintegration occurred after the second discharge cycle. Examination of several pieces of the electrode, which had fallen to the bottom of the cell, revealed a large hole pattern had developed in the central portion of the electrode. This system should be eliminated from further study.

4. Copper Fluoride Electrode in Dimethylformamide-$LiPF_6$

The test procedure remained the same except that an initial discharge is introduced to bring the electrode to an initial discharged state.

Discharge of active material occurred readily for the CuF_2/DMF-$LiPF_6$ system at 5 ma/cm^2. The discharge time to a cutoff voltage of - 0.6 v corresponded to 20 coul/cm^2, which was better than 80% utilization based on weight gain measurements for a controlled electrode. The regular test procedure was then followed after this initial discharge.

Prolonged discharge (utilization efficiency greater than 120%) occurred for

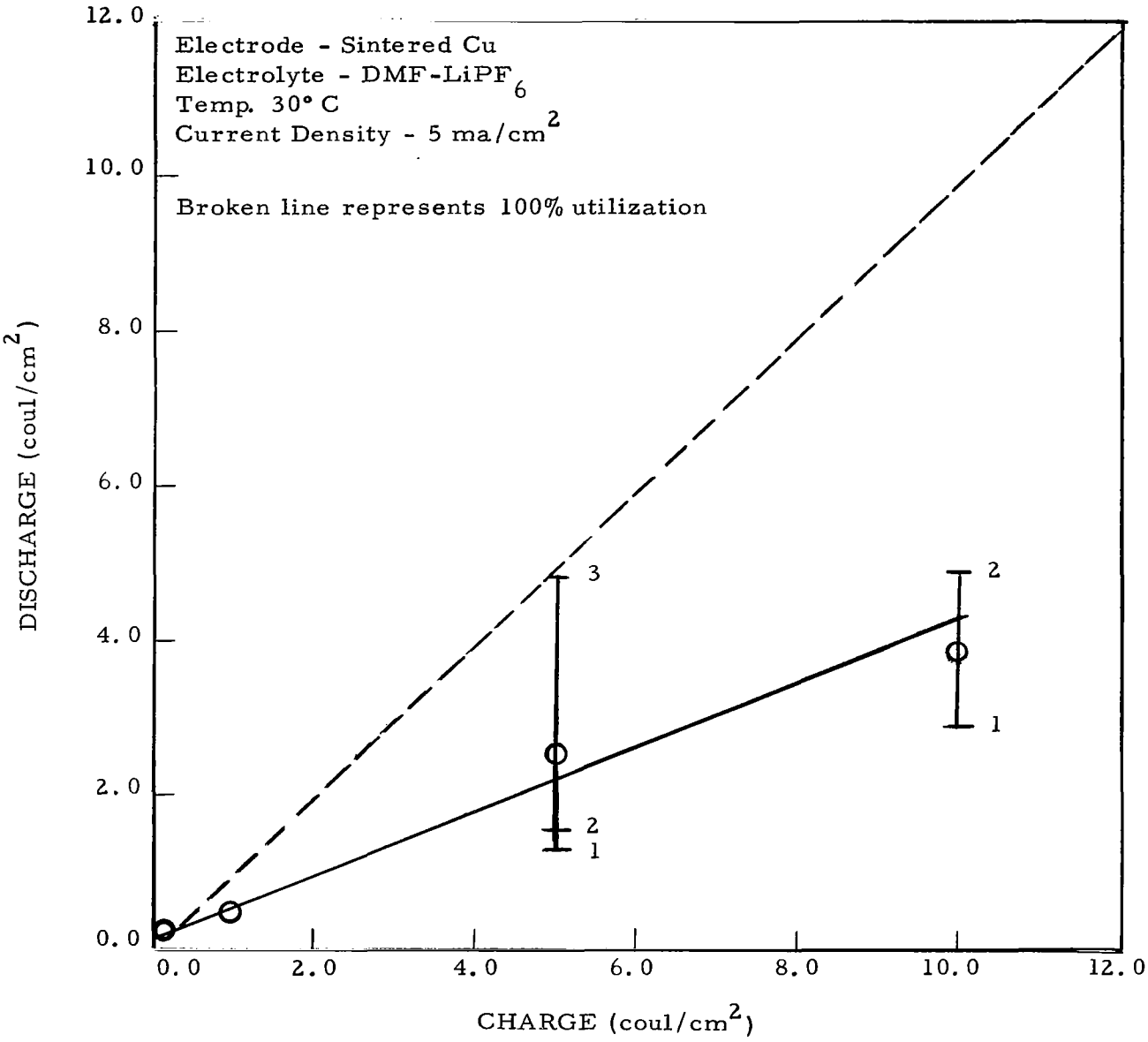

Figure 39. Coulombs delivered as a function of coulombs passed

all tests at 1 ma/cm^2. The charge-discharge plot for the 5 ma/cm^2 tests is shown in Figure 40. The utilization efficiency based on the best straight line through all the points is 72%. Polarization between charge and discharge plateaus is 0.3 volts. The discharge curve for the largest charge input is shown in Figure 41. Further testing of this system is recommended.

5. Copper Fluoride Electrode in Propylene carbonate-$LiPF_6$

Initial discharge of chemoformed fluoride material for the CuF_2/PC-$LiPF_6$ system was nil. A discharge plateau resulted only for currents less than 0.5 ma/cm^2. However, charge-discharge curves at 1 ma/cm^2 revealed measurable charge utilization and therefore the regular testing procedure was followed. The time-voltage curves showed polarization between charge and discharge plateaus of 0.5 and 1.2 volts respectively for the 1 and 5 ma/cm^2 tests. The charge-discharge plots (Figures 42 and 43) also show strong dependence on current density, giving an average utilization efficiency of 75% at 1 ma/cm^2 and 5% for the 5 ma/cm^2 tests. Only one point was obtained at the 10 coul/cm^2 charge input due to separation at the wire lead-electrode junction. This is one of the few systems in which the discharge at the 1 ma/cm^2 current density is not masked by prolonged discharge of dissolved active material. It is likely that the chemoformed fluorination product on the electrode surface is a controlling factor affecting the charge-discharge process. Further characterization of this system is in order.

6. Copper Chloride Electrode in Dimethylformamide-$LiPF_6$

Initial discharge of the chemoformed copper chloride electrode at 4 ma/cm^2 corresponded to 21 coul/cm^2. The regular testing procedure was followed after this initial test.

Tests on this system showed a variation in the charge and discharge

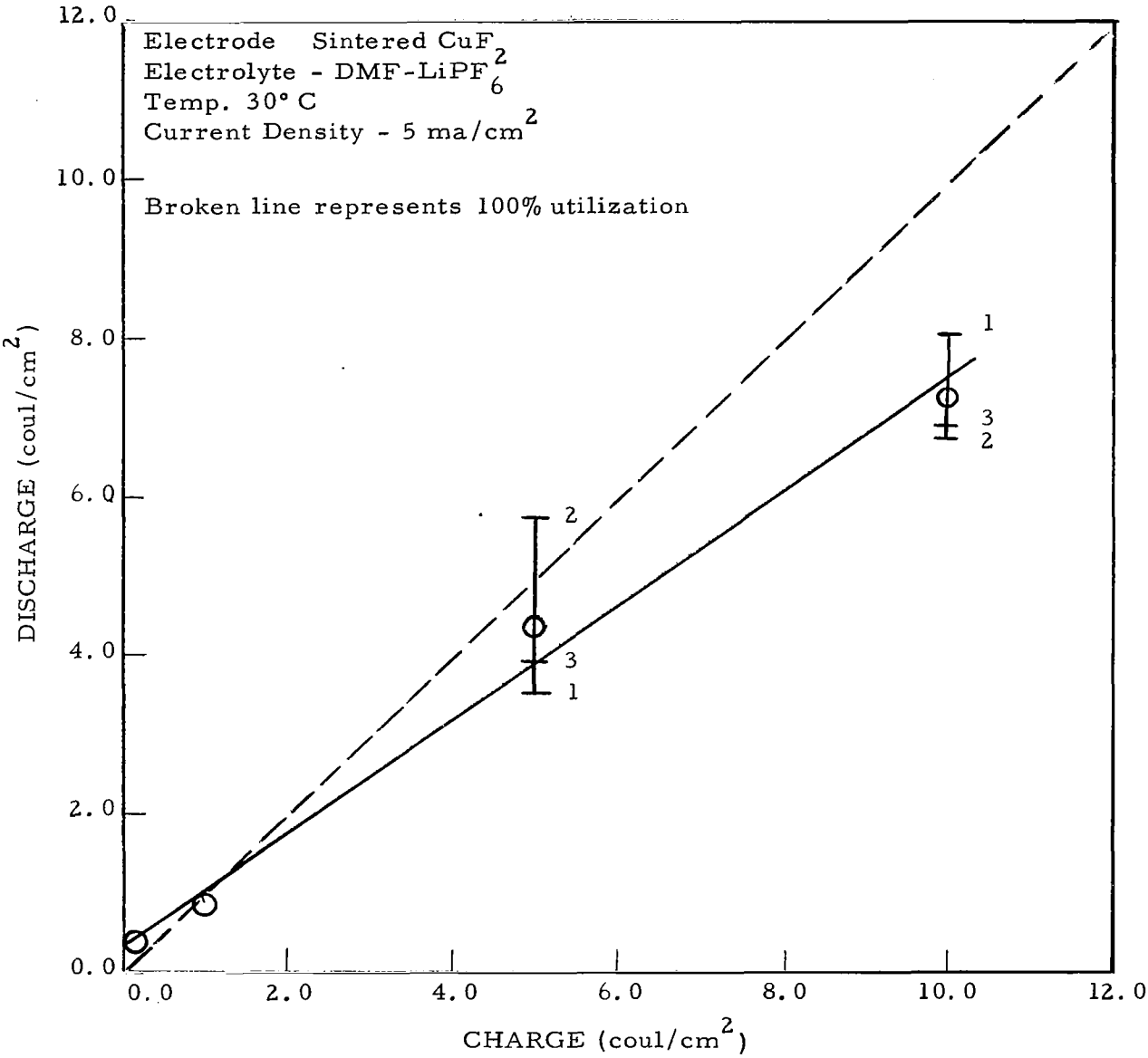

Figure 40. Coulombs delivered as a function of coulombs passed

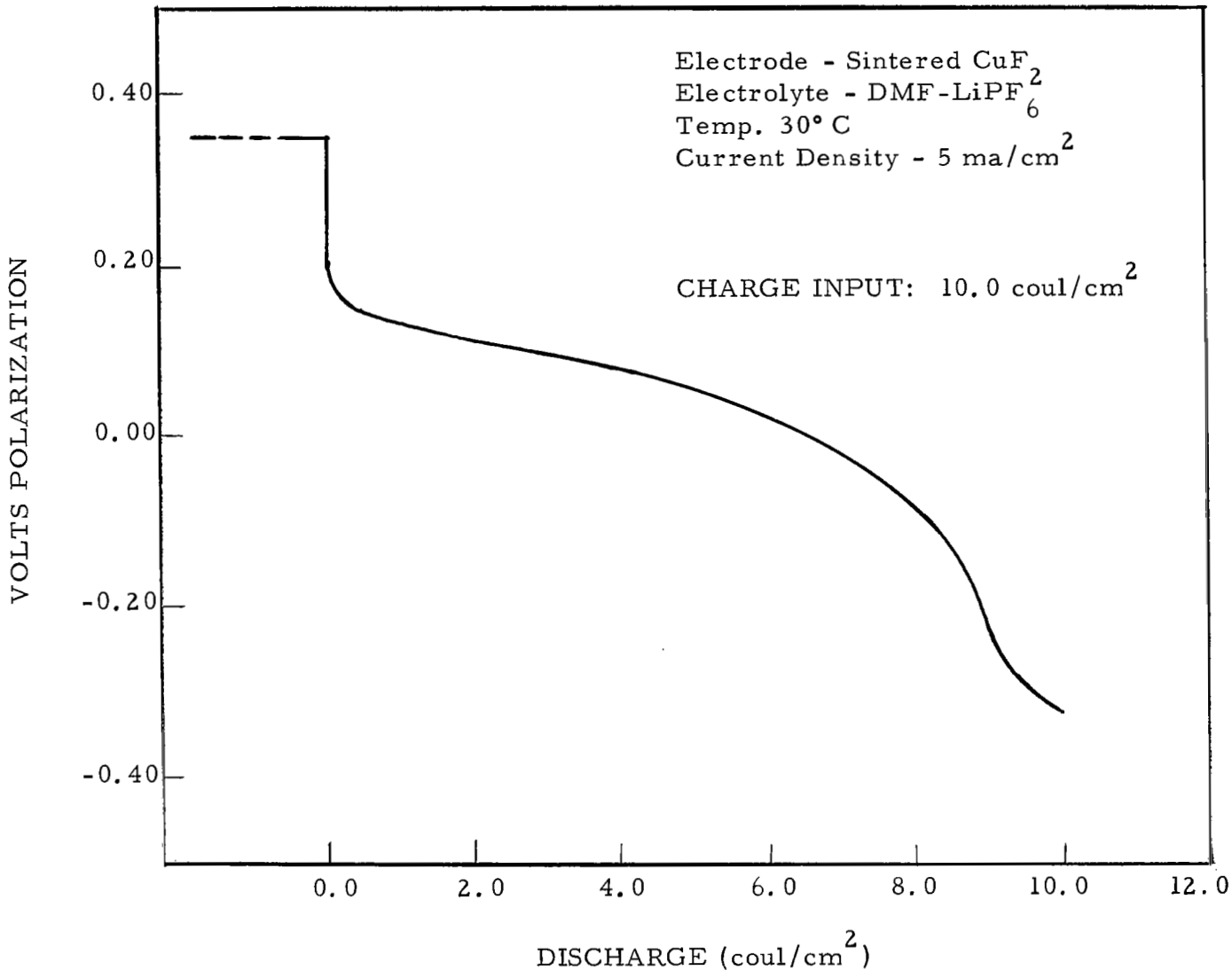

Figure 41. Discharge curve for CuF_2/DMF-$LiPF_6$

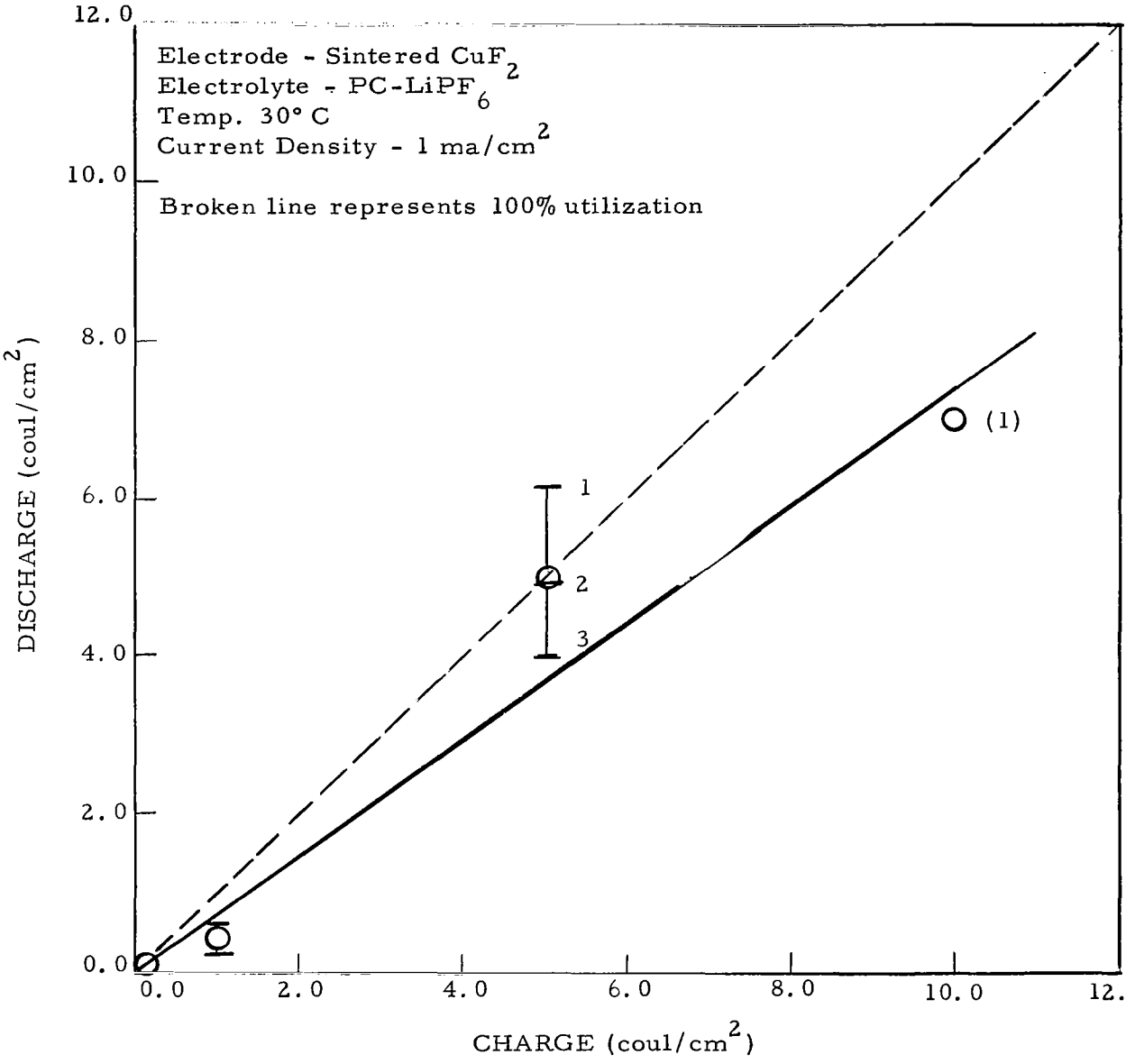

Figure 42. Coulombs delivered as a function of coulombs passed

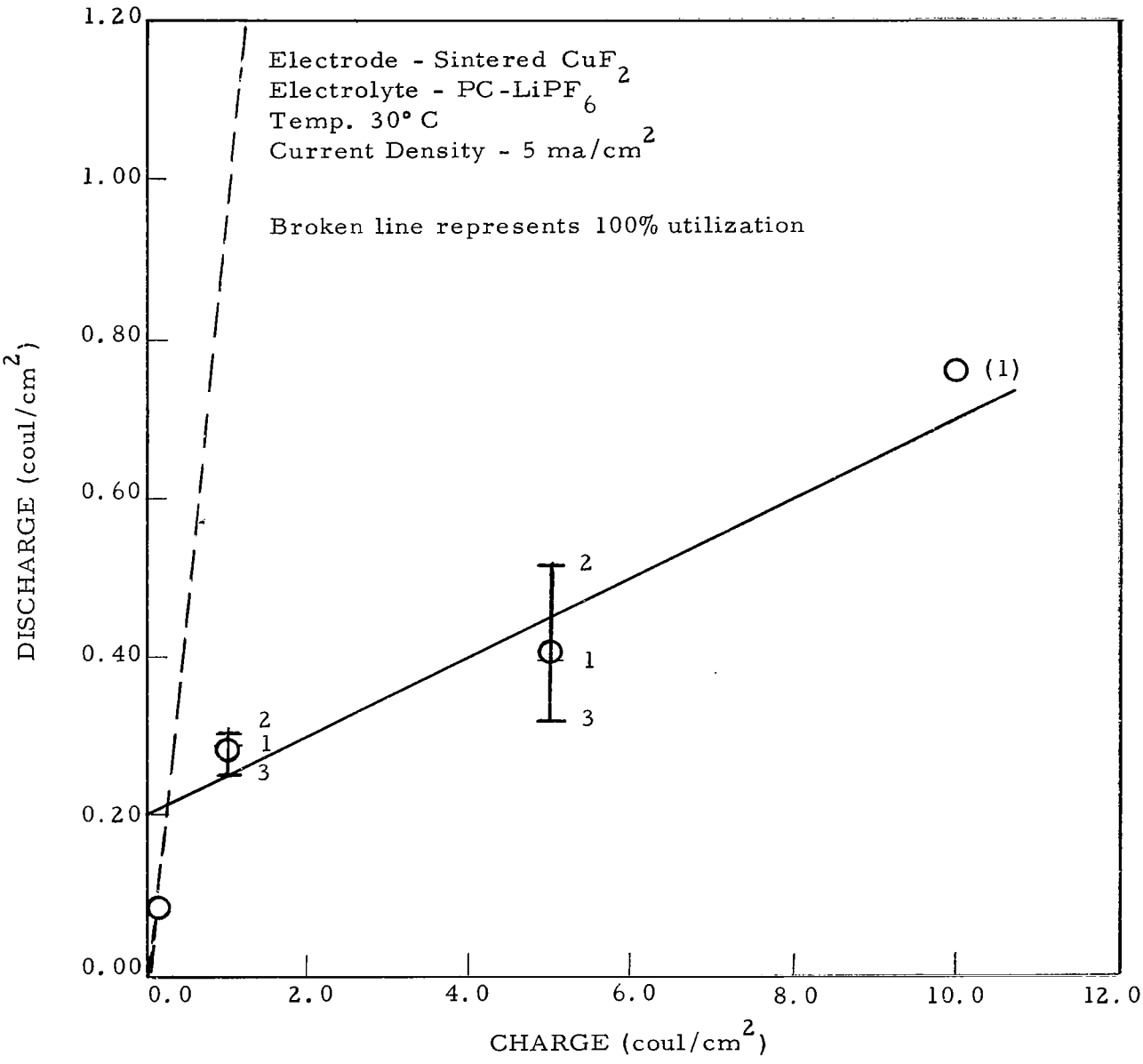

Figure 43. Coulombs delivered as a function of coulombs passed

potential for the first few charge input values. During this time both the charge and discharge plateaus occurred at positive potentials. The tests at 1 ma/cm^2 showed a two plateau charge at + 0.2 and + 0.4 volts, with a discharge at + 0.2 volts, with about 50% utilization efficiency at 0.10 coul/cm^2 charge. The 5 ma/cm^2 tests for the 0.10 coul/cm^2 charge showed a single charging plateau at + 0.25 volts with no discharge. A second charging plateau was observed at + 0.7 volts (at the 1.0 coul/cm^2 charge) with about 20% utilization. Similar results occurred for 1 ma/cm^2 at the 1 coul/cm^2 test. These effects disappeared after an overnight stand whereupon all tests at 1 ma/cm^2 showed prolonged discharge, and only single charge plateaus were observed for both high and low current densities. The remainder of the tests at 5 ma/cm^2 showed two discharge plateaus within - 0.3 v relative to the reference electrode, with overall utilization varying between 80 and 130%, indicating a high contribution due to dissolved material. The charge-discharge plot for the 5 ma/cm^2 tests is shown in Figure 44. The results suggest an effect due to residual chloride material remaining within the pores of the electrode from the initial discharge of the chemoformed copper chloride. The chloride ion would be expected to diffuse gradually to the bulk solution because of the high solubility (greater than 2 m) of LiCl in DMF. Further testing with controlled chloride ion concentration is required to clarify these results.

7. Copper Chloride Electrode in Acetonitrile-$LiPF_6$

Initial discharge of this system occurred readily at 5 ma/cm^2, indicating greater than 90% utilization of the chemoformed material. The regular tests which followed this initial discharge showed no drop-off in the discharge plateau for either the 1 or 5 ma/cm^2 tests. The voltages separating the charge and discharge plateaus were 0.3 and 0.5 volts for the low and high current densities respectively. The results are similar to those observed for the Cu/AN-$LiPF_6$ + KPF_6 system and suggest that diffusion of residual chloride ion away from the electrode surface occurs

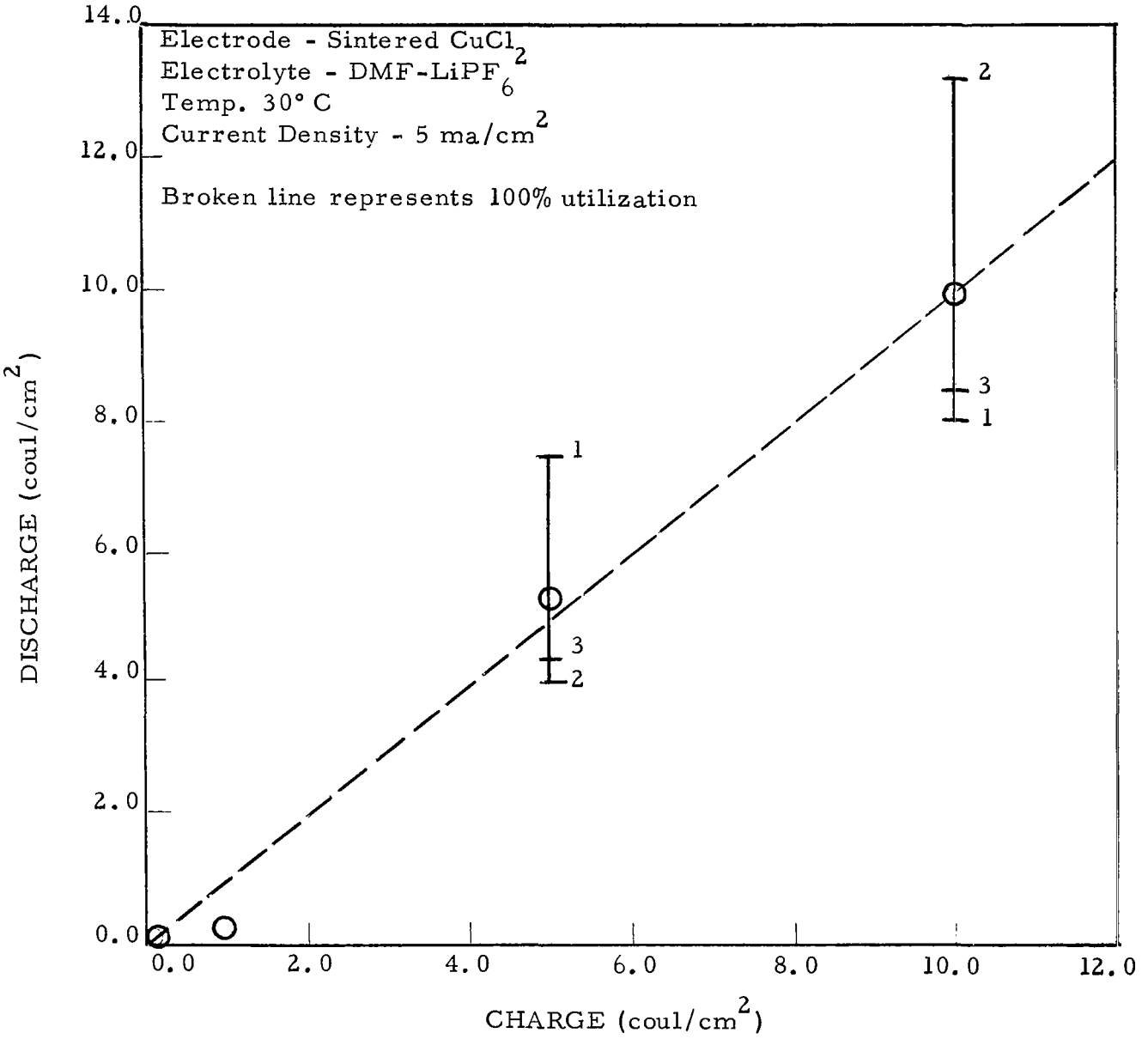

Figure 44. Coulombs delivered as a function of coulombs passed

rapidly, most of it taking place probably during the preconditioning phase of the test procedure. This system is not recommended for further study.

8. Copper Chloride Electrode in Propylene carbonate-$LiClO_4$

Initial discharge of chemoformed copper chloride in this electrolyte was poor. Electrode polarization at current densities greater than 1 ma/cm^2 was more than 1 volt and therefore no measure of active chloride material was obtained. The regular testing procedure was followed after these initial tests.

Prolonged discharge for the 1 ma/cm^2 tests occurred at charge inputs of 0.10 and 1.0 coul/cm^2, while drop-offs in the discharge plateau occurred for the 5 and 10 coul/cm^2 tests. No tests at 5 ma/cm^2 were completed since electrode polarization greater than 1 volt for both charge and discharge cycles was observed. The voltage separating the charge and discharge plateaus for the 1 ma/cm^2 tests was initially greater than 0.7 v, but then began to decrease with cycling during the 5 coul/cm^2 tests, and was less than 0.4 v for the 10 coul/cm^2 test. Only one test at 1 ma/cm^2 was completed at this highest charge input due to loss of contact as a result of electrode disintegration.

The charge-discharge plot for this system is shown in Figure 45. The average utilization efficiency for the three tests at 5 coul/cm^2 is 84% while the point at 10 coul/cm^2 corresponds to 96%. This system merits further study in view of the improvement of the charge-discharge characteristics with cycling, and the high utilization efficiency.

9. Zinc Electrode in Acetonitrile-$LiClO_4$

This system showed prolonged discharge at 1 ma/cm^2 with relatively no polarization separating the charge and discharge plateaus, indicating, high

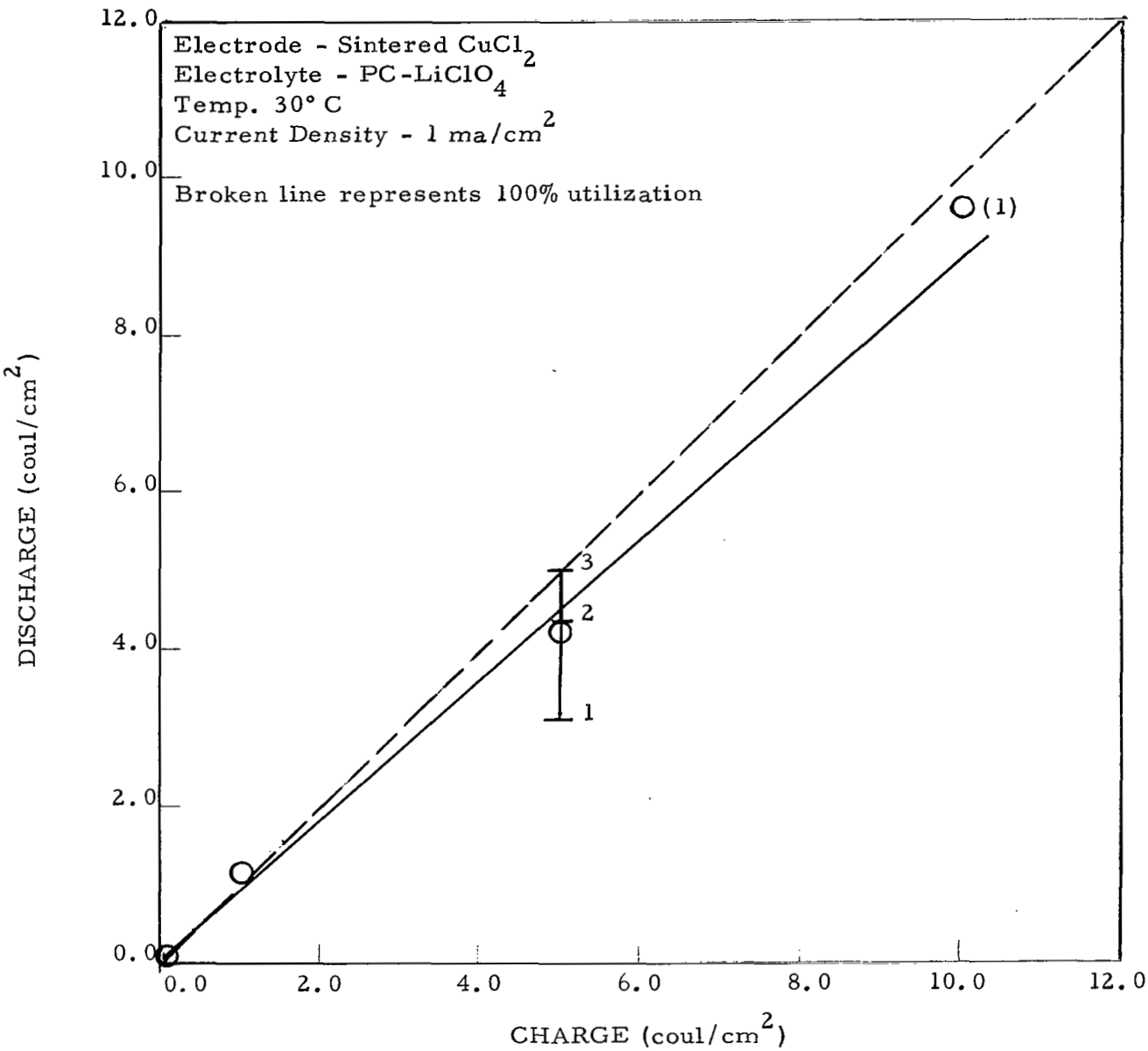

Figure 45. Coulombs delivered as a function of coulombs passed

electrochemical activity for dissolved active material.

The charge-discharge plot for this system (Figure 46) for the 5 ma/cm^2 tests shows discharge capacities less than 0.8 coul/cm^2 at all charge inputs. These results indicate poor utilization of solid state active material. No further tests are recommended.

10. Zinc Electrode in Dimethylformamide-$LiClO_4$

Test results were similar to those for Zn/AN-$LiClO_4$. The charge-discharge plot is shown in Figure 47. This system is not recommended for further tests.

11. Zinc Electrode in Dimethylformamide-$LiPF_6$

The system Zn/DMF-$LiPF_6$ shows prolonged discharge with low polarization at 1 ma/cm^2 indicating high electrochemical activity for dissolved material. The utilization efficiency at 5 ma/cm^2, while linear up to the 5 coul/cm^2, is less than 60% and then tends to drop off to an average of 37% at 10 coul/cm^2. The charge-discharge plot is shown in Figure 48. The results indicate that charging of this electrode to higher charge inputs proves detrimental to its utilization efficiency. This system does not merit further study.

12. Zinc Electrode in Dimethylformamide-KPF_6

Charge-discharge tests were carried out in two electrolyte concentrations at 0.75 m and 2.0 m. Both systems show prolonged discharges at 1 ma/cm^2 with low polarization, indicating activity for dissolved material. At 5 ma/cm^2, the voltage separating the charge and discharge plateaus was 0.3 v for the lower concentration, and 0.6 v for the high concentration, as seen in Figure 49. A pronounced cycling effect is evident in the charge-discharge

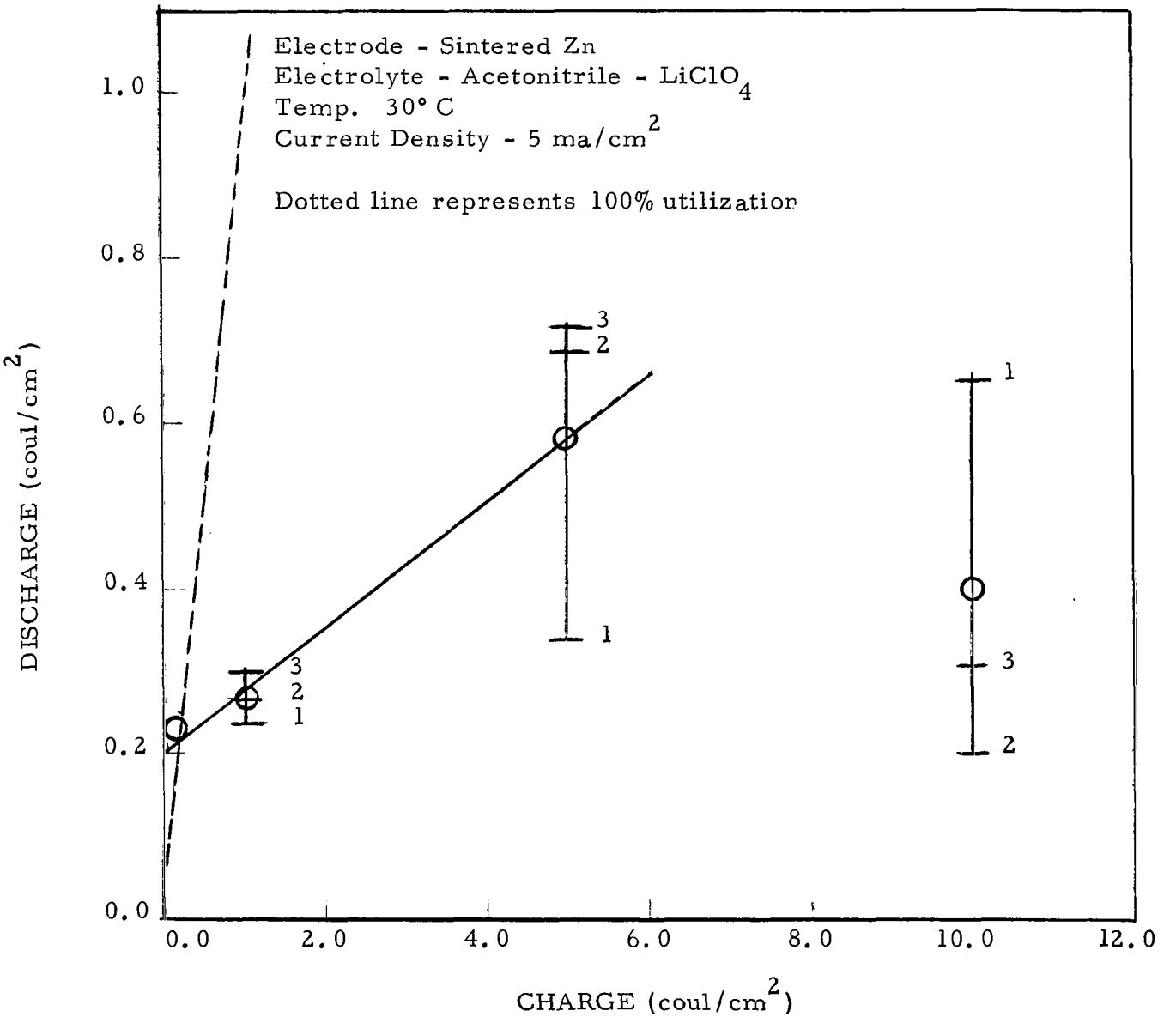

Figure 46. Coulombs delivered as a function of coulombs passed

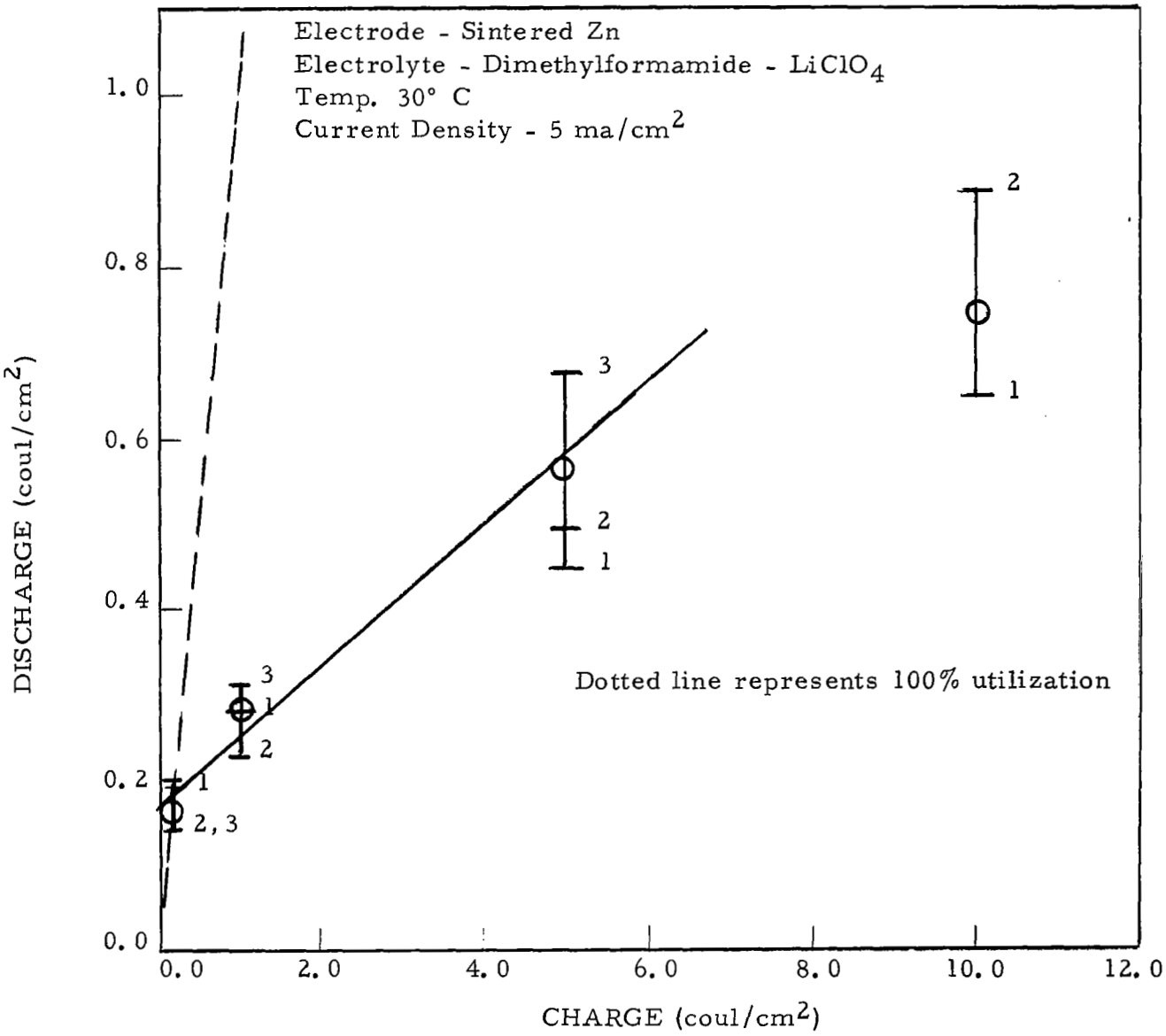

Figure 47. Coulombs delivered as a function of coulombs passed

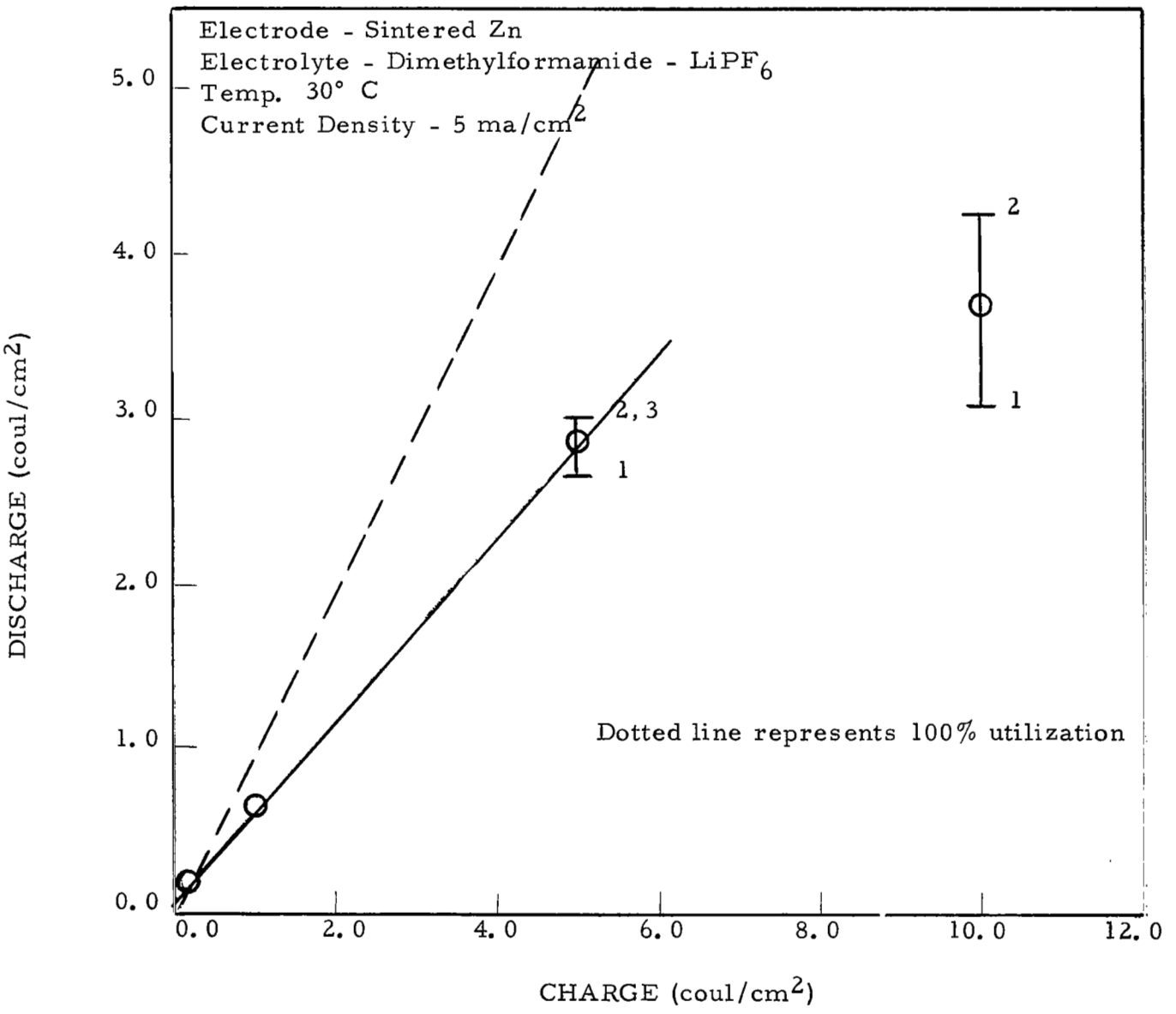

Figure 48. Coulombs delivered as a function of coulombs passed

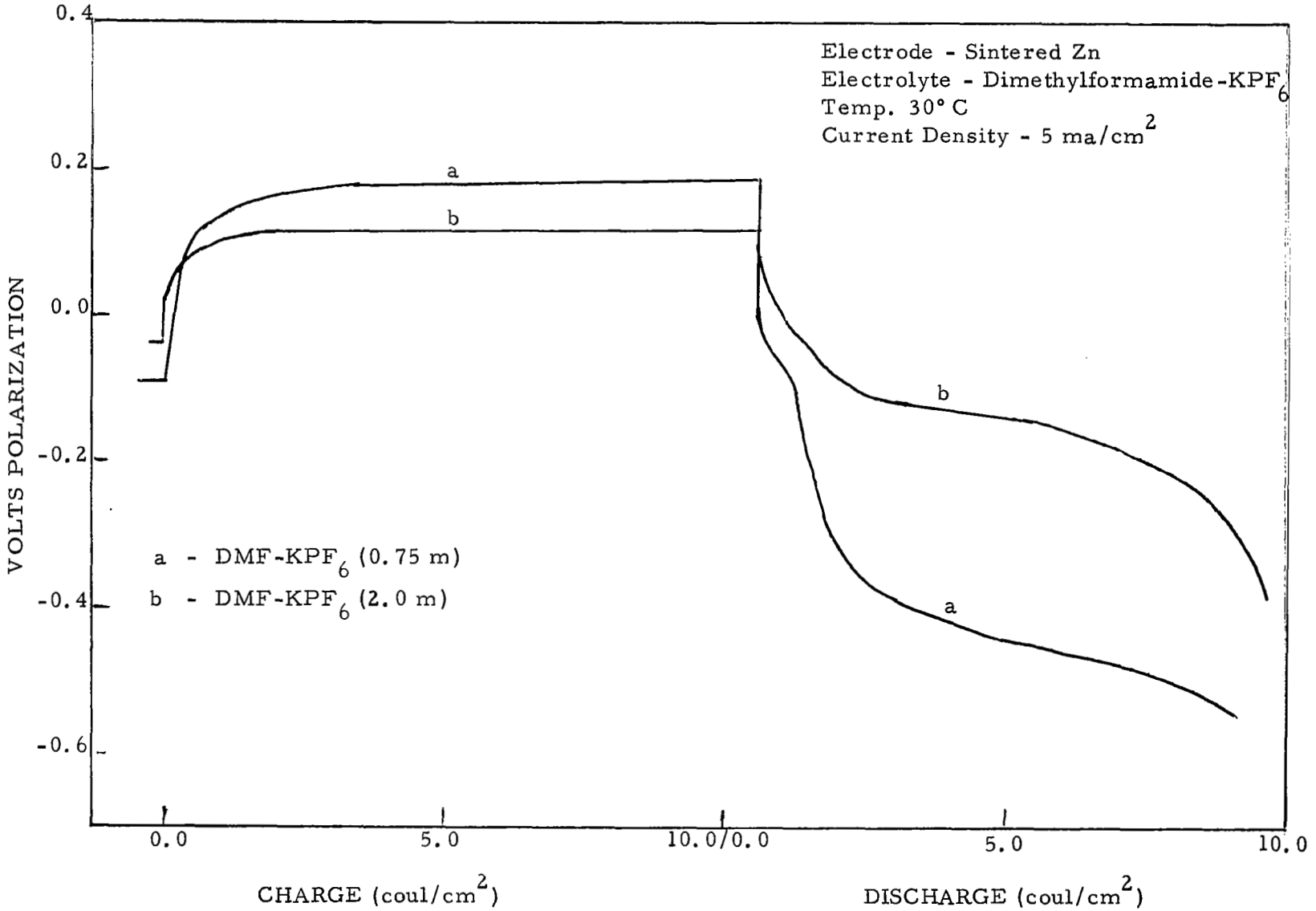

Figure 49. Charge and discharge curves for Zn/DMF-KPF_6

plots for these two systems as indicated in Figures 50 and 51. At the lower concentration (0.75 m) the utilization increases progressively with each cycle at the 5 coul/cm^2 charge input, having an average of 62% compared to 16% for the high concentration (2.0 m) where no significant cycling effect is noted. A cycling effect improves the utilization for the high concentration at the 10 coul/cm^2 charge input to an average of 42%. The utilization for the low concentration at 10 coul/cm^2 is 74%. A test at 5 coul/cm^2 on the high concentration system was made after the regular testing sequence had been followed and showed a utilization efficiency of 46%.

These data illustrate the significant effect of concentration and cycling, on utilization efficiency, and point out the importance of these factors in the optimum electroformation of high charge density positive plates. From this viewpoint the system is of interest.

13. Zinc Electrodes in Butyrolactone and Propylene carbonate-KPF_6

The systems Zn/Bl-KPF_6 and Zn/PC-KPF_6 behaved similarly. Both showed prolonged discharge at 1 ma/cm^2 (discharge capacity over 120% of the charge input) indicating reduction of dissolved material, and less than 15% utilization efficiency at 5 ma/cm^2 for charge inputs up to 5 coul/cm^2. The curves for this and lower charge inputs show relatively flat charging plateaus, followed by smaller polarized discharge (less than 1.0 coul/cm^2) with half-cell voltages dropping rapidly to greater than - 0.5 volt. The voltages separating the charge and discharge reaction are 0.2 and 6.0 volts for the Zn/BL-KPF_6 and Zn/PC-KPF_6 systems respectively. At the 10 coul/cm^2 charge input, a second apparently overlapping discharge becomes evident as seen in the discharge curves for the Zn/BL-KPF_6 system shown in Figure 52. The resulting enhancement in utilization efficiency at 10 coul/cm^2 charge can be seen in the charge-discharge plots for these two systems in Figures 53 and 54.

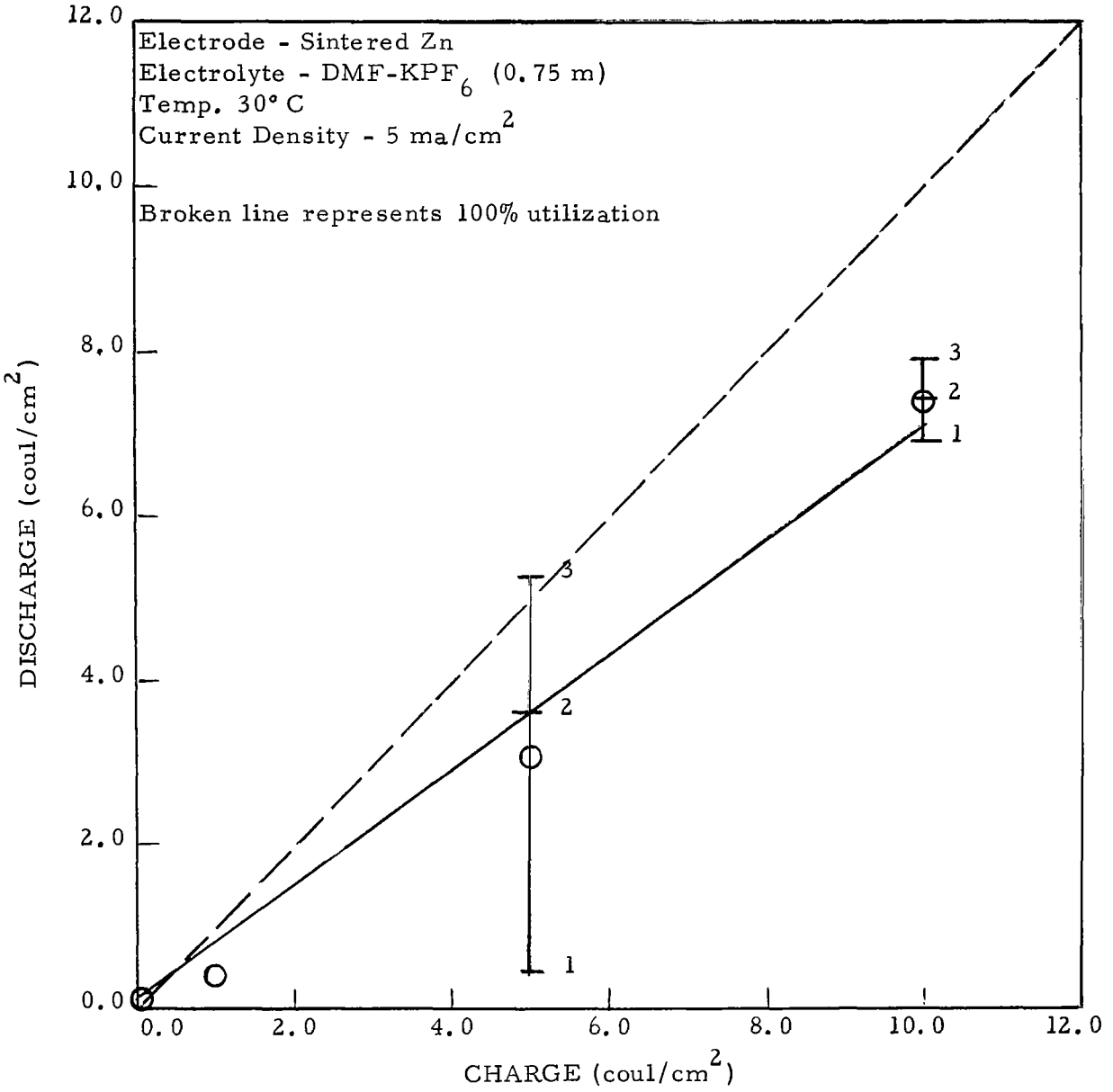

Figure 50. Coulombs delivered as a function of coulombs passed

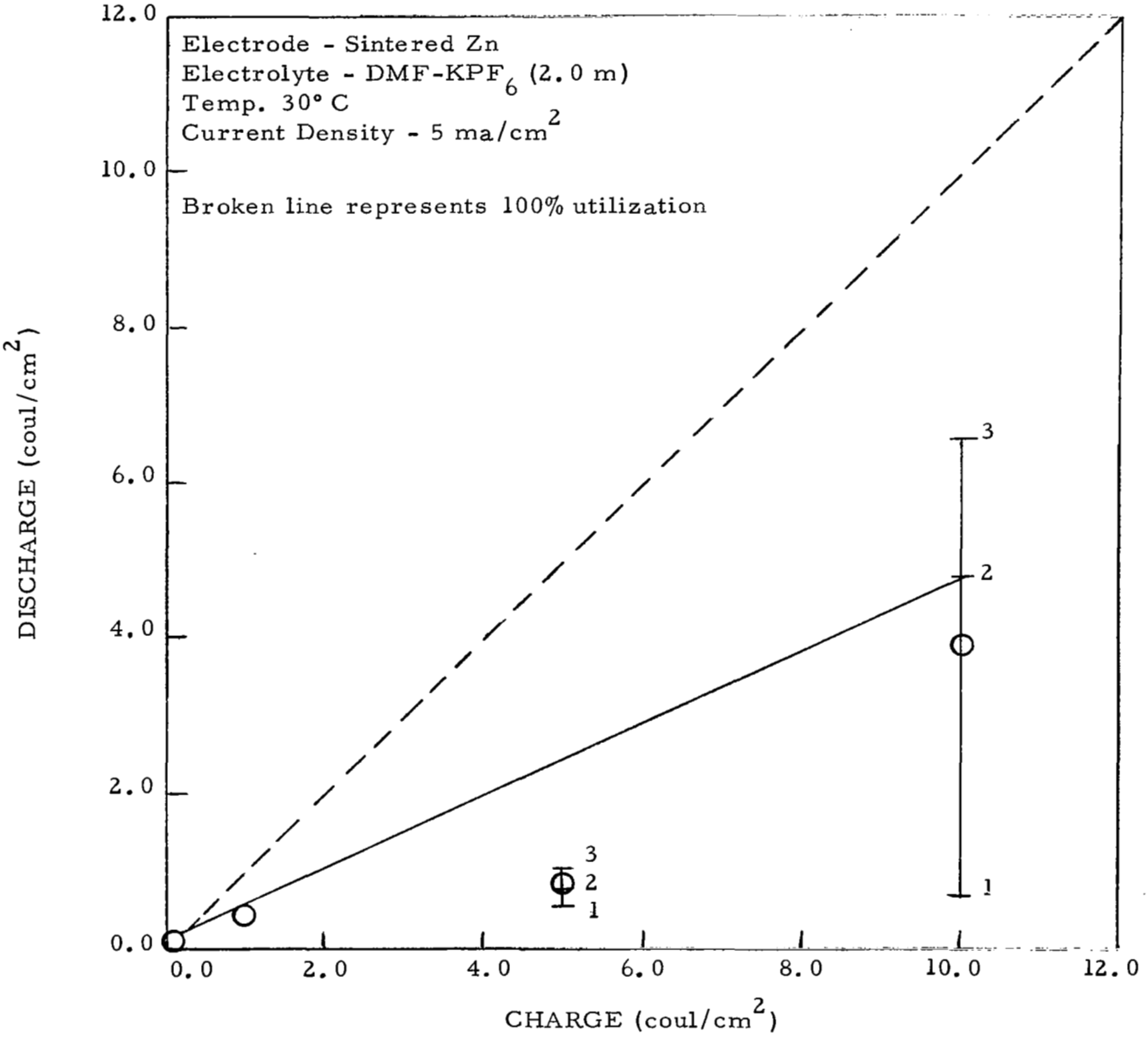

Figure 51. Coulombs delivered as a function of coulombs passed

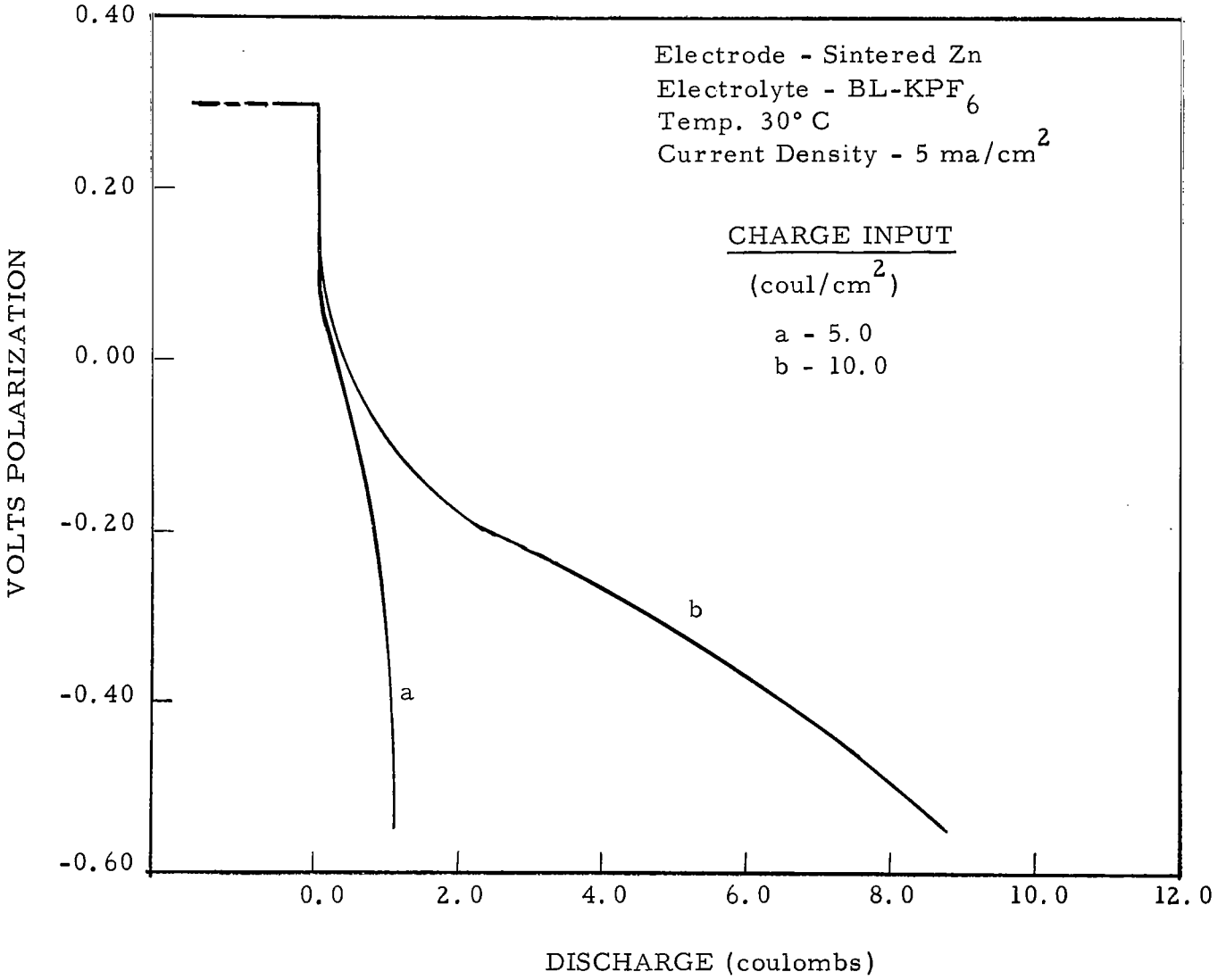

Figure 52. Discharge curve for Zn/BL-KPF_6

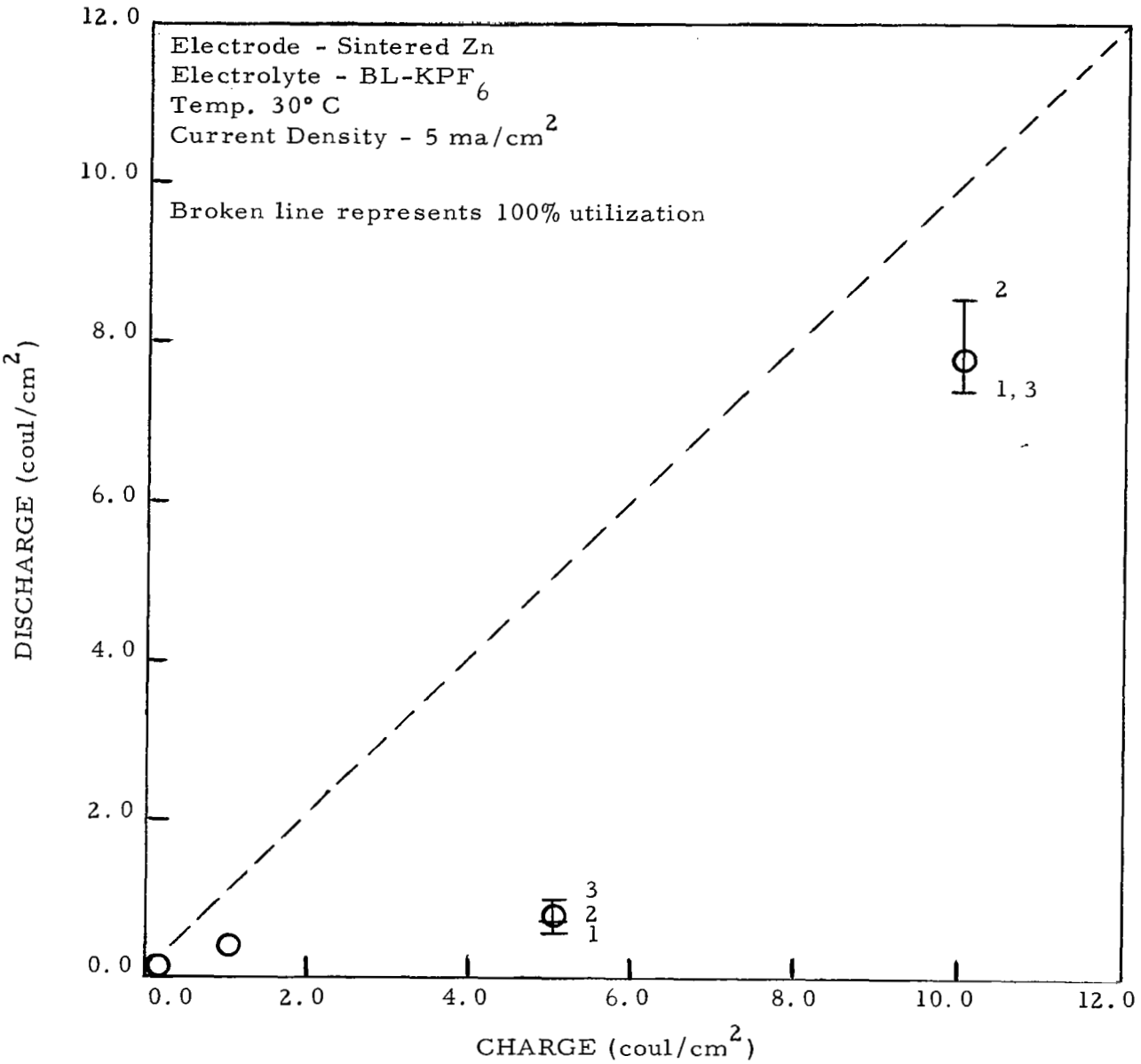

Figure 53. Coulombs delivered as a function of coulombs passed

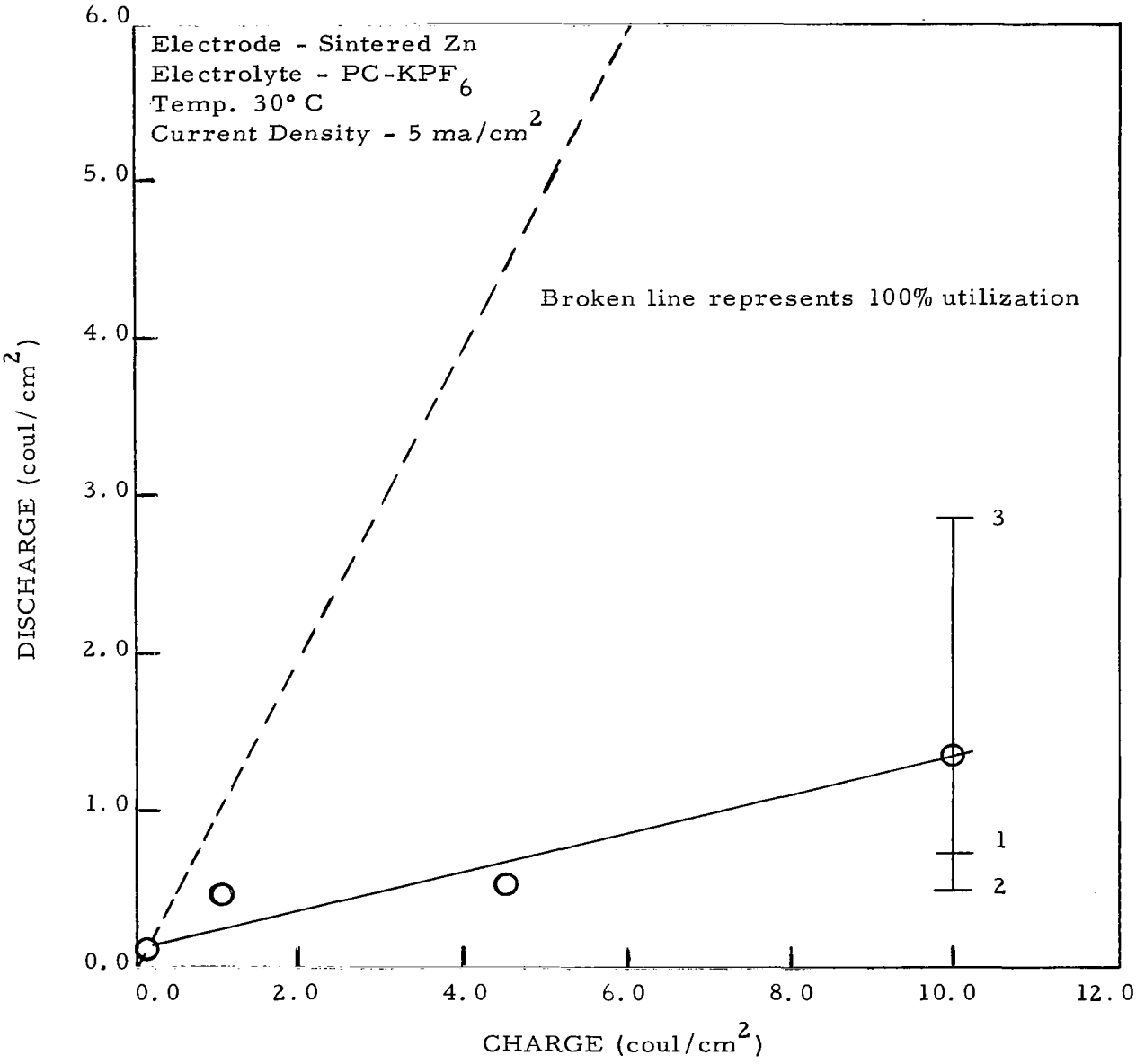

Figure 54. Coulombs delivered as a function of coulombs passed

The enhanced utilization at the 10 coul/cm^2 charge input may result from an increase in the effective porosity of the electrode, caused by the penetration of the charging reaction to deeper levels within the pores of the electrode, resulting in improved charge retention and utilization efficiency.

14. Cadmium Electrode in Dimethylformamide-KPF_6

This system shows prolonged discharge for the 1 ma/cm^2 tests with low polarization between charge and discharge plateaus, indicating high electrochemical activity of dissolved material. The charge-discharge plot for this system at 5 ma/cm^2 is shown in Figure 55. Although the utilization efficiency is about 46% taken up to 5 coul/cm^2, the discharge capacity at 10 coul/cm^2 of charge is greater than 100% indicative of discharge due to dissolved material. Examination of the working electrode revealed a build-up of a spongy grey material adhering to the electrode surface, which appears to represent a mixture of reduced metal and anodic product. It is likely that dissolution of this material near the electrode tends to raise the limiting current for reduction of dissolved active material.

15. Cadmium Electrode in Dimethylformamide-$LiBF_4$.

Sintered cadmium in DMF-$LiBF_4$ shows prolonged discharge at 1 ma/cm^2 with 0.03 v polarization between charge and discharge plateaus, indicating high electrochemical activity for dissolved material. The tests at 5 ma/cm^2 gave a small discharge plateau near 0.00 v which increased from 0.3 to 0.8 coul/cm^2 with cycling, followed by a second discharge plateau at - 0.07 v which did not drop off within 120% of the charge time. The charge-discharge

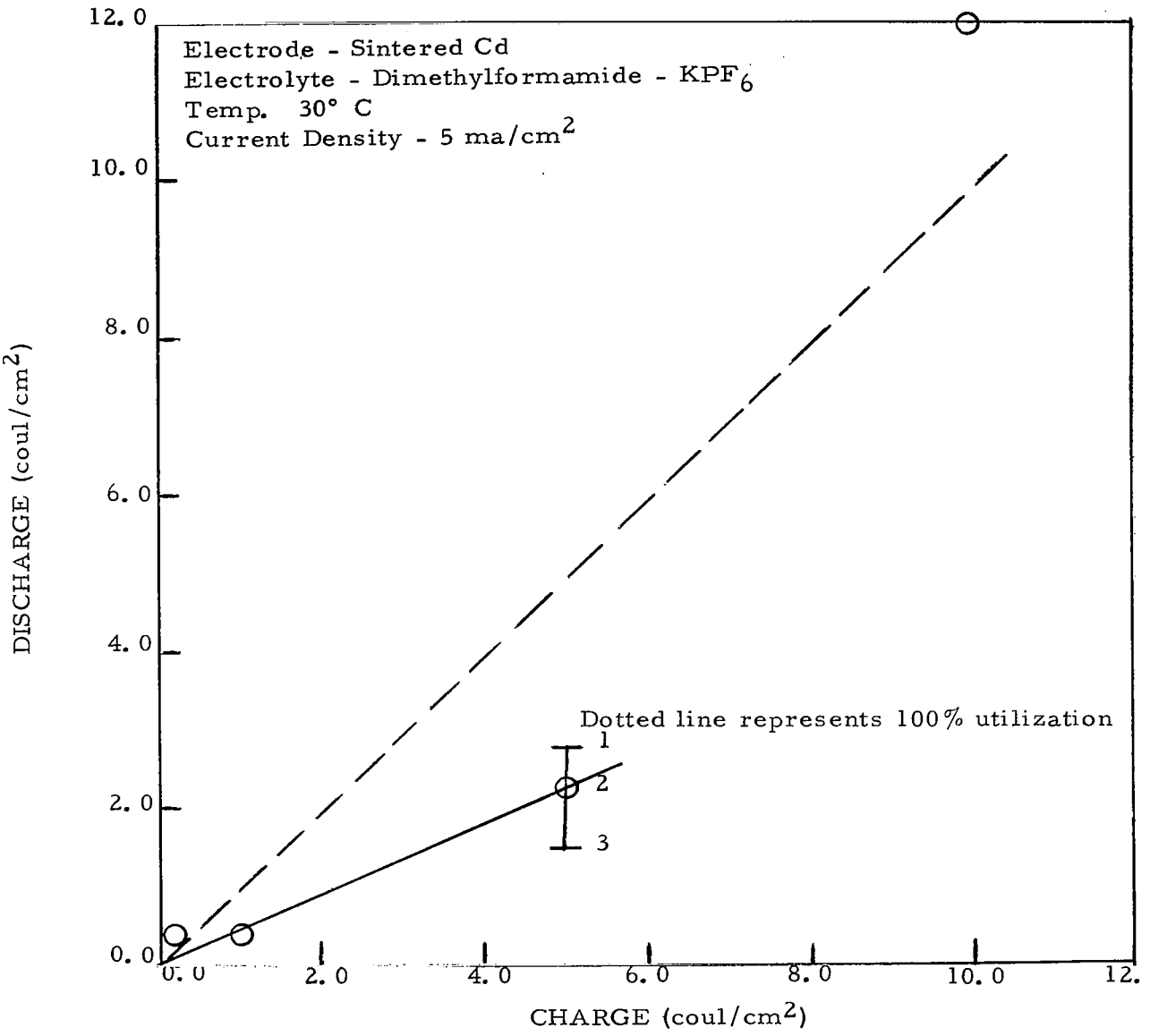

Figure 55. Coulombs delivered as a function of coulombs passed

plot for the first plateau is shown in Figure 56 representing a utilization efficiency of less than 15% for all charge inputs. The results indicate a low availability of solid material and a high availability of dissolved material at the electrode surface, which may result from a high dissolution rate of the electroformed product.

This system is not recommended for further testing.

16. Cadmium Electrode in Dimethylformamide-$LiClO_4$

The charge-discharge plot for this system is shown in Figure 57. A utilization efficiency of 53% is calculated from the best straight line through all points. The discharge at the lower charge inputs (0.10 and 1.0 coul/cm^2) is reproducible and falls within the circular points. At the higher charge inputs the spread of individual points among a given set is greater than 2 coul/cm^2. At 5 coul/cm^2, the lowest discharge is comparable to values obtained at the lower charge levels. The average utilization efficiency (calculated only for the largest charge input, 10.0 coul/cm^2) is 63%, a value greater than the average for all the tests. These effects may be explained as follows. The large spread at the higher charge level (10.0 coul/cm^2) can result from the expected formation of solid state material at deeper levels within the pores of the electrode where contact to the metal is favored, thus minimizing the relative significance of gross loss effects. It is expected on this basis that this system and others with similar behavior will show an improvement of the utilization efficiency at larger charge inputs (20-50 coul/cm^2).

This system is recommended for further consideration.

17. Cadmium Electrode in Butyrolactone-KPF_6

The discharge curve for the system Cd/BL-KPF_6 is shown in Figure 58.

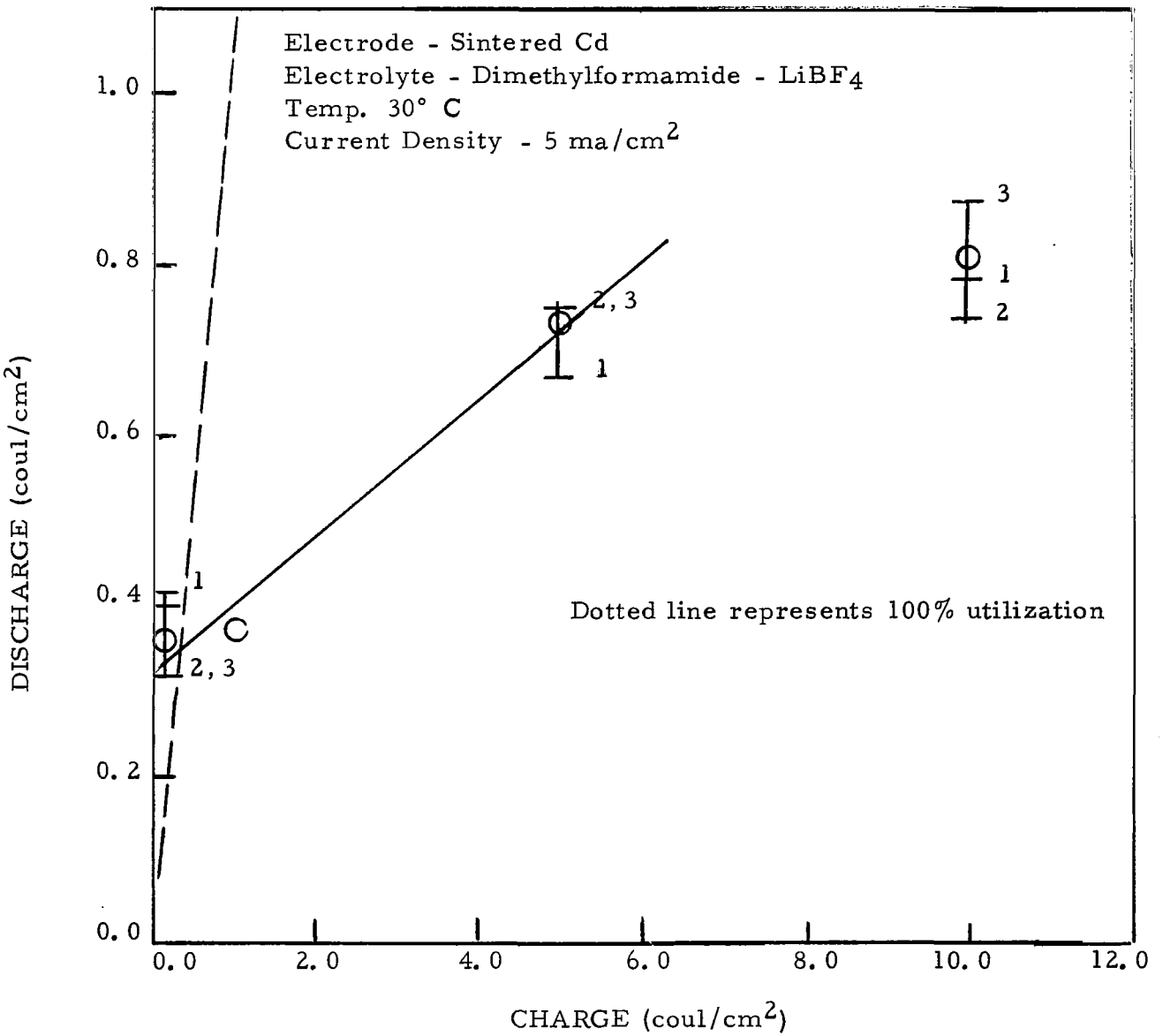

Figure 56. Coulombs delivered as a function of coulombs passed

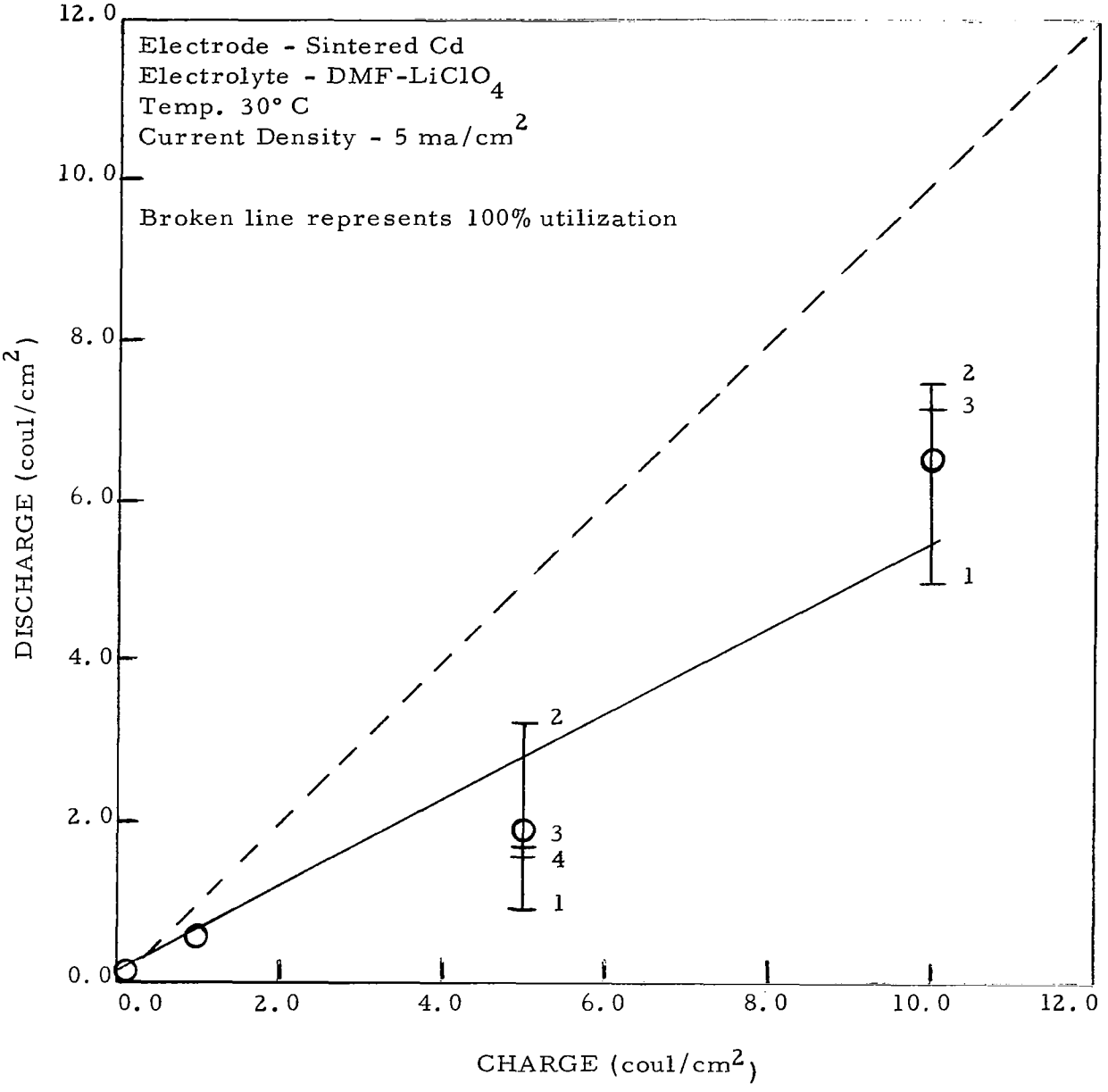

Figure 57. Coulombs delivered as a function of coulombs passed

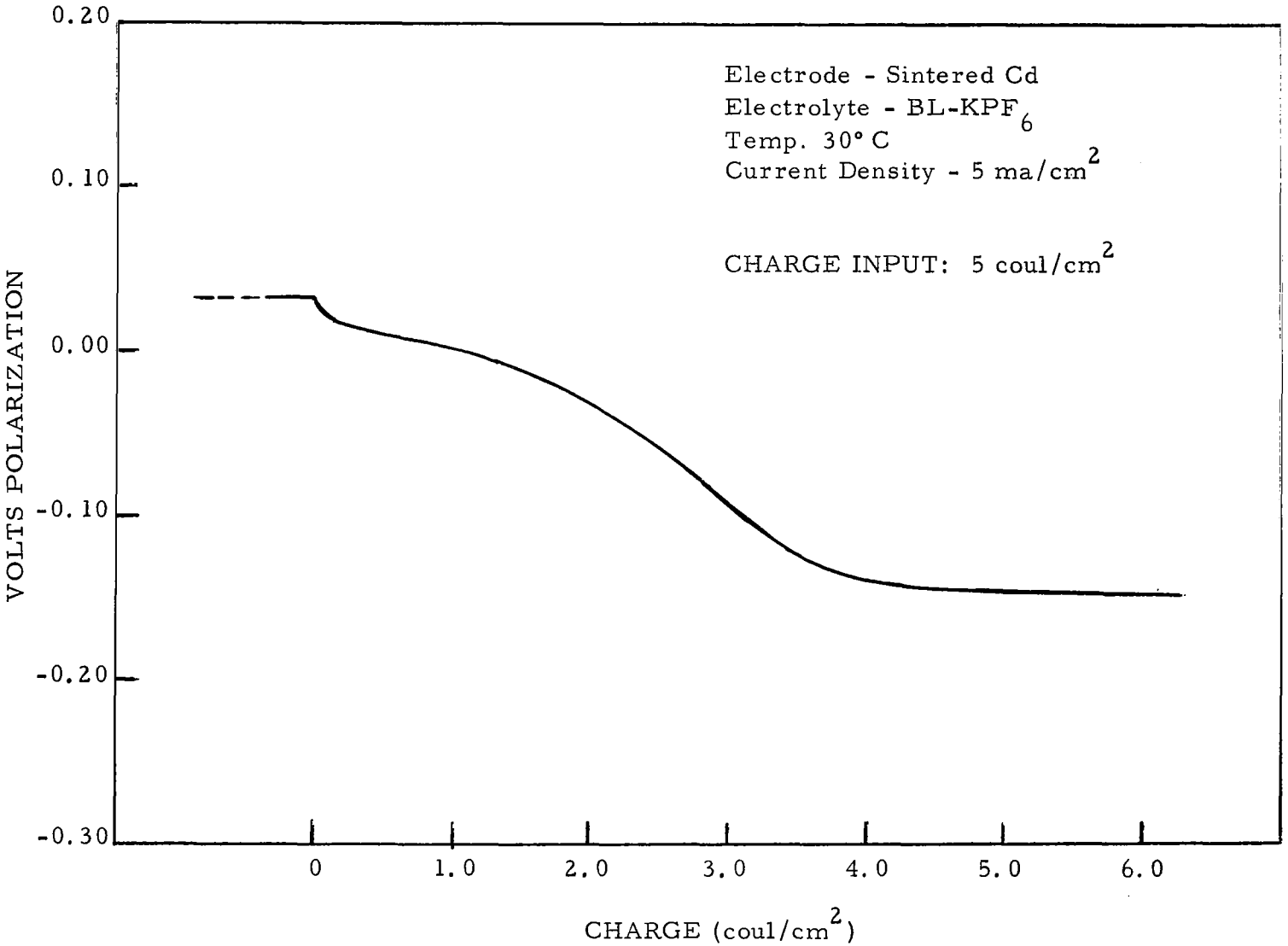

Figure 58. Discharge curve for Cd/BL-KPF_6

The curve shows very low initial polarization (50 mv) relative to the charge plateau, a portion of which is shown. The discharge plateau then drops gradually levelling off at - 120 mv, following which it continues until greater than the corresponding charge input. This effect is not evident in the discharge curves for the smaller charge inputs (0.10 and 1.0 coul/cm^2), where in fact a sharp break occurs with the discharge potential dropping rapidly to negative values greater than 0.5 volts vs the cadmium reference electrode. The charge-discharge plot for this system is shown in Figure 59, where the large spread for the discharge capacity at the 5 coul/cm^2 charge input, and the relative low utilization at 10.0 coul/cm^2 charge input, are evident.

It appears that in this system loss of charged solid state material caused by gross effects predominates during the charging process. The prolonged discharge at potentials slightly less than that for the solid state discharge is most likely caused by dissolved material. The appearance of the prolonged discharge for the larger charge inputs indicates an increase in the effective concentration of dissolved species possibly resulting from dissolution of solid material which builds up with cycling.

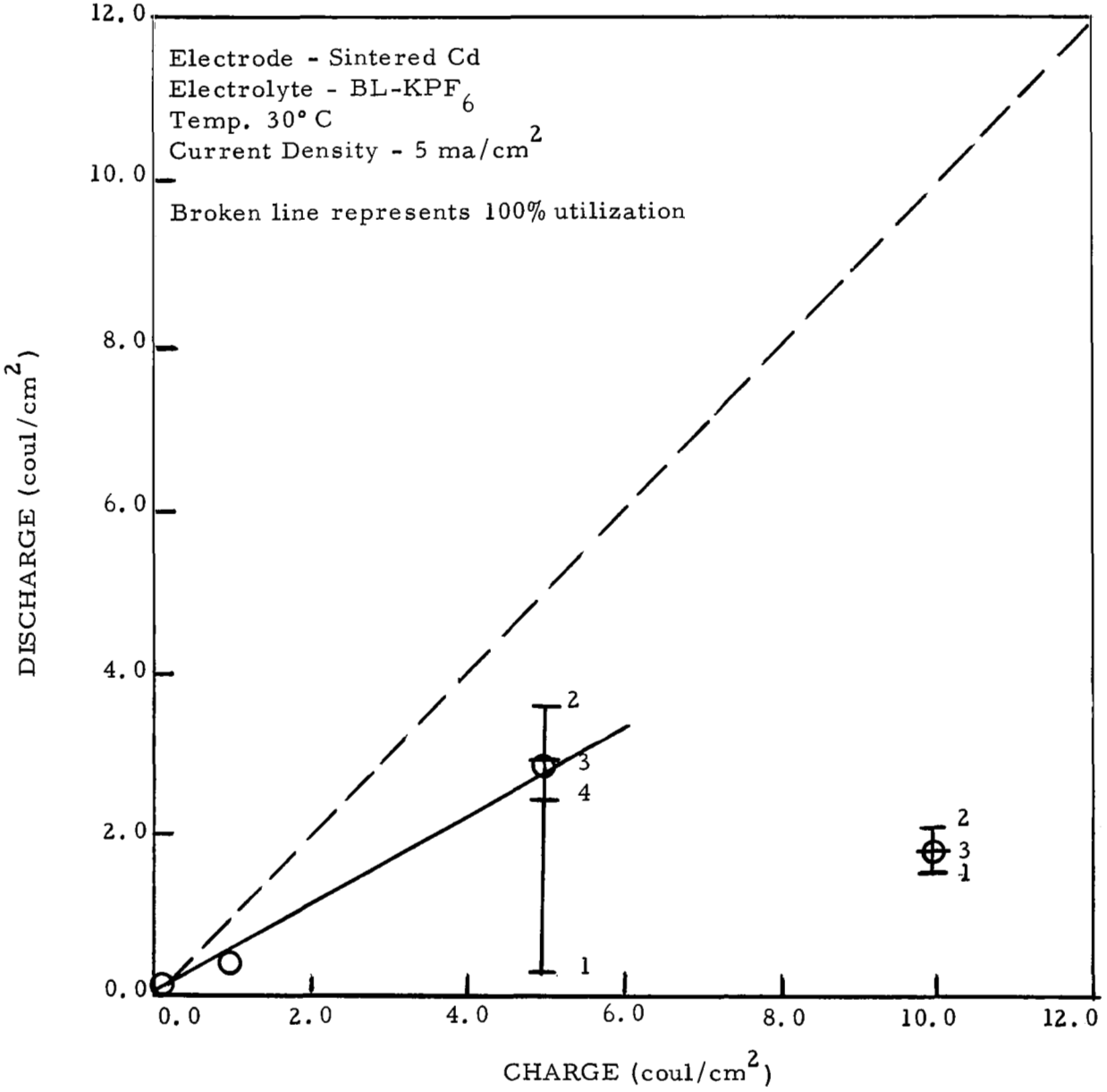

Figure 59. Coulombs delivered as a function of coulombs passed

18. Silver Fluoride Electrode in Propylene carbonate-$LiBF_4$

The initial discharge for this system corresponded to 40% utilization of a 20 coul/cm^2 chemoformed fluoride electrode. The regular testing procedure was followed after this initial discharge.

Tests at 1 ma/cm^2 showed prolonged discharge with less than 0.3 volt separating charge and discharge plateaus. The polarization at 5 ma/cm^2 was initially greater than 1 volt, but decreases with cycling and increasing charge input to less than 0.4 volts between the two plateaus. The charge-discharge curve in Figure 60 shows an average utilization of 60%. For the 10 coul/cm^2 tests, where the polarization had decreased to its lowest value, a prolonged discharge resulted. Examination of the cell revealed a fine dispersion of a grey metallic particle and a spongy like material on the electrode surface.

Results indicate that non-discharged fluoride material initially blocks the electrode surface. Cycling gradually activates the surface and finally a prolonged discharge results due to contributions from dissolved charged state material. This system indicates good electrochemical activity and is recommended for further characterization.

19. Copper Chloride Electrode in Butyrolactone-$AlCl_3$

The initial discharge for this system exhibits 27% utilization of the 20 coul/cm^2 chemoformed product. The regular testing procedure was followed after this initial discharge.

Tests at 1 ma/cm^2 showed prolonged discharge and 0.4 volt polarization

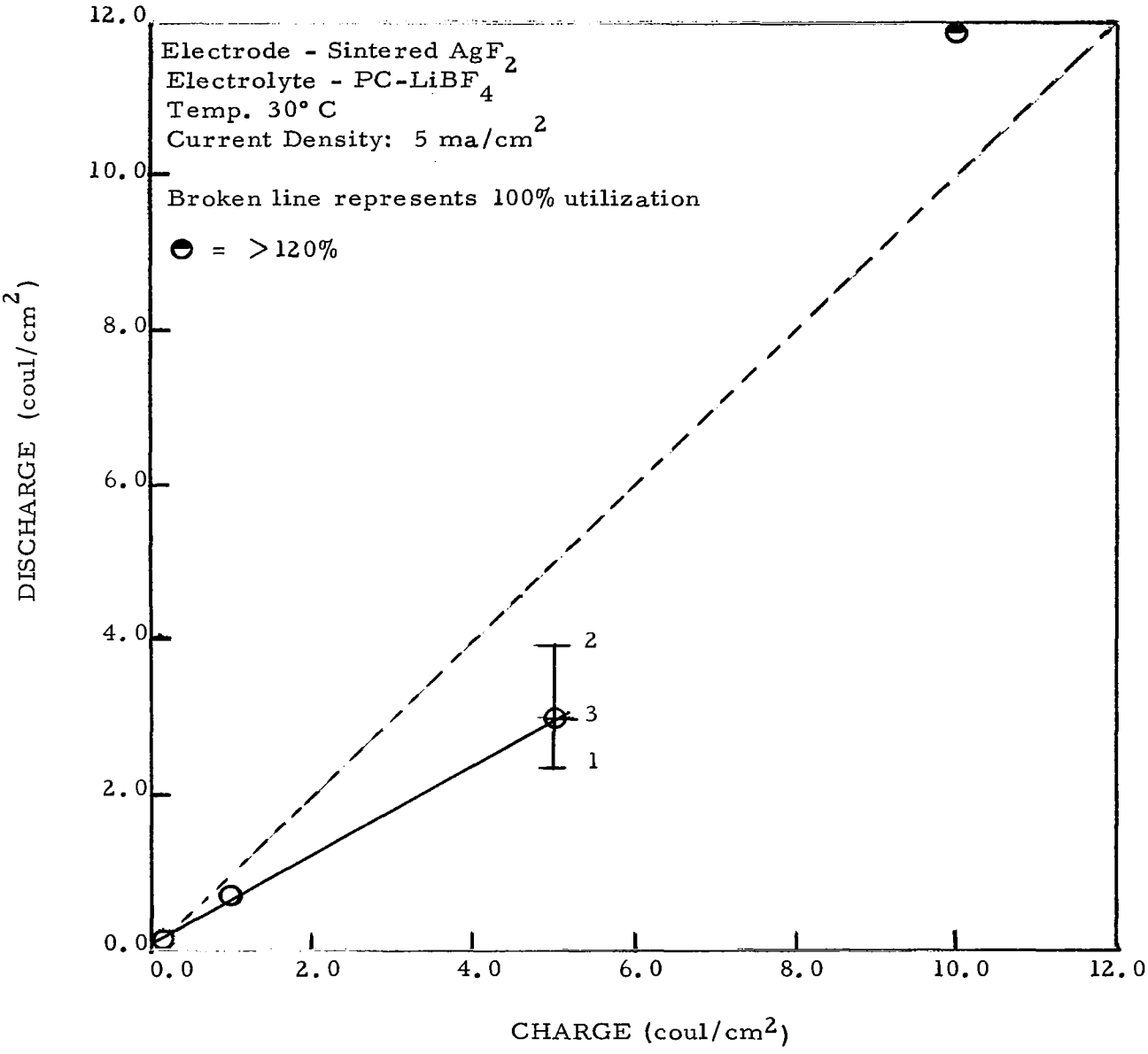

Figure 60. Coulombs delivered as a function of coulombs passed

separating the charge and discharge plateau. At 5 ma/cm^2, the polarization increased from 0.7 to 1.2 volts with increase in charge input. The charge-discharge plot, shown in Figure 61 is linear indicating only 19% utilization efficiency. This system is not recommended.

20. Copper Chloride Electrode in Dimethylformamide-LiCl + $LiClO_4$

Initial discharge equivalent to 32% utilization of chemoformed chloride was obtained at 5 ma/cm^2 for this system. The regular testing procedure followed after this initial test gave results similar to those for the preceding system ($CuCl_2$/BL-$AlCl_3$). The polarization at 5 ma/cm^2 increased with cycling from 0.5 to 0.9 volt lowering the utilization efficiency to 25%. The charge-discharge plot is shown in Figure 62. This system is not recommended for further testing.

21. Copper Fluoride Electrode in Propylene carbonate-$LiClO_4$

The initial discharge at 5 ma/cm^2 amounted to 18% of a 20 coul/cm^2 capacity chemoformed chloride electrode. Regular testing procedure followed this initial test.

Polarizations of 0.6 volt at 1 ma/cm^2 and 0.8 volt at 5 ma/cm^2 separated the charge and discharge plateaus for this system. Prolonged discharge was observed only for the 0.10 coul/cm^2 charge input at 1 ma/cm^2, otherwise the charge-discharge plots are linear for both low and high current densities. This is shown in Figures 63 and 64. Utilization efficiencies of 12 and 36% are indicated at 1 and 5 ma/cm^2 respectively. This system is not recommended.

22. Zinc Fluoride Electrode in Dimethylformamide-$LiClO_4$

The initial discharge of the chemoformed zinc fluoride at 5 ma/cm^2 in

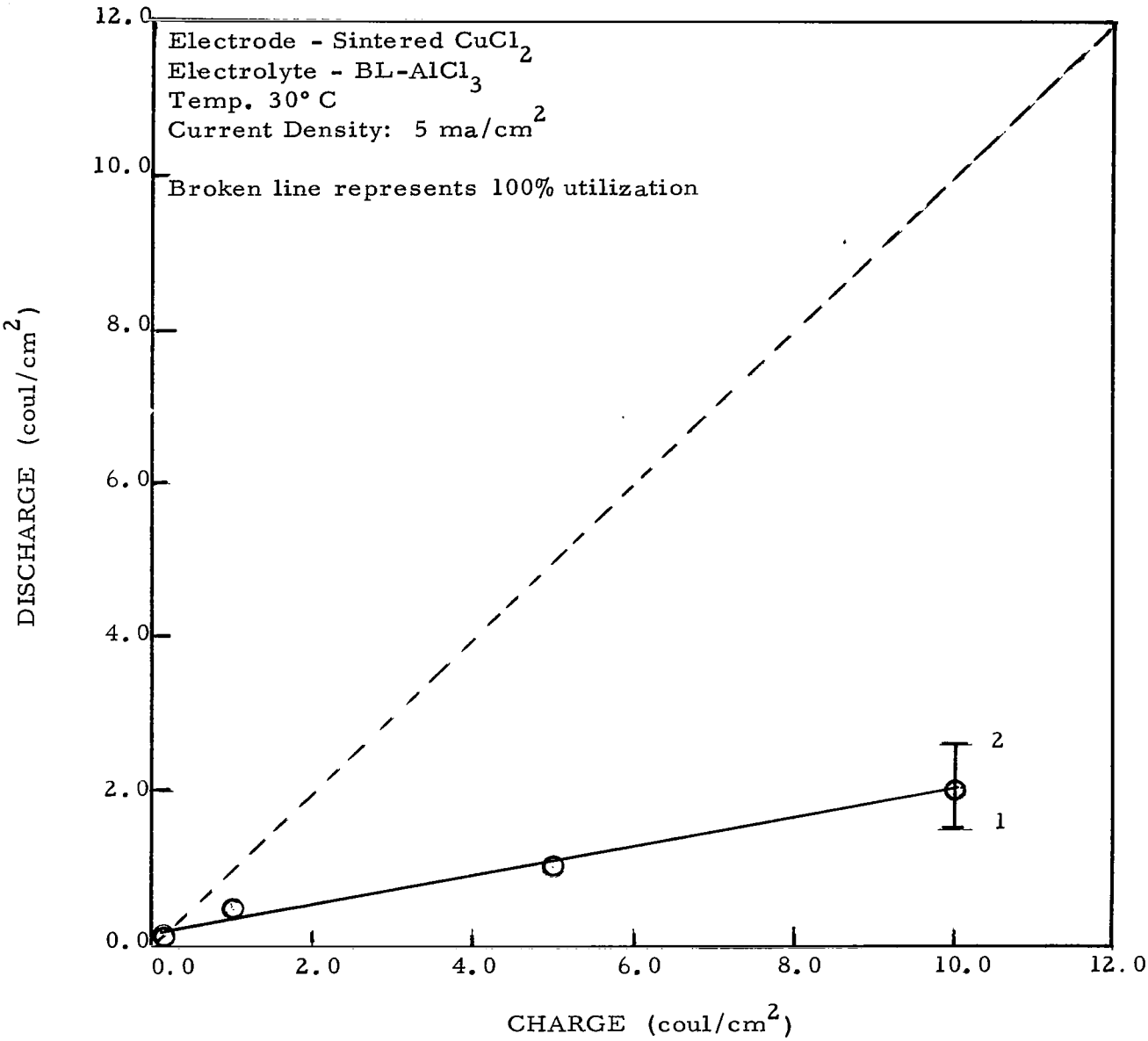

Figure 61. Coulombs delivered as a function of coulombs passed

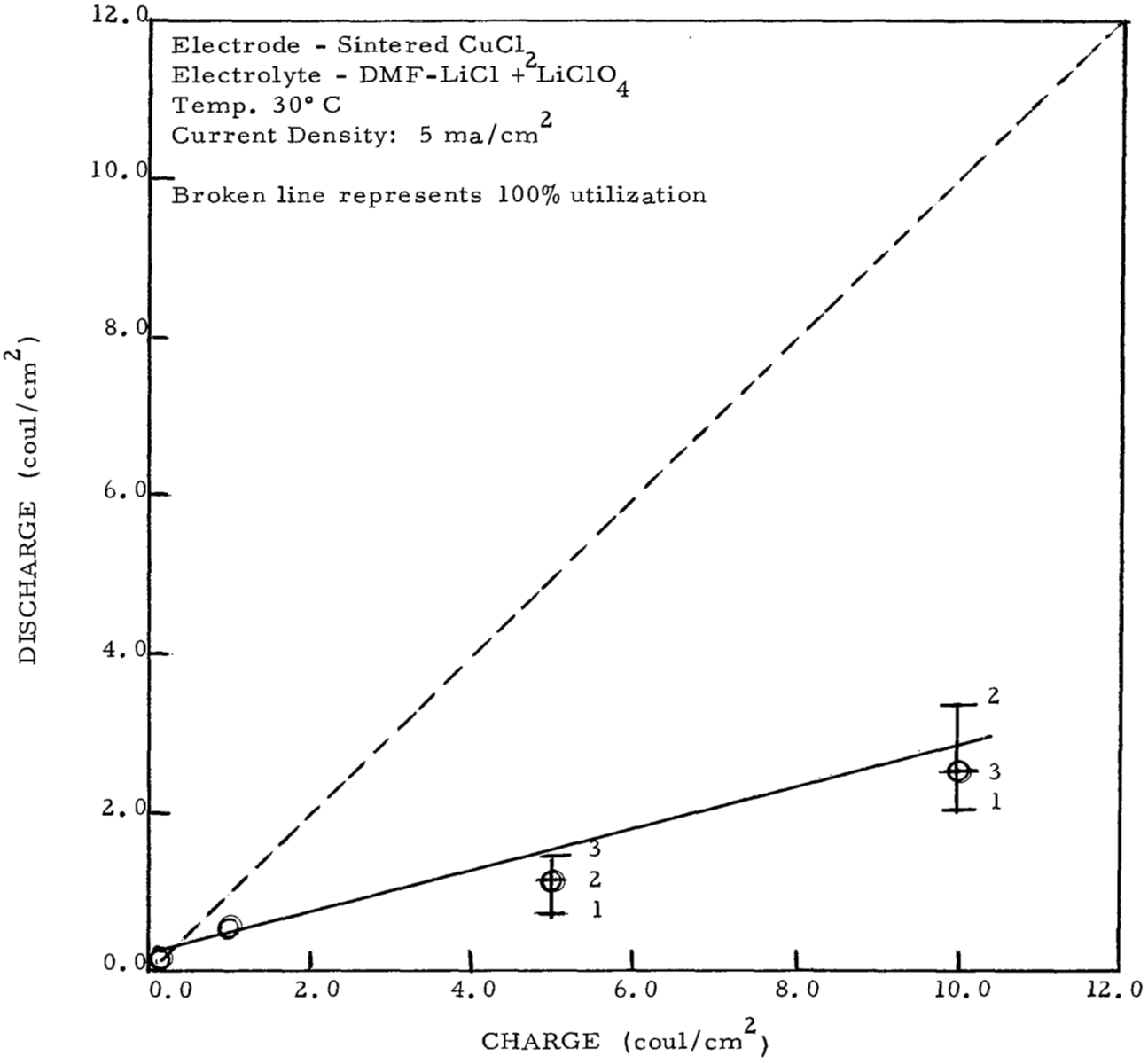

Figure 62. Coulombs delivered as a function of coulombs passed

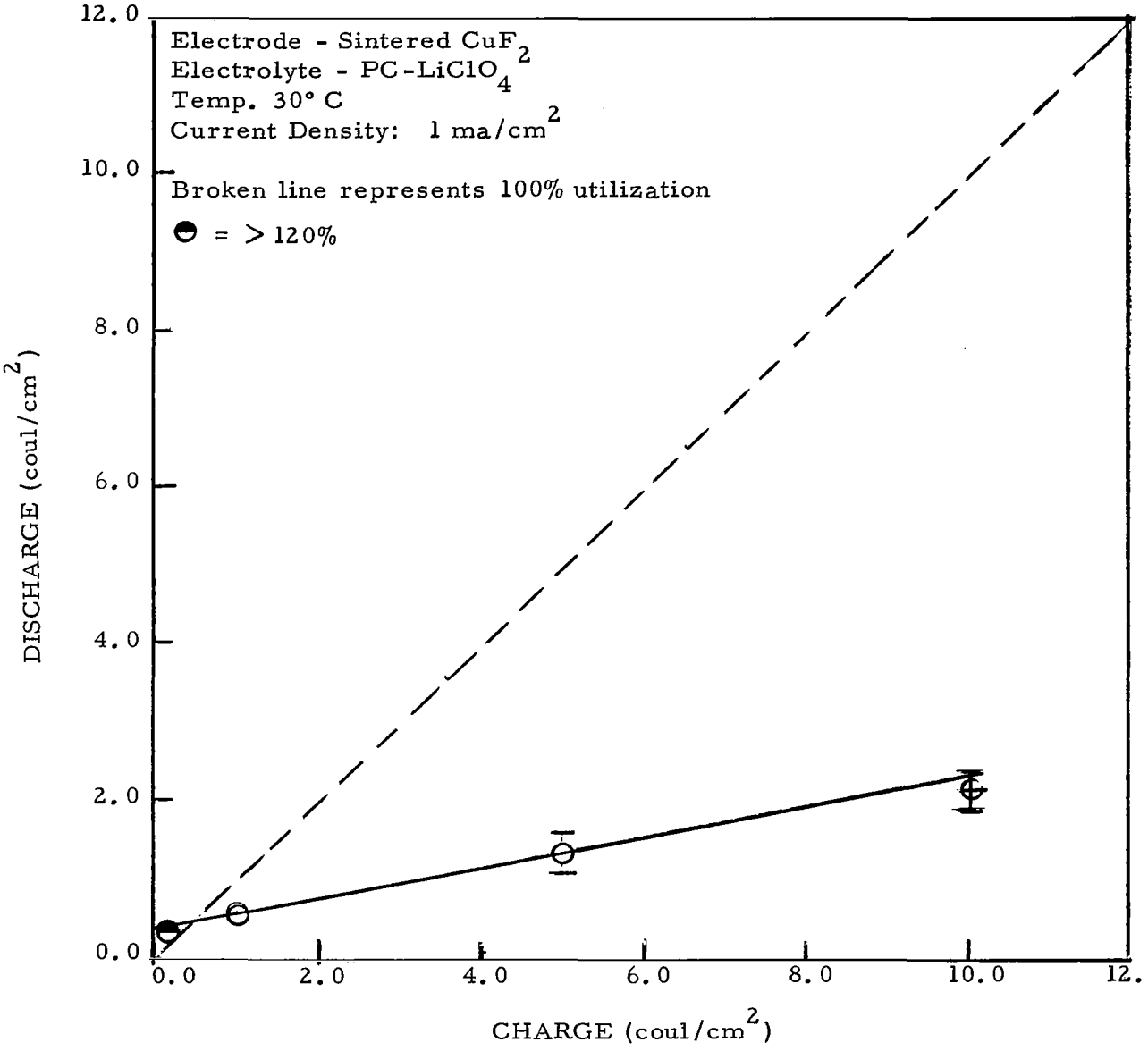

Figure 63. Coulombs delivered as a function of coulombs passed

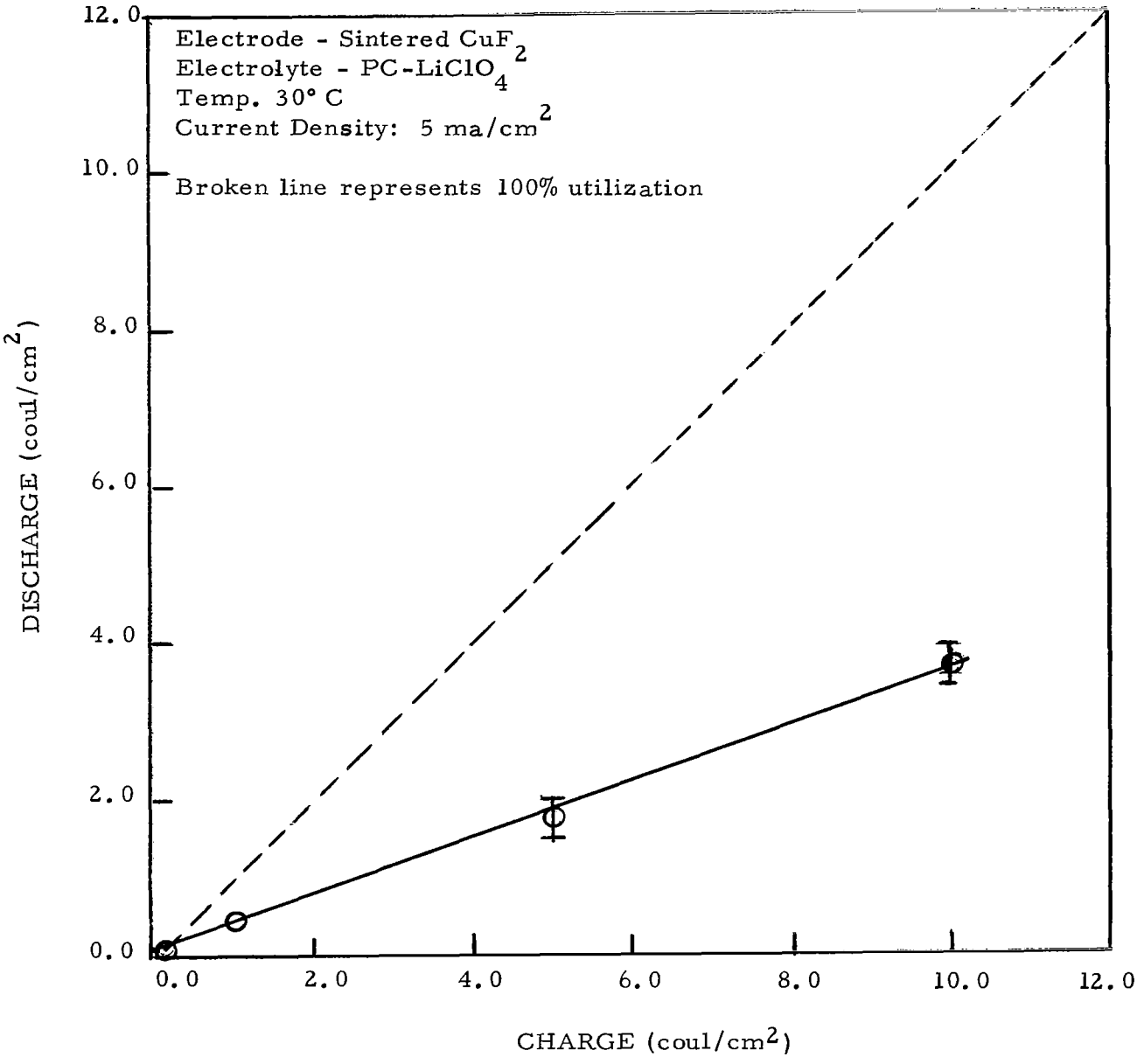

Figure 64. Coulombs delivered as a function of coulombs passed

this electrolyte amounted to 42% of the initial 15.1 coul/cm^2 of fluorination product. Polarization on discharge was 0.6 volts relative to the ocv, and the cut-off was taken at 1 volt. Regular testing procedure was followed after this initial discharge.

The test at 1 ma/cm^2 showed prolonged discharge with less than 0.2 volts polarization between charge and discharge plateaus. The polarization for the tests at 5 ma/cm^2 decreased as the tests progressed to higher charge inputs. The voltage separation was initially greater than 1 volt but levelled off at 0.3 - 0.4 volt indicating a surface activation process, perhaps the removal of a surface blocking zinc fluoride film. The discharge capacity at 5 ma/cm^2 appeared limited to values less than 2 coul/cm^2 as shown in Figure 65. The utilization efficiency at 10 coul/cm^2 was 18%. This system is not recommended for further study.

23. Zinc Fluoride Electrode in Dimethylformamide-KPF_6

Initial discharge of chemoformed zinc fluoride in this electrolyte was nil. The regular testing procedure, followed after this initial discharge, gave results similar to those for the zinc fluoride electrode in the preceding system. The charge-discharge for the 5 ma/cm^2 tests plot is shown in Figure 66. The utilization efficiency is 22%. This system is not recommended for further characterization.

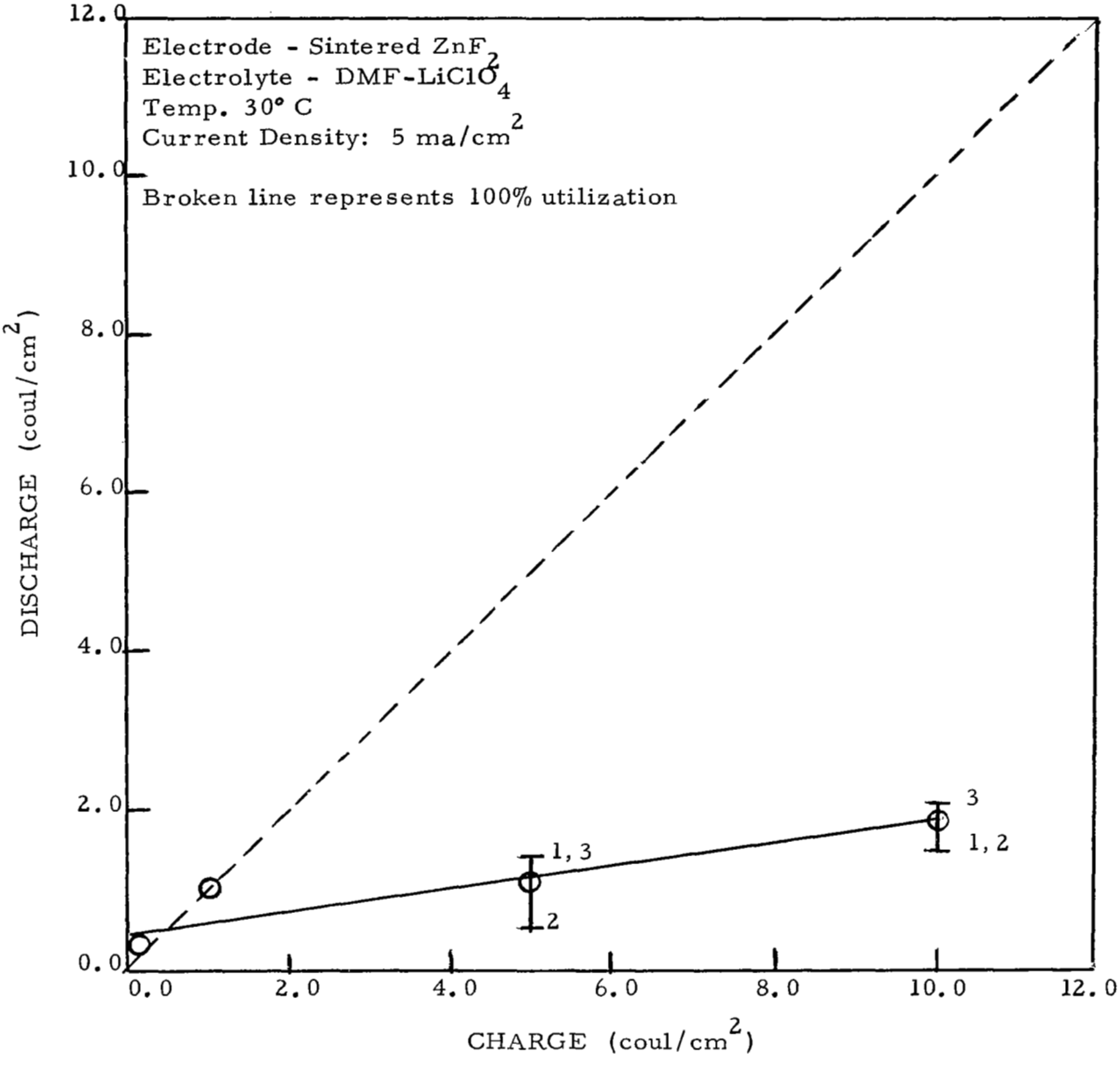

Figure 65. Coulombs delivered as a function of coulombs passed

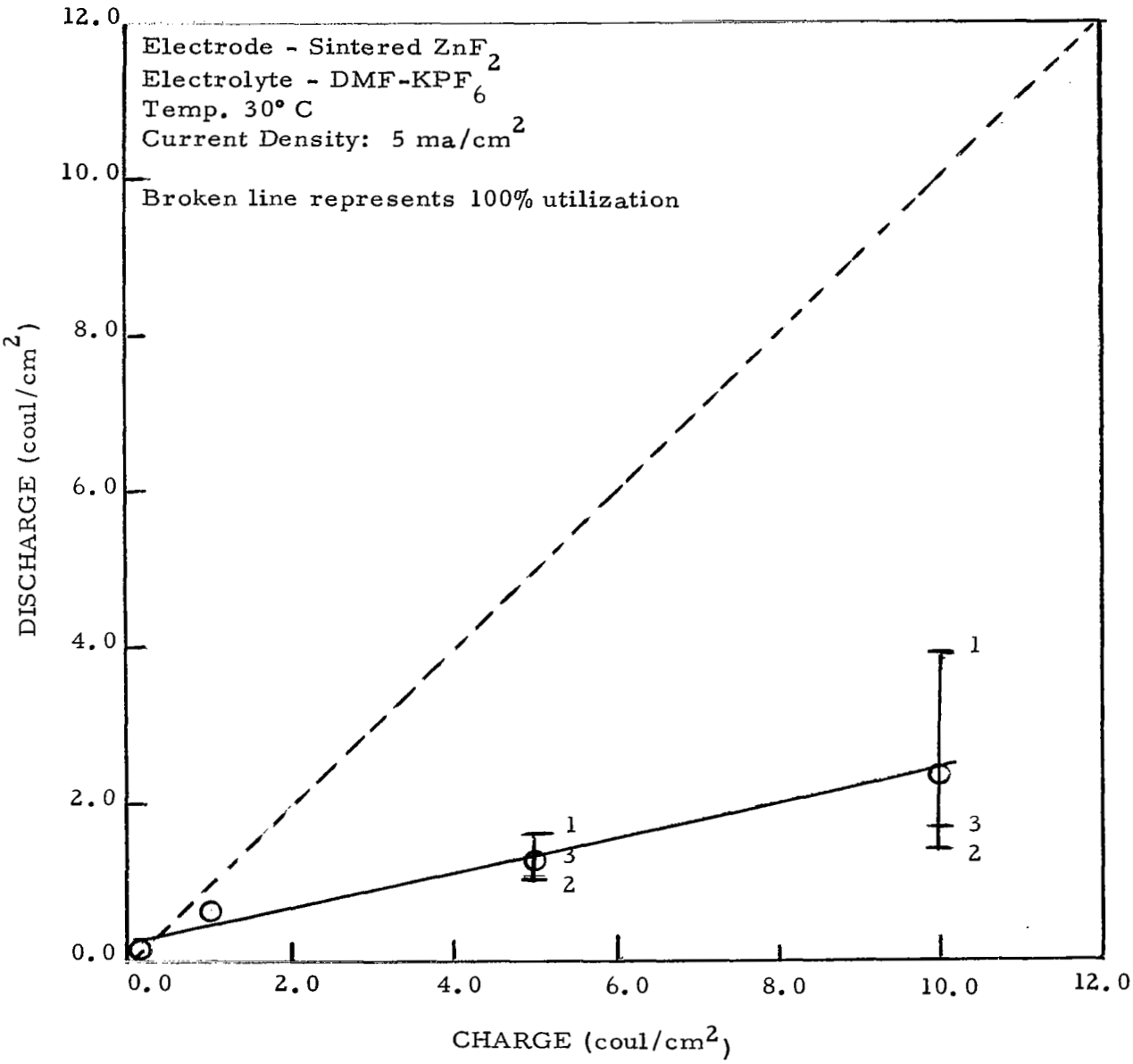

Figure 66. Coulombs delivered as a function of coulombs passed

The purpose of the charge-discharge tests on the twenty-four recommended systems was to obtain an order of suitability whereby a minimum number of promising systems could be selected for further study and eventual development of high energy density secondary cells for battery application.

The cyclic voltammetric selection of these systems was based on low polarization between charge and discharge reactions and single high current density peaks. This singled out the most promising systems from the standpoint of electrochemical activity and reversibility. The charge-discharge tests on the sintered electrodes specifically characterized the charge and discharge properties of the electrode.

The results of the galvanostatic charge-discharge tests are summarized in Table 31. The systems are listed in order of decreasing utilization efficiency obtained at 5 ma/cm^2, since a minimal contribution due to dissolved material is expected at this current density. In addition, remarks on the visual appearance of the electrode after testing, with regard to the physical integrity, are included to augment the information and reveal detrimental behavior such as loss of physical integrity on cycling.

For the sake of clarity, Figure 67 illustrates the manner in which the charge-discharge data was compiled. The time intervals C and D correspond to the charge and discharge time, with D measured to an appropriate cut-off point near the break of the discharge plateau. The polarization voltage separating the charge and discharge plateau, ΔV, was measured from the difference in the medium values of the flat portions of the charge and discharge plateaus as indicated on the curve. The charge-discharge plots were obtained from the coulombs corresponding to the times C and D for each charge input. The slope of the best straight line through the points obtained in this manner was used to calculate the utilization efficiency.

TABLE 31

CHARGE-DISCHARGE DATA FOR SINTERED ELECTRODES

System	% Utilization Efficiency 1 ma/cm^2	% Utilization Efficiency 5 ma/cm^2	Polarization Voltage 1 ma/cm^2	Polarization Voltage 5 ma/cm^2	
$CuCl_2$/DMF-$LiPF_6$		100	0.20	0.70	ml
AgO/BL-LiCl + $AlCl_3$	82	87	0.30	0.50	i
CuF_2/DMF-$LiPF_6$	P	72	0.30	0.40	i
Zn/DMF-KPF_6(.75 m)	P	69	0.06	0.30	i
AgF_2/PC-$LiBF_4$	P	60*, P**	0.20	0.70	ml
Zn/DMF-$LiPF_6$	P	56*	0.10	0.30	i
Cd/BL-KPF_6	P	54*	0.05	0.10	i
Cd/DMF-$LiClO_4$	P	53	0.05	0.20	i
Zn DMF-KPF_6 (2.0 m)	P	47	0.15	0.60	i
Cd/DMF-KPF_6	P	46*, P**	0.05	0.20	i
Cu/DMF-$LiPF_6$	P	42	0.03	0.10	d
CuF_2/PC-$LiClO_4$	17	36	0.60	0.80	i
$CuCl_2$/DMF-LiCl + $LiClO_4$	P	25	0.40	0.60	i
ZnF_2/DMF-KPF_6	P	22	0.10	0.50	i
$CuCl_2$/BL-$AlCl_3$	P	19	0.40	0.90	d
ZnF_2/DMF-$LiClO_4$	P	18**	0.10	0.60	ml
Zn/BL-KPF_6	P	12*, 77**	0.20	0.40	i
Zn/PC-KPF_6	P	12	0.30	0.70	i
CuF_2/PC-$LiPF_6$	75	5	0.50	1.20	ml
Zn/AN-$LiClO_4$	P	7*	0.07	0.20	ml
Zn/DMF-$LiClO_4$	P	4*	0.05	0.30	i
Cd/DMF-$LiBF_4$	P	4*	0.06	0.07	i
$CuCl_2$/AN-$LiPF_6$	P	P	0.30	0.50	d
$CuCl_2$/PC-$LiClO_4$	90	nil	0.60	>2.00	i
Cu/AN-$LiPF_6$ + KPF_6	P	P	0.10	0.12	d

P >120% due to contribution from dissolved material

* Calculated from best straight line through all points up to 5 coul/cm^2 charge input

** Calculated for 10 coul/cm^2 charge input

AN Acetonitrile

BL Butyrolactone

DMF Dimethylformamide

PC Propylene carbonate

i intact

ml moderate loss

d disintegrated

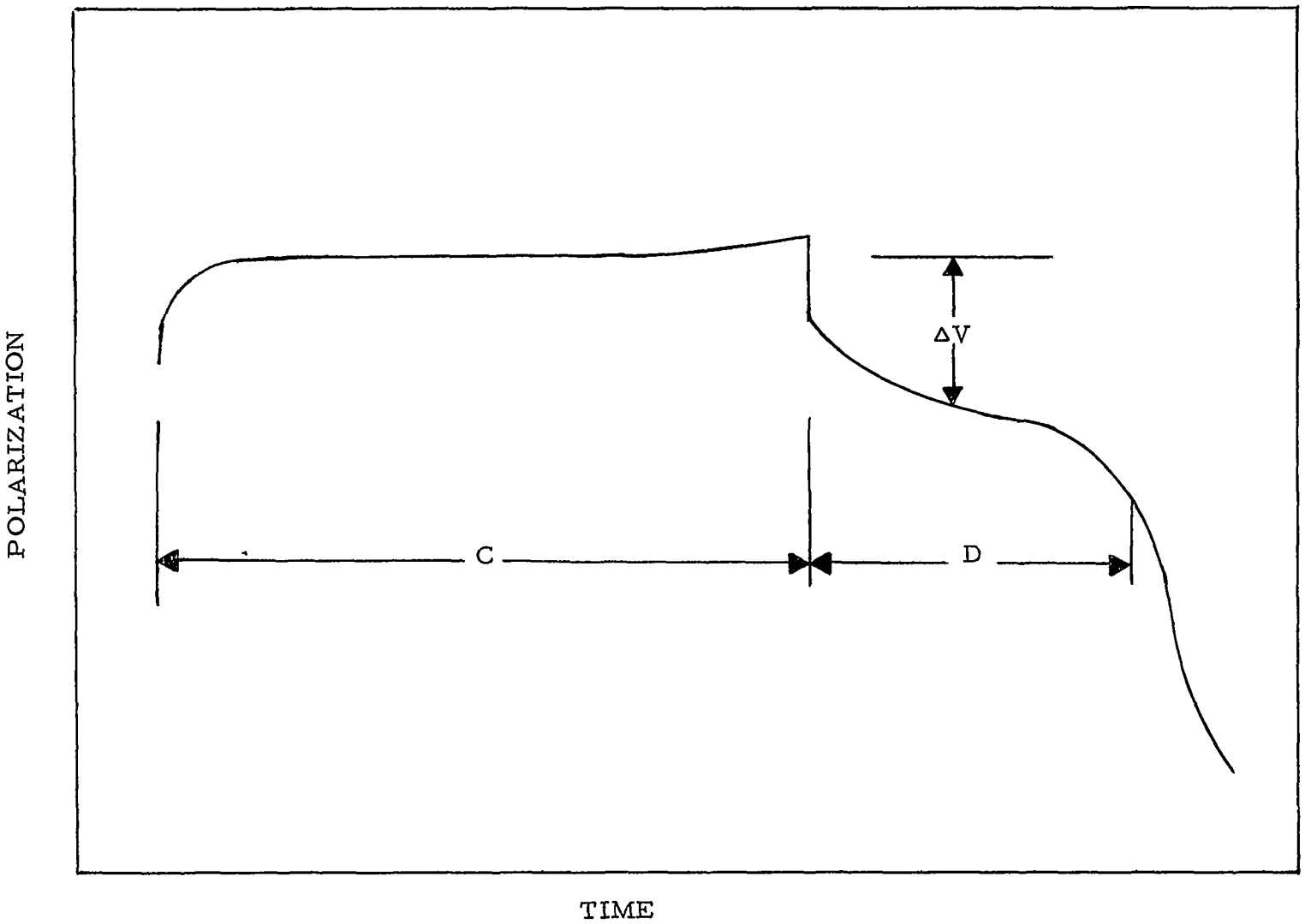

Figure 67. Representative charge and discharge curve

From the data shown in Table 31, the following seven systems were recommended for further characterization and cell development:

- AgO in butyrolactone - $LiCl + AlCl_3$
- AgF_2 in propylene carbonate - $LiBF_4$
- $CuCl_2$ in propylene carbonate - $LiClO_4$
- CuF_2 in dimethylformamide - $LiPF_6$
- CuF_2 in propylene carbonate - $LiPF_6$
- Zn in dimethylformamide - KPF_6
- Cd in dimethylformamide - $LiClO_4$

Although galvanostatic charge-discharge measurements were not carried out on the following systems, based on the cyclic voltammetric data, they are offered here as second choice candidates:

$CuCl_2$/BL-$MgCl_2$
CuF_2/PC-$LiCl + AlCl_3$
CuF_2/AN-$LiBF_4$
CuO/PC-$LiClO_4$
Zn/PC-$Ca(PF_6)_2$
Cd/DMF-$Mg(ClO_4)_2$
In/PC-$Mg(ClO_4)_2$
In/PC-$MgCl_2$

L. Chronopotentiometry of Some Recommended Systems

Chronopotentiometric measurements were made on some of the positive systems selected for further electrochemical characterization. The purpose of these measurements was to attempt to characterize the anodic (charge) reaction product. Reverse chronopotentiometry was used to characterize the location of reaction product with respect to the electrode; i.e. whether the reaction product was deposited on the electrode as an insoluble product or whether the product dissolved in the solution.

The Sand equation may be written in the form:

$$\frac{i\tau^{1/2}}{nC} = K = \frac{\pi^{1/2} FD^{1/2}}{2} \qquad (1)$$

where i is the constant current density, τ is the transition time, n is the number of Faradays per mole of reacting (diffusing) species, C is the concentration in the bulk solution, F is the Faraday, D is the diffusion coefficient of the diffusing species and K is a constant. If no supporting electrolyte is present, D may be replaced by an "effective" diffusion coefficient calculated from the transference number of the diffusing species and the equivalent conductance of the electrolyte salt (Ref. 16). By calculation of an effective D value, excellent agreement between theory and experiment has been obtained (Ref. 16).

We are concerned with anodic charge, in which a metal atom is oxidized and forms a reaction product with one or more ions diffusing to the electrode. An insoluble film may form on the electrode surface. The applicability of the Sand equation, under these circumstances, was demonstrated by Delahay et al (Ref. 17) by means of the constancy of $i\tau^{1/2}$ for the anodization of silver electrodes in 5 mM KBr aqueous solutions (no supporting

electrolyte). The insoluble AgBr film formed on the electrode did not affect the value of the diffusion coefficient. In more concentrated solutions the thickness of the film may however be large enough to have an effect on the diffusion of the reacting species.

The value of n can be useful in characterizing the reaction product resulting from oxidation of the metal electrode. As stated above, n is the number of Faradays per mole of reacting species diffusing to the electrode. For example, if the reaction

$$Cd + 2\ PF_6^- \longrightarrow Cd(PF_6)_2 + 2e^-$$

takes place at the electrode, then 2 Faradays are involved per 2 moles of PF_6^-, so that n = 1. This assumes that all oxidized cadmium ends up as $Cd(PF_6)_2$. If, however, the complex ion

$$Cd + 4\ PF_6^- \longrightarrow Cd(PF_6)_4^= + 2e^-$$

should form, then n would equal 1/2. The assumption is made that the reaction takes place at the electrode surface rather than elsewhere in the diffusion layer.

Other conceivable reactions might be:

a. $$Cd + PF_6^- \longrightarrow Cd(PF_6)^+ + 2e^-$$

In this case n = 2.

b. $$Cd + xPF_6^- \rightarrow CdF_2 + \frac{6x-2}{6-y} PF_{6-y}^{y-1} + 2e^-$$

where x is a small integer, $6x-2/6-y$ is an integer and $n = \frac{2}{x}$. This equation is usable only with $y = 1$ or 2, for which $x = 2$ or 1 respectively.

For example, a possible reaction might result in PF_5 as a product. In this case $y = 1$ and $x = 2$, so that the reaction is

$$Cd + 2PF_6^- \rightarrow CdF_2 + 2PF_5 + 2e^-$$

with n equal to 1.

This last example illustrates that a given value for n could indicate more than one reaction product, so that additional analysis would have to be made to pinpoint a probable reaction product.

If the CdF_2 or $Cd(PF_6)_2$ postulated above are soluble and undissociated, then the ratio of the reverse (cathodic) transition time to the anodic transition time would approach 1/3. For an insoluble product on the electrode surface the ratio would approach unity.

The above discussion assumes (a) only a single half-cell electrode reaction occurs (b) data can be obtained so that the "effective" diffusion coefficient can be calculated (c) solutions are dilute enough so that film thickness can be minimized (d) the reactions occur at the electrode surface and are rapid enough to be diffusion controlled (e) the equilibrium constant for the ionic dissociation of the reaction product heavily favors the undissociated species,

and (f) the transference number of any ionized reaction product is small enough so as not to alter the transference number of the reacting species.

These above restrictions may seem severe enough to limit the usefulness of chronopotentiometry, but it is likely (as indicated by the cyclic voltammetric data) that a single reaction forming an unionized product may occur under certain conditions. In such cases the technique may be useful in gaining further insight into the characterization of the positive electrode reaction species on charge and discharge.

Transference numbers were not obtained for the systems of interest, so that values of n could not be obtained, since small variations in transference number have a large effect on the effective diffusion coefficient. Initial chronopotentiometric data was obtained, however, in order to test the constancy of $K = i\tau^{1/2}/nC$ and to obtain the ratio τ_c/τ_a, i.e. the reverse cathodic transition time to the anodic transition time.

Results are presented in Tables 32 to 37. Smooth surface sheet metal electrodes (as described in the Experimental Section) were used in all cases, except for the experiment reported in Table 35 for which a porous sintered electrode was used. Linear diffusion was obtained in the cell, and transition times were short enough so that convection should not have caused any major disturbances. The anodic transition times for the smooth surface sheet electrodes were reproducible to better than ± 10%. For the porous Zn electrodes, the transition times were reproducible to better than ± 3%. A sample chronopotentiometric and reverse chronopotentiometric curve is shown in Figure 68.

Since the measurements were of a preliminary nature, only a few observations will be made. Tables 32, 33, and 36 show a constancy for $i\tau^{1/2}C^{-1}$.*

* Except for the low value at the highest c.d. (Table 36).

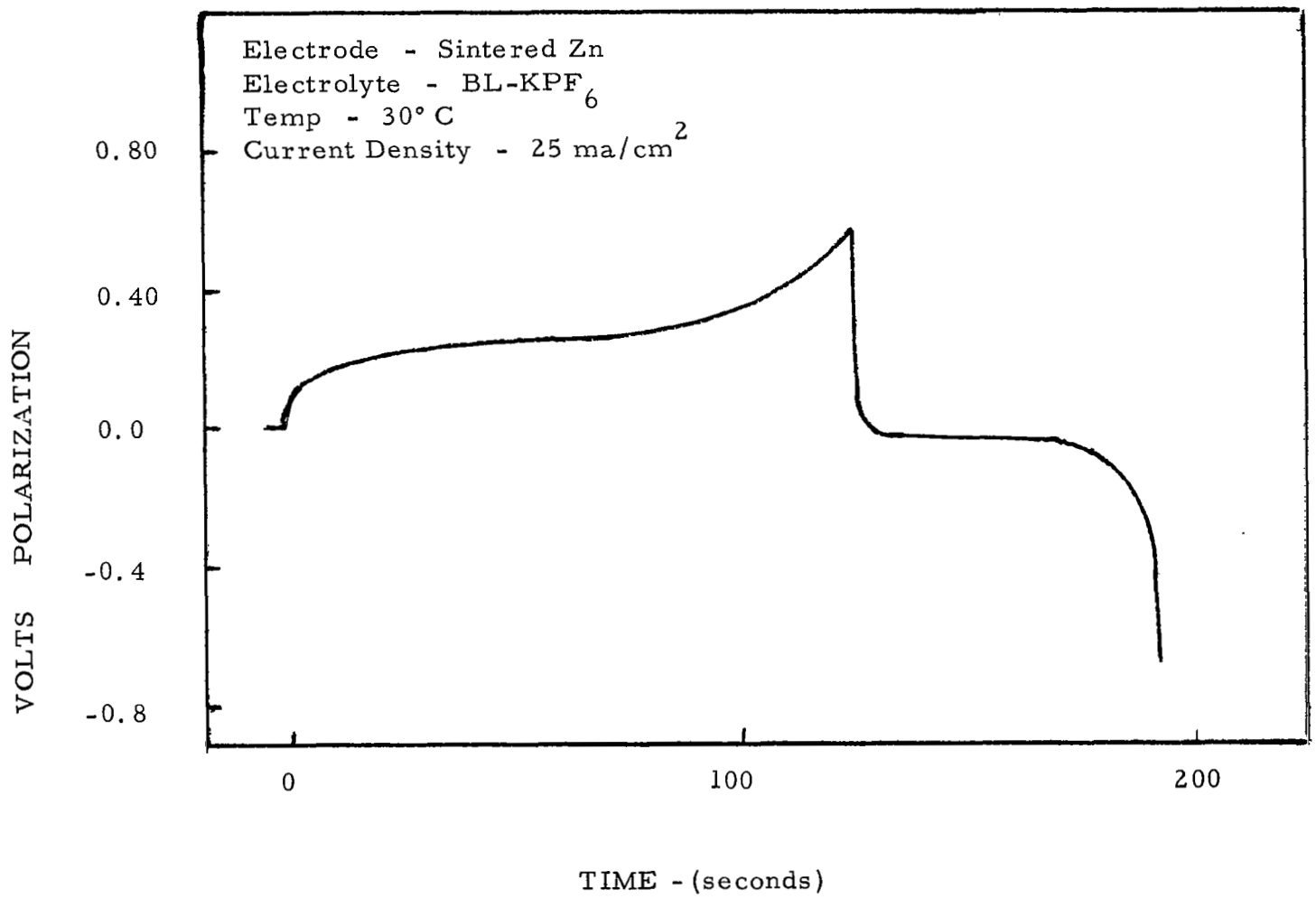

Figure 68. Chronopotentiometric curve.

TABLE 32

CHRONOPOTENTIOMETRIC DATA
FOR Zn/BL-KPF_6 (0.80 M)

i / ma cm^{-2}	τ / sec	$i\tau^{1/2}C^{-1}$ / ma cm^{-2} $sec^{1/2}$ M^{-1}	τ_c/τ_a
15	99.4	188	0.33
20	41.4	160	0.47
25	30.7	172	0.55
40	15.3	188	0.62
50	9.9	197	0.74
70	5.4	208	0.74

TABLE 33

CHRONOPOTENTIOMETRIC DATA
FOR Zn/BL-KPF_6 (0.40 M)

i / ma cm^{-2}	τ / sec	$i\tau^{1/2}C^{-1}$ / ma cm^{-2} $sec^{1/2}$ M^{-1}
15	39.4	233
20	31.9	280
25	15.5	247
40	5.7	229
50	3.3	228

The remaining tables show an increase of $i\tau^{1/2}C^{-1}$ with current.

The thickness of a film (caused by deposition of an insoluble product) is proportional to $i\tau$, which will decrease with increasing current as long as a diffusion process is the controlling factor. The slow rate of diffusion through the film is proportional to the film thickness and $i\tau^{1/2}C^{-1}$ will reflect this change in diffusion rate. In Table 37, the indicated increase of $i\tau^{1/2}C^{-1}$ with current is probably due to a film since the high values of τ_c/τ_a indicate the presence of a film.

In Tables 34 and 35, the increase of $i\tau^{1/2}C^{-1}$ with current is probably due to an increase of n with current. Table 35 data show an increase with current of τ_c/τ_a suggesting a changeover from a soluble product to an insoluble one. Though this may suggest film formation, it is doubtful that a thick film will form for a porous electrode, which has a large surface area, when a thick film does not form for exactly the same system at a smooth sheet electrode (Table 32). Also, the increase of $i\tau^{1/2}C^{-1}$ with current in Table 34 is probably due to a change in n since increasing $i\tau^{1/2}C^{-1}$ was not observed in the same system at higher concentrations of electrolyte salt (see Tables 32 and 33). Thick film formation is enhanced at high concentration rather than low.

Finally, from Tables 32, 33, and 34 it is noted that $i\tau^{1/2}C^{-1}$ increases with a decrease in electrolyte salt concentration, whereas equation (1) predicts it should remain constant. The indication is that n is increasing as the concentration decreases. This means that an actual change in reaction occurs. It has been pointed out above that for the Zn system reported in Tables 32-34 there is no thick film formation and therefore the results cannot be explained on the basis of a changing film thickness. Support for the idea of a change in reaction with concentration of electrolyte salt is also obtained from the

TABLE 34

CHRONOPOTENTIOMETRIC DATA

FOR Zn/BL-KPF_6 (0.20 M)

i / ma cm^{-2}	τ / sec	$i\tau^{1/2}C^{-1}$ / ma cm^{-2} $sec^{1/2}$ M^{-1}
10	39.0	312
15	20.4	341
20	9.3	320
25	11.5	425
40	7.5	525

TABLE 35

CHRONOPOTENTIOMETRIC DATA

FOR Zn/BL-KPF_6 (0.80 M)*

i / ma cm^{-2}	τ / sec	$i\tau^{1/2}C^{-1}$ / ma cm^{-2} $sec^{1/2}$ M^{-1}	τ_c/τ_a
15	151.0	232	0.38
20	103.0	258	0.47
25	72.2	266	0.54
40	36.6	290	0.64
50	24.4	323	0.65
70	14.8	344	0.67

* Porous electrodes were employed in this set of measurements.

TABLE 36

CHRONOPOTENTIOMETRIC DATA
FOR Cd/BL-KPF_6 (0.80 M)

i / ma cm^{-2}	τ / sec	$i\tau^{1/2}C^{-1}$ / ma cm^{-2} $sec^{1/2}$ M^{-1}	τ_c/τ_a
25	58.3	239	0.26
30	37.1	244	0.24
40	21.3	231	0.36
50	9.0	188	0.46

TABLE 37

CHRONOPOTENTIOMETRIC DATA
FOR Cu/PC-LiCl + $AlCl_3$ (0.80 M)*

i / ma cm^{-2}	τ / sec	$i\tau^{1/2}C^{-1}$ / ma cm^{-2} $sec^{1/2}$ M^{-1}	τ_c/τ_a
10.0	144.0	158	0.83
15.0	93.2	181	0.74
25.0	49.6	214	0.93
40.0	23.8	231	0.79
50.0	20.1	255	0.65
70.0	10.3	281	0.90

* Concentration with respect to each salt.

earlier discussion of concentration effects on cyclic voltammetric sweep curves. A final possibility is that due to the change of transference number and equivalent conductance with concentration, the value of K in equation (1) is changing. The final understanding of this effect must await the gathering of additional data.

III. EXPERIMENTAL

A. Material Purification and Characterization

Of critical importance to the electrochemical characterization of nonaqueous electrode-electrolyte systems is the prior chemical characterization of all materials comprising these systems or used to prepare them. The molecular complexity of the organic-inorganic solutions alone demands that wherever possible, within the limits of practicability, extraneous impurities be removed, and whatever remains at least be known and characterized. The most obvious impurity in nonaqueous systems is water. For this reason, preparation and storage of all solutions was performed in a dual chamber gloved dry box under a nitrogen atmosphere. The box was maintained at 30 ± 1° C by a recirculating gas heating system. All conductance and electrochemical measurements (with the exception of PF_5 and BF_3 systems) were performed in the dry box, with lead connections to the instruments on the outside via sealed couplings. In a number of cases, known amounts of water were deliberately added to determine the effect on the voltammograms.

Wherever possible, materials were analyzed by an outside testing laboratory. In some cases, however, it was not possible to characterize the material. This was particularly true for the complex fluoride materials (hexafluorophosphates and tetrafluoroborates) prepared in-situ in the solvent. Also, characterization by X-ray diffraction of the fluorinated metal wire electrodes proved to be experimentally difficult. Recognition of the limitations in chemical characterization is a necessity to proper interpretation of the electrochemical data. The minimum requirements are reproducibility of results, unless the complexity of the electrochemical reaction prohibits it within the scope of the measurement technique, and assurance that the results are not due to some artifact. Wherever practically possible in the screening of more than a thousand systems these requirements have been met.

1. Solvent Purification and Characterization

The solvents employed were dimethylformamide, butyrolactone, propylene carbonate, and acetonitrile. With the exception of dimethylformamide, purification of each of these materials was accomplished by vacuum distillation. Solvents were distilled at the indicated temperature and pressure in the same apparatus. Usually 1500 ml portions were distilled, with about 100 ml comprising the main cut, the remainder being divided between the head fraction and pot residue. The distillation apparatus consisted of 1 inch by 3 feet vacuum jacketed (and silvered) column packed with 3/8" beryl saddles, and equipped with a total reflux return head. The head was connected to a revolving type multiple distillation receiver through a stopcock which was used to adjust the take-off rate. Connection was also made to the usual vacuum manifold consisting of rough and fine manometers connected in series with a Cartesian manostat, dry ice trap and vacuum pump. After distillation startup and removal of low boiling impurities, the column was purposely flooded to insure proper wetting. It was then allowed to equilibrate over a 1-2 hour period and fractionation commenced. The main fractions were usually taken over a 48-hour period at a reflux ratio of 20-25/1. Use of higher reflux ratios did not improve the fractionation characteristics.

Although initially a single distillation had sufficed for the purification of propylene carbonate, this method did not suffice for the purification of later quantities. It was found that water apparently reached a constant level in all fractions obtained in the distillation. Since it was known that the distillation procedure was capable of removing water originally present, it was suspected that an impurity was present in the propylene carbonate which slowly decomposed under the distillation conditions, yielding water as one of the products. Therefore, following the first distillation, the main cuts of propylene carbonate were dried over calcium sulfate, filtered, and carefully redistilled. This procedure afforded propylene carbonate of reproducible purity.

Analysis of the solvents was usually carried out by vapor phase chromatography (VPC). An aerograph A-90-P vapor phase chromatograph equipped with a hot wire detector was used for the analysis under the conditions shown in Table 38.

TABLE 38 VAPOR PHASE CHROMATOGRAPHY CONDITIONS

Solvent	Column Temp. °C	Injector Temp. °C	Detector Temp. °C	Helium Flow Rate ml/min
Propylene carbonate	190	240	260	85
Dimethylformamide	160	238	260	40
Butyrolactone	171	235	250	120

All analyses were obtained on a 1/4 inch by 6 feet s.s. column packed with 20% PEG 1540 on HMDS-treated 60/80 mesh chromosorb P. Use of a column packed with GE SF-96 silicone oil on 60/80 mesh firebrick afforded little or no resolution for the compounds investigated. Usually 3-4 μl samples were used in the order to reveal trace impurities without overloading the column. Stable baselines were obtained at maximum instrument sensitivity.

a. Butyrolactone (MCB*, b.p. 91-93° C/17 mm)

This material showed water ($\sim$ 0.1 mole %) as the only impurity by VPC analysis on a polyethylene glycol (PEG) 1540 column. The butyrolactone

* MCB - Matheson, Coleman, and Bell.

was fractionally distilled through a 3-foot column at 91-93° /17 mm. Four cuts were taken, the first two comprising about 10% of the total volume. VPC's of the latter two fractions showed no impurities. VPC of the first fraction, however, showed two additional impurities close to the main peak. These impurities were also present in the second fraction to a lesser extent. Since it was evident these impurities were readily concentrated in the head cuts, a somewhat larger head fraction (300-400 ml) was usually taken to insure their removal from the main fraction of distilled butyrolactone. VPC analysis following distillation showed less than 100 ppm water. Butyrolactone (main fraction) stored in glass bottles showed no change after two weeks.

b. Dimethylformamide (MCB, Spectroquality grade)

This material was subjected to VPC analysis on a PEG 1540 column. No impurities were detected under conditions where as little as 0.01 mole % water would have been evident. Distillation of dimethylformamide at 80° C/40 mm yielded material showing no impurities of any of the fractions by VPC analysis. It therefore appeared unnecessary to distill dimethylformamide, and subsequent solution preparation was accomplished using "as received" material.

c. Acetonitrile (MCB, chromatoquality)

This material was distilled at 80° C through a 3-foot column. VPC analysis of this specific lot by Matheson, Coleman and Bell on 3,3' - iminodipropionitrile column showed acrylonitrile (0.15%) as the only impurity. Resolution of trace amounts of water in acetonitrile was not possible on a PEG column,

since the large acetonitrile peak obscured possible small quantities of water. Resolution of water was attempted on a tris.cyanoethoxy-propane column as well as on a diethyleneglycol stearate column. Neither of these substrates were successful, requiring that analysis of water be made by the Karl Fischer method. Distilled under the above conditions, the acetonitrile contained 60-80 ppm water.

d. Propylene Carbonate (MCB, b.p. 108-110° /10 mm)

This was subjected to VPC analysis on a PEG 1540 column. The material showed five peaks in addition to the air peak. The first peak probably contained both air and carbon dioxide, but resolution of these components under the conditions employed was not possible. The second peak (probably propylene oxide) was 0.22 to 0.25 mole %. The third peak, identified as water by peak enhancement techniques, was 0.02 to 0.03 mole %. A fourth peak of the same area as the third was unidentified. The fifth peak, tentatively identified as propanediol by boiling point considerations, usually comprised 0.16 to 0.25 mole %. The sixth peak corresponded to propylene carbonate. The indicated variation was between various lots of "as received" propylene carbonate. Distillation of propylene carbonate at 109° /10 mm. followed by VPC analysis indicated that the impurities corresponding to the fourth and fifth peaks were removed. The amount of propylene oxide was reduced to 0.01 - 0.02 mole %, while the amount of water was 0.015 - 0.025 mole %. The variations in the amount of these impurities did not occur between samples obtained in a single batch distillation (neglecting the head cuts which were discarded) but were obtained between the main cuts of separate distillations. Alteration of such factors as reflux ratio (100:1 to 25:1) produced no change (within analytical limits) in the amounts of propylene oxide or water. Some unobserved variation in distillation technique may have produced a small change in the amounts of residual impurities. Propylene carbonate distilled in this manner contained 90 - 150 (low and high) ppm water.

2. Solute Purification and Characterization

In the initial portion of the program, most of the reagent grade solutes chosen for screening were further purified only by vacuum drying. Analysis of these materials (Table 39) indicated that they were reasonably pure and that expected impurities would not markedly affect the interpretation of the cyclic voltammograms. Any salts or mixtures of salts used in the program and not specified in this section were prepared in-situ as described in Section 3 (Solution Preparation). After drying of the salts described in this section, dry nitrogen was the only atmosphere brought in contact with them.

a. Lithium chloride (J. T. Baker, reagent grade) was initially dried at 110° C for 3 hours, and was then analyzed for lithium and chloride content. Analysis by flame photometry yielded 16.4% lithium, and analysis by Volhard's method gave 82.8% chloride for a total of 99.2% LiCl in the Sample. The LiCl was then dried in a flask at 25° C for 24 hours by evacuating to a pressure of 2 torr through a dry ice-acetone trap. After 24 hours the temperature of the evacuated flask was gradually raised over a 48 hour period to promote the removal of the remaining water. Possible hydrolysis under the drying conditions would leave a small amount of lithium oxide in the material. It was felt that the lithium oxide, because of its insolubility, would not affect the electrochemical reaction (except to act as a partial water scavenger for the solvents).

Results of spectrographic analysis of the lithium chloride for trace constituents are reported in Table 39.

b. Lithium fluoride (J. T. Baker, reagent grade) was initially dried at 110° C for 3 hours, and was then analyzed for lithium and chloride content. Analysis by flame photometry yielded 26.7% lithium, and determination of fluoride as lead chlorofluoride gave 73.24% fluoride for a

TABLE 39

SPECTROGRAPHIC ANALYSIS OF METAL SALTS* (In per cent)

Element	$LiCl$	LiF	MgF_2	$MgCl_2$	$LiClO_4$	$Mg(ClO_4)_2$	$CaCl_2$	CaF_2
Fe	0.0060	0.00042	0.0170	0.0052	nil	nil	nil	0.0097
Al	0.0092	0.00017	nil	nil	nil	nil	nil	0.0073
Cu	0.00012	0.00025	0.00033	0.0027	0.00005	0.0013	0.00007	0.00003
Ni	nil	0.00014	nil	nil	nil	nil	nil	nil
Ca	0.0260	0.0016	0.0430	0.0024	0.0020	0.0070	nil	nil
Si	0.0036	0.0015	0.0510	0.0051	nil	nil	0.0054	0.27
Mg	0.00038	0.00012	nil	nil	0.00061	nil	0.47	0.36
Na	nil	nil	nil	nil	nil	nil	nil	nil
K	nil	nil	nil	nil	nil	nil	nil	nil
Mn	nil	0.00005	0.0110	0.0110	nil	nil	nil	0.0015
B	nil	nil	0.0330	nil	nil	nil	nil	nil
Ti	nil	nil	0.0055	0.0022	nil	nil	nil	nil
Sr	nil	nil	nil	nil	<0.0002	nil	0.012	0.016
Ag	-	-	-	-	-	-	0.00022	nil
Cr	-	-	-	-	-	-	nil	0.00080

*Analysis by emission spectroscopy (Truesdail Laboratories, Inc., Los Angeles, Calif.). Limits of detector of sodium and potassium by this method approximately 0.02%.

total of 99.9 + % LiF in the sample. The LiF was then dried at 110° C for 74 hours and thereafter kept under a dry, inert atmosphere. Titration with Karl Fischer reagent indicated a water content of 120 ppm. At 110° C there is some possibility of hydrolysis (by trace moisture) to lithium hydroxide and hydrogen fluoride. The hydroxide was not expected to interfere with the measurements. Since the lithium fluoride-hydrogen fluoride complex is unstable even at room temperature, contamination due to hydrogen fluoride is not expected.

Results of spectrographic analysis of the lithium fluoride for trace constituents are reported in Table 39.

c. Magnesium fluoride (Research Inorganic Chemical Co., powder, 99% purity) was initially dried at 110° C for 3 hours, and was then analyzed for magnesium and fluoride content. Magnesium, determined as a pyrophosphate, was present to the extent of 35.2%. Determination of fluoride as lead chlorofluoride gave 55.3% fluoride for a total of 90.5% magnesium fluoride in the sample. This low percentage is hard to reconcile for three reasons: the advertised purity of the MgF_2 is 99%, the salt is not particularly hygroscopic, and the ratio of 35.2% Mg to 55.3% F_2 is the expected ratio of atomic weights for pure MgF_2. We will assume that the purity of the MgF_2 was 99%. The primary impurity expected was magnesium oxide (< 1%) which is essentially insoluble in organic solvents. Since hydrogen fluoride (possibly formed by hydrolysis) does not form a complex with magnesium fluoride, acidic contamination should not have been a factor. The MgF_2 was then dried at 110° C for 72 hours and thereafter kept under a dry, inert atmosphere.

Results of spectrographic analysis of the magnesium fluoride for trace constituents are reported in Table 39.

d. Lithium fluoride - magnesium fluoride mixture was prepared from an equimolar mixture of the dried salts by dry mixing.

e. Magnesium chloride (Research Inorganic Chemical Co., grade: 98 + %) was initially dried at 110° C for 3 hours, and was then analyzed for magnesium and chloride content. Magnesium determined as a pyrophosphate was present to the extent of 24.31%, and analysis by Volhard's method gave 68.69% chloride for a total of 93.00%. Since $MgCl_2$ is hygroscopic, the 7% impurity is expected to be mainly water. A maximum of 2% MgO is the only other major impurity listed in the analysis reported by the supplier. The ratio of 24.31% Mg to 68.69% Cl_2 indicates that about 1.3% MgO is present in the sample. MgO is essentially insoluble in organic solvents, and it is expected that the MgO will not have any appreciable effect upon the electrochemistry.

The $MgCl_2$ was then vacuum dried in a flask at 25° C for 24 hours at 1 torr, the dry ice-acetone trap being checked and cleaned after eight hours. After 24 hours no H_2O was observed in the trap and the temperature was then raised to 80° C. After 72 hours the salt was removed and pulverized in a dry box. The salt was then maintained at 80° C and 1 torr for 48 additional hours. At the end of this time, no H_2O was observed in the trap. Some $MgCl_2$ was further dried at 125° C and 2 torr. A temperature of 125° C was chosen, since it was stated in the literature that complete dehydration would occur under these conditions, and hydrolysis would be kept at a minimum.

Results of spectrographic analysis of the magnesium chloride for trace constituents are reported in Table 39.

f. Magnesium chloride - lithium chloride mixture was prepared from equimolar quantities of dried salts by dry mixing.

g. Lithium perchlorate (Research Inorganic Chemical Co., grade: anhydrous, 99% purity) was initially dried at 110° C for 3 hours, and was then analyzed for lithium and perchlorate content. Analysis by flame photometry indicated 6.00% lithium. Perchlorate was reduced to chloride by fusion with ammonium chloride followed by the gravimetric determination of the resulting chloride ion. 82.09% perchlorate was found in the sample. Less than 0.006% chloride and chlorate were found in the sample. The ratio of 6.00% Li to 82.1% perchlorate indicates that over 99.5% of the lithium salt is lithium perchlorate. Any LiO formed on further drying should have no deleterious effects as has been discussed earlier. About 12% water is present in the sample after 3 hours drying at 110° C. The salt was further dried in a flask at 25° C for 24 hours by evacuating to a pressure of 1 torr through a dry ice-acetone trap. Then the evacuated flask was heated and kept at 90° C for 72 hours. The temperature was then raised and kept at 140° C (under 1 torr) for 24 hours and finally the evacuated sample was held at 175° C for 24 hours. No additional H_2O was found in the trap at the final temperature.

Results of spectrographic analysis of the magnesium chloride for trace constituents are reported in Table 39.

h. Lithium chloride - lithium perchlorate mixture was prepared from an equimolar mixture of the dried salts by dry mixing.

i. Magnesium perchlorate (J.T. Baker, anhydrous Anhydrone grade) was analyzed directly upon removal of the sample from its container. Magnesium was determined by atomic absorption spectroscopy and 9.83% was found. The perchlorate anion was analyzed by fusion with sodium carbonate to effect reduction to chloride. The chloride was then determined by Volhard titration. The determination yielded 85.10% perchlorates. The ratio of 9.83% Mg to 85.10% perchlorate indicates a slight excess of per-

chlorate over that expected for pure $Mg(ClO_4)_2$. Total halides ($Cl^- + Br^- + I^-$) were determined turbidimetrically by measuring the opalescence produced with silver nitrate against standards of known chloride concentrations. Total halides found were 0.0007%. Fluoride was determined by distillation with sulfuric acid and colorimetrically by the Alizarin method; fluoride found was 0.0018%. The total salt content of 95% indicates that 5% water was in the sample. Therefore the salt was vacuum dried at 25° C and 1 torr for 24 hours. The vacuum drying was then continued for 72 hours at 250° C in order to remove the remaining water.

Results of spectrographic analysis of the magnesium perchlorate for trace constituents are reported in Table 39.

j. Calcium chloride (Mallinckrodt, anhydrous reagent grade, 40 mesh) was analyzed for major constituents directly upon removal of the sample from the container. Calcium, determined by oxalate precipitation and permanganate titration, was present in the amount of 35.40%. Chloride, determined by the Volhard titration method, was present in the amount of 62.39%. The ratio of 35.40% calcium to 62.39% chloride is very close to that expected for pure $CaCl_2$. Fluoride was analyzed by distilling with sulfuric acid followed by colorimetric determination by the Alizarin Method. The amount of fluoride found was 265 parts per million. The total $CaCl_2$ content of 97.8% compares favorably with the minimum assay of 96.0% $CaCl_2$ specified by Mallinckrodt. Mallinckrodt specified that 1.0% magnesium and alkali salts are present. Therefore, the sample contained 1% water or less. The calcium chloride was vacuum dried for a short period of time at 150° C.

Results of spectrographic analysis of the calcium chloride for trace constituents are reported in Table 39.

k. Calcium fluoride (Matheson, Coleman, and Bell reagent grade, powder) was analyzed for major constituents directly upon removal of the sample from the container. Calcium was determined by oxalate precipitation and permanganate titration; percentage calcium found was 49.80%. Fluoride was determined by fusion of the sample with K_2CO_3-KNO_3 flux. The soluble fluoride was then precipitated and weighed as chlorofluoride. Percentage fluoride found was 47.54%. Trace halides ($Cl^- + Br^- + I^-$) were determined turbidimetrically by measuring the opalescence produced with silver nitrate against standards of known chloride concentrations. Total halides found (calculated as chloride) was 0.0015%. The ratio of 49.80% calcium to 47.54% fluoride is very close to that expected for the pure salt. The total CaF_2 content is 97.3%. The salt was vacuum dried for a short period of time at 200° C.

Results of spectrographic analysis of the calcium fluoride for trace constituents are reported in Table 39.

1. Aluminum chloride (Matheson, Coleman, and Bell anhydrous reagent grade). No analysis for major constituents or spectrographic analysis for trace impurities was performed. Instead the standard procedure for purification by sublimation was followed. A very pure product is obtained by this procedure. A sublimation flask and a receiving flask were connected by a short wide, connecting tube. A stream of dry nitrogen was continually passed through the sublimation flask and out through the receiving flask. The entire system was flamed (heated) prior to sublimation in order to degas the walls. The sublimation was carried out by gently heating (to approximately 170° C) the sublimation flask and the connecting tube and cooling the receiving flask in a water bath. Upon completion of the sublimation, the $AlCl_3$ was kept under dry nitrogen during cooling and then during storage.

No spectrographic analysis for trace constituents was made for this salt.

m. Potassium hexafluorophosphate (Ozark-Mahoning, 98% minimum purity) was analyzed by fluoride analysis. The assay indicated the sample was 99.6% KPF_6. This salt was then vacuum dried at 25° C and 1 torr for 24 hours. The salt was further dried at 130° C and 1 torr for 24 hours. Since the salt may be recrystallized from water, it was not expected that appreciable hydrolysis or dissociation would occur under the drying conditions. The small amount of impurity indicated by the analysis is probably due to the presence of lithium oxide, which would not be expected to interfere with the sweep determinations.

No spectrographic analysis for trace constituents was made for this salt.

n. Phosphorous pentafluoride (Matheson Co., 99% minimum purity) was used directly from the gas cylinder as described in Section 3 (Solution Preparation).

o. Boron trifluoride (Matheson Co., C.P. grade, 99.5% minimum purity) was used directly from the gas cylinder as described in Section 3 (Solution Preparation).

p. Lithium hexafluorophosphate and lithium tetrafluoroborate have appreciable dissociation pressures at 25° C. Therefore these materials were prepared in-situ from $LiF + PF_5$ and $LiF + BF_3$ respectively, as described in Section 3 (Solution Preparation).

3. Solution Preparation

All materials were stored after drying in closed containers in a glove bag under nitrogen. All manipulation of solvents and solutes was accomplished

in the dry box under nitrogen. Where necessary, cooling was furnished by a cold-finger which was flame-dried and positioned in the exterior wall of the dry box. After cooling with the cold-finger, the flask in which the solution was to be prepared was positioned around the cold-finger while coolant was added externally. Usually the rate of addition of solute was controlled so as to maintain the temperature in the solution flask at -5° to 10° C.

The procedure used in preparing the solution was to prepare an initial solution in such proportions as to yield a 0.5 m solution. If the solute was insufficiently soluble, the solution was allowed to stand overnight, (48 hours in the mixed salts) filtered, and the conductivity determined. If the solute was soluble, an increment of solute (sufficient to bring the solution to 0.75M) was added and the conductivity redetermined. If the conductivity had not changed by 0.5×10^{-n} ohm $^{-1}$cm^{-1} (n being the same order as that in the initial conductivity measurements) the solution was filtered and used at this concentration for the cyclic voltammetry procedure. If the conductance changed by more than 0.5×10^{-n} ohm^{-1}cm^{-1}, the incremental addition procedure was repeated until the change in conductivity was less than 0.5×10^{-n} ohm^{-1}cm^{-1}. Subsequent preparation of new batches of the same solution were prepared directly at that concentration giving this optimum conductivity. In all cases, conductivities were redetermined for all newly-prepared solutions

Conductivity measurements were obtained at 1000 cycles per second using an Industrial Instruments Inc. Model RC 16B2 conductivity bridge. A Tektronic Type 536 oscilloscope was placed in the detector arm for increased null sensitivity.

Solutions of lithium chloride - aluminum chloride were prepared by initially

saturating 150 ml of solvent with excess LiCl. An equimolar quantity of aluminum chloride was added to this solution over a 2-hour period at 0° to 5° C. If saturation was maintained after stirring for 24 hours at room temperature, the solution was filtered and used. If saturation was not maintained, further solute was added as described above. Since the complex salt $LiAlCl_4$ was not prepared by the fusion procedure, no assumption of dissolved $AlCl_4$ - ion will be made, and such systems will be described as mixtures of LiCl and $AlCl_3$. Equimolar solutions of lithium perchlorate - aluminum chloride were prepared as described above for LiCl - $AlCl_3$ except that the $AlCl_3$ was added at -15° C.

Preparation of PF_5, BF_3, and lithium salts of complex fluorides required special handling.

a. PF_5 solutions

The stainless steel gas manifold used for the preparation of PF_5 solutions is shown in Figure 69. The manifold was conditioned by evacuating for several hours at 0.05 mm, refilling with PF_5 to 15 psig, and re-evacuation to remove any gaseous reaction products.

After filling the three-neck flask with about 240 ml of solvent in the inert atmosphere chamber, the pyrex gas inlet tube of the flask was connected to the manifold by means of a short Tygon connector. The entire system was then flushed with nitrogen. After removal of nitrogen by evacuation, the gas bulbs were filled to 60 psig with PF_5. The latter was then slowly introduced to the solvent at a rate allowing complete absorption of the gas. The amount of gas being absorbed was monitored by the oil-filled bubbler on the gas exit tube. Following solution preparation, the gas exit tube was replaced by a special dip tube which allowed direct transfer of the solution to the measurements involving either PF_5 of BF_3 solutions. The cell was

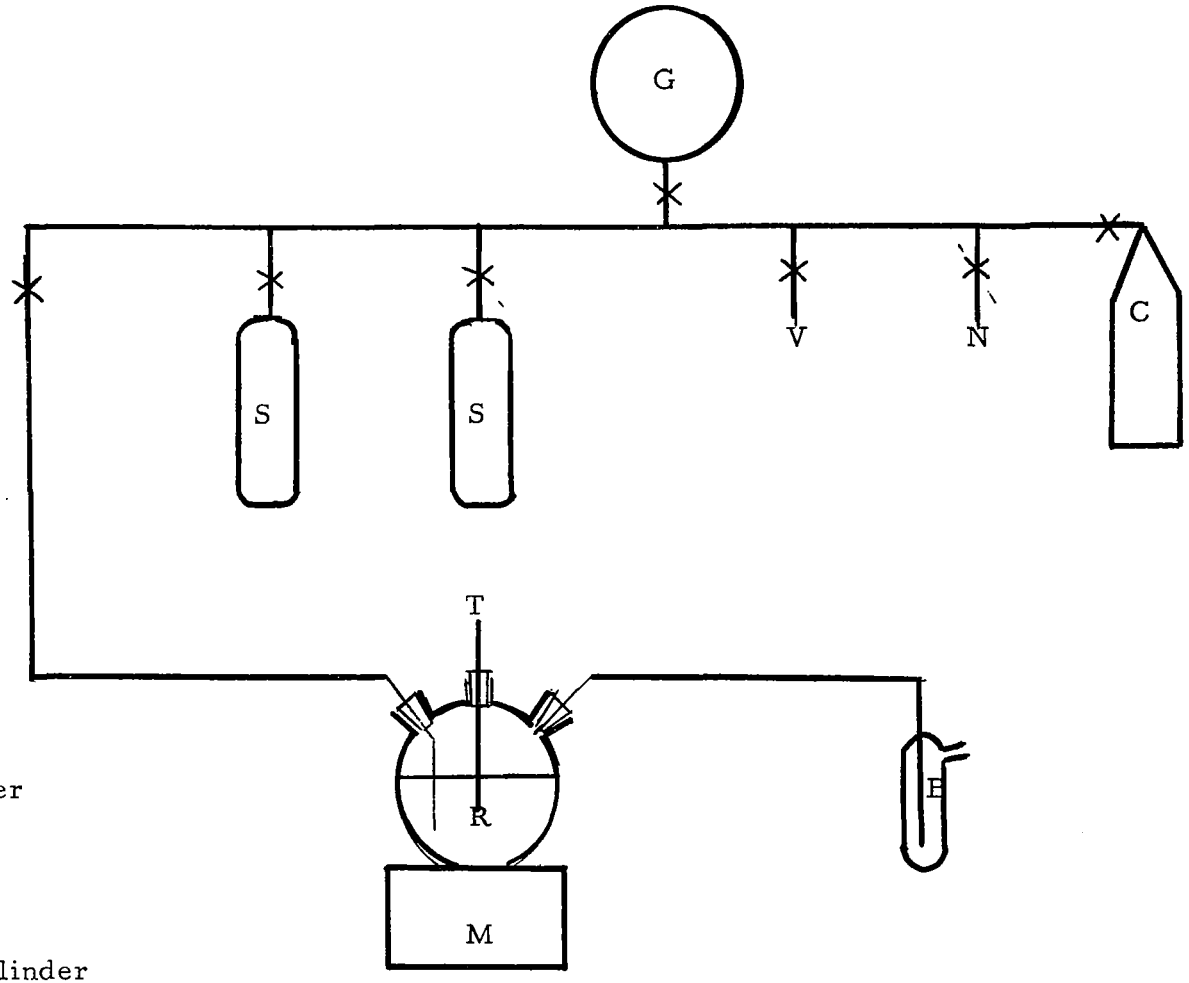

G - gauge
B - bubbler
M - magnetic stirrer
R - reaction flask
S - storage bulb
V - vacuum
N - nitrogen
C - PF_5 or BF_3 cylinder
T - thermometer

Figure 69. Schematic of apparatus for preparing complex fluoride salts in-situ.

not placed in the dry box in order to avoid possible contamination of the chamber with these gases.

All solutions were prepared at room temperature. In the case of dimethylformamide, propylene carbonate, and acetonitrile, there was evidence of deposition of a solid complex on the walls of the gas addition tube. (The complex was apparently soluble in the solvent). Solutions of PF_5 in dimethylformamide and propylene carbonate were colorless and did not discolor after several hours. The PF_5-acetronitrile solutions were yellow. This color persisted for several hours but could be removed by the addition of LiF. The addition of PF_5 to butyrolactone caused immediate discoloration of the solution which intensified on longer standing.

b. BF_3 solutions

Solutions of BF_3 were prepared in the same manner as for PF_5 except for the fact that the solvent temperature was usually maintained at 8-10° C in order to increase the apparent BF_3 solubility. After BF_3 addition was completed, the solution was allowed to warm to room temperature before transferring to the conductance or CV measuring cell. As in the case of PF_5, addition of BF_3 to butyrolactone caused extensive discoloration.

c. $LiPF_6$ and $LiBF_4$ solutions

Solutions of $LiPF_6$ and $LiBF_4$ were prepared in a manner similar to that described above except that a known quantity of LiF was suspended in the solvent before addition of the PF_5 or BF_3 respectively. Essentially all of the LiF dissolved on addition of equimolar quantities of the gases, indicating relatively complete formation of the complex fluoride salts. Additions were carried out at 8-10° C.

Since PF_5 appeared to react in a deleterious manner with butyrolactone, the preparation of $LiPF_6$ in-situ was not deemed advisable. Direct reaction of LiF with PF_5 was attempted without success. A 5.0 g sample of LiF was placed in a nickel tube connected to the gas manifold. The tube was evacuated and filled with PF_5 to 25 psig. This quantity of PF_5 was insufficient to react with all of the LiF. Even after slowly heating to 290° C, no pressure drop was observed, indicating little or no formation of $LiPF_6$ under these conditions. An alternate procedure involving solution of LiF in liquid PF_5 at -88.5° C afforded no product.

d. $Mg(PF_6)_2$, $Ca(PF_6)_2$, $Mg(BF_4)_2$, and $Ca(BF_4)_2$ solutions

The magnesium and calcium salts of the complex fluorides were prepared as in c. above from MgF_2 and CaF_2, respectively. In most cases undissolved material remained, either unreacted fluoride or precipitated complex fluoride. Although the conductivity compared with BF_3- or PF_5- solvent mixture was generally not significant, the voltammetric data indicated marked differences with the complex fluoride solutions, depending on the electrode. Thus although BF_3, $Mg(BF_4)_2$, and $Ca(BF_4)_2$ in dimethylformamide all resulted in instrument overload for zinc and cadmium electrodes, iron gave overload only in DMF-BF_3. Iron exhibited both anodic and cathodic peaks in the high current density range in the case of DMF-$Mg(BF_4)_2$. In DMF-$Ca(BF_4)_2$, iron showed a very high anodic peak with the total absence of a cathodic peak. Again, the cyclic voltammogram of cadmium in propylene carbonate - PF_5 exhibited a peakless anodic current of 160 ma/cm^2, and a cathodic peak of 90 ma/cm^2, although Cd in PC-$Ca(PF_6)_2$ and $Mg(PF_6)_2$ resulted in voltage overload of the instrumentation, with current densities of 1.2 amps/cm^2 for the former solution, and 300-400 ma/cm^2 for the latter solution. Other examples of varying electrochemical behavior exist, indicating that although the complex fluoride solutions are not well characterized, existence of complex fluoride ions must be suspected.

4. Electrode Preparation and Characterization

a. Wire electrodes

The following metals were used for electrodes:

(1) Copper (Matheson Scientific Co., soft #65710-10, 0.051" dia.)

(2) Silver (E.H. Sargent & Co., 99.5 - 99.8% pure, #S-85235, 0.051" dia.)

(3) Nickel (Matheson Scientific Co., pure grade #65730-10, 0.064" dia.)

(4) Cobalt (Leico Industries, Inc., 99.9% pure, 0.040" dia.)

(5) Zinc (Stamford Processing Co., 99.9% pure, 0.050" dia.)

(6) Cadmium (Stamford Processing Co., 99.9% pure, 0.050" dia.)

(7) Molybdenum (Climax Molybdenum Co., Climent R. (0.040" dia.)

(8) Indium (Leico Industries, 99.97% pure, 0.032" dia.)

(9) Iron (Atomergic Chemicals Co., 99.998% pure, 0.040" dia., Leico Industries, Inc., 99.99% pure, 0.030" dia.)

(10) Chromium plate (Matheson, Coleman and Bell, 99% technical grade CrO_3)

(11) Manganese plate (Matheson, Coleman and Bell, reagent grade $MnSO_4 \cdot H_2O$, reagent grade $(NH_4)_2 SO_4$)

(12) Vanadium (Leico Industries, Inc., 99.8% pure, 0.040" dia.)

(13) Lithium (Foote Mineral Co., 99.9% pure, extruded to 0.050" dia.)

(14) Magnesium (Leico Industries, Inc., 99.9% pure, 0.032" dia.)

(15) Calcium (United Mineral and Chemical Corp., 99.9% pure, 0.92" rod, machined to 1/4" dia. and extruded to 0.050" dia.)

Results of spectrographic analysis for trace constituents for most of the electrode metals are given in Table 40. It is probable that the indicated

TABLE 40

SPECTROGRAPHIC ANALYSIS OF WIRE ELECTRODES* (In per cent)

Element	Cu[a]	Ag[a]	Ni[a]	Co[b]	Zn[c]	Cd[c]	Mo[b,c]	In[c]
Co	nil	nil	0.1600	-	nil	nil	nil	nil
Ti	nil	nil	0.0140	nil	nil	nil	nil	nil
Cu	-	0.0091	0.0320	0.0020	0.00057	0.00043	nil	0.00022
Al	nil	nil	<0.003	nil	nil	nil	nil	nil
Fe	0.00091	<0.001	0.0540	0.0050	0.0030	nil	0.078[c]	nil
Si	nil	nil	0.0500	0.0010	0.0027	0.0046	<0.01[c]	0.0078
Mn	nil	nil	0.1300	nil	nil	nil	nil	nil
Mg	0.00019	0.00024	0.0320	nil	0.0038	0.00030	nil	0.00038
B	nil	nil	0.0063	nil	nil	nil	nil	nil
Ag	0.0013	-	nil	nil	0.00094	nil	nil	nil
Ni	<0.001	nil	-	<0.1	nil	<0.0005	<0.001[b]	nil
Ca	0.00078	<0.0002	nil	nil	nil	<0.0002	nil	0.0011
Pb	nil	<0.004	nil	nil	0.020	<0.005	nil	<0.005
C	-	-	-	0.0400	-	-	0.002[b]	-
S	-	-	-	0.0300	-	-	-	-
Sn	nil	nil	nil	nil	0.0072	nil	nil	nil
Zn	nil	nil	nil	nil	-	0.043	nil	nil

a. Emission spectrography by Truesdail Labs., Los Angeles.

b. Typical analysis supplied by seller.

c. Emission spectrography by Pacific Spectrochemical, Los Angeles.

TABLE 40 (Cont'd)

SPECTROGRAPHIC ANALYSIS OF WIRE ELECTRODES* (In per cent)

Element	Fe[c] (99.99)	Fe[c] (99.998)	Cr(Ni)[c]	Mn(Ni)[c]	V[c]	Li[b]	Mg[b]	Ca[b]
Co	0.0064	nil	nil	nil	nil	nil	nil	nil
Al	nil	nil	nil	nil	nil	0.0005	0.005	0.0090
Cu	0.14	<0.0005	nil	0.014	nil	nil	nil	<0.004
Cr	0.021	nil	-	0.0041	nil	nil	nil	<0.004
Fe	-	-	nil	0.019	0.020	0.0005	0.001	<0.004
Si	nil	nil	0.017	<0.005	0.060	0.001	0.005	nil
Mn	0.093	nil	nil	-	nil	nil	0.004	<0.004
Mg	nil	nil	nil	0.0048	nil	nil	-	nil
*K	nil	nil	nil	nil	nil	0.07	nil	<0.001
Ag	nil	nil	nil	0.0023	nil	nil	nil	nil
Ni	0.024	nil	0.019	0.025	nil	nil	0.001	<0.004
Ca	nil	nil	nil	0.0070	nil	0.0001	nil	-
Pb	nil	<0.010	nil	nil	nil	nil	nil	nil
C	-	-	-	-	0.032	-	-	-
B, Cd	-	-	-	-	-	-	-	<0.0002
Sn	0.016	nil	nil	nil	nil	nil	nil	nil
Cl	nil	nil	nil	nil	nil	0.04	nil	nil
Mo	0.032	<0.003	nil	nil	0.020	nil	nil	nil

b. Typical analysis supplied by seller.

c. Emission spectrography by Pacific Spectrochemical, Los Angeles.

* The same analysis was obtained for Li and Na.

impurities do not affect the nature of the electrochemical processes involved in the electrochemical measurements. The electrodes were used without any pre-treatment other than the ten cyclic voltammetric sweeps made prior to the final sweep.

The chromium and manganese electrodes consisted of these metals plated onto nickel. Spectrographic analyses were performed on samples of the electroplate taken by scraping off the plate. The manganese plating was done as follows The nickel wire was cleaned in a 20 weight % H_2SO_4 bath for 20 minutes. A one inch length of the 0.050" dia. nickel wire was then electroplated for 2 1/2 hours at 50 ma at 45° C in an aqueous bath consisting of 100 grams/liter of $MnSO_4 \cdot H_2O$ and 130 grams/liter of $(NH_4)_2 SO_4$. A lead-silver anode was used. The bath was degassed with N_2. Typically, under these conditions 95 milligrams of Mn were plated onto the nickel, giving a good smooth surface.

The chromium plating was done as follows. The 0.050" nickel wire was cleaned by cathodic treatment in a 10 weight % H_2SO_4 bath for 15 seconds at 150 ma/cm^2. The wire was then allowed to sit in this solution for an additional five minutes.

A one inch length of the cleaned nickel wire was then electroplated for 5 hours at 400 ma at 45° C in an aqueous bath consisting of 230 grams/liter of CrO_3 and 5cc/liter of concentrated H_2SO_4. A lead-silver anode was used. Typically, under these conditions 70 mg of chromium were plated onto the nickel. A bright, tightly adhering plate was obtained.

b. Fluoride, chloride, and oxide wire electrodes

Fluoride electrodes were prepared by exposing short lengths of 0.040 - 0.060" dia. wire of the desired metal to pure fluorine (Matheson Co., 98.0% purity) in a nickel (passivated) reactor at 30 psia (20° C) under the conditions given in Table 41. (Prior to heating, the reactor was evacuated and filled with argon at 20° C and 15 psia four times, before fluorine was finally admitted and the heating begun.) Evidence of reaction was indicated by a 1-2% weight gain and a change in visual appearance. (A typical weight gain was 15 mg for a 3-inch length of Cu wire.)

TABLE 41

FLUORINATION CONDITIONS

Metal	Exposure Time (hours)	Temperature, ° C
Ag	5	100
Co	7	480
Cu	4	480
Ni	14	600
Zn	8	350
Cd	4	270
In	2	100
Fe	6	350

Chloride electrodes were prepared by exposing short lengths of 0.040 - 0.060" dia. wire of the desired metal to pure chlorine (Matheson Co., 99.5% minimum purity) in a nickel (passivated) reactor at 45 psia (20° C) under the conditions given in Table 42. The chlorination procedure was similar to that given for fluorine above.

TABLE 42

CHLORINATION CONDITIONS

Metal	Color of Chloride	Exposure Time (hours)	Temperature, ° C
Ag	white (AgCl)	16	200
Cu	brown ($CuCl_2$)	20	25
Co	blue ($CoCl_2$)	20	380
Ni	yellow ($NiCl_2$)	6	680

Copper, nickel, and cobalt oxides were prepared by heating the 0.040 - 0.060" dia. metal wires in a stream of air in a vycor tube furnace at 15 psia under the conditions given in Table 43. The cobalt wire, as received, had a black coating which was removed with emery cloth prior to heating.

TABLE 43

OXIDATION CONDITIONS

Metal	Exposure Time (hours)	Temperature, ° C
Cu	0.3	200
Co	1.5	365
Ni	1.0	300

After preparation of the above fluorides, chlorides and oxides, they were allowed to cool, and their atmospheres were replaced by dry nitrogen under which they were stored.

Attempted preparation of silver oxide wire electrode by heating in air was not successful; instead these electrodes were prepared by electrolytic oxidation of 0.050" dia. silver wire at 25° C at 2.0 ma/cm^2 (constant current supply) in a 30 weight % KOH solution against a silver counter-electrode. After about 5 minutes, the voltage reached its second plateau and the electrolysis was stopped. The oxidized electrode was then washed with water, air dried, and finally dried under vacuum at 25° C.

Although the specific compositions of the fluoride, chloride, and oxide electrodes were not investigated, these electrodes gave reproducible results in the voltage sweep measurements.

c. Sintered electrodes

Porous, sintered metal electrodes (2.0 cm x 2.0 cm) were used to measure discharge capacity as a function of charge inputs. The zinc and cadmium electrodes were prepared by a proprietary chemosintering process, using -100 mesh metal powder pressed onto nickel grids. Sintered copper felt electrodes were obtained from Huyck Metals Company. Standard silver plates from silver oxide - zinc batteries were provided by the Power Sources Division of Whittaker Corporation. These were charged to silver oxide, in KOH at 2 ma/cm^2 to a specific capacity of 10 coul/cm^2 of electroactive material.

Silver fluoride, copper fluoride, zinc fluoride, and copper chloride electrodes were prepared by direct reaction of the metal with the active gas. The reaction was carried out in a closed passivated nickel reactor system with pressure set at 30 psig (25° C), and with an argon-to-active gas ratio chosen so as to limit the extent of reaction to about 20 coul/cm^2, assuming complete reaction. Control electrodes, weighed before and after reaction, were used in all preparations to estimate the amount of reacted material per unit area on the electrode surfaces.

Some typical fluorination and chlorination conditions are given in Table 44.

TABLE 44

FLUORINATION AND CHLORINATION OF SINTERED METAL ELECTRODES

Metal	Exposure Time (hours)	Temp., °C	Charge (coul/cm^2)
CuF_2	15.0	550	9
ZnF_2	17.0	350	15
AgF_2	1.5	90	15
$CuCl_2$	50.0	250	20

B. Cyclic Voltammetric Measurements

1. Instrumentation

The instrumentation employed for the cyclic voltammetric measurements is schematically shown in Figure **70**. Basic to the method is a potentiostat which maintains the voltage between the reference - working electrode couple at a value equal to the sum of the input reference voltages represented by the dc reference and function generator values. The potentiostat accomplishes this by controlling the current between the working and counterelectrodes. The potentiostat senses the difference between the reference - working electrode voltages and the sum of the reference input voltages by means of a high gain amplifier system, and feeds the output through the working electrode - counterelectrode couple. This amplifier has high input and low output impedance, and a rise-time less than 10^{-4} sec. The system permits the measurement of current-voltage-time relationships under well-defined conditions. No voltage change is possible at the reference electrode, and the measurements reflect only the voltage changes at the working electrode - electrolyte interface independent of ohmic losses through the electrolyte and polarization at the counterelectrode.

The potentiostat was designed and built at Whittaker R and D. Employing solid state operational amplifiers, the instrument was limited to ± 10 volts at 100 ma. Use of a Harrison type 6824A current amplifier extended the capability to 100 volts peak-to-peak at 1.2 amp. The function generator was a Hewlett Packard Model 3300. Voltammograms were recorded using the Moseley type 7035A X-Y recorder. The dc reference voltage was a simple circuit consisting of mercury cells in series with a 10-turn precision potentiometer and a voltage trim pot.

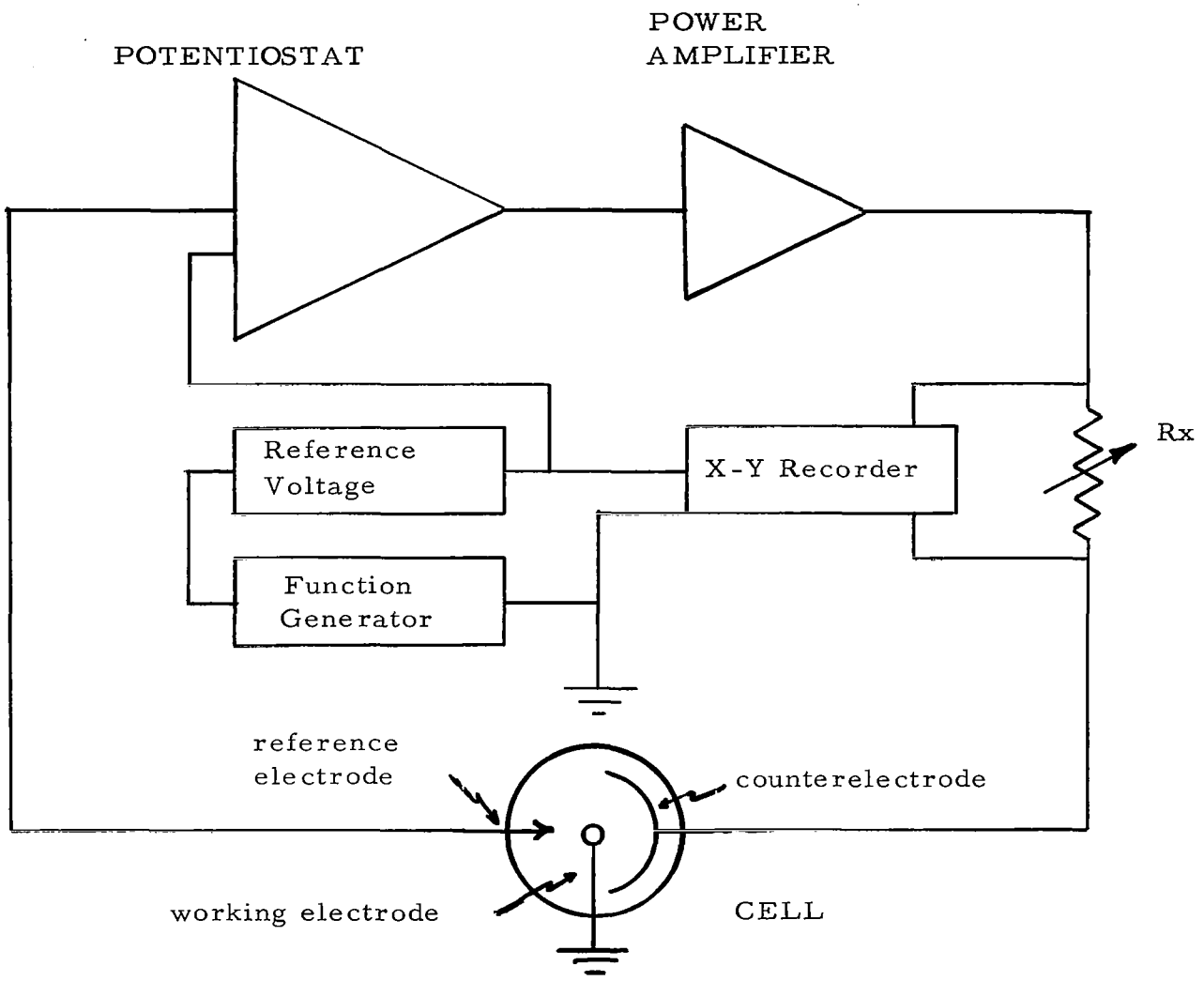

Figure 70. Block diagram of instrumentation.

2. Measurement Procedure

The dc reference voltage was set at the value of the open circuit voltage of the working electrode. The function generator was then set at the desired frequency with an output amplitude of 2.0 v peak-to-peak, causing the instrument to scan 1.0 volt anodic to 1.0 volt cathodic with respect to the open circuit potential. With the recorder at minimum sensitivity to prevent overloading, the instrument was switched to the cell just as the function generator voltage passed through zero. The cell was allowed to cycle at least 10 times at 200 mv/sec, during which time the current sensitivity was increased until the pattern covered a maximum area. During this time the pen was left in the "up" position. After 10 cycles had passed, the pen was switched to the "down" position and a recording made, unless the voltammogram was still undergoing an obvious change, at which time further cycling was permitted prior to recording. Voltammograms were obtained in triplicate at this sweep rate. Individual recordings were also made at 80 and 40 mv/sec. Comparison of systems was made at the lowest sweep rate.

In the early part of the program, for those systems where little or no electrochemical reaction occurred, the sensitivity of the instrument was sufficiently increased until a pattern was observed on the X-Y recorder. Since this pattern was invariably a flat ellipse typical for a leaky capacitor, it was decided to set a maximum sensitivity to avoid loss of time in attempting to obtain an X-Y pattern for a system obviously having no interest. This maximum sensitivity was equivalent to 0.1 ma/cm^2 per cm length measured along the Y-axis. This figure was well below the unit divisional setting for the poorest systems containing an electroactive species, so there was no danger of eliminating any systems that might be of interest.

The voltage scan was always in the clockwise direction, becoming more positive to the right, and more negative to the left, so that the anodic reaction

occurs above the X-axis (voltage axis), and the cathodic reaction below this axis. For the screening of positive plate materials, this corresponds to the charge reaction above the X-axis, and the discharge reaction below this axis. In screening the negative plate materials, the anodic and cathodic reactions remain oriented as above, but these now represent the discharge and charge reactions respectively.

3. Instrument Overloading

A number of electrochemical systems were exceedingly active, resulting in currents in excess of 1.2 amps causing current overload of the amplifier. This in turn resulted in driving the amplifier voltage to an overload condition (greater than ± 50 v). The effect was a sharp break-off on the XY pattern preventing the recording of the voltammogram. Many other systems also exhibited voltage overload, but without the accompanying current overload. This is due to the relatively low electrolyte conductance accompanied by an appreciable current so that the ± 50 v limit of the instrument is exceeded. Although both cases cause voltage overload of the instrument, in order to distinguish those systems having currents greater than 1200 ma (irrespective of the solution conductivity) from those in which the currents are sufficiently high (but less than 1200 ma), but which possess a relatively low conductance, the term current overload was reserved for the former, and voltage overload for the latter. The approximate maximum current (both anodic and cathodic) for the latter systems is indicated on the amplifier meter, so could be noted and recorded. A maximum current of 1200 ma corresponds to a current density of 4.8 amps/cm^2 for a 1/4 inch length electrode, indicating the excessively high non-steady state current densities available. During the early period of the program, instrument overload was infrequently observed so no current recordings were made.

For a number of systems, voltage overload did not occur even though the

electrolyte conductance was one and two orders of magnitude lower than systems giving overload. This occurred whenever currents were exceedingly low, owing to poor availability of electroactive species (very low solute solubility).

4. Electrochemical Cell

Cyclic voltammetric measurements were made in a 3-electrode type cell shown in Figure 71. The reference electrode compartment and that of the main cell are filled with the same electrolyte to prevent solution junctions leading to voltage errors. The two compartments are attached to each other via an electrolyte bridge culminating in the main compartment at a luggin capillary. The tip of the luggin capillary is notched in a vertical direction, allowing the reproducible positioning of the working electrode. The cell is equipped with a ground glass ball-joint connection for the working electrode compartment. The ball-joint facilitates the positioning of the electrode into the luggin capillary notch, and the joint clamp holds the electrode rigidly in place during the measurements.

The working electrode was generally a 50-mil diameter wire contained in a glass capillary tube capped at the end by a Teflon plug. The capillary tube was covered with Teflon tape in the region of the vertical tube portion of the glass ball-joint. This assured a snug fit and permitted limited vertical adjustment of the capillary tube so that the working electrode could be properly set in place in the luggin capillary. The Teflon plug was machined from Teflon rod to a slightly undersized fit for the glass. The hole through the Teflon plug was also undersized. The cold flow property of Teflon resulted in a good seal. The wire was normally exposed to a 1 inch length, and was renewed by pulling it out further and cutting away the used portion. For those systems having high activity, it was necessary to expose a shorter length in order to reduce the current requirement.

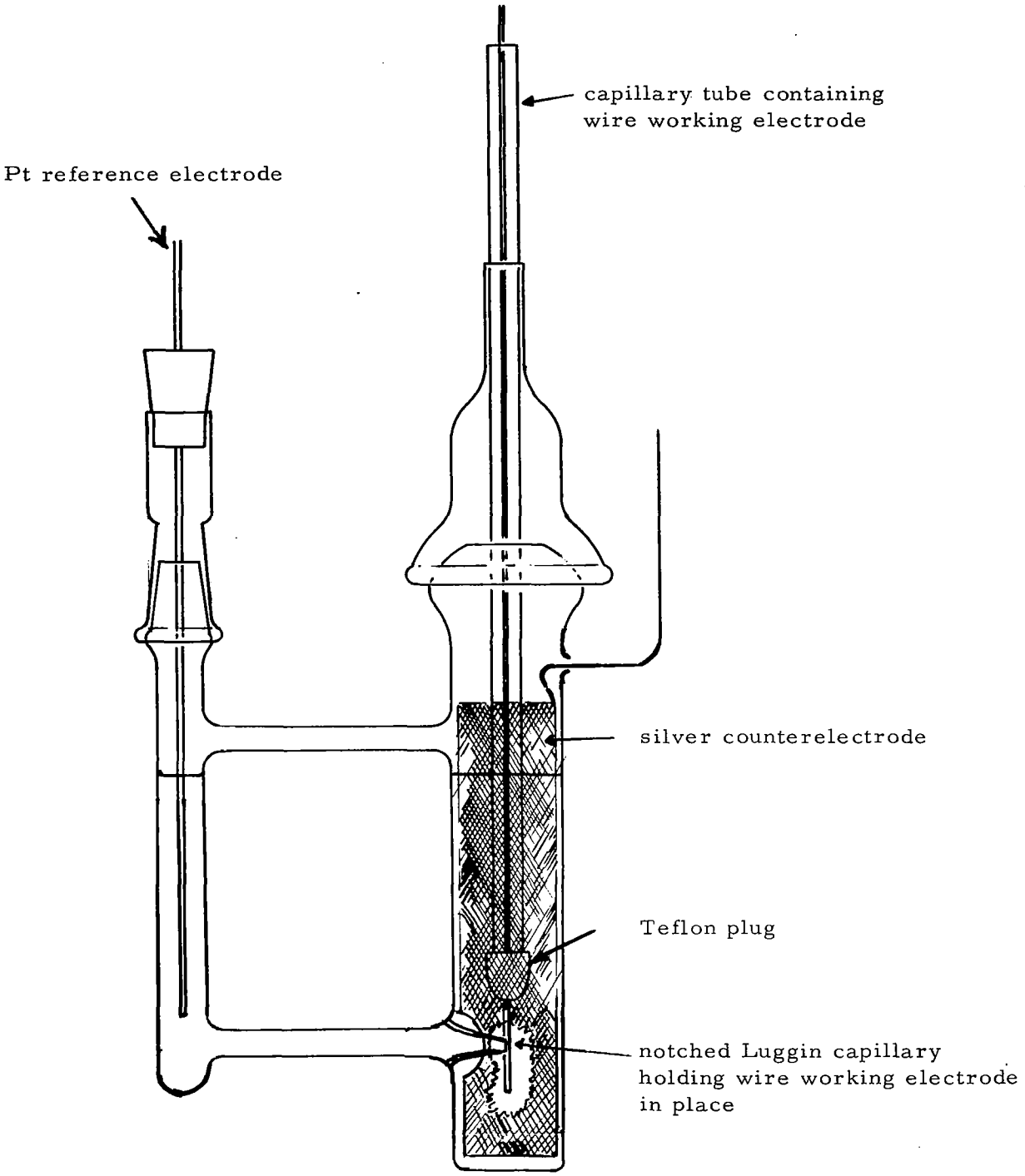

Figure 71. Measuring cell for cyclic voltammetry

The full exposure of the 1 inch length of the 50-mil diameter electrode gave an apparent surface area of 1 cm^2.

The counterelectrode consisted of a silver screen tube totally surrounding the working electrode to insure good current distribution. A platinum "reference" electrode was used only for the purpose of establishing a zero reference point for the cyclic voltammogram. Important to the screening was the nature of the charge and discharge peaks, and their orientation relative to each other, obviating the need of a true reference electrode.

5. Effect of ir Drop on Cyclic Voltammograms

Figure 72 shows the effect of solution ir drop on the peak shape. The cyclic voltammograms were obtained by placing the working electrode in the normal position in the notched luggin capillary, then moving it further from the capillary. Curve A shows the cyclic voltammogram obtained with the working electrode at its proper position at the luggin capillary. Curve B was obtained by moving the working electrode 2-3 mm from the luggin, and Curve C, 4-6 mm distant. Measurements were then repeated using an ir compensating circuit, and with the working electrode still 4-6 mm from the luggin. The resulting sweep curve coincided with Curve A.

These results established that as long as the working electrode was maintained at the prescribed position in the luggin capillary notch, the cyclic voltammograms would not be distorted or blanked out by solution resistance. This permitted measurements to be made without the use of a resistance compensating circuit, which would have complicated and restricted the scope of the program.

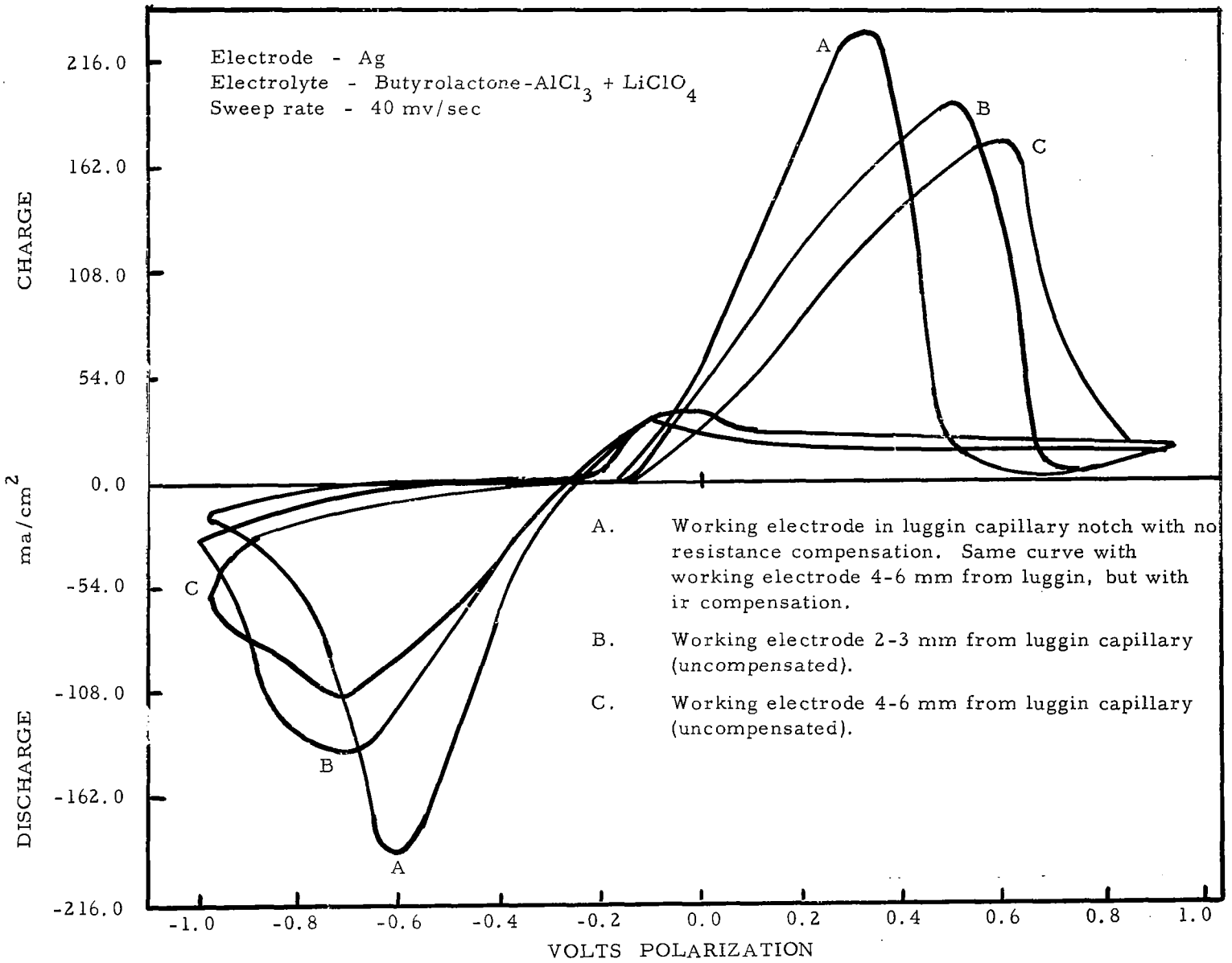

Figure 72. Effect of solution ir-drop on cyclic voltammogram.

C. Galvanostatic Charge-Discharge Measurements

On completion of the screening program by cyclic voltammetry, recommended systems were further characterized by charge and discharge of sintered electrodes.

Tests were conducted in a 3-compartment cell, with the working and reference electrodes positioned in the central compartment, and the counter-electrodes in the outer compartments. Cell dimensions were such as to provide at least a ten-fold excess of electrolyte to the working electrode at current densities well above those used in these tests. The cells were constructed from polypropylene sheets (3 x 2 1/2 x 1/8 inch), cut in appropriate shapes of sides and spacers to form the compartments when assembled. The separate parts were fused together along the outer edges using a heat torch. The working electrode was positioned in the current path provided for by 1.8 cm bore diameter holes in the spacers separating the working and counterelectrode compartments. Total exposed electrode area was 5.0 cm^2. Pyrex fritted, glass disks (Corning F) were affixed with a polypropylene melt onto the spacers to act as separators and retard diffusion of reaction by-products from the counterelectrode compartments. Figure 73 shows an illustration of the test cell.

The working, counter-, and reference electrodes consisted of the same metal for any given test. Porous, sintered, working electrodes were used. The zinc and cadmium electrodes were prepared by a chemosintering process, using -100 mesh metal powder pressed onto nickel grids. Sintered copper felt electrodes were obtained from Huyck Metals Company. Standard silver plates from silver oxide - zinc batteries were provided by the Power Sources Division of Whittaker Corporation. These were charged to silver oxide in KOH at 2 ma/cm^2 to a specific capacity of 10 $coul/cm^2$ of electroactive material.

Figure 73. Experimental cell.

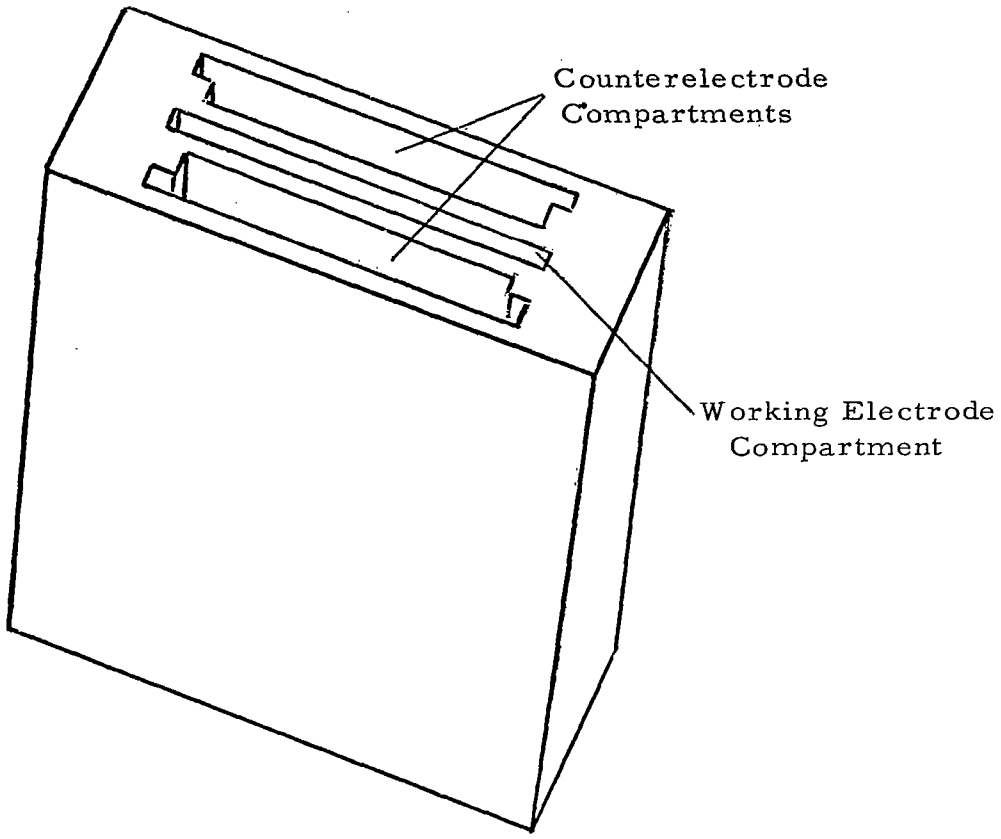

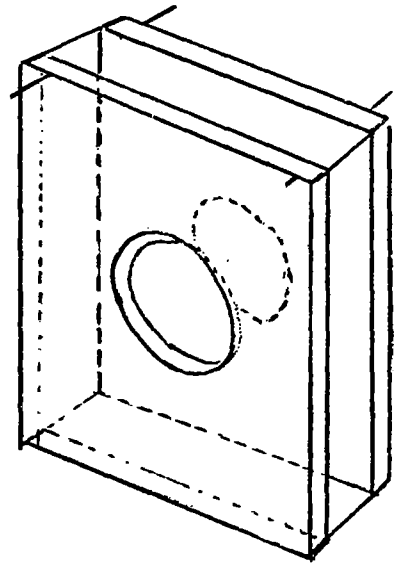

Working Electrode
Compartment Detail

Showing openings to counterelectrode compartments. (During charge-discharge experiments, these were covered by pyrex glass frits.)

Silver fluoride, copper fluoride and copper chloride electrodes were prepared by direct reaction of the metal with the active gas. The reaction was carried out in a closed system with pressure set at 30 psig (25° C), and with an argon-to-active gas ratio chosen so as to limit the extent of reaction to about 20 coul/cm^2, assuming complete reaction. Control electrodes, weighed before and after reaction, were used in all preparations to estimate the amount of reacted material per unit area on the electrode surfaces. In all cases, the weight gain on the control electrodes corresponded to between 20 and 25 coul/cm^2. Counterelectrodes were made either from metal sheet or wire coils (total surface area = 100 cm^2). Reference electrodes consisted of the corresponding fluoride in wire form.

All test solutions were saturated with respect to the corresponding electrode material. This was done in a two compartment H-cell by subjecting electrodes to a constant current of 10 ma/cm^2 for a minimum of three hours. This was more than sufficient to saturate the solutions, since the coulombs passed exceeded an equivalent value of 40 millimoles/liter, which is the cation concentration for the most soluble of the systems.

Since it was impractical to sweep cycle the electrodes (due to electrode geometry and test cell setup), the electrodes were preconditioned by cycling the cell using a linearly varying current applied between the working and counterelectrodes. This current varied between 0 and ± 10 ma/cm^2 at a cycling frequency of 5 seconds per charge-discharge cycle. This frequency was chosen to maintain the polarization potential within ± 0.5 volts. Preconditioning was carried out for ten minutes prior to the charge-discharge tests. This was equivalent to 120 charge-discharge cycles.

The charge-discharge tests consisted of galvanostatic charging at coulombic capacities of 0.1, 1.0, 5.0, and 10.0 coul/cm^2, and discharging to an appropriate cutoff voltage within 0.5 volts negative to the rest potential. Current densities of 1 and 5 ma/cm^2 were employed. Tests were started at the lowest coulombic input, then progressed to the larger charge capacity. A minimum of three tests were made for each charge capacity. Voltage-time curves were recorded during both the charge and discharge processes, measurements being made relative to the reference electrode. In cases of charged electrode systems such as with the copper fluoride, a reduction current was applied to bring the electrode to an initial discharged state. The regular procedure was then followed.

D. Chronopotentiometric Measurements

CPM data were taken by operating a Whittaker designed potentiostat in a galvanostatic mode as shown in the block diagram in Figure 74. A manual reversing switch on the reference voltage input to the amplifier was used for current reversal.

The experimental cell constructed from polypropylene is illustrated in Figure 73. The working electrode was a flat thin sheet, 2.0 cm x 2.0 cm, and was positioned in the current path established by the 1.8 cm diameter holes in the inter-compartment spacers. Both sides of the electrode were used, giving a total area of 5.0 cm^2. The two counterelectrodes were of the same metal as the working electrode for any given test, as was also the reference electrode. The reference electrode metal would usually achieve a stable potential, and proved unsuitable in only a few instances (in which case a metal/metal halide reference electrode was used).

The reference electrode configuration consisted of a modified Luggin tip using 1/8" diameter teflon tubing as the reference electrode compartment. The teflon tube was notched to fit over the working electrode, thereby achieving a minimum set distance of the Luggin tip from the electrode surface. Roughly, the average ir drops intercepted by the reference electrode at 50 ma/cm^2 were: 0.1 v in PC-$LiBF_4$, 0.1 v in PC-$LiClO_4$, 0.3 v in PC-$LiPF_6$, 0.6 - 0.8 v in PC-LiCl + $AlCl_3$, and 0.5 - 1.0 v in BL-KPF_6. No ir drop corrections were made in the CPM figures shown in this report. The positioning of the reference electrode was reproducible to the extent that the intercepted ir drop might vary by ± 30%.

CE = Counterelectrode

RE = Reference Electrode

WE = Working Electrode

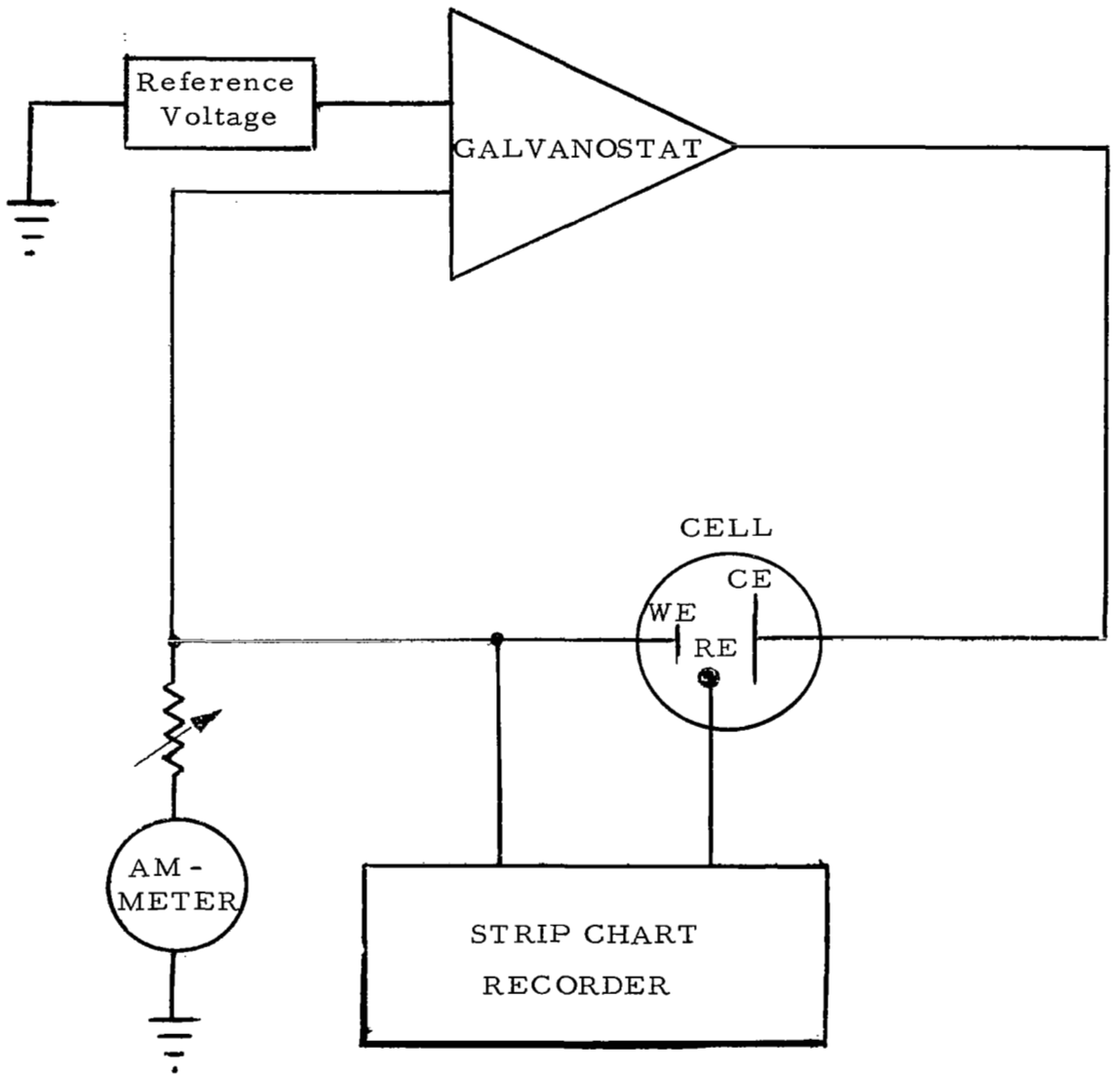

Figure 74. Block diagram for CPM experimental circuit.

IV. REFERENCES

1. Globe-Union Inc., Final Report, NASA Contract NAS3-2790 NASA Report CR-54153, January 1965

2. Nicholson, R.S., Shain, I., Anal. Chem. 36, 706 (1964)

3. Nicholson, R.S., Shain, I., Ibid., 37, 178 (1965)

4. Polcyn, D.S., Shain, I., Ibid., 38, 370 (1966)

5. Nicholson, R.S., Ibid., 37, 1351 (1965)

6. Breiter, M.W., J. Electrochem. Soc., 109, 42 (1962)

7. Breiter, M.W., Gilman, S., Ibid., 109, 622 (1962)

8. Gilman, S., Breiter, M. W., Ibid., 109, 1099 (1962)

9. Breiter, M.W., Ibid., 110, 449 (1963)

10. Juliard, A.L., Shalit, H., Ibid., 110, 1002 (1963)

11. Buck, R.P., Griffith, L.R., Ibid., 109, 1005 (1962)

12. Mann, C.W., Anal. Chem., 36, 2424 (1964)

13. Rhodes, D.R., and Steigelmann, E.F., J. Electrochem. Soc., 112, 16 (1965)

14. Davis, D.G., and Orleron, D.J., Anal. Chem., 38, 179 (1966)

15. Delahay, P., New Instrumental Methods in Electrochemistry, Interscience, 1954.

16. P. R. Mallory and Co., Inc., Final Report, NASA Contract 3-6017 NASA CR-54969, October 1964 - December 1965.

17. Delahay, P.D., Mattax, C.C., and Berzins, T., J. Am. Chem. Soc., 76, 5322 (1954).

NASA-Langley, 1969 —— 3 E-5131